POLITECNICO
MILANO 1863

DIPARTIMENTO DI MECCANICA

Steel metallurgy

Volume I

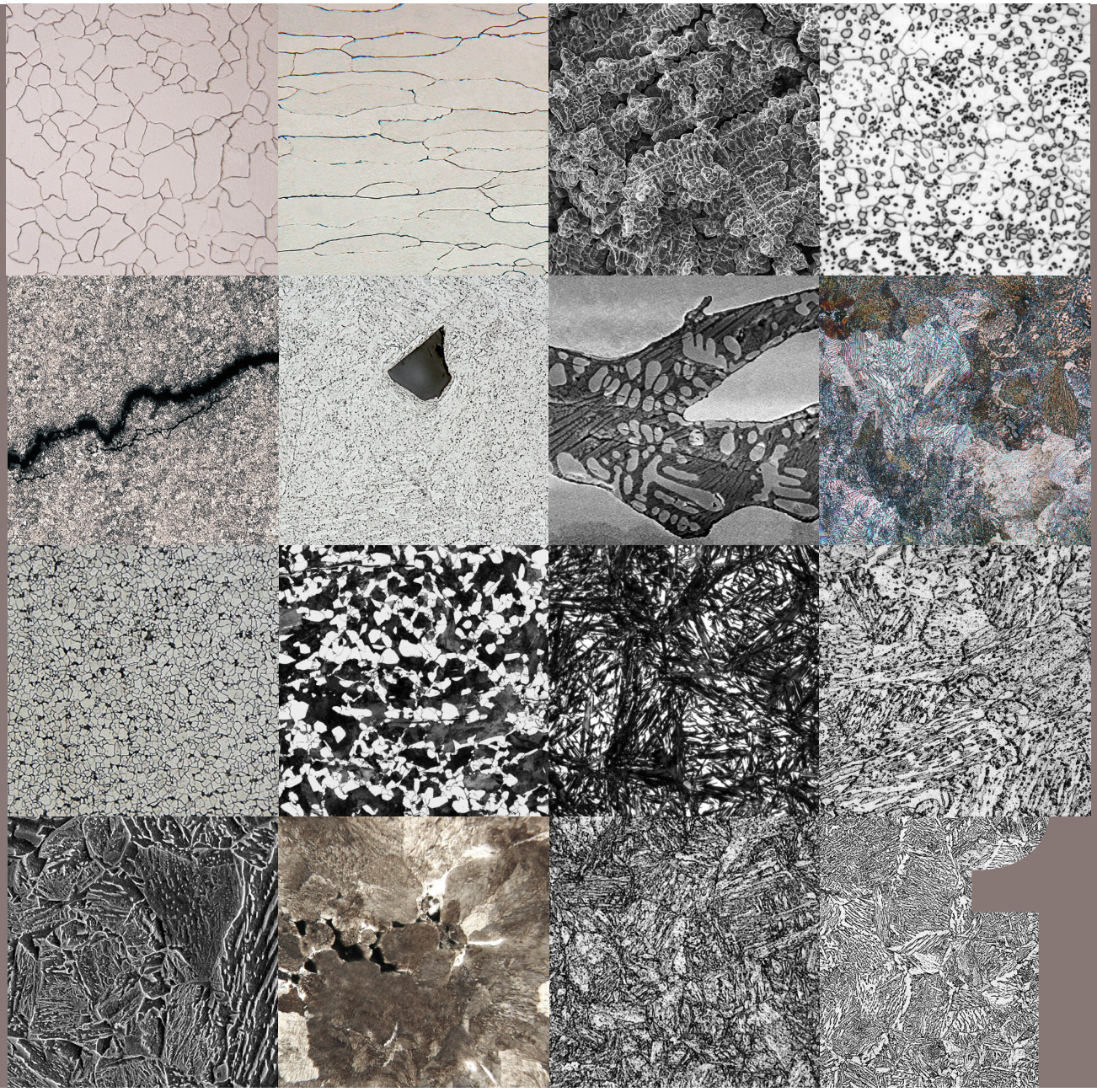

Marco V. Boniardi e Andrea Casaroli

TRAFILIX
INDUSTRIES

This book is dedicated to Davide and Pietro:
before them lays a future that awaits them.

You do not teach what you wish to.
I would even dare to say that you do not teach what you know or what you think you know.
You teach, and you can only teach, what you are.

Jean Jaurès, Speech to the Chamber, 1910.

TABLE OF CONTENTS

PREFACE

"Steel Metallurgy": procedure towards continuing to recount our materials and our history... since we have always believed in this!
We believe in what we do, with professionalism, commitment, and dedication.
We believe in culture. In the culture of the industry and in the culture of knowledge, turning towards those who live this profession with intensity and passion, or to those who are just simply at the beginning.
We believe that our work, to which we dedicate a lifetime, should not just be an everyday experience, but the desire for continuity.
We believe in the collaboration among people and the value of projects that arise from collaborations.
In the end, we believe that the future of our industry depends only on us.

I thank the authors. Great professionals but, above all, great people, and I thank all those who made this initiative possible.

Giorgio Buzzi, Esine - Brescia - April 15th, 2017

I think I will not wrong anyone in saying that the preface of a book is usually written last, even if the term indicates precisely the opposite. Usually, in a preface, authors explain why they have decided to write that certain book, why it is useful, and for which readers it was thought for and created.
I, who work as a teacher (it would be nice to say "a master"... but that is not a profession), I always write and teach with a mental tare in my head: Will I be able to make them understand what I'm trying to say or not?
With this idea, my intention was to print the volume you are holding. I wanted to write a simple - but not simplistic - book that explained the basics of steel metallurgy with a language that was comprehensible to everyone. Often, when I read technical-scientific texts in this discipline (but also in others), I have the unpleasant feeling that the author is only talking to those who are in the field, the so-called "initiates", whom are already familiar with metallurgy. That is exactly what I did not want to do.
I thought of a "bottom-up" approach towards the problems. Something that could be useful to my students and all those who already work in the metallurgic industry. For the first, my desire was to whet their interest in a topic not yet known to them. For the latter, I wanted to complete some theoretical gaps that will explain the relevant daily practice.
If you want to write well, you must have an altruistic approach. Writing a book is an act of love for the reader. A good writer, like a good teacher, is not one who sums up all possible knowledge regarding a given topic or one who is capable of effectively transferring a great deal of information. Instead, a good writer is one who seduces, suggests, stimulates. One who, in order to convey true knowledge, generates in those who read a kind of void that, from that moment forward, must be filled. Or else, as Massimo Recalcati observed, "True teachers are not those who have filled our heads with already established knowledge, therefore already dead knowledge, but those who have created gaps, in order to animate a new desire towards "knowing". They are those who have raised questions without offering pre-established answers.[1]
I wonder if I have succeeded in all this? Only the readers will be able to say.

Marco V. Boniardi, Cusano Milanino - Milano - March 4th, 2017

[1] *Massimo Recalcati, L'ora di lezione - per un'erotica dell'insegnamento, Giulio Einaudi Editore, Torino, 2014.*

This book represents the continuation of a work begun back in 2014, along with the Lucefin group: the first result was the publication of the volume, "Stainless steels".
Over the last three years, a recurring question has continued to spin in my head: why write another book on metallurgy? Certainly not for money or academic "honor": there are better ways to achieve these goals. The real motivation is found in the individual. "Writing a Book" has to do with the will to create a useful tool for the reader (... not just for the writer).
We live in a time that precedes the race. Perhaps it would be best to learn to walk before running. One must be efficient; even better if effective.
The book you have in your hands holds the presumption to serve this purpose: to learn how to walk one step at a time, to solve problems, and to be effective.
In the pages that follow, you will find yourself walking through the paths - sometimes winding - that have led metallurgy to what it is today. Roads that are often neglected and forgotten, without which it is not possible to fully appreciate the "why" and "how" of a very important discipline that, unfortunately, is taken for granted by now.
My hope is that this work has not been created in vain. That the time I have devoted to it passes from me to you and that it will allow you to run or take new roads in the future.

Andrea Casaroli, Sarmato - Piacenza - February 27th, 2017

ACKNOWLEDGMENTS

Writing a book is like contracting a debt with many. Not wanting to recognize it is not only wrong but presumptuous. In the case of this book, the list of people and institutions to be thanked has been necessarily very large. We apologize in advance for anything or anyone forgotten.
First of all, a heartfelt thank you to our teachers.
The love and passion for Metallurgy - as for any other thing - always arises from an encounter with a person. In this case, with Prof. Giuseppe Silva and with his way of teaching, working, and being. We certainly learned a lot more than what the professor himself thought to have left us.
We also owe a great deal to Professor Mario Balbi and Professor Walter Nicodemi, to what they have constructed, to the work they achieved, and to what they have transmitted to us.
An acknowledgment of equal importance goes to all of our students in mechanical engineering at the Politecnico di Milano (Bovisa, Leonardo, Lecco, and Piacenza branches), and Università di Pavia. During the years, they have urged and forced us to question ourselves, induced us to better understand things, and to improve our way of recounting them. Many of them have also made a significant contribution to revising the final drafts of this book.
We cannot forget the colleagues from our department - professors and researchers - with whom we discuss all the issues of this very interesting discipline on a daily basis. Therefore, we also thank all the Professors. Maurizio Vedani, Carlo Mapelli, Elisabetta Gariboldi, Barbara Rivolta, Nora Lecis, Fabrizio D'Errico, Riccardo Gerosa, Silvia Barella, Andrea Gruttadauria, Riccardo Casati, and Davide Mombelli.
Another duly deserved acknowledgment goes to Mr. Piero Pellin, Mr. Maurizio Pardi, Engineer Ludovica Rovatti, and Engineer Luca Signorelli, some of the most valued technicians in the Laboratories of the Department of Mechanical Engineering of Politecnico di Milano: their scientific competence - this term is not used at random - has always been of great support and help. We cannot forget our secretary, Mrs. Cinzia Farina: she is the best in understanding people and always knows how to "deal with them".
The things you will find written in this book are also the result of collaborations developed over time with many university colleagues that are not from the Politecnico di Milano: Professor Benedetto Bozzini of the Università di Lecce, and Professors Roberto Roberti and Marina La Vecchia from the Università di Brescia, Professor Francesco Iacoviello from the Università di Cassino, Professor Donato Firrao from the Politecnico di Torino, and Professor Giovanni Straffelini from the Università di Trento. We also owe a great deal to Engineers Gianmatteo Martinelli, Mattia Bellogini, Marco Feraboli, Gianmarco Vimercati, Silvia Cincera, and Alessia Sironi who have by now transferred their sphere of interest outside the academic world.
It is not possible to speak of metallurgy without also looking at the industrial world. Studying steel is not a theoretical experiment, but a continuous practical application.Therefore, a thank you to Mr. Emilio Rocchi at Acciai Vender, to Engineer Mario Cusolito, and Engineer Enrico Mariani at Rodacciai, to Mr. Antonio Vienna, to Mr. Gabriele Rampinini, and to Engineer Chiara Tagliabue at Forgiatura Vienna, to Engineer Valentina Vicario at Fomas, and to Engineer Guido Perricone at Brembo. A special thought goes to all the technicians and friends at Tenaris Dalmine, Engineers Renato Spelgatti, Barbara Scarabelli, Stefano Farè, Gianluca Bassanini, Maurizio Bellingardi, Emanule Paravicini Bagliani, and Tiziana Nani and Carolina Lussana, Phds.

We also must not forget the support received from industrial laboratories that work in the field of steel metallurgy. Confronting oneself with intelligent individuals helps to increase your wealth of knowledge: thank you Engineer Luca Bonvini and Engineer Andrea Tombretta at Hammer, to Mrs. Patrizia Maio and Engineer Matteo Borgonovo at Kaizenlab, to Engineer Alessandra Marelli, Engineer Marco Casaril and Engineer HC Clemente Marelli at Omeco, Mr. Giovanni Rivolta at RTM Breda, Mrs. Elena Bresciani, and Dr. Mauro Ostacoli at Exova.
Last but not least, immense thank you to Luigi and Giorgio Buzzi, Massimo Sperto, Vittorio Boneschi, and Domenico Surpi at the Lucefin steel group, who have believed in us and who have offered us this editorial opportunity.
Our final thought goes to those who are always close to us and who support us every day: Dolores, Piero and Marcella, Pinuccia, Francesco and Elena.

For all the micrographs in the text, we received support from the following organizations:
- Laboratories of the Department of Mechanical Engineering, Politecnico di Milano, I-20156 Milano Via La Masa, 1;
- Hammer S.r.l. Laboratories, I-20017 Rho - Milano - Via Risorgimento, 69/22;
- Omeco S.r.l. Laboratories, I-20900 Monza - Monza Brianza - Via Monviso, 56;
- Exova S.r.l. Laboratories (now Element Materials Technology Milan S.r.l.), I-26013 Crema - Cremona Via della Pierina, 9/11.

Although it is true that the work involved in preparing and observing the samples was performed by people - and our thanks goes to them - without the required laboratory tools, not much could have been done.

Marco V. Boniardi and Andrea Casaroli, Milano February 24th, 2017

Each book - and this is not a flaw - is "alive",
and wishes to continue to live.

For this to occur, your help is needed.
Any suggestions or advice you would like to give us,
and any images or micrographs you would like to send us,
will be well accepted and very appreciated.
You will help us improve the quality of the next edition.

We urge you to write to the following addresses:
marco.boniardi@polimi.it and andrea.casaroli@polimi.it

Thank you everyone in advance... for everything!

1. IRON AND ITS CRYSTAL STRUCTURE

1.1 What is iron?

Iron (symbol: *Fe*) is a metal chemical element belonging to the eighth group of the periodic system (transition metals), with atomic number 26, an atomic mass of 55.847amu[1], and an atomic radius at room temperature of 0.124nm.

Iron is one of the chemical species most commonly found on the Earth's crust, second only to aluminum. It has a melting temperature of 1,538°C and a density of about 7,870kg/m^3. It is a ferromagnetic metal and its magnetic behavior decreases as temperature increases, until it disappears at 770°C (Curie temperature). The thermal conductivity of iron at room temperature is in the order of 80W/mK, while its electrical conductivity is approximately $10 \cdot 10^6$ $(\Omega m)^{-1}$.

Iron, like most pure metals, has no significant mechanical properties. The ultimate tensile strength ranges between 250MPa and 270MPa, while hardness is between 70HB and 80HB.

The main physical and mechanical properties of pure iron are shown in Table 1.1.

Physical and mechanical properties of pure iron (*)	
Atomic number	26
Atomic mass [amu]	55.85
Number of protons/electrons	26
Number of neutrons	30
Symbol	*Fe*
Color	silvery gray
Density ρ [kg/m^3]	7,860 -7,875
Electro-negativity [Pauling scale]	1.83
Melting temperature [°C]	1,538
Boiling temperature [°C]	2,750-2,870
Specific heat [J/kg·K]	440-450

Physical and mechanical properties of pure iron (*)	
Electrical conductivity $[\Omega \cdot m]^{-1}$	$9.90 \cdot 10^6$-$10.4 \cdot 10^6$
Thermal conductivity [W/m·K]	79.5-80.4
Linear thermal expansion [μm/m·K]	11.7-1.8
Speed of sound [m/s]	4,910-5,120
Mohs Hardness [Mohs scale]	4
Longitudinal elastic modulus *E* [GPa]	196-205
Transverse elastic modulus *G* [GPa]	79-82
Ultimate tensile strength [MPa]	250-270
Yield strength [MPa]	80-120
Elongation after fracture [%]	40-60
Brinell Hardness [HB]	70-80

(*) Unless otherwise specified, they are measured at 20°C and at atmospheric pressure.

Table 1.1 - Physical and mechanical properties of pure iron.

[1] *L'amu (atomic mass unit) is the unit of measure used to express the mass of atoms or of their molecules.The amu is defined as the twelfth part of the mass of a carbon-12 atom and corresponds to $1.660538921 \cdot 10^{-27}$ kg. This unit of measure is convenient because, in general, each atom has a mass equal to the sum of its protons and neutrons. Therefore, with carbon having 6 protons, 6 neutrons, and 6 electrons, it has an atomic mass of about 12amu (electrons have a negligible mass), while hydrogen, with only one proton, has an atomic mass equal to 1amu.*

The chemical bond that allows iron atoms to join together is referred to as a metal bond: it has specific characteristics that are very different from those of the ion bond or the covalent bond, typical of non-metal solids (ceramic materials and polymeric materials).
Let us see in detail what a metal bond is.
Iron, like most of the so-called "metal elements" of the periodic table, has a limited number of electrons in its outer orbit (valence electrons). As a consequence to the element has low electronegativity and low ionization energy and, therefore, it can easily lose its valence electrons (in the case of iron, there are two electrons).
The metal bond develops when valence electrons reach energy levels above a threshold, called the Fermi level. The electrons are separated from the original atoms and generate a cloud with a negative charge that surrounds all the iron cations (i.e., all the iron atoms that have lost their valence electrons and, consequently, gained a positive charge).
Iron cations occupy equilibrium positions and are surrounded by an electronic cloud formed by all the valence electrons. The cloud of delocalized electrons (or electronic gas) is the adhesive that holds the iron cation system together. The binding energy derives from the electromagnetic interaction between the negative charges of the valence electrons and the positive charges of the iron cations. Figure 1.1 shows an exemplification of the described model.

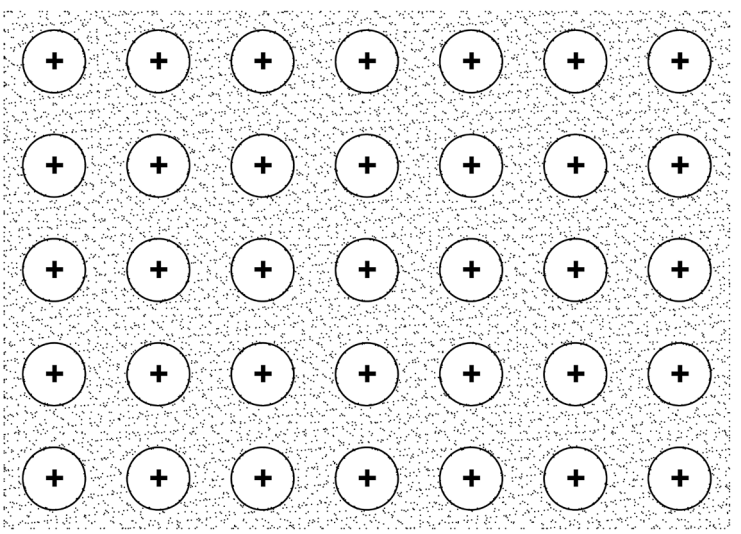

Figura 1.1 – Schematic representation of the metal bond of an iron crystal.

The metal bond model explains many physical and mechanical properties of iron and metallic materials. For example, thermal conductivity and electrical conductivity are closely related to the cloud of valence

electrons. The mobility of valence electrons also explains the transfer of thermal and electrical energy in metals and alloys[2].

The ability of iron, and all metal materials, to reflect light is also due to the interaction of the photons from light radiation with the electronic cloud that surrounds the iron cations.

The mobility of the valence electrons justifies the ductility and malleability of iron and metal materials, as well[3]: if we apply a shear stress to the lattice, the cations slide with respect to each other within the valence electron cloud which like a gelatinous adhesive, holds together the system. On the contrary, this deformation mode is prevented in ceramic materials that show brittle fracture, due to the repulsion between ions with the same electric charge (Figure 1.2).

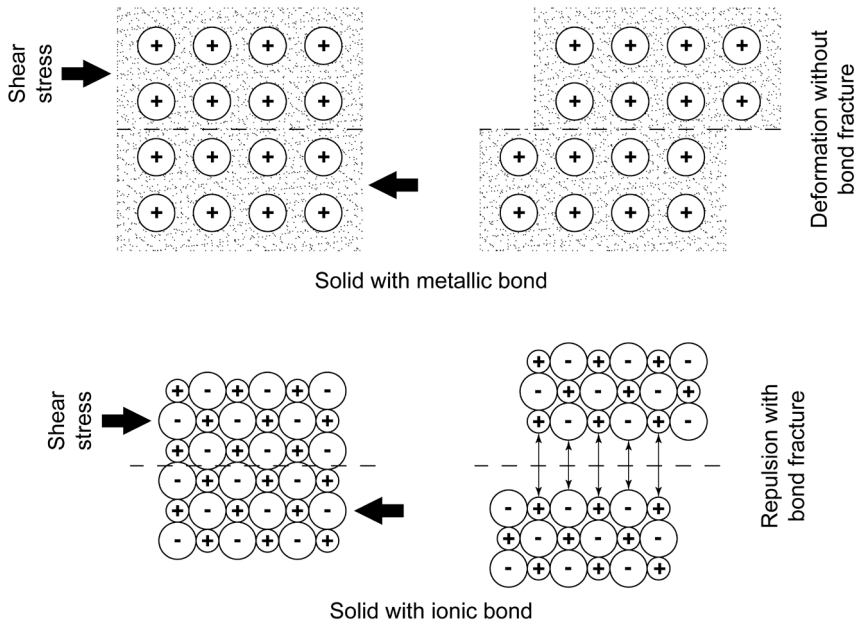

Figure 1.2 - Schematic representation of the plastic deformation mechanism of a solid with a metal bond (above) and of the brittle fracture of a solid with an ion bond (below).

[2] Polymeric materials and ceramic materials generally have poor electrical and thermal conductivity, due to the covalent or ion bond that keeps the electrons of the outer orbits engaged in the bond.

[3] Ductility is defined as the capacity of a metal (or metal alloy) to be reduced to wires. Malleability, on the other hand, describes the aptitude to be reduced to plates. Both properties are closely related to the metal deformability.

1.2 Crystal lattices of iron

The position of iron atoms[4] in space is not random but follows a well-defined order. In particular, a basic arrangement of atoms is always detectable and is repeated indefinitely in the three dimensions.

The base unit of this regular repetition is called elementary unit cell. The crystalline grain of the metal material is obtained by repeating the unit cell in the space. The elementary unit cell is, therefore, the smallest set of atoms that, repeated in the three dimensions, generates the entire crystal structure (Figure 1.3).

This repetitive structure is typical of metal materials, and it is the characteristic feature of all crystalline solids[5].

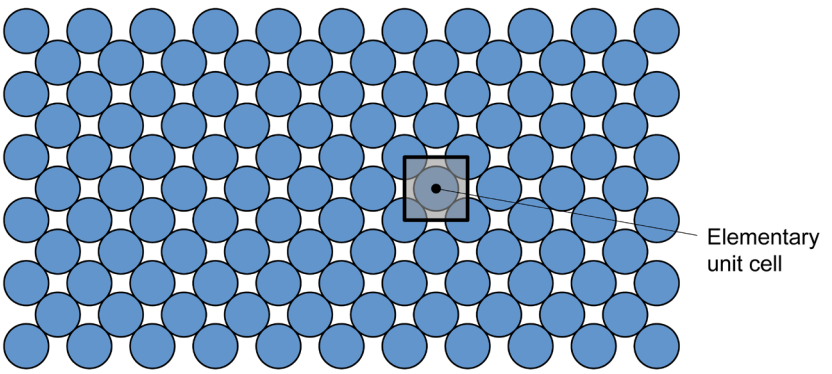

Figure 1.3 - Schematic representation of a metal lattice. Atoms are represented by the rigid sphere model.

A crystalline grain is formed by placing many identical unit cells next to each other. This is somewhat like piling many identical bricks in order to build the wall of a house (Figure 1.4).

The unit cell of iron does not always have the same characteristics. Iron is, in fact, a polymorphic metal. Its lattice takes on various shapes, called allotropic forms, as temperature varies.

Continuing with the analogy of the construction industry, it can be said that the elementary unit cells of iron are not all the same just like the bricks that form the walls of a building, they may have very different characteristics.

[4] The term "iron atoms" will always be used, as usual in the metallurgic field. However we are speaking of iron cations, i.e. atoms that have lost valence electrons.

[5] The term, crystalline solids, is used because the spatial regularity of the crystal is a common element, not only to metal materials, but also in many ceramic materials and some polymeric materials. Glass, on the contrary, is an amorphous solid, that is, non-crystalline. Its atoms are randomly arranged in space without a well-defined regularity.

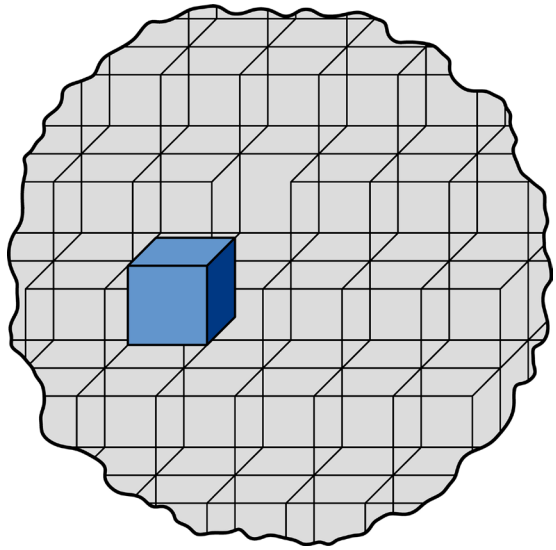

Figure 1.4 - Schematic representation of the elementary unit cell (brick) and the crystalline grain (wall).

The material used for making bricks - the iron atoms - is the same, but the bricks - the unit cells - can be of different types: full bricks, semi-full bricks, perforated bricks, etc. Therefore, the walls, meaning the supporting structure of the metal mass, can be constructed using bricks that are full, semi-full, perforated, and so on.
At atmospheric pressure, there are two different unit cells (i.e. allotropic forms) of iron[6]: the elementary unit cell with body-centered cubic lattice and the elementary unit cell with face-centered cubic lattice. Usually, we speak of B.C.C. and F.C.C. cells or lattices, also called α-iron (or δ-iron)[7] and γ-iron. In both cases the side of the cubic cells is called lattice parameter and is indicated by the letter "*a*".
Figure 1.5 shows the graphic representation of the two iron lattices, using the rigid sphere atomic model[8].

[6] If pressure is considered in addition to temperature, a third allotropic form can be observed, called ε-iron. ε-iron has a compact hexagonal lattice and forms at room temperature for pressures greater than 100,000 bar.

[7] One of the two allotropic forms of iron, exists in two different temperature ranges. This is the body-centered cubic lattice (B.C.C.), called α-iron, between 20°C and 912°C or δ-iron, between 1,394°C and 1,538°C. The name changes (α-iron or δ-iron), but the characteristics of the lattice are the same. By contrast, γ-iron, with a face-centered cubic lattice (F.C.C.), only exists between 912°C and 1,394°C.

[8] This is a simple representation method where the atoms are assimilated to rigid spheres having a radius equal to the atomic radius of the chemical element.

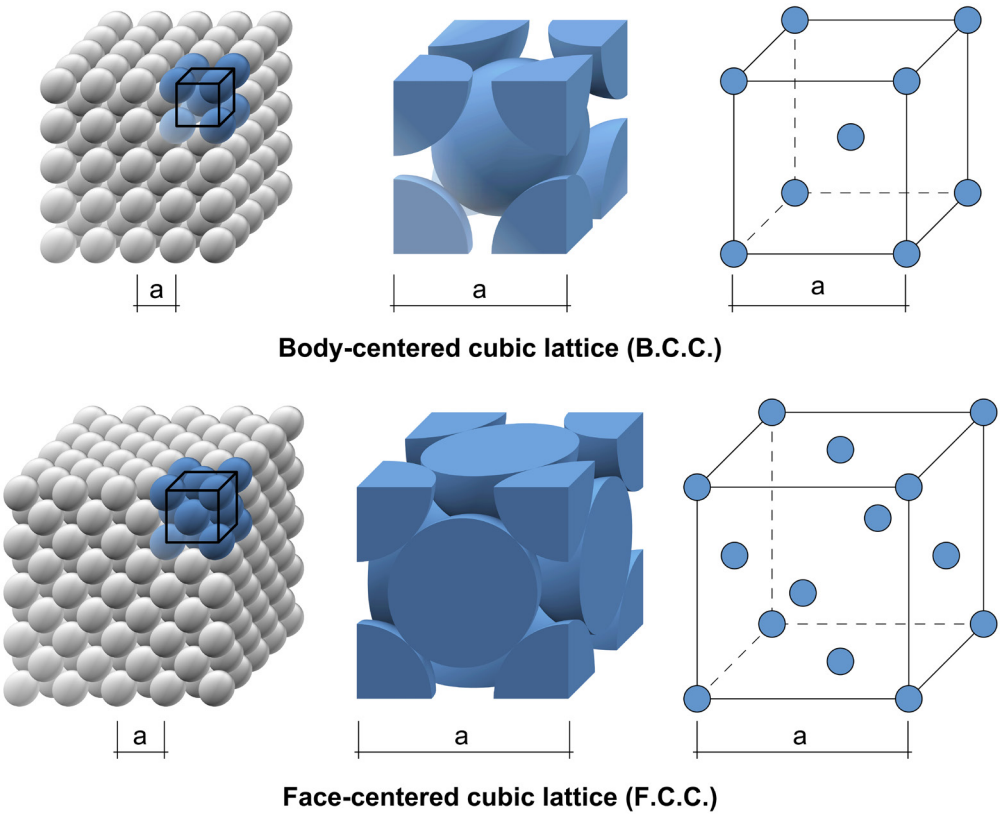

Figure 1.5 - Elementary unit cells of the body-centered cubic lattice (above) and the face-centered cubic lattice (below) [from Callister 2007].

1.3 Characteristics of iron lattices

The B.C.C. unit cell has an iron atom at the center of the cube. Sorrounded by eight iron atoms (four above and four below) located at each of the eight vertices of the cell. In the body-centered cubic system, the rigid spheres, representing the iron atoms, are tangent along the diagonal of the cube[9].

On the contrary, in the F.C.C. unit cell, an iron atom is centered on each of the six sides of the cube. Also, in this second case, there are eight iron atoms at each of the eight vertices. However, in the face-centered cubic system, the contact between the iron atoms takes place along the diagonals of the sides of the cube.

[9] *The diagonal of each of the side of the cube equals to $a \cdot \sqrt{2}$ while the diagonal of the cube equals to $a \cdot \sqrt{3}$ (a is the lattice parameter, i.e. side of the unit cell.*

The value of the cell side a can be obtained through simple calculations starting from the ray R of the atom and the diagonals along which the atoms are tangent. The cell side is $a \cong 2{,}309 \cdot R$ for the B.C.C. lattice and $a \cong 2{,}828 \cdot R$ for the F.C.C. lattice.

Consequently, the volume a^3 of the body-centered cubic cell is much less than the volume of the face-centered cubic cell ($V_{B.C.C.} \cong 12.32 \cdot R^3$ and $V_{F.C.C.} \cong 22.63 \cdot R^3$).

However, F.C.C. cell contains twice as many atoms as B.C.C. cell: four atoms for the face-centered cubic cell, two for the body-centered cubic cell[10].

As a result the so-called, Atomic Packing Factor (A.P.F.) of the cell[11], or the volume of the cell that is occupied by its atoms, is greater for the F.C.C. cell (~74%) than the B.C.C. cell (~68%). Therefore, the F.C.C. cell is slightly denser than the B.C.C. cell and occupies a smaller volume.

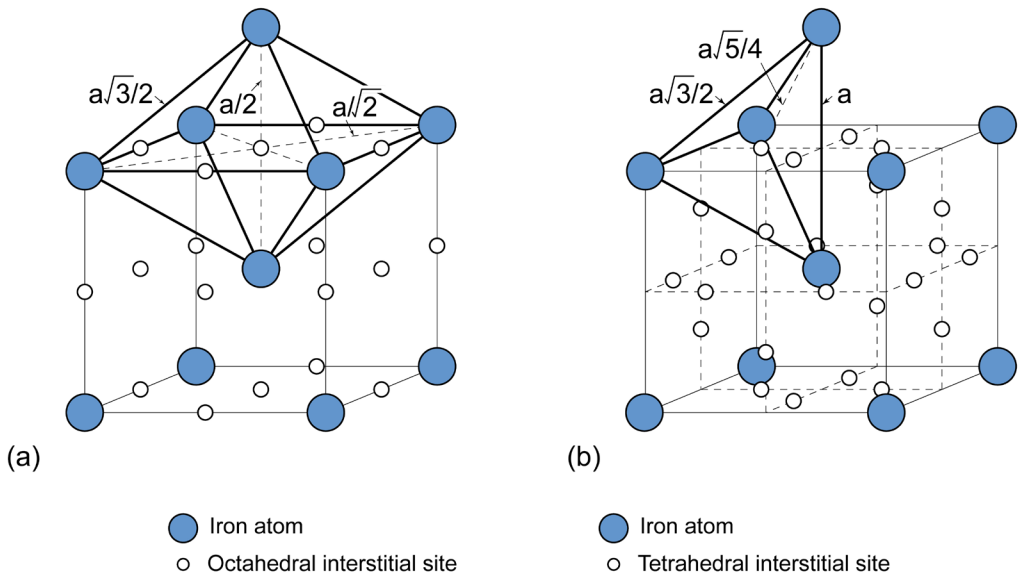

Figure 1.6 - (a) octahedral interstitial site and (b) tetrahedral interstitial site of the body-centered cubic lattice [from Krauss 2005].

[10] In the B.C.C. system, there is an atom at the center of the cell (1) and eight atoms at the eight vertices of the cell shared with other eight adjacent cells (8 ·1/8 = 1): total of two atoms (1 + 1). In the F.C.C. system, however, there are six atoms on the six sides of the cell shared with the adjacent cells (6 ·1/2 = 3) and eight atoms at the eight vertices of the cell shared with another eight adjacent cells (8 ·1/8 = 1): total of four atoms (3 + 1).

[11] The "Atomic Packing Factor" is the fraction of volume in a elementary unit cell that is occupied by atoms.

Another important aspect to consider is the free space within the lattice: these portions of cell volume not occupied by atoms are called interstitial sites. Figures 1.6 and 1.7 show octahedral and tetrahedral interstitial sites of the body-centered cubic cell and the face-centered cubic cell. The white balls identify the center of the interstitial sites, while the blue balls represent the iron atoms[12].

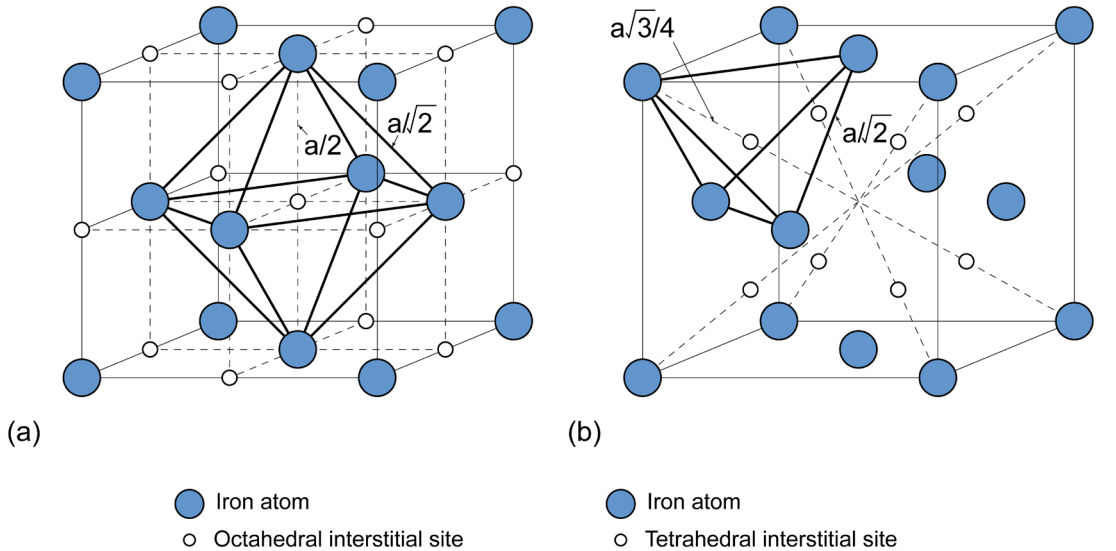

Figure 1.7 - (a) octahedral interstitial sites and (b) tetrahedral interstitial sites of the face-centered cubic lattice [from Krauss 2005].

If on one hand the face-centered cubic lattice has a interstitial site with the greatest absolute volume (the octahedral interstitial site at the center of the cell), on the other hand, the body-centered cubic lattice has the largest total number of interstitial sites (B.C.C.: 6 octahedral interstitial sites + 12 tetrahedral interstitial sites; F.C.C.: 4 octahedral interstitial sites + 8 tetrahedral interstitial sites).
Table 1.2 shows the characteristics of the two iron lattices.

[12] *The interstitial sites in crystal lattices are called octahedral or tetrahedral in relation to the shape of the solid that delimits the portion of lattice not occupied by the atoms. The vertices of this solid are the iron atoms around the interstitial site.*

Properties of the iron crystal lattice			
	α-Iron (20°-912°C)	γ-Iron (912°-1,394°C)	δ-Iron (1,394°-1,538°C)
Atomic Radius R [nm]	0.124-0.126	0.126-0.127	0.127
Type of lattice	B.C.C.	F.C.C.	B.C.C.
Theoric lattice parameter a [nm] as a function of R	$(4/\sqrt{3})\cdot R \cong 0.286\text{-}0.290$	$(4/\sqrt{2})\cdot R \cong 0.356\text{-}0.359$	$(4/\sqrt{3})\cdot R \cong 0.293$
Experimental lattice parameter a [nm]	~0.287 at 20°C ~0.291 at 912°C	~0.369 at 912°C ~0.373 at 1394°C	~0.293 at 1394°C ~0.294 at 1538°C
Number of atoms (N_A) per cell	$1 + 8 \cdot \frac{1}{8} = 2$	$6 \cdot \frac{1}{2} + 8 \cdot \frac{1}{8} = 4$	$1 + 8 \cdot \frac{1}{8} = 2$
Atom volume (V_A) as a function of R	$\frac{4}{3}\cdot\pi\cdot R^3$	$\frac{4}{3}\cdot\pi\cdot R^3$	$\frac{4}{3}\cdot\pi\cdot R^3$
Cell volume (V_C) as a function of R	$\frac{64\cdot\sqrt{3}}{9}\cdot R^3$	$16\cdot\sqrt{2}\cdot R^3$	$\frac{64\cdot\sqrt{3}}{9}\cdot R^3$
Atomic Packing Factor ($N_A \cdot V_A / V_C$)	~0.68	~0.74	~0.68
Number of octahedral interstitial sites per cell	6	4	6
Number of tetrahedral interstitial sites per cell	12	8	12
Radius of the octahedral interstitial site [nm] as a function of R	$0.155\cdot R \cong 0.0194$	$0.414\cdot R \cong 0.0524$	$0.155\cdot R \cong 0.0197$
Radius of the tetrahedral interstitial site [nm] as a function of R	$0.291\cdot R \cong 0.0364$	$0.225\cdot R \cong 0.0285$	$0.291\cdot R \cong 0.0370$

Table 1.2 - Properties of the body-centered cubic lattice (B.C.C.) and of the face-centered cubic lattice (F.C.C.) of pure iron.

1.4 Allotropic transformations of iron

The allotropic forms of iron are not random, but depend on temperature.

To understand this concept we can heat slowly an iron bar from room temperature, to its melting point. Then we cool it down very slowly[13]. Figure 1.8 shows the iron bar temperature over time.

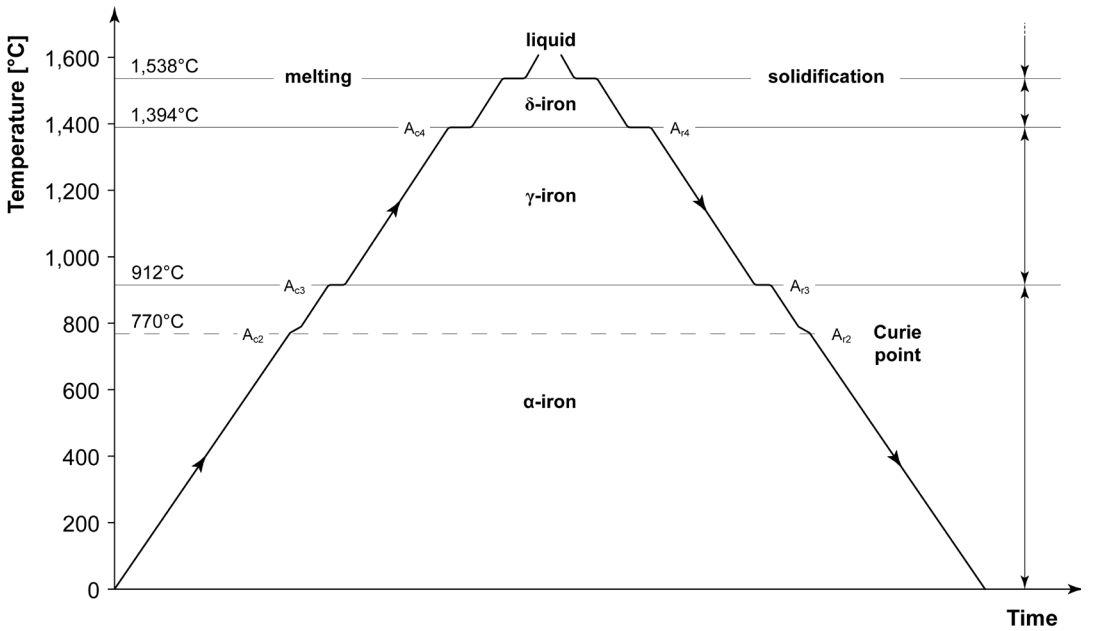

Figure 1.8 - Heating and cooling of an iron bar with indication of the critical points [from Thelning 1975].

Both in heating and cooling, the curve shows three points (912°C, 1,394°C, 1,538°C), where the temperature remains constant over a short interval of time. These temperatures, called critical points, indicate the allotropic transformations temperature of iron, i.e., the transformations temperatures of the iron lattice (critical point $A_3 = 912°C$; critical point $A_4 = 1{,}394°C$; melting temperature $T_f = 1{,}538°C$).

[13] *We can speak of equilibrium transformations if the change in temperature (T) over time (t), tends to zero ($dT/dt \rightarrow 0$). In this condition, heat is supplied or subtracted from the system very slowly, giving the time to the system to return to its equilibrium state, that is, in a contition in which temperature, pressure, chemical composition and state of aggregation are the same everywhere.*

Pure iron has[14]:

- body-centered cubic lattice cell (B.C.C.) from 20°C up to 912°C (called: α-iron);
- face-centered cubic lattice cell (F.C.C.) from 912°C to 1,394°C (called: γ-iron);
- body-centered cubic lattice cell (B.C.C.) from 1,394°C to 1,538°C, (called: δ-iron);
- liquid state over 1,538°C.

Further observations are required, in order to explain some of the characteristics of the curves in Figure 1.8. First of all, the allotropic transformations of iron always involve the absorption of heat from the surrounding environment if they occur during heating, or release of heat to the surrounding environment if they occur during cooling. Consequently, thermostatation (temperature stop) are always observed at critical points, both for heating and cooling. In summary, allotropic transformations of iron occur at a constant temperature, similar to what occurs with changes in the state of aggregation of pure substances[15].

In addition to the three critical points, a further discontinuity at 770°C can be observed: this temperature, called the Curie point, does not represent an allotropic transformation, but the transition of iron from ferromagnetic ($T < 770$°C) to paramagnetic ($T > 770$°C)[16] behavior.

All critical points are indicated by the letter *A* (from the French, *arrêter* = to stop) and by a progressive number (1, 2, 3, and 4). There is also the letter *c* if the measurement of the critical point occurred when heating (*chauffer* = to heat), or the letter *r* when cooling (*refroidir* = to cool).

Lastly, let us consider that the distinction between δ-iron and α-iron is only formal, since in both cases, iron has same B.C.C. crystal lattice. In this respect, Figure 1.9 shows the effect of temperature on the lattice paramiter *a*.

---

[14] Numerous references about critical points of iron and of iron-carbon alloys are available in literature. In this book we follow what was proposed in [Chipman 1972]. The same data are also taken up in [Abbaschian et al.2009], [Krauss 2005] and in italian university textbooks, as in [Nicodemi 2007].

[15] The iron bar absorbs heat when the allotropic transformations ($\alpha \leftrightarrow \gamma$; $\gamma \leftrightarrow \delta$; $\delta \leftrightarrow$ liquid) occur during the heating phase: this heat is called latent heat and it is released from the bar during the cooling phase. As a result, the linear temperature trend shows discontinuities when the allotropic transformations take place ($\alpha \leftrightarrow \gamma$; $\gamma \leftrightarrow \delta$; $\delta \leftrightarrow$ liquid). A bit like the evaporation of pure whater at 100°C: also in this case the thermostatation is caused by the absorption of the latent heat during the phase change.

[16] At the dawn of scientific studies in the metallurgic field, it was mistakenly believed that between 770°C (critical point A_2) and 912°C, there was another allotropic transformation which was indicated as iron ß.

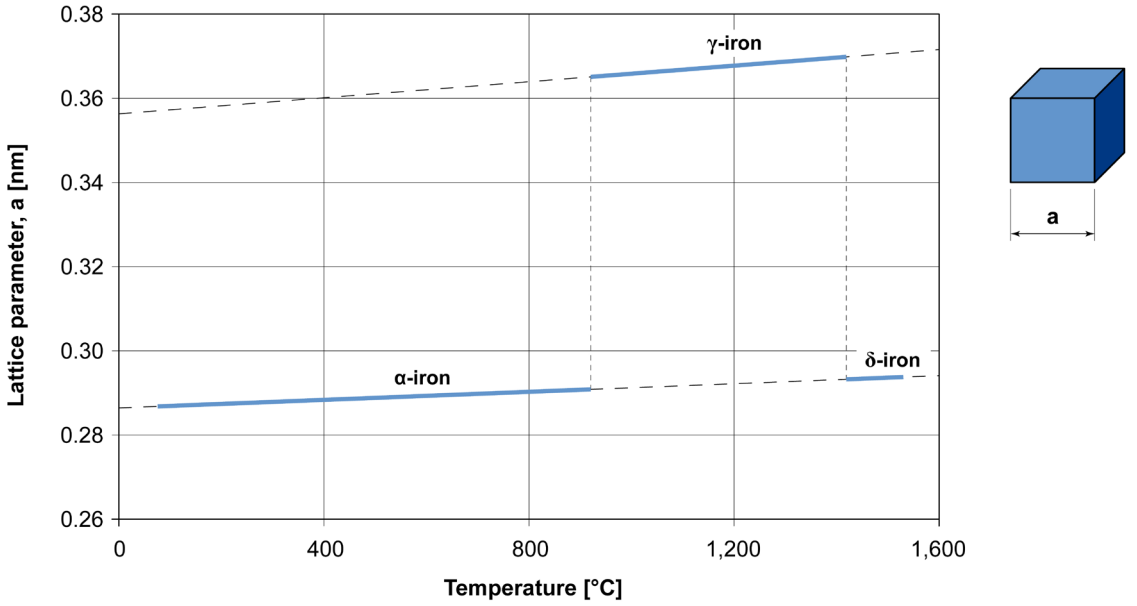

Figure 1.9 - The effect of temperature on the lattice paramiter *a* [from Onink et al.1993].

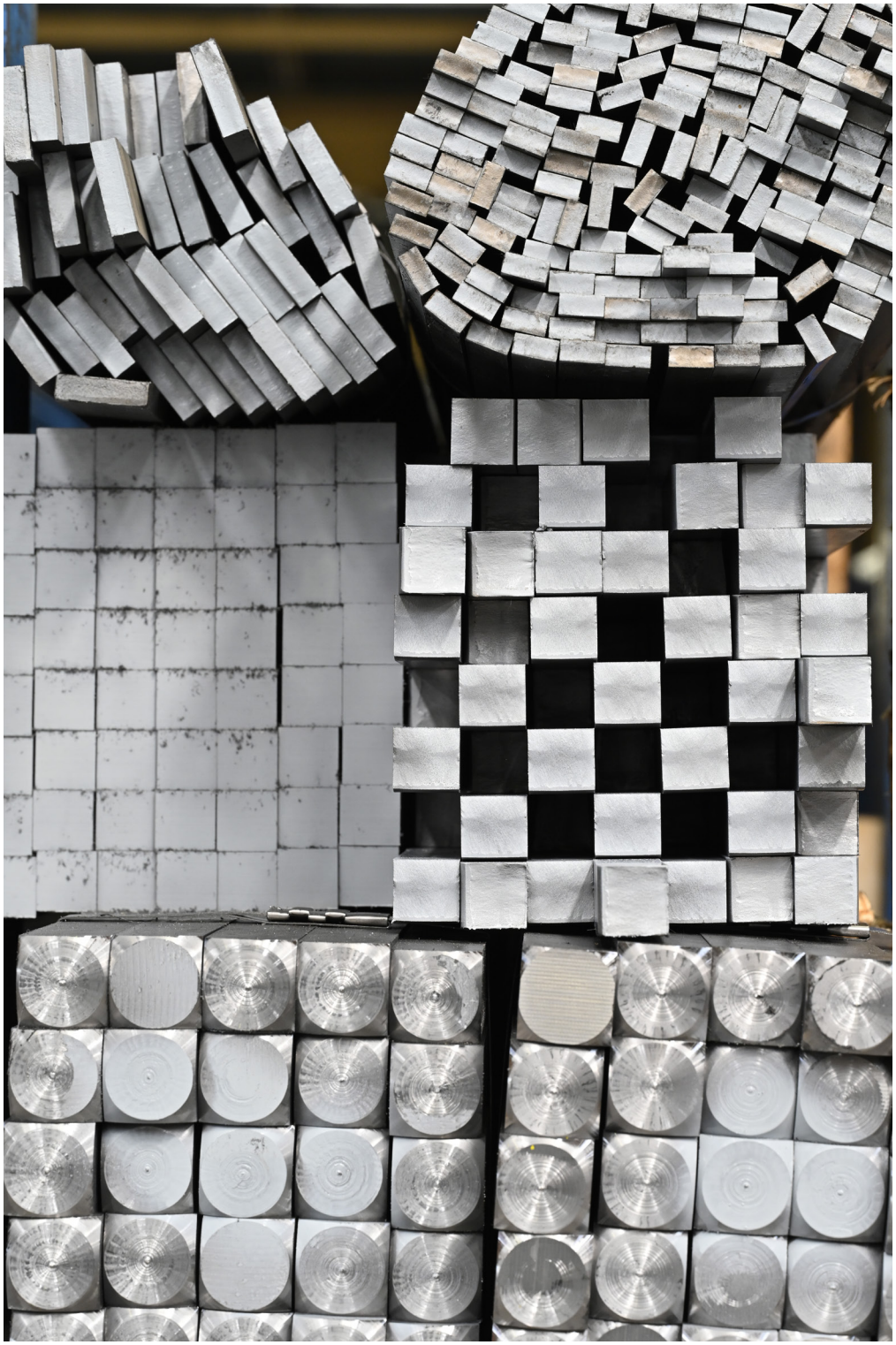

2. DEFECTS OF THE CRYSTAL LATTICE

2.1 Classification of crystal lattice defects

The crystal lattice of iron, as ideally shown in Chapter 1, should have a regular geometry. However, in practice, all metals and metal alloys always have a certain number of defects, where the original order of the lattice disappears[1].

Some types of lattice defects are due to the entropy[2] of the system and, therefore, increase when the temperature increases: these defects are called "thermodynamic equilibrium defects". At absolute zero, thermodynamic equilibrium defects can be considered absent while a progressive increase of the temperature causes an increase of their number as a consequence of the higher thermal agitation of the atoms.

Most other defects, are called "not in thermodynamic equilibrium" and their numbers do not increase when temperature increases although their size and distribution can be modified through appropriate heat treatments.

Another classification is related to the dimensional characteristics of lattice defects. Four different types can be distinguished:

- point defects (zero-dimensional defects);
- line defects (one-dimensional defects);
- surface defects (two-dimensional defects);
- volume defects (three-dimensional defects).

2.2 Point defects

Point defects are an atomic discontinuity and are normally associated with one or two atomic positions. All point defects are thermodynamic equilibrium defects.

The main types of point defects are:

- vacancies;
- substitutional atoms;
- interstitial atoms.

[1] Generally, in common language, a negative connotation is given to the term "defect". In the case of crystal lattices, however, the term only indicates a lack of regularity. Sometimes, there are negative effects and, therefore, the defect is a defect in its full sense. In other cases, defects guarantees benefits to the metal.

[2] In statistical mechanics, entropy is a physical quantity, indicated by the letter S, that represents the disorder level of a generic system. An increase in the disorder of the system is associated with an increase in entropy, while a decrease in disorder leads to a decrease in entropy.

A first type of point defect is the vacancy, i.e., a lack of an iron atom within the regular crystal lattice. The consequence of a vacancy is a local distortion of the lattice due to the movement of the surrounding atoms from their original position in order to compensate the electromagnetic void (Figure 2.1).
Vacancies are point defects that originate mainly during solidification, plastic deformation, or heat treatments. Vacancies and lattice interstitial sites explain the movement of the atoms within the metal lattices. This phenomenon, called diffusion, is important for understanding many metallurgical phenomena[3].

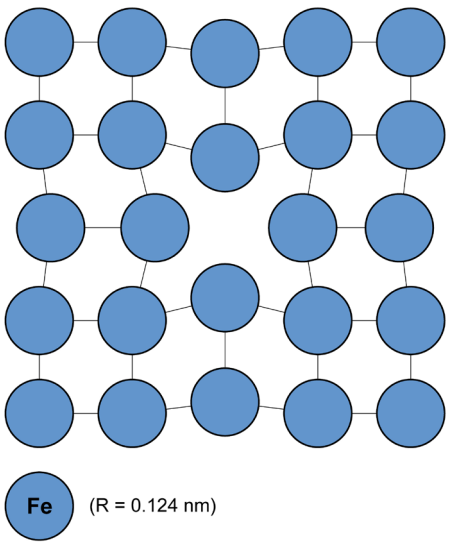

Figure 2.1 - Example a vacancy in a crystal lattice.

A second type of point defect is the substitutional atom. This defect is due to the replacement of one or more atoms of the iron lattice with atoms of other chemical elements having an atomic radius comparable to the atomic radius of iron (R_{Fe} = 0.124nm). Typical examples of substitutional atoms in the iron lattice are nickel (R_{Ni} = 0.124nm), chromium (R_{Cr} = 0.125nm), molybdenum (R_{Mo} = 0,136nm), vanadium (R_{V} = 0.131nm), manganese (R_{Mn} = 0.126nm), aluminum (R_{Al} = 0.143nm), and silicon (R_{Si} = 0.117nm). The example of this defect is shown in Figure 2.2.

[3] *For a broad discussion on diffusion see Chapter 3.*

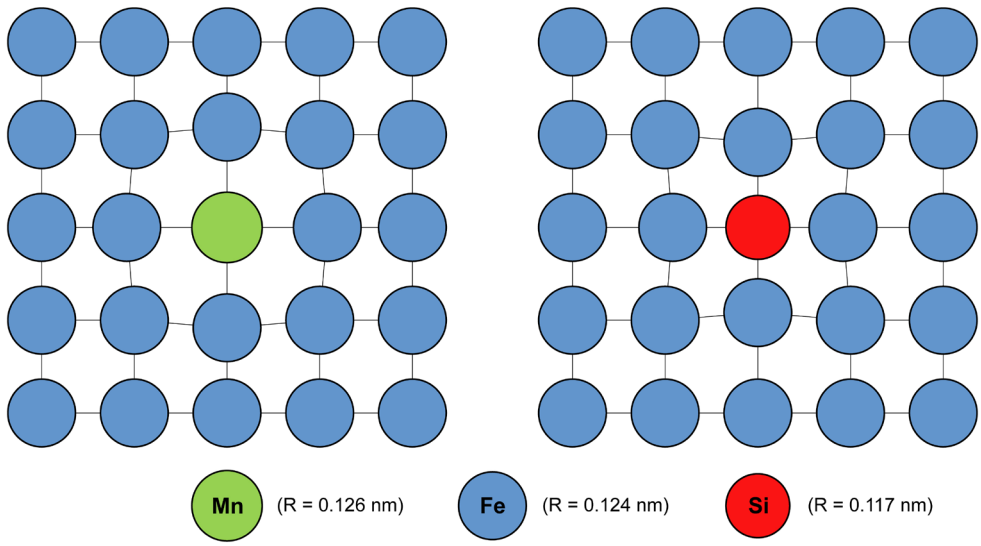

Figure 2.2 - Examples of substitutional atoms in the iron crystal lattice. Manganese, an atom larger than an iron atom (left); silicon, an atom smaller than an iron atom (right).

The last type of point defect is the interstitial atom. This defect is due to atoms extraneous to the iron lattice entering into the lattice interstitial sites.

In this case atoms must have an atomic radius much smaller than the atomic radius of iron, as is typical with carbon (R_C = 0.077nm), nitrogen (R_N = 0.070nm), oxygen (R_O = 0.066nm), hydrogen (R_H = 0.030nm). Only small atoms have the potential to occupy the interstitial spaces of F.C.C. or B.C.C. cells, i.e. the tetrahedral and octahedral interstitial sites in the iron lattice (Figure 2.3).

2.3 Solid solutions and compounds

Point defects (vacancies, substitutional atoms, and interstitial atoms) are important to explain the existence of steel and metal alloys, in general. Steel, as is known, is an alloy of iron and carbon. In many cases, in addition to carbon, it contains other alloying elements.

Let us understand how this can occur. Steel can be thought as a lattice of iron atoms with interstitial atoms of carbon. One can imagine that iron is the solvent while carbon is the solute that dissolves in the iron lattice. This is somewhat like sugar that is dissolved in water, resulting in a more or less sweet water solution, depending on the greater or lesser quantity of sugar. It is no coincidence that, referring to steel, the solid solution of carbon in iron is mentioned.

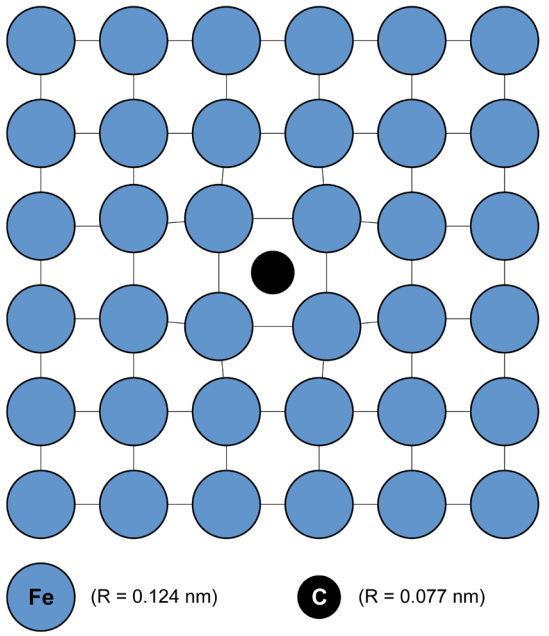

Figure 2.3 - Example of an interstitial atom in the crystal lattice of iron.

The presence of other alloying elements besides carbon, such as manganese, silicon, nickel, chromium, molybdenum, or vanadium, can be explained with the concept of the substitutional atom. Also in this case, iron is the solvent and the alloying elements are the solute that dissolves in the lattice.
Therefore, at a first approximation, steel can be conceived as a solid solution of carbon and other chemical elements in iron[4]. The iron lattice is partially filled with carbon in the form of interstitial atoms and partially replaced with other chemical elements in the form of substitutional atoms (Figure 2.4).

In addition, it should be noted that, as is the case for the liquid solution of water and sugar, even solid solutions have solubility limits for the solute in the solvent, depending on temperature. Beyond the solubility limit, it is no longer possible to dissolve sugar in water and the sugar precipitates to the bottom of the container. Something similar is also true for the iron lattice when adding carbon and/or other alloying elements beyond the solubility limit.

[4] This is true only at a high temperature (i.e. at 1,000°C) when carbon is completely in solution in the lattice of γ-iron (at least for commonly used steels). When temperature decreases, the carbon solubility in the iron lattice is greatly reduced, and the schematic representation in figure 2.4. is no longer true.

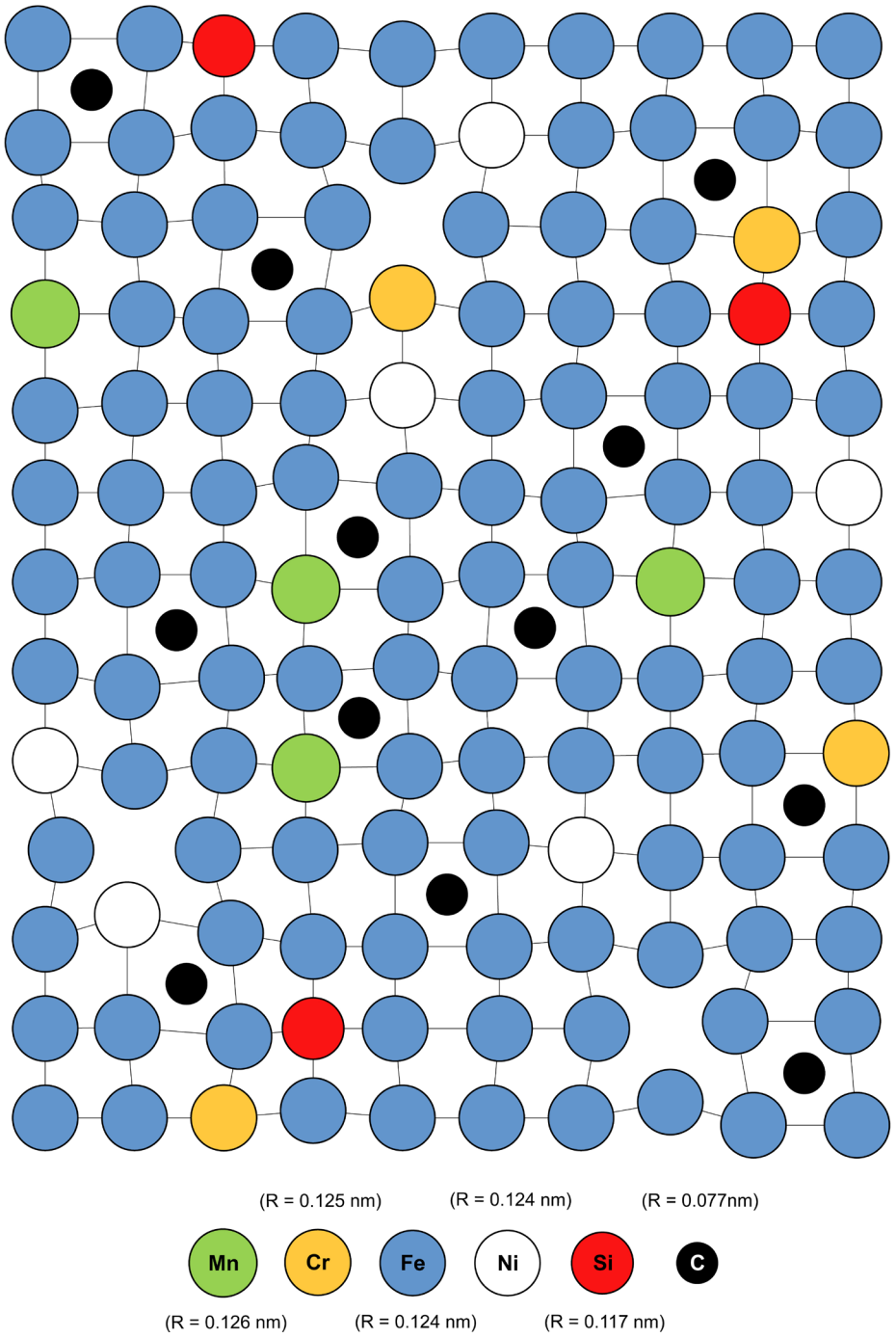

Figure 2.4 - Example of a solid solution of iron, carbon, and other alloying elements (steel).

The carbon case is typical. After exceeding a given composite threshold, it is no longer possible to insert additional carbon atoms into the iron lattice. Beyond the solubility limit, a chemical compound is formed between iron and carbon, called iron carbide, with stoichiometry Fe_3C.

The solubility of carbon in iron is highly dependent on the characteristics of the crystal lattice. In γ-iron (F.C.C. lattice), it is easier to fill carbon atoms because interstitial sites are larger than those of α-iron (B.C.C. lattice). The B.C.C. lattice has great difficulty to accept carbon atoms because the lattice interstitial sites are very small in size.

Consequently, the carbon solubility limit is higher for F.C.C. systems than for B.C.C. systems: at a temperature of 727°C, for example, the carbon solubility limit in γ-iron is equal to 0.77% and in α-iron it is equal to 0.02%[5]. Carbon solubility is also dependent on temperature. As can be seen from Figure 2.5, the carbon solubility is virtually nil in the α-iron lattice at room temperature, while it is in the order of 0.02% at 727°C.

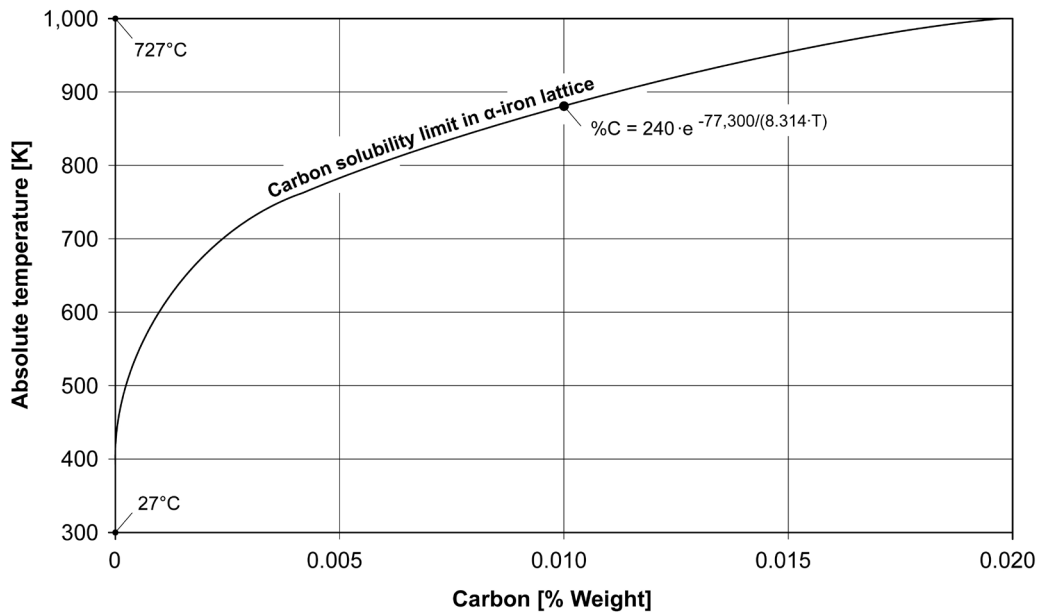

Figure 2.5 - Carbon solubility limit in α-iron lattice [from Abbaschian et al.2009].

[5] *The transformation from γ-lattice (C = 0.77%) to α-lattice (C = 0.02%) plus iron carbides of Fe_3C type (C = 6.69%) occurs at 727°C.*

In addition to iron carbide, Fe_3C, many other chemical compounds[6] can also be present in steel.

The compounds are divided into two categories: interstitial compounds when they are formed between a metal and a non-metal, and intermetallic compounds when they are formed between two metals. Interstitial compounds, such as carbides, nitrides, sulphides, and oxides are rather common in steel where as intermetallic compounds are less common.

Iron can form all four types of interstitial compounds mentioned above: carbides, (Fe_3C, $Fe_{2,4}C$), nitrides (Fe_4N, $Fe_{2-3}N$), sulphides (FeS), oxides (FeO, Fe_2O_3, Fe_3O_4). In addition, many alloying elements may also form interstitial compounds, such as[7]:

- *Ti*, *V*, *Mo*, *W*, and *Cr* for the formation of carbides;
- *Ti*, *Al*, *V*, *Mo*, and *Cr* for the formation of nitrides;
- *Cr*, *Al*, *Si*, and *Mn* for the formation of oxides;
- *Mo*, *Cr*, and *Mn* for the formation of sulphides.

Frequently, compounds are not formed by only one metal and/or one non-metal. Two or more metals in combination with two or more non-metals can contribute to the formation of compounds, as in the case of iron-carbon nitride, $Fe_{2-3}(CN)$, iron-silicon oxide, $2(FeO)\cdot SiO_2$, or manganese oxide sulphide, $MnS\cdot MnO$.

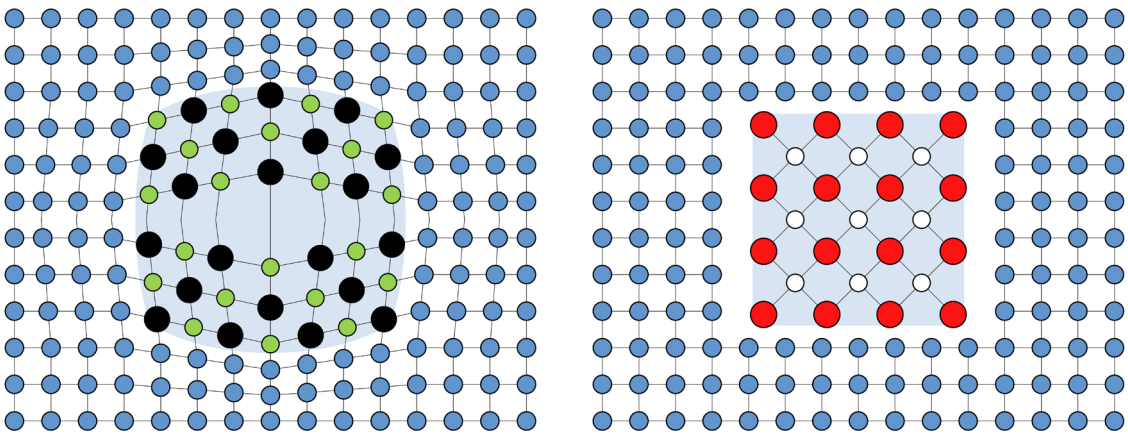

Figure 2.6 - Schematic representation of coherent compounds (left) and incoherent compounds (right).

[6] *All the chemical compounds present in metal materials have a ionic or covalent bond, in relation to the elements involved.*

[7] *The list proposed here does not indicate the aptitude of the element to form a compound (affinity).*

Another important classification of compounds is related to the characteristics of their crystal lattice. They are called coherent compounds if their lattice have the same crystallographic orientation of the surrounding lattice or incoherent compounds in the opposite case (Figure 2.6).
The analogy with liquids also explains why it is common to call the compounds with the term precipitates: when the solubility limit is reached in a liquid sugar solution, the sugar precipitates to the bottom of the container. It is similar for compounds, when the solubility limit of the solute in the iron lattice is reached.

2.4 Line defects

A typical line defect of metal lattices is dislocation. This is a defect that is not in thermodynamic equilibrium. Dislocations are discontinuities of the lattice that are formed during solidification and heat treatment, or due to mechanical stresses.
The most simple form of a dislocation is the so-called "edge dislocation" that consists in the lack of a crystallographic semi-planes within the lattice.
Let us try to understand how an edge dislocation is formed with an example (Figure 2.7).

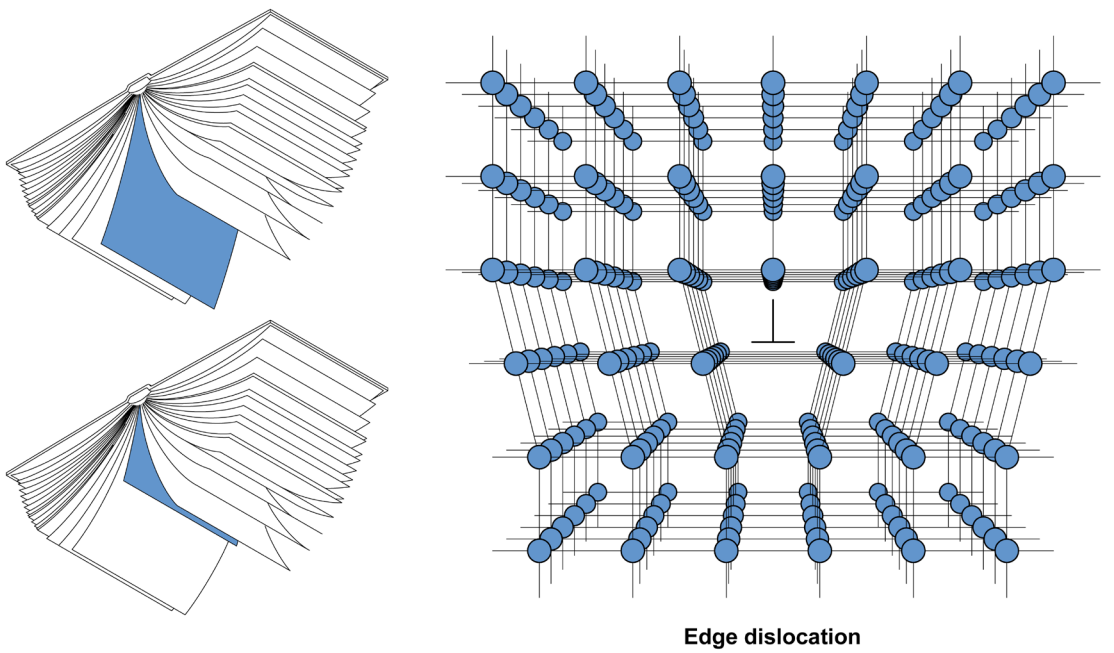

Figure 2.7 - Example of an edge dislocation and analogy with the pages of a book.

For convenience, the crystal lattice of iron can be thought as a book. The pages of the book represent the planes, occupied by the atoms. The sum of all the pages, side-by-side, creates the book, that is, the three-dimensional crystal.

To create an edge dislocation, just take a page of the book and tear it lengthwise, leaving half the page attached to the book. Closing the book and placing the pages next to each other again, the book is put back together and the crystalline solid is reformed, without, however, a crystallographic semi-plane (i.e. the page torn in half). The end of the crystallographic semi-plane (the edge of the torn page) defines the dislocation line where the atoms are slightly shifted from their original position.

From a section, perpendicular to the dislocation, the defect appears as a point that is indicated by an inverted letter *T* (⊥).

Edge dislocations are not the only type of line defects. Other types are screw dislocations or mixed[8] dislocations. These are linear irregularities, that make easier the deformation of the metal mass (Figure 2.8).

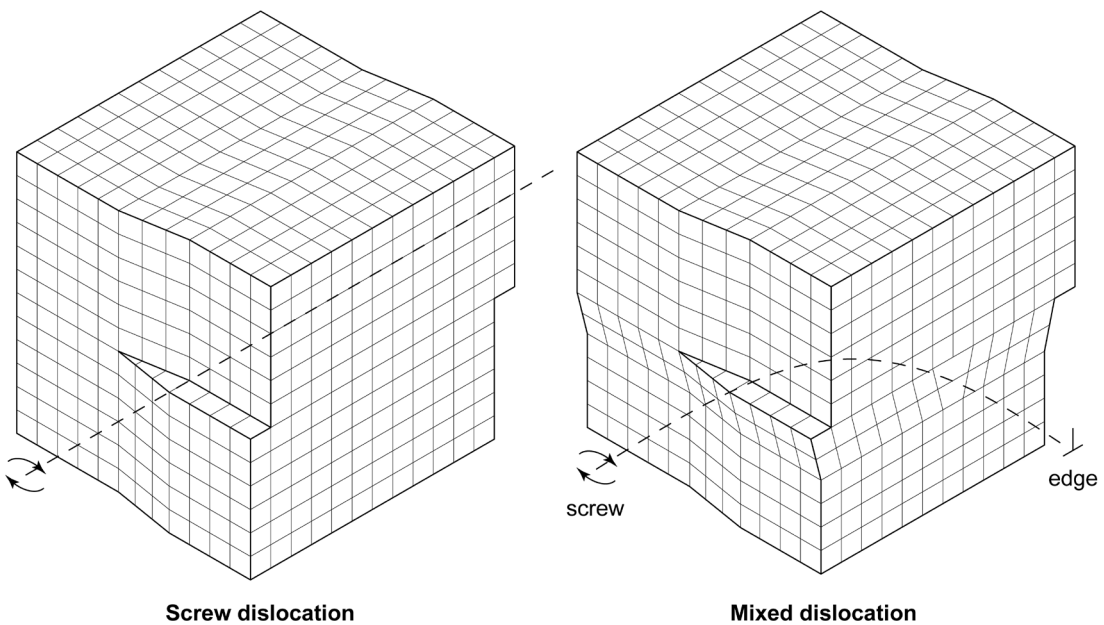

Figure 2.8 - Example of a screw dislocation and a mixed dislocation [from Campbell 2008].

[8] *Mixed dislocations derive from the sum between an edge dislocation and a screw dislocation.*

2.5 The dislocation motion and the deformability of metal lattices

Dislocations are very important because they explain the mechanical properties of iron, steel, and all metallic materials.

First of all, let us see how the plastic deformation of a metal lattice would occur if there were no dislocations. In order to deform the crystal, as indicated in Chapter 1, a shear stress τ must be applied on the lattice. Pure tensile stress applied to the lattice does not produce any permanent deformation[9].

If the lattice is ideal, i.e. if all the atoms are regularly arranged in space, deformation occurs along the shear plane when shear stress is applied.

The deformation mechanism causes the breakage of the existing bonds between the atoms and the sliding of all the atoms along the shear plane[10] (Figure 2.9). It's important to note that all atoms slide forward one lattice step simultaneasly.

The shear stress τ required to deform the lattice can be theoretically calculated based on the bonding energies between the atoms. This results in:

$$\tau \cong \frac{G}{2\pi}$$

where G is the shear modulus of the material[11]. Since, in the case of steel, G is approximately 80-82GPa, the theoretical stress is in the order of 13GPa.

Let us now consider the deformation of the actual lattices.

If the crystal has an edge dislocation the deformation mechanism is different.

---

[9] We are speaking of shear stress or tensile stress that acts on the crystal lattice, not of stress on the whole metallic mass. The case of a macroscopic tensile stress on a metallic bar as occurs is very different, for example, during a mechanical tensile test. In this case, by effect of the tensile stress σ, a macroscopic shear stress τ is generated. The shear stress τ is maximum on directions at 45° with respect to the tensile direction. This stress condition gives rise to typical phenomena of macroscopic deformation of the specimen (elongation and necking).

[10] The notion of breaking the bonds between the atoms does not have to suggest that the bond is a sort of mechanical connection. It is rather an electromagnetic interaction: if the atoms approach each other, repulsing forces intervene, which tend to bring them back to their position of equilibrium. If they move away from each other, attracting forces are created that lead them back to their original position. The analogy with a mechanical spring is evident, even though there is no real physical connection between the atoms.

[11] The shear modulus G is related to the elastic modulus E through the Poisson's ratio υ according to the relation: $G = E/2(1+\upsilon)$. Remember that for steel, υ it is 0.27-0.3.

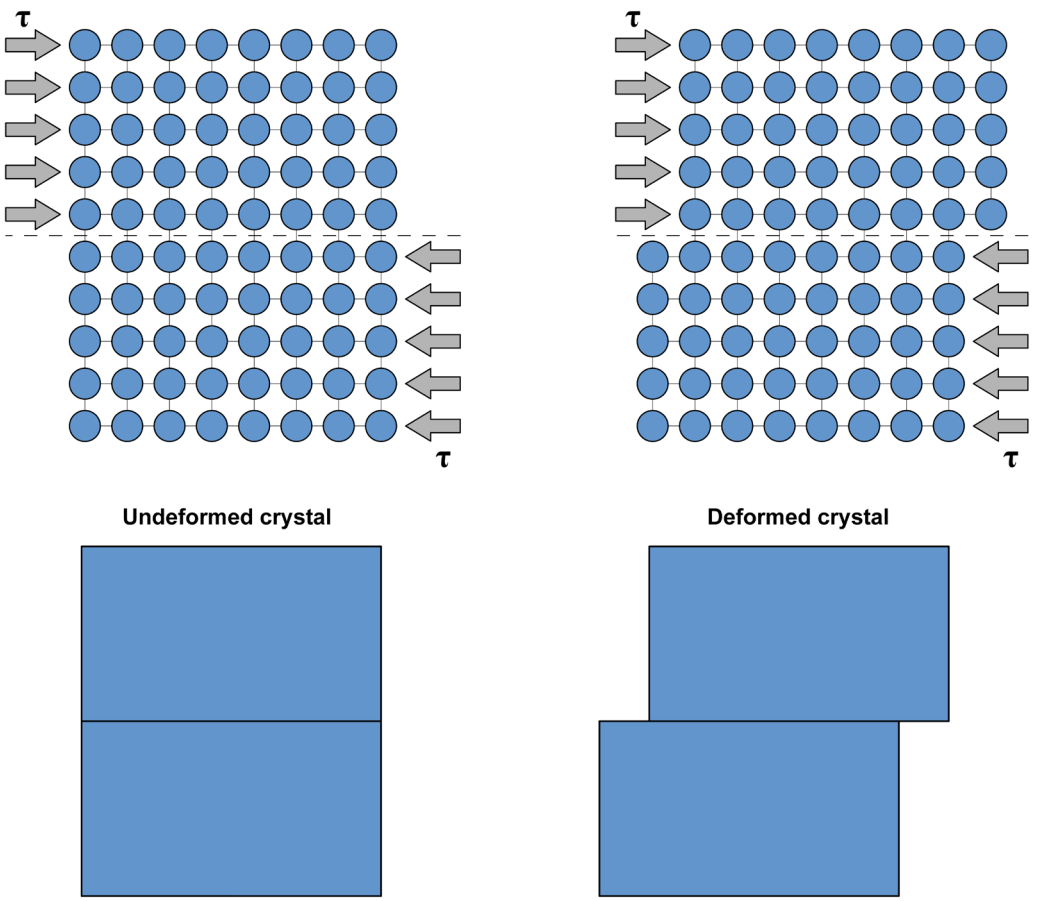

Figure 2.9 - Plastic deformation of an ideal crystal lattice. The dotted line represents the shear plane.

As a result of the applied stress τ, sliding still occurs along the shear plane but the dislocation significantly reduces the stress required to cause the crystal deformation. In fact, 5-10MPa are enough to start dislocations that require less energy input and not ~13GPa, as previously evaluated according to theoretical models[12]. Figure 2.10 shows in detail what effect dislocations have on deformation.

[12] *The term "defect" - in this case, line defect - should be taken as a positive meaning: without dislocations, the deformation would be very difficult.*

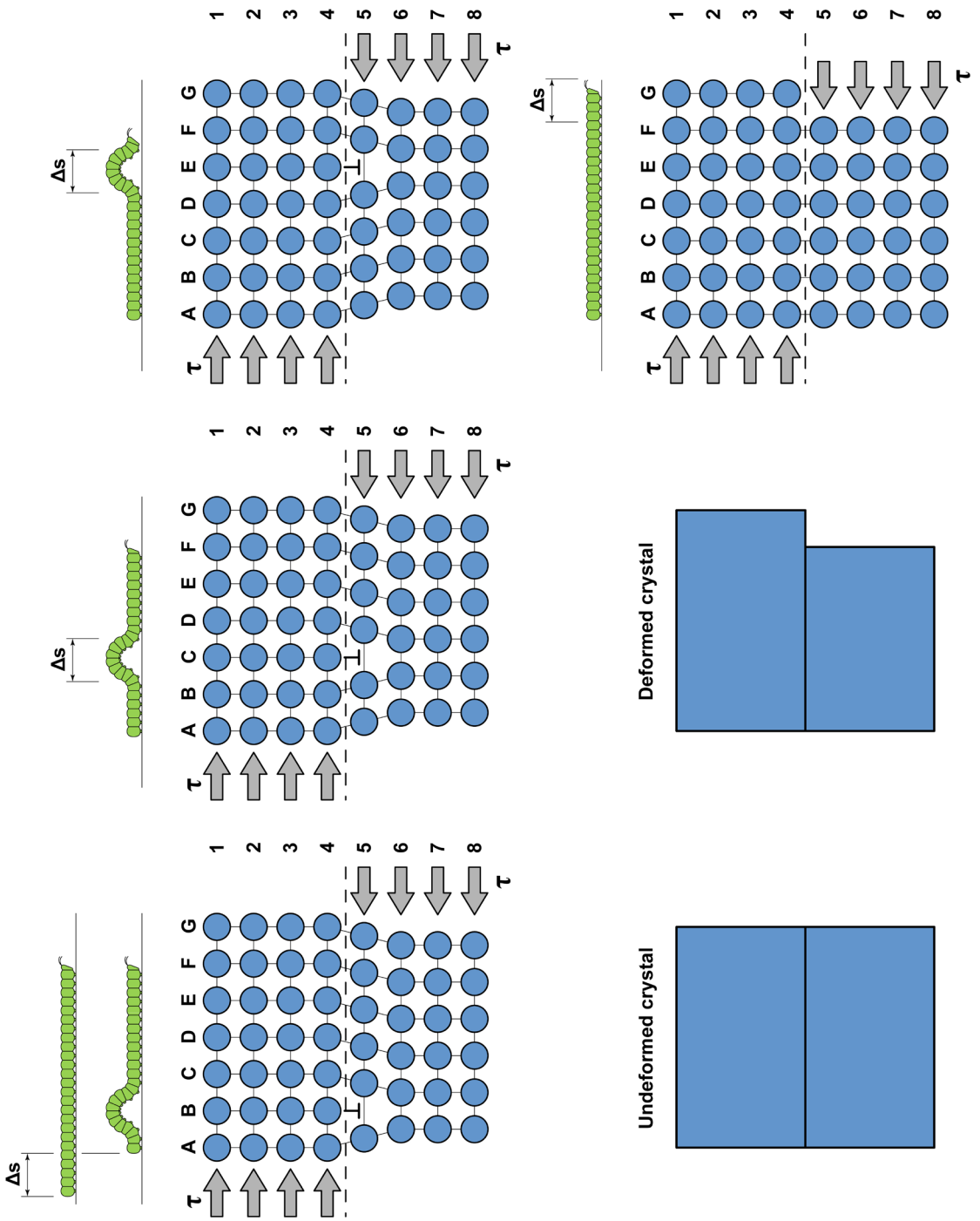

Figure 2.10 - Plastic deformation of a crystal lattice with an edge dislocation. The dotted line represents the shear plane.

When the stress τ is applied to the lattice, atom *C4* progressively moves away from atom *C5*. Consequently, the link between the two atoms (*C4* and *C5*) becomes more labile. At the same time, however, atom *B4*, at the end of the missing semi-plane of the dislocation, increasingly approaches atom *C5*. Therefore, it is progressively affected by the electromagnetic interaction developed by the atom *C5*.

When a certain energy threshold is exceeded (i.e. if the shear action τ is adequate), atom *C4* frees itself from the bond it originally had with *C5*, and a new bond is created between *B4* and *C5*. As a result, atom *C4* becomes the end atom of the missing semi-plane and the dislocation has moved forward one lattice step.

The dislocation motion, one step at a time, causes the deformation of the lattice and, in the end, the defect emerges at the opposite end.

The movement described, one step at a time, is a bit like the motion of a caterpillar that has to cross a generic space Δs. The caterpillar does not move forward Δs because all its feet instantly increase by an amount equal to Δs. In contrast, the caterpillar moves itself because its legs, one after the other, move forward Δs : the sum of the individual advancement of the feet in succession, ultimately produces the overall movement Δs of the caterpillar.

The comparison of the two deformation mechanisms (perfect crystal and crystal with defects), clearly shows that the mechanical stress required to deform the lattice is much less when dislocations are present. For this reason, all metallic materials - some more, others less - are plastically deformable.

Dislocations also explains why, in metals and in alloys, the values of the shear stress required to deform the lattices is lower than an order of magnitude than the theoretically calculated values for ideal crystals. Real crystals have a very high density of dislocations. This means that they contain a large number of line defects, which can be moved if correctly stressed: this promote deformability.

Mechanical resistance, as deformability, is also a direct consequence of the dislocation motion. While it is true that the lattice deformability is correlated to dislocation motions, it is equally true that also mechanical strength - the opposite of deformability - is due to a limited dislocation motions.

In summary: the more the dislocations move, the more the lattice is deformed. The more the dislocation motion is limited, the less the lattice is deformed and the higher the mechanical strength of the metallic mass becomes.

2.6 Surface defects

Iron, steel, and all metal alloys have a polycrystalline structure with many crystalline grains, which is the result of the solidification process. This means that any pure metal or metal alloy, if observed at a microscopic level, always shows an aggregate of irregular polygonal grains. Figure 2.11 shows the case of pure iron.

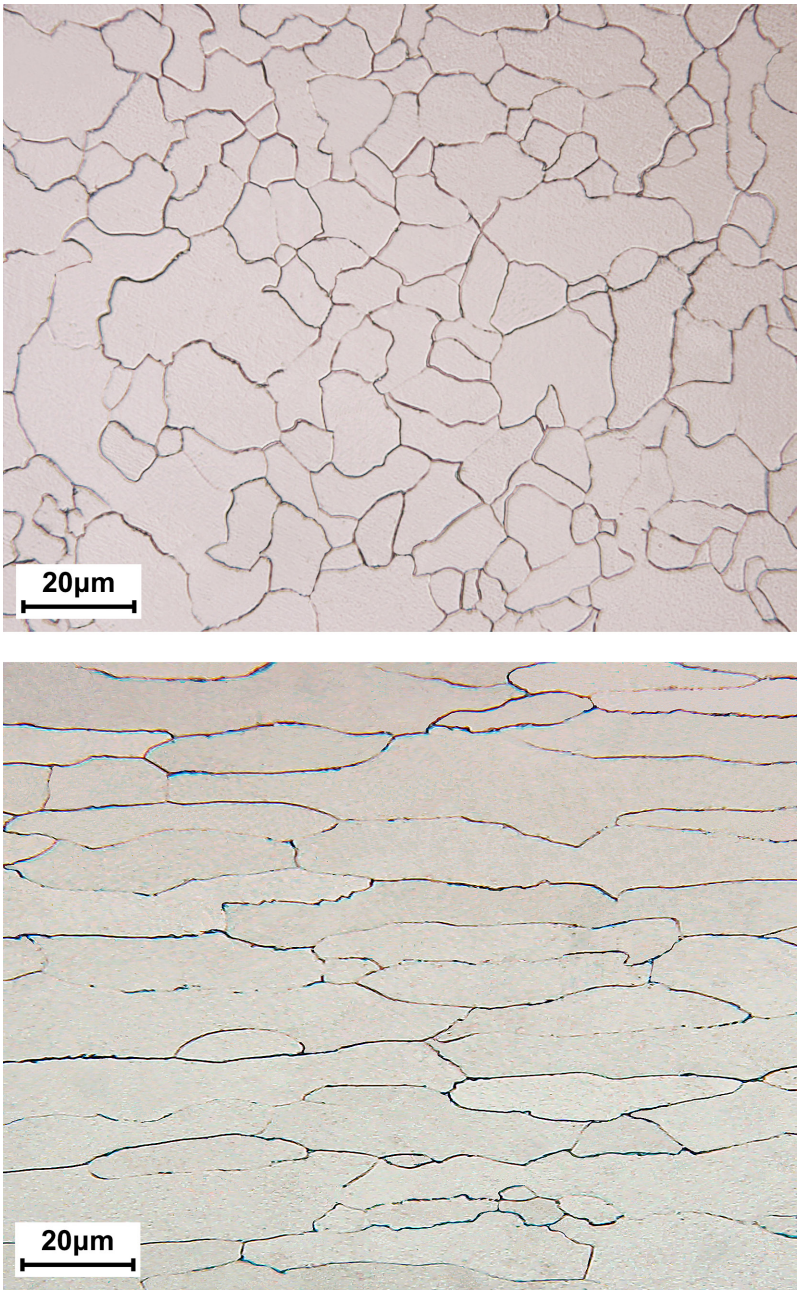

Figure 2.11 - Polycrystalline structure of pure ARMCO iron[13]: in the annealed state (above), and after cold work (below). Appearance under the metallographic microscope - Nital 2% etch. [Laboratories of the Department of Mechanical Engineering, Politecnico di Milano - Milano].

[13] Pure industrial iron with Fe > 99.8%, developed for the first time in 1909 by ARMCO (American Rolling Mill Company). The term, "Iron ARMCO", is now synonymous with pure industrial iron.

Each grain has a homogeneous crystal lattice made up of atoms that are uniformly oriented[14]. The crystalline lattice of each grain, however, has an orientation that is statistically different from the other grains. The problem arises along the border area, where a transition between a lattice and the adjacent one is created, both regular but with different orientations.

Atoms located along the border area can not keep the smooth arrangement of the two contiguous crystalline lattices and are forced to assume an irregular position. Therefore, there is a local distortion of the lattice, i.e. a defect, called "grain boundary" (Figure 2.12).

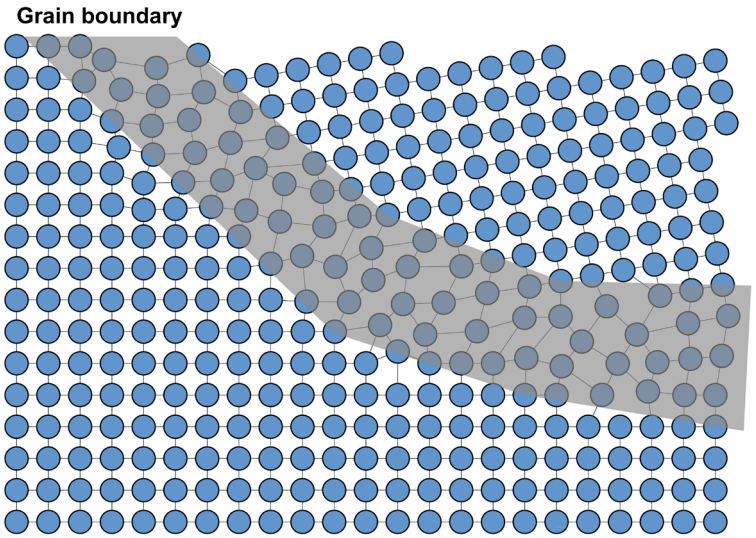

Figure 2.12 - Schematic representation of the boundary between two grains (grain boundary).

The grain boundaries have a typical extension of about 2-4 atomic diameters and they are surface defects (two-dimensional defects). Like dislocations, grain boundaries are also defects that are not in thermodynamic equilibrium.

Grain boundaries are areas characterized by a lower atomic density, and atoms located near grain boundaries have higher free energies than atoms located within the crystallite. Consequently, the grain boundary areas have a higher resistence to plastic deformation as compared to the core of the grains[15].

[14] *In many material science books, the uniformity of the crystalline lattice within grains is also defined as short-range regularity.*

[15] *An exception is the case of the grain boundary segregation of chemical elements that are harmful to steel (sulfur, phosphorous, hydrogen, etc.). In these cases, the grain boundary is subjected to embrittlement phenomena and intergranular type of fractures can occur.*

Moreover, the grain boundaries are much more reactive than the inner portion of the crystal lattice. Diffusion phenomena[16] (oxidation, carburizing, nitriding), precipitation of compounds, and segregation of impurities occur more easily along the grain boundaries.

2.7 Solidification

We will now analyze the metallurgic phenomena that occurs during solidification. The solidification of a pure metal (iron) or a metal alloy (steel) develops through two physical mechanism called nucleation and growth. At first, the atoms of liquid metal join together to give rise to solid nucleus called nuclei, which subsequently increase their dimension through the aggregation of the atoms in the liquid phase. The process continues as long as the liquid has not completely used up. Only at this point the grains meet together, creating the grain boundaries (Figure 2.13).

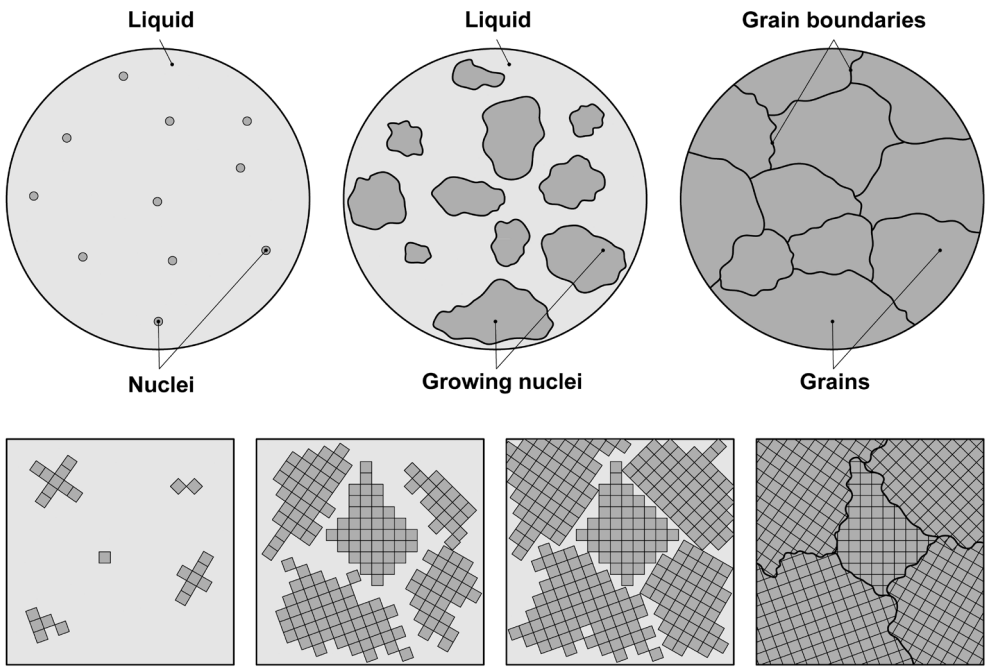

Figure 2.13 - Schematic representation of the solidification process of a generic metallic mass.

[16] *For a broader discussion on diffusion phenomena, see Chapter 3.*

Initially the system is in a liquid state and atoms are free to move randomly. As a matter of fact, if the temperature is higher than melting point, the kinetic energy of the atoms is enough to prevent the formation of stable bonds.

During the cooling phase, the movement of the atoms progressively decrease. Therefore, the probability that some atoms have a lattice configuration equal to that of solid metal increases even more. When the temperature falls below the melting point, this probability becomes very high and many solid nuclei form in the liquid metal. This nucleation mechanism is called homogeneous nucleation and is very rare in industrial practice. In almost all cases, solidification is characterized by the heterogeneous nucleation mechanism. In this second case the nucleations starts from the inner surface of the ingot mould and/or the solid impurities which act as trigger points for solidification[17].

For iron, and all pure metals, solidification never occurs exactly at the melting point. Before starting to solidify the liquid must cool below its solidification temperature: this phenomenon is called "undercooling". Undercooling decreases the mobility of atoms and promotes the solidification process. If undercooling is limited, also the number of nuclei is limited and the liquid solidifies forming few coarse grains. However, if undercooling increases, the number of nuclei also increase and the liquid solidifies forming many small grains (Figure 2.14).

Similar considerations are also true for steel and for all alloys, in general. The main difference is that pure metals have a single liquid/solid transition temperature, instead, metal alloys solidify in a thermal interval (solidification interval)[18].

Undercooling also influences the morphology of the solidified microstructure. If the undercooling is limited, the solidification rate is very slow and the solid nuclei grow along all the directions, with the formation of planar or cellular crystalline grains.

[17] Solid impurities of microscopic size are always present in the liquid metal. Typically, these impurities are oxides and/or nitrides deriving from steel-making process (Al_2O_3, SiO_2, MnO, AlN, TiN,, and so on).

[18] For a closer examination of this topic, see Chapter 5.

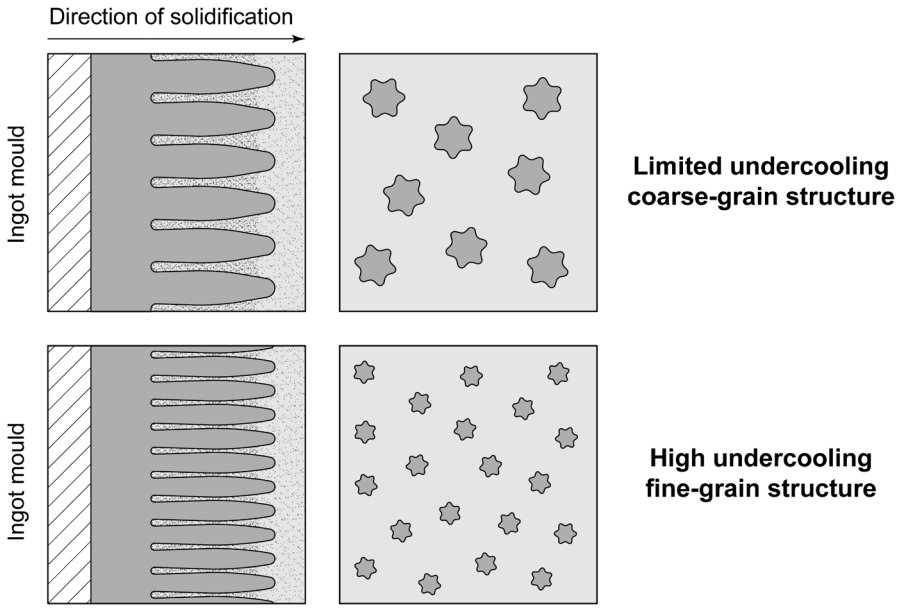

Figure 2.14 - The effect of undercooling on the nucleation mechanism.

On the other hand, if the undercooling is high the grains grow along the heat exchange direction with the formation of multi-branched grains, called dendrites (Figure 2.15).

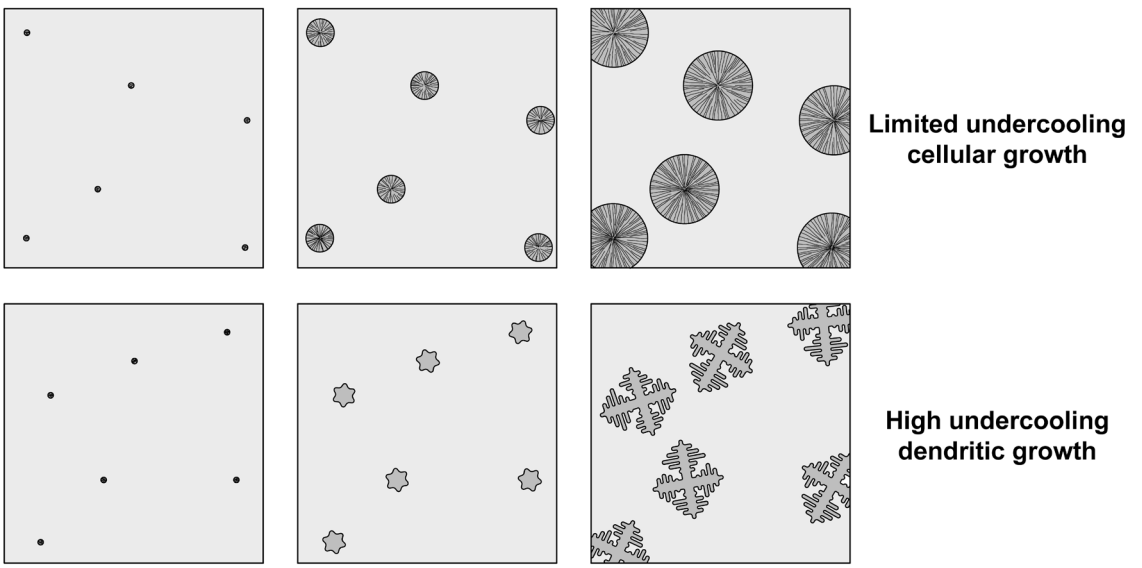

Figure 2.15 - Schematic representation of the cellular solidification process (limited undercooling) and the dendritic solidification process (high undercooling) [from Kurz and Fisher 1992].

The term "dendrite" comes from the Greek, *dendron* (tree) and derives from the tree-like shape formed by the crystalline grains during solidification. The secondary and tertiary branches of dendrites originate from the main grain when the lateral heat gradients become relevant. The dendrite size is measured through the average distance between the secondary branches and is closely related to undercooling phenomenon. Figures 2.16 and 2.17 show some typical examples of dedritic structures.

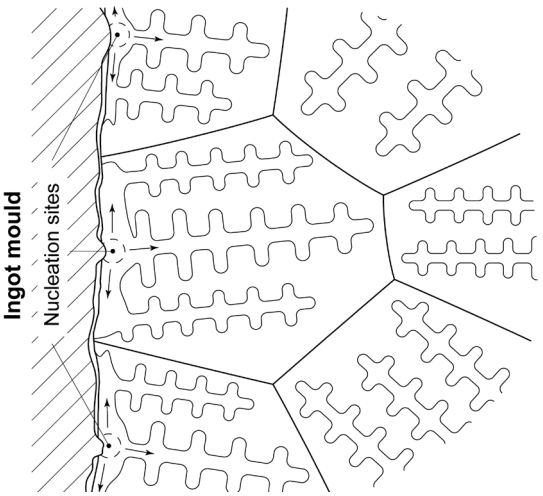

Figure 2.16 - Schematic representation of the dendritic solidification process [from Campbell 2003].

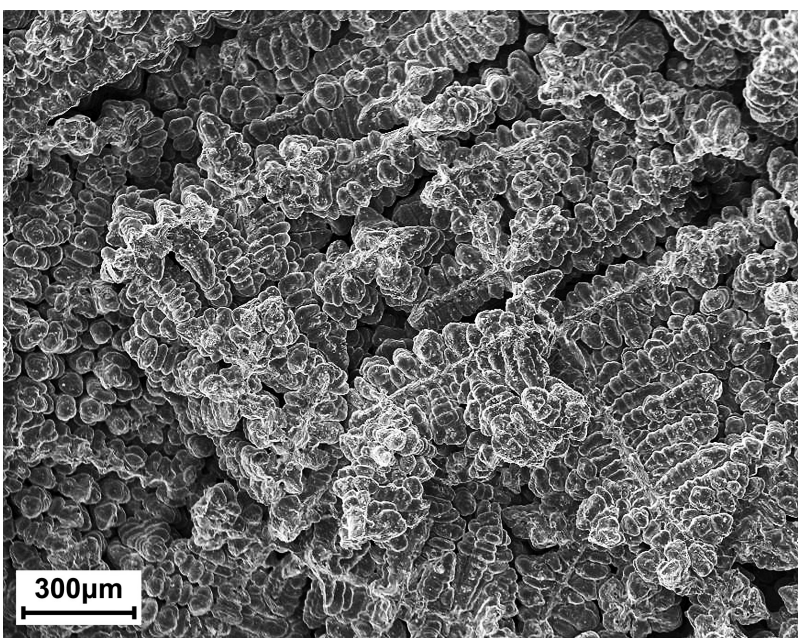

Figure 2.17 - Dendritic solidification structure. Appearance under the scanning electron microscope - without etching [Laboratories of the Department of Mechanical Engineering, Politecnico di Milano - Milano].

2.8 Volume defects

Volume defects are three-dimensional discontinuities of the crystal lattice. This type of defects is not in thermodynamic equilibrium.There are essentially two categories of volume defects:

- micro-voids and macro-voids (shrinkage cavity, porosity, cracks, etc.);
- inclusions.

Micro-voids/Macro-voids

Micro-voids and macro-voids are three-dimensional or volume defects caused by the lack of atoms in the lattice. Macro-voids are visible to the naked eye, on the contrary, micro-voids are visible only under the metallografic microscope. Micro-voids and macro-voids are due to the volumetric contraction of the liquid (shrinkage cavity) and the entrapment of gaseous bubbles (porosity) during the solidification of steel.

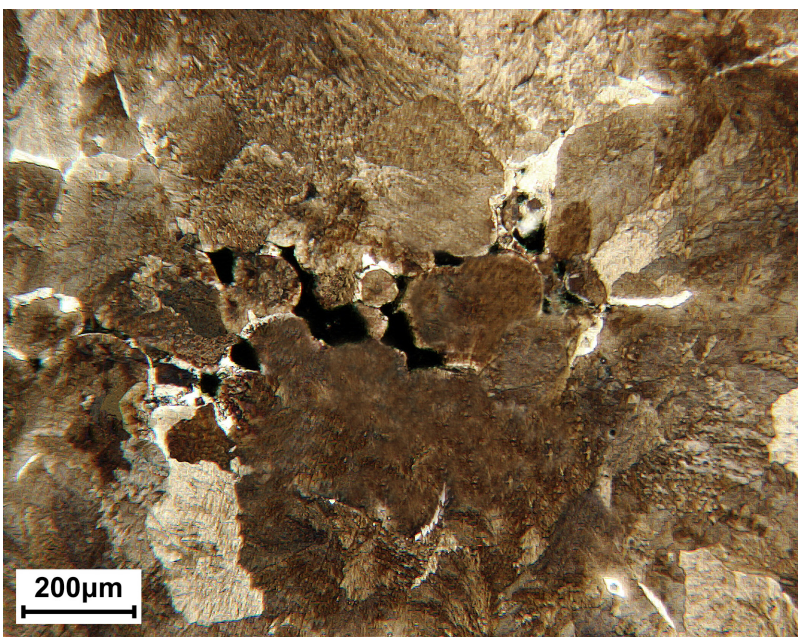

Figure 2.18 - Shrinkage cavities in a continuous casting billet of an EN C45 steel with a pearlitic-ferritic microstructure. Appearance under the metallographic microscope - Nital 2% etch. [Laboratories of the Department of Mechanical Engineering, Politecnico di Milano - Milano].

Cracks are volume defects caused by external stresses (mechanical, thermal, environmental, etc.) or harmful chemical elements (i.e. hydrogen flakes).
Shrinkage cavities, porosity and cracks always have a negative effect, as they reduce mechanical strength, impact strength and fracture toughness of steel[19] (Figures 2.18 and 2.19).

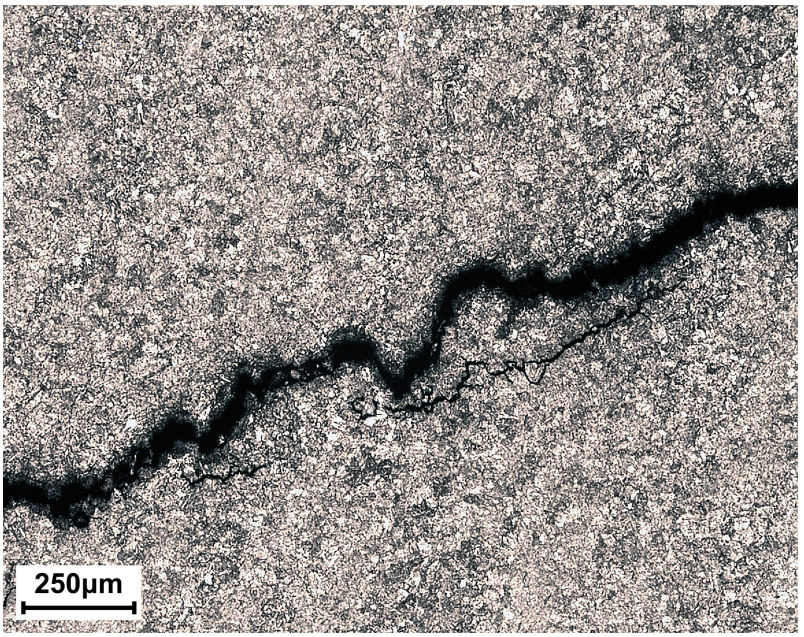

Figure 2.19 - Crack in an EN 34CrMo4 steel, with tempered martensitic microstructure. Appearance under the metallographic microscope - Nital 2% etch. [Hammer S.r.l. Laboratories, Rho - Milano].

Inclusions

Another important type of volume defect are inclusions which are interstitial compounds[20] with a different lattice than the surrounding metal.

[19] Macro-voids and/or micro-voids have a negative effect both in static or quasi-static conditions (tensile strength) and in dynamic conditions (fatigue resistance, impact strength, fracture toughness).

[20] There are many types of steel inclusions: they range from few microns particles up to few dozen millimeters defects.

Inclusions are classified in endogenous (originating within the system) or exogenous (originating from outside). Endogenous inclusions are formed through separation from liquid during the steel-making process, for example during processes of deoxidation, dephosphorylation, desulphurization, and degassing. This is the case of the medium-small sized sulphides, oxides, and nitrides (Figures 2.20 to 2.23).

The term, exogenous inclusions refers to particles that remain trapped in the liquid metal during the solidification phase. This type of inclusions are typically refractory material, deriving from slag or from walls of the ingot mould (Figure 2.24).

In general, inclusions have a negative effect on steel, since they represent preferred zones for cracks nucleation. On the other hand, inclusions can also have positive effects. Just think of iron and/or manganese sulphides (*FeS*, *MnS*, or mixed $Fe_xMn_{1-x}S$), in free-machining steel. These inclusions decrease the impact strength and ductility of steel but greatly increase its machinability.

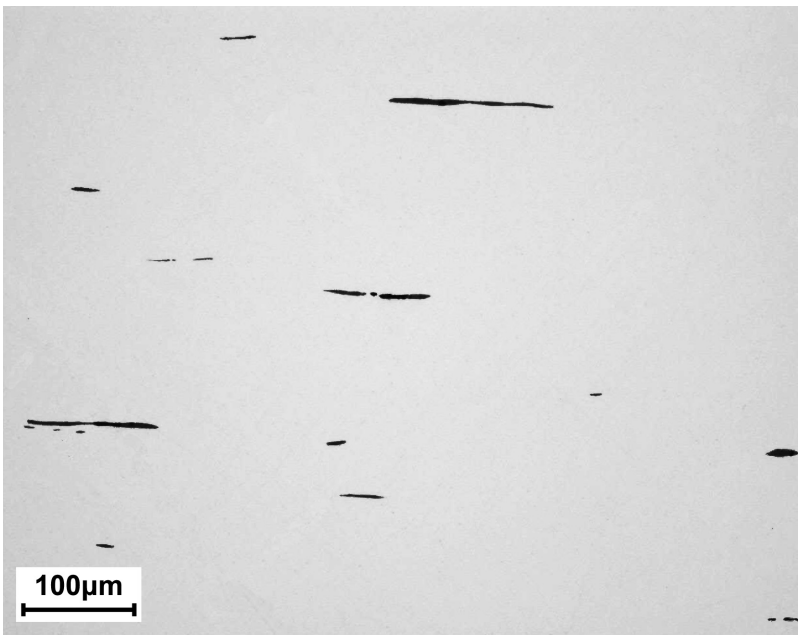

Figure 2.20 - Iron manganese sulphide inclusions in a special steel. Appearance under the metallographic microscope - without etching [Omeco S.r.l. Laboratories, Monza - Monza Brianza].

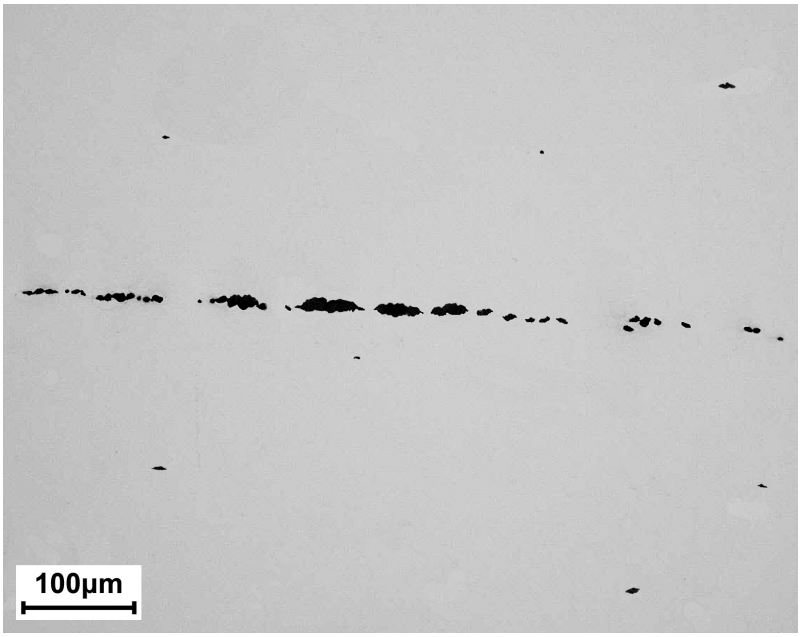

Figure 2.21 - Alumina inclusions in special steel. Appearance under the metallographic microscope - without etching [Omeco S.r.l. Laboratories, Monza - Monza Brianza].

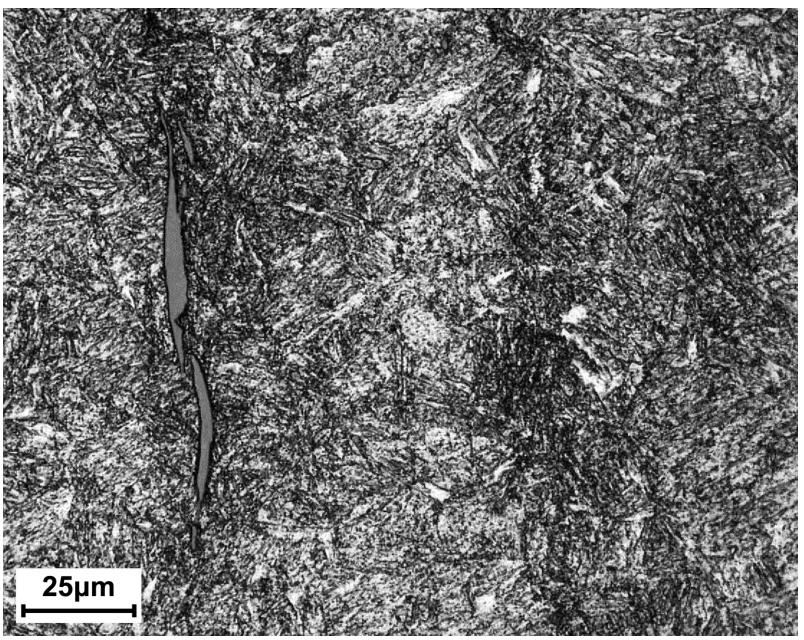

Figure 2.22 - Inclusion of iron/manganese sulphide in an EN 42CrMo4 steel with tempered martensitic structure. Appearance under the metallographic microscope - Nital 2% etch. [Hammer S.r.l. Laboratories, Rho - Milano].

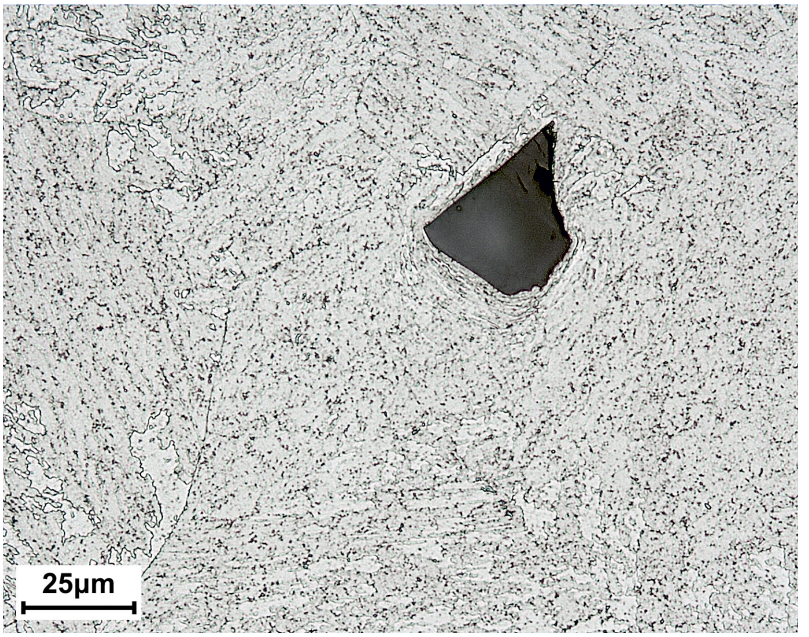

Figure 2.23 - Inclusion of titanium nitride in an ASTM SA336 F22V steel (2.25Cr-1Mo-0.25V) with bainitic structure. Appearance under the metallographic microscope - Nital 2% etch. [Hammer S.r.l. Laboratories, Rho - Milano].

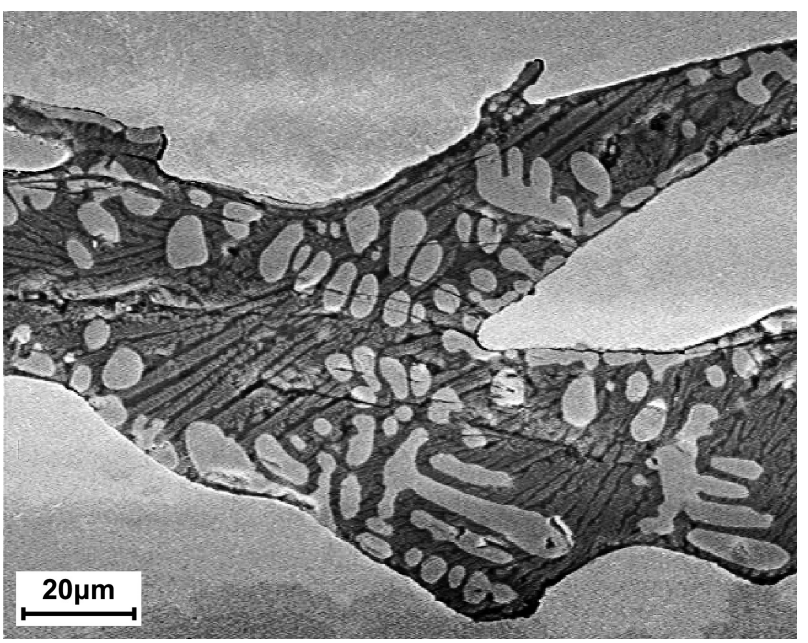

Figure 2.24 - Exogenous inclusion of ferrous scrap (iron, iron oxides, silicon oxides, calcium aluminates) in a 16th century artifact. Appearance under the scanning electron microscope - without etching [Laboratories of the Department of Mechanical Engineering, Politecnico di Milano - Milano].

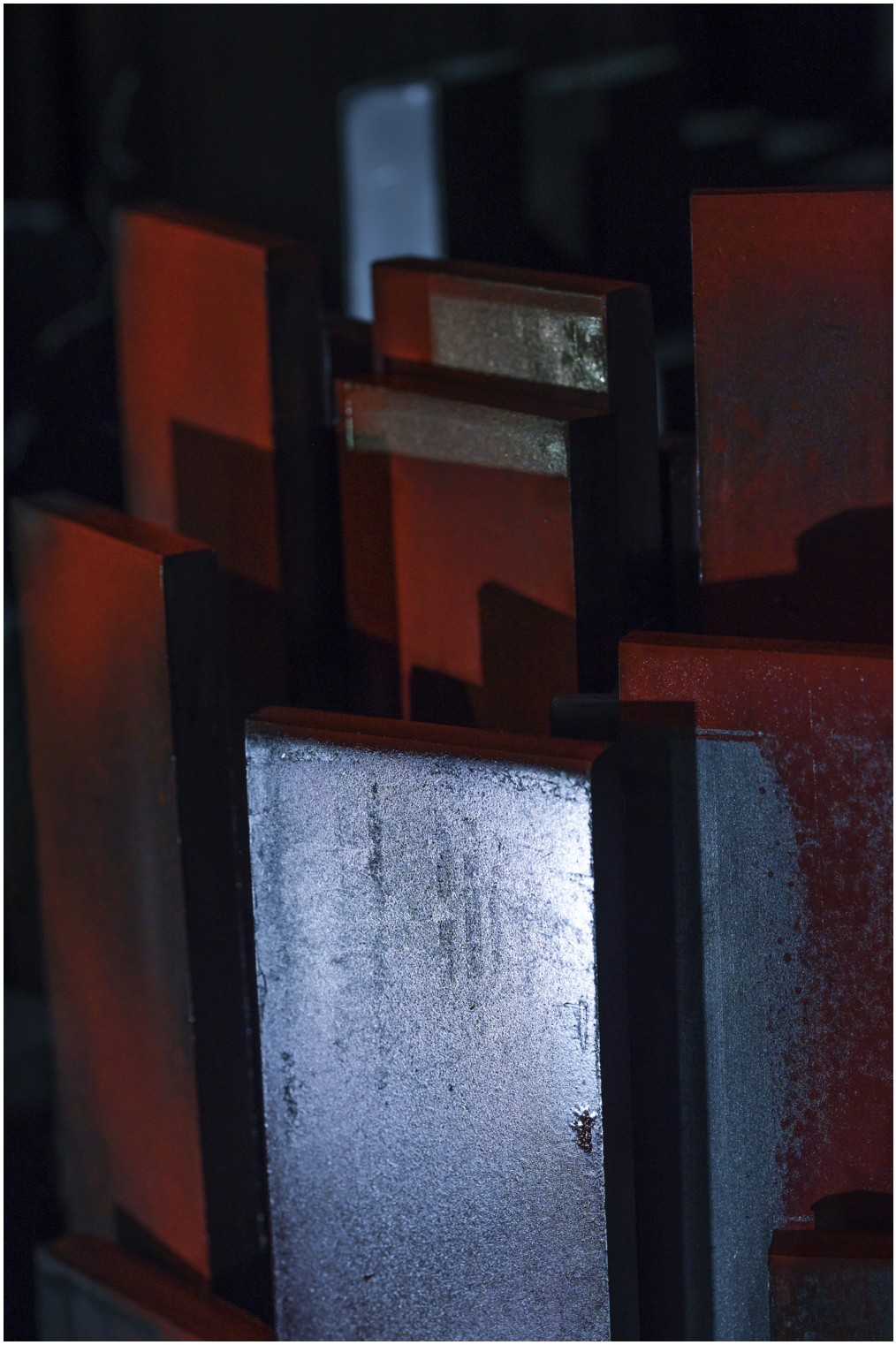

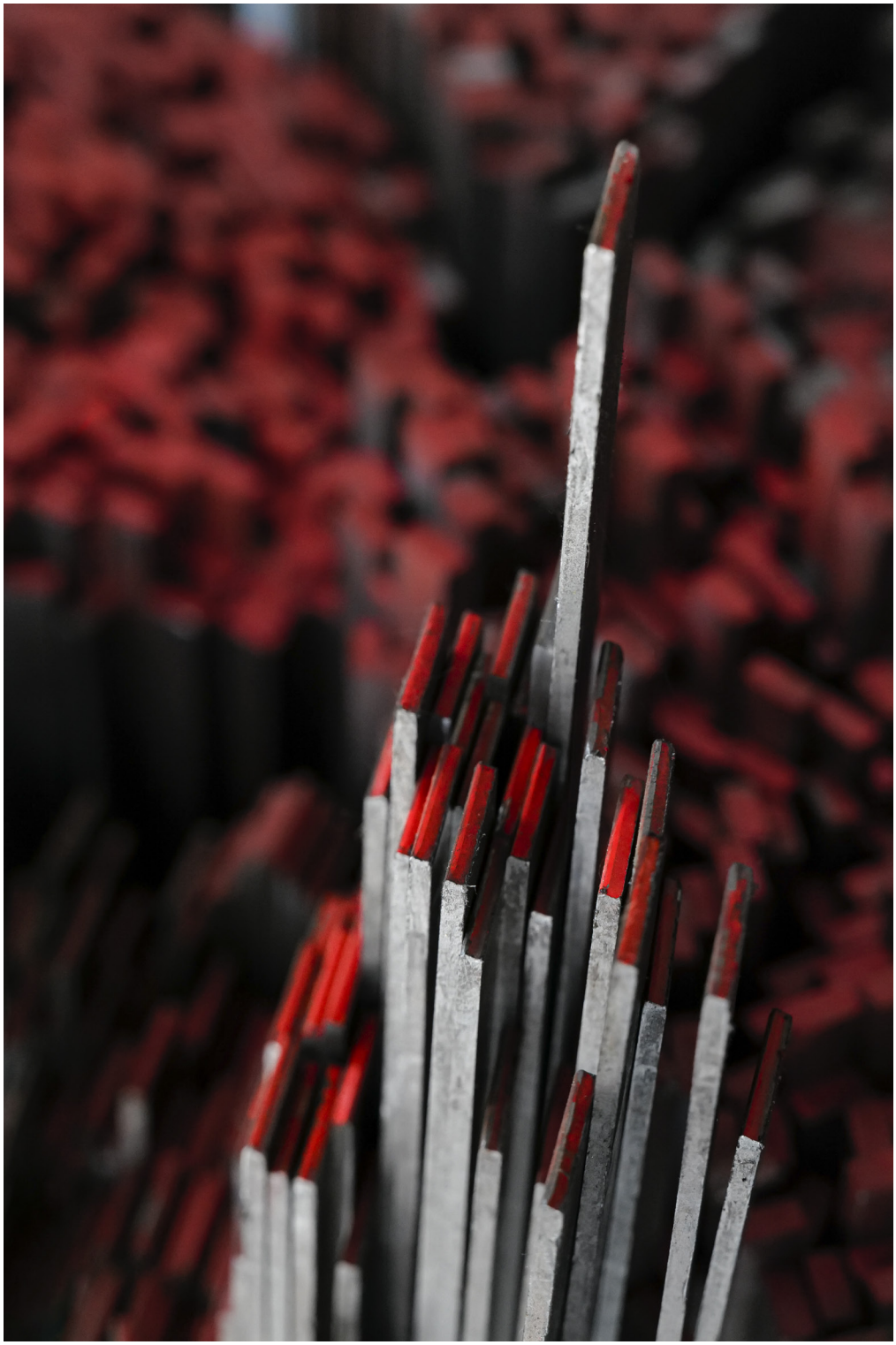

3. DIFFUSION

3.1 What is diffusion?

Diffusion is a mass transport phenomenon, a mechanism that allows the movement of atoms within matter due to their thermal agitation. Diffusion can occur in gases, liquids, and solids and depends on temperature and time. In fact, the increase in temperature causes an increase in the thermal agitation of the atoms and therefore an increase in the diffusion rate.

Diffusion explains many metallurgical phenomena, such as the formation of new phases, structural transformations, nucleation and growth mechanism of crystalline grains, recrystallisation, thermo-chemical treatments, creep, sintering, etc.

The simple example shown in Figure 3.1. Is useful to understand the diffusion phenomenon. It is a typical self-diffusion mechanism via vacancies, as can occur in a homogeneous crystalline solid, when the vacancies of the lattice allow the movement of atoms within the system.

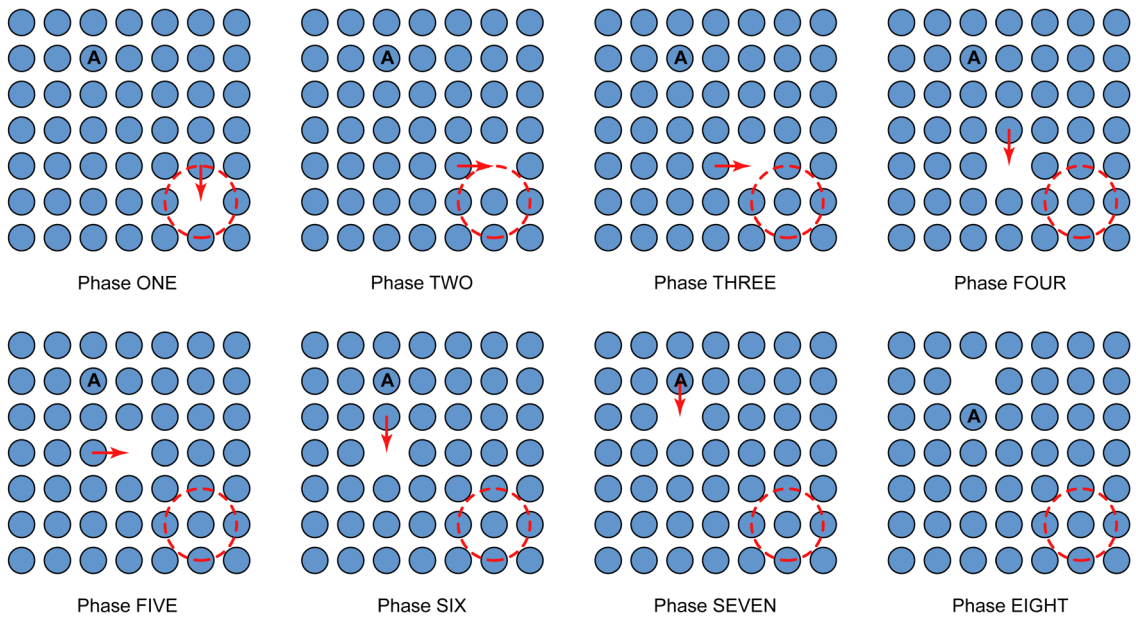

Figure 3.1 - Self-diffusion via vacancies in a homogeneous system. Note the original positions of atom *A* and vacancy (dotted line circle) and their movement due to the diffusion phenomenon.

Diffusion also occurs between atoms of a different types. In this case, we talk about inter-diffusion in heterogeneous systems. If the atom of the diffusing species has dimensions similar to the atoms of the system (such as, iron and nickel), diffusion occurs via vacancies (Figure 3.2). If, on the other hand, the diffusing chemical species has a much smaller atomic size (such as, iron and carbon), diffusion occurs via the interstitial sites in the crystal lattice (Figure 3.3).

In both cases, in addition to temperature and time, the diffusion mechanism is governed by the concentration of the diffusing chemical species within the heterogeneous system.

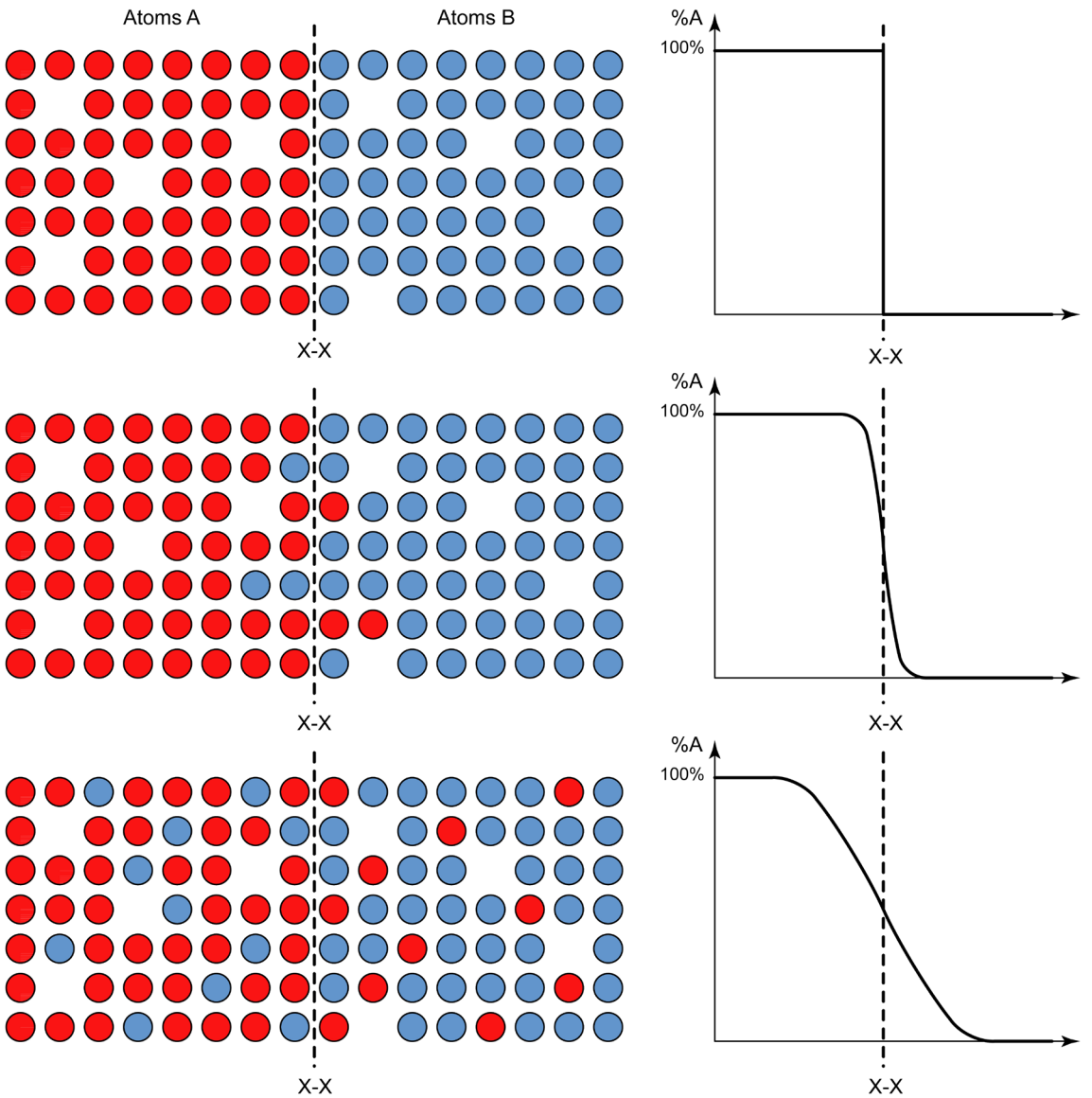

Figure 3.2 - Inter-diffusion via vacancies in a heterogeneous system between two crystalline solids.

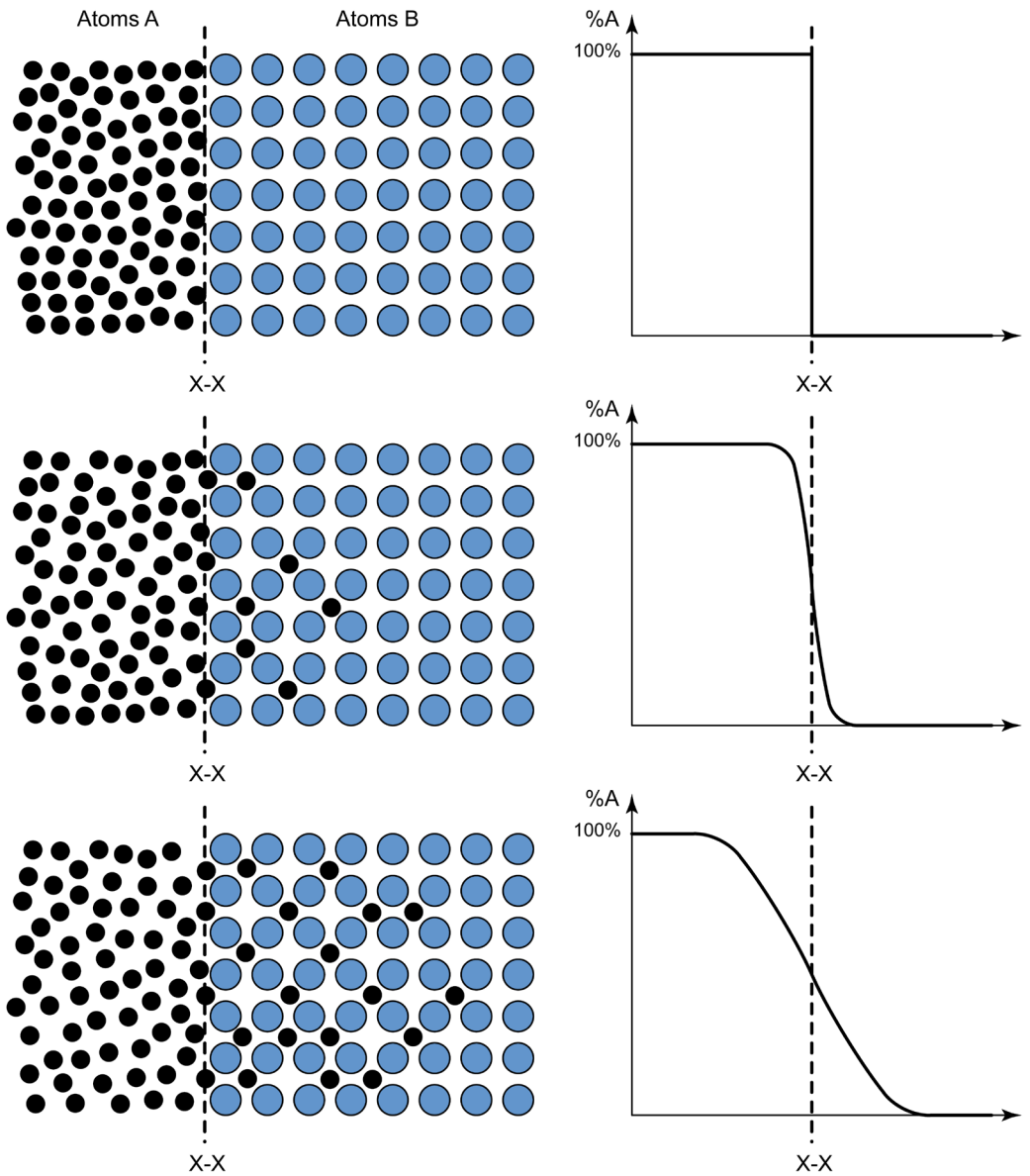

Figure 3.3 - Inter-diffusion via lattice interstitial sites in a heterogeneous system between gas and solid.

3.2 Mathematical model of the phenomenon

Diffusion mechanisms can also be treated quantitatively. In 1855, the physiologist, Adolf Eugen Fick, was the first to propose the two equations that describe the phenomenon.

The equations proposed by Fick are based on the experimental observation that the diffusion of a chemical species depends on its concentration in space, temperature and time.

A first type of problem to be evaluated is the rate of the diffusion process or, in other words, how quickly a given chemical species moves from an area of greater concentration C_1 towards an area of lesser concentration C_2.

The described phenomenon is called diffusion flow and is indicated by the letter J. The unit of measurement is [atoms/m^2·s]. J Represents the amount of atoms that, in steady state, cross a perpendicular surface A with a thickness of x in a unit of time t.

The Fick's first law can predict the diffusion flow J through the relation:

$$J = \frac{\partial C}{\partial t} = -D\frac{\partial C}{\partial x} \cong -D\frac{\Delta C}{\Delta x} = -D\frac{(C_2 - C_1)}{(x_2 - x_1)} \qquad [3.1]$$

where D [m^2/s] is the diffusivity and C [atoms/m^3] is the concentration of the chemical species along direction x. Equation 3.1 shows that the variation in time of C depends on the variation of C along direction x. The minus sign (-) indicates that the direction of the diffusion is opposite to the gradient of concentration, i.e. the atoms tend to move from areas where their concentration is greater (C_1) towards areas where their concentration is lower (C_2). It is useful, observe the schematic representation in Figure 3.4 in this regard.

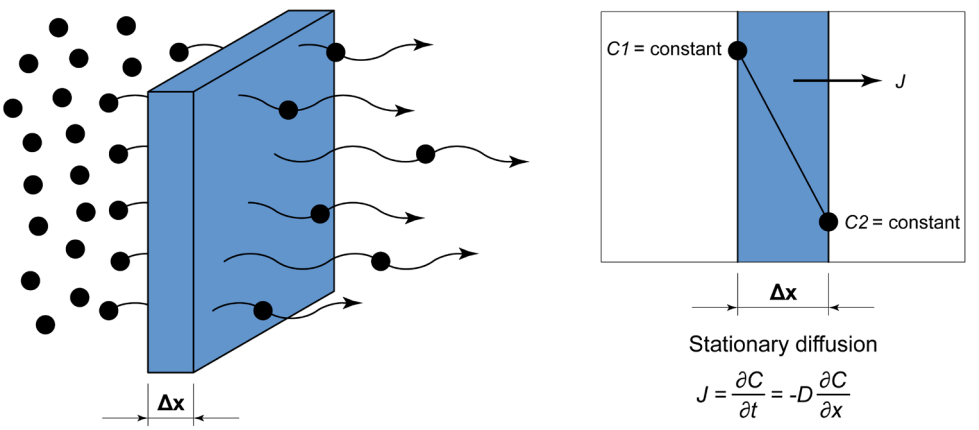

Figure 3.4 - Schematic representation of stationary diffusion (Fick's first law).

The diffusivity D depends on temperature: approximately the value of D doubles for an increase in temperature of 20 degrees (°C or K). The equation to derive D from T is an Arrhenius type equation:

$$D = D_0 e^{\left(-\frac{Q}{RT}\right)} \qquad [3.2]$$

where D_0 [m²/s] is the diffusion coefficient that depends on the diffusing chemical species and the chemical species in which diffusion takes place, Q [J/mole] is the activation energy[1], T [K] is the temperature in Kelvin, and R is the gas constant equal to ~8.3145J/mole·K.
Table 3.1 shows the values of the diffusion coefficient D_0 and the activation energy Q for several chemical species that diffuse into the iron lattice.

Diffusing chemical species	Chemical species in which diffusion occurs	Diffusion coefficient, D_0 [m²/s]	Activation energy, Q [J/mole]
Fe	γ-*Fe*	$5.0 \cdot 10^{-5}$	284,000
Fe	α-*Fe*	$2.8 \cdot 10^{-4}$	251,000
C	γ-*Fe*	$2.3 \cdot 10^{-5}$	148,000
C	α-*Fe*	$6.2 \cdot 10^{-7}$	80,000
N	γ-*Fe*	$3.4 \cdot 10^{-7}$	145,000
N	α-*Fe*	$6.6 \cdot 10^{-7}$	78,000
H	γ-*Fe*	$6.3 \cdot 10^{-7}$	43,000
H	α-*Fe*	$1.2 \cdot 10^{-7}$	15,000
O	α-*Fe*	$2.0 \cdot 10^{-7}$	86,000
Ni	γ-*Fe*	$5.0 \cdot 10^{-5}$	276,000
Mn	γ-*Fe*	$3.5 \cdot 10^{-5}$	282,000
Cr	γ-*Fe*	$5.4 \cdot 10^{-5}$	286,000

Table 3.1 - Diffusion coefficients D_0 and activation energies Q for several chemical species that diffuse into γ-iron and α-iron lattice.

Fick's first law (equation 3.1) is valid only when there are stationary diffusion phenomena, i.e., when the gradient of concentration C remains unaltered over time (J constant).
More useful is the diffusion in a non-stationary mode, i.e. when the gradient of concentration C varies in space x over time.
In this second case, the diffusion equation, called Fick's second law, becomes:

$$J = \frac{\partial C}{\partial t} = -D \frac{\partial^2 C}{\partial x^2} \qquad [3.3]$$

where D, C and x have the same meaning as defined above (Figure 3.5).

[1] *Activation energy Q is the minimum amount of energy needed to trigger a chemical reaction or a specific phenomenon in a system in equilibrium state.*

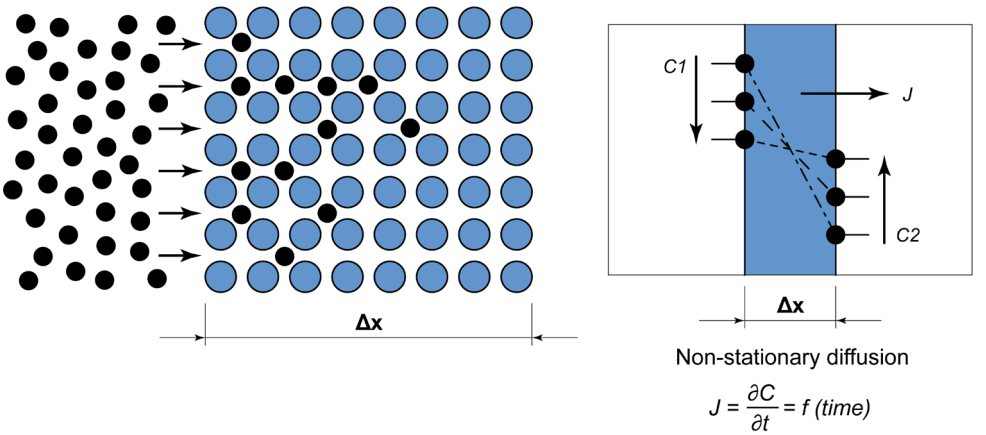

Figure 3.5 - Schematic representation of non-stationary diffusion (Fick's second law).

Equation 3.3 has been solved for some geometries that are of interest to the metallurgical field.
A first example is a semi-infinite solid, where the flow of the diffusing substance never reaches one of the two external surfaces[2]. In this case the equation 3.3 can be solved as proposed by van Ostrand-Dewey:

$$C_x - C_0 = (C_s - C_0)\left[1 - erf\left(\frac{x}{2\sqrt{Dt}}\right)\right] \qquad [3.4]$$

where C_x is the concentration of the diffusing chemical species at distance x from the exchange surface, whilst C_s and C_0 are the initial concentration of the diffusing chemical species at the interface with the semi-infinite solid and in the semi-infinite solid.
Erf (z) is the function of Gauss's error whose values are listed in Table 3.2.

[2] *It is the case of carburizing and nitriding. In these surface heat treatments a gas-phase element (carbon or nitrogen) diffuses near the surface of the steel component.*

z	erf (z)	z	erf (z)	z	erf (z)
0	0	0.55	0.5633	1.3	0.9340
0.025	0.0282	0.60	0.6039	1.4	0.9523
0.05	0.0564	0.65	0.6420	1.5	0.9661
0.10	0.1125	0.70	0.6778	1.6	0.9763
0.15	0.1680	0.75	0.7112	1.7	0.9838
0.20	0.2227	0.80	0.7421	1.8	0.9891
0.25	0.2763	0.85	0.7707	1.9	0.9928
0.30	0.3286	0.90	0.7970	2.0	0.9953
0.35	0.3794	0.95	0.8209	2.2	0.9981
0.40	0.4284	1.0	0.8427	2.4	0.9993
0.45	0.4755	1.1	0.8802	2.6	0.9998
0.50	0.5205	1.2	0.9103	2.8	0.9999

Table 3.2 - Values of the *erf (z)* error function as a function of the argument $z = \frac{x}{2\sqrt{Dt}}$

3.3 Practical applications of diffusion equations

Several practical applications may be helpful to clarify the use of the proposed equations. A reader unfamiliar with metallurgical topics must keep in mind that the following examples refer to topics that will be clarified in the following chapters.

Case 1

Suppose you want to carburise a steel component with 0.18% carbon, using a furnace at 920°C in contact with a carburazing atmosphere with 0.9% carbon.

You want to know how long the workpiece will have to stay in the furnace to achieve a carbon content of 0.4% at a distance of 0.5mm from the surface[3] (figure 3.6).

The data to be included in equation 3.4 are:

$$C_x = 0.4\% \qquad C_s = 0.9\% \qquad C_0 = 0.18\%$$

from which we obtain:

$$0.4\% - 0.18\% = (0.9\% - 0.18\%)\left[1 - erf\left(\frac{x}{2\sqrt{Dt}}\right)\right]$$

$$erf\left(\frac{x}{2\sqrt{Dt}}\right) \cong 0.6944$$

[3] *0.4% carbon guarantees a martensitic structure, with a hardness of approximately 550HV, after hardening i.e. the hardness used to measure the effective case depth.*

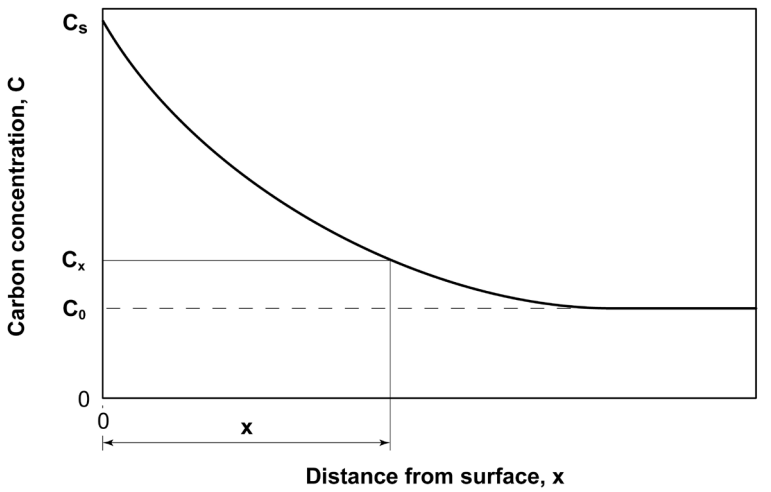

Figure 3.6 - The effect of carburizing on carbon concentration [from Thelning 1975].

The value of the argument $\frac{x}{2\sqrt{Dt}}$ when the error function is 0.6944 can be derived from Table 3.2:

$$\frac{x}{2\sqrt{Dt}} \cong 0.725$$

The diffusivity D of carbon in the γ-iron lattice at 920°C (1193 K) can be calculated with equation 3.2, using the appropriate values of D_0 and Q shown in Table 3.1.
This results is:

$$D = 2.3 \cdot 10^{-5} e^{\left(-\frac{148{,}000}{8.3145 \cdot 1193}\right)} \cong 7.617 \cdot 10^{-12}\ \ m^2/s$$

Since the carbon content at 0.5mm ($0.5 \cdot 10^{-3}$ m) must be equal to 0.4%, we obtain:

$$\frac{x}{2\sqrt{Dt}} \cong 0.725 \qquad x = 1.45\sqrt{Dt}$$

$$0.5 \cdot 10^{-3} = 1.45\sqrt{7.617 \cdot 10^{-12} \cdot t}$$

$$t \cong 15{,}600s \cong 4h\ and\ 20min$$

Therefore, the steel reaches 0.4% carbon at a distance of 0.5mm from the surface after aproximately 4 hours and 20 minutes in contact with the carburizing atmosphere.

Case 2

Another application of equation 3.4 refers to the problems of steel decarburization. It is, in fact, well known that during normal heat treatments, the surface of semi-finished steel product may be depleted of carbon through a reaction with the oxygen in the atmosphere (oxidation). This phenomenon must be limited, since it may result in surface hardness levels below the technical standards.

Consider a round steel bar, of carbon steel, with $C = 0.4\%$. The heating process is performed in a furnace, operating in air, and holding is performed at 920°C for 2 hours. In the surface of the semi-finished piece, the carbon content is zero, due to decarburization.

You want to know at what distance x from the decarburated external surface the carbon content is at least equal to 0.36%, that is 10% less than the nominal value (Figure 3.7).

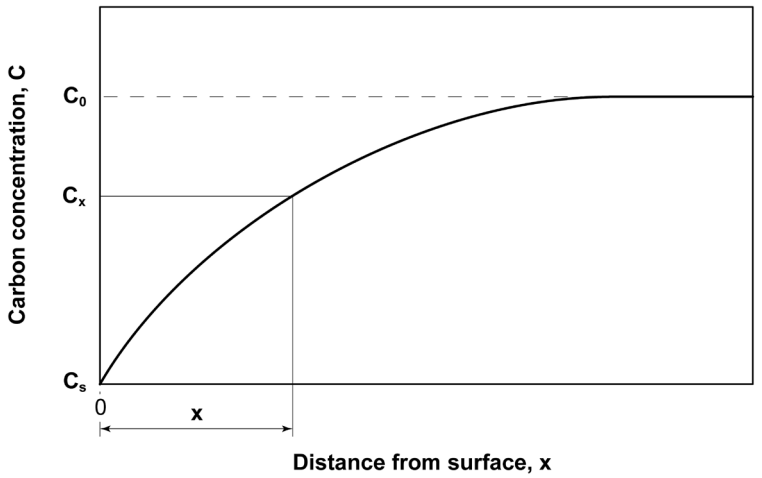

Figure 3.7 - The effect of decarburization on carbon concentration [from Thelning 1975].

To solve this problem, you can always use equation 3.4, but note that:

$$C_s = 0\%$$

therefore, equation 3.4 becomes:

$$C_x = C_0 erf\left(\frac{x}{2\sqrt{Dt}}\right)$$

Since t = 7200 seconds (2 hours), C_x = 0.36%, and C_0 = 0.4% , with a diffusivity value of $D = 7.617 \cdot 10^{-12}$ [m^2 / s] (identical to the previous example), the result is:

$$0.36 = 0.4 \cdot erf\left(\frac{x}{2\sqrt{7.617 \cdot 10^{-12} \cdot 7{,}200}}\right)$$

$$0.9 = erf\left(\frac{x}{2\sqrt{5.484 \cdot 10^{-8}}}\right)$$

$$1.165 = \frac{x}{2\sqrt{5.484 \cdot 10^{-8}}}$$

$$x \cong 0.00055m = 0.55mm$$

This means that, before using the bar, you have to remove about 0.6-0.7mm of material on the radius (1.2-1.4mm on the diameter) using a metalworking lathe, in order to ensure that the entire decarburised layer is removed. Or else, in the future, it will be more appropriate to perform the treatment in a non-oxidizing atmosphere (i.e. nitrogen atmosphere).

Case 3

The last interesting application related to Fick's laws refers to the problem of segregation in semi-finished steel products. As is well known, any semi-finished product is affected by a variability in its chemical composition along the section. The phenomenon is strictly dependent on the chemical composition of steel, the methods of solidification for the metallic mass (ingot or continuous casting billet), and the subsequent phases of hot working. In some cases, it is possible to reduce the effects of segregation through appropriate homogenization heat treatments at high temperatures.

Consider steel with a nominal chemical composition of 0.4% carbon and 0.8% manganese. As a result of segregation, the chemical composition is not constant but shows a fluctuation along the section with a regular spacing between segregation bands, l , equal to 100μm ($0.1 \cdot 10^{-3}$ m): carbon fluctuates between 0.36% and 0.44% and manganese fluctuates between 0.72% and 0.88%, with a change in nominal value of ± 10% for both elements.

You want to know the duration of the homogenization treatment at 1,200°C to reduce the differences in chemical composition within the ± 2.5% interval of the nominal value of each element. In the case of carbon, the desired final variation is between 0.39% and 0.41%, and for manganese between 0.78% and 0.82%.

The diffusive phenomenon can be schematized as in Figure 3.8 in the hypothesis that the fluctuation of the chemical composition is sinusoidal.

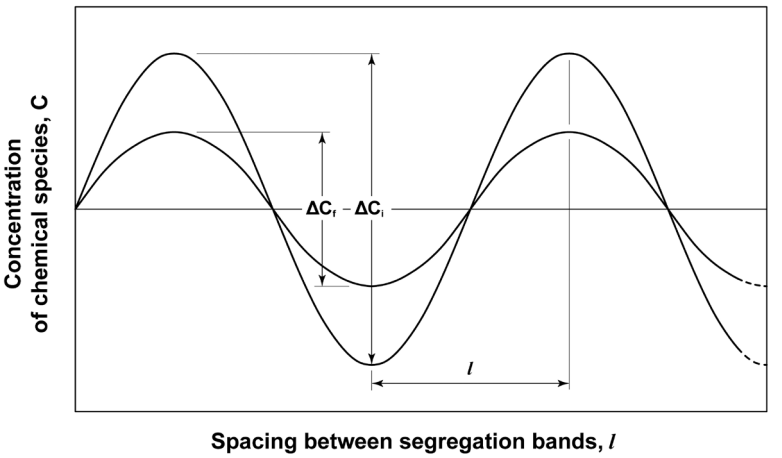

Figure 3.8 - The effect of homogenization heat treatment on concentration of a chemical species [from Hosford 2005].

The equation to use in this case is: $\Delta C_f = \Delta C_i e^{\left(-\frac{D \cdot t \cdot \pi^2}{l^2}\right)}$

where ΔC_i and ΔC_f represent the oscillation of the chemical composition before and after the homogenization treatment, D is the diffusivity of the element taken into consideration, t is time, and l is the spacing between two segregation bands.

First of all, the carbon and manganese diffusivity at 1,200°C (1473 K) should be calculated:

$$D_C = 2.3 \cdot 10^{-5} e^{\left(-\frac{148{,}000}{8.3145 \cdot 1473}\right)} \cong 1.299 \cdot 10^{-10} \ \ m^2/s$$

$$D_{Mn} = 3.5 \cdot 10^{-5} e^{\left(-\frac{282{,}000}{8.3145 \cdot 1473}\right)} \cong 3.501 \cdot 10^{-15} \ \ m^2/s$$

This simple calculation highlights that the diffusivity of carbon (interstitial element) is much higher than that of manganese (substitute element), and consequently, it is much easier to equalize the chemical composition of the first element than the second.

In order to make the chemical composition fall within ± 2.5% of their nominal value, the holding time for carbon is equal to:

$$0.02 = 0.08 e^{\left(-\frac{1.299 \cdot 10^{-10} \cdot t \cdot \pi^2}{0.0001^2}\right)}$$

$$t_C \cong 10.8 s$$

while for manganese, the holding time is equal to:

$$0.04 = 0.16 e^{\left(-\frac{3.501 \cdot 10^{-15} \cdot t \cdot \pi^2}{0.0001^2}\right)}$$

$$t_{Mn} \cong 401{,}200 s \cong 111 h \ and \ 30 min$$

Now, let us see what happens, if the spacing between the segregation bands was more limited, for example 20μm ($0.02 \cdot 10^{-3}$ m). In this case, the holding time for manganese is equal to:

$$0.04 = 0.16 e^{\left(-\frac{3.501 \cdot 10^{-15} \cdot t \cdot \pi^2}{0.00002^2}\right)}$$

$$t_{Mn} \cong 16{,}048 s \cong 4 h \ and \ 30 min$$

This example clearly shows how the effect of hot working is very important, in order to refine the segregation band structure and to homogenize the chemical composition during subsequent heat treatments.

The thinner the segregation bands the easier it is to eliminate the segregation in the semi-finished product (forged, molded, laminated). In fact, reducing the spacing between the segregation bands by a fifth (100μm as compared to 20μm), the homogenization time is reduced by about 25 times.

4. STRENGTHENING MECHANISMS OF STEEL

4.1 Classification of steel strengthening mechanisms

The considerations presented in Chapter 2 on crystal lattice defects are of fundamental importance for understanding the mechanisms that increase or decrease the mechanical strength of an iron alloy.

As we have seen, the deformation of a metallic mass essentially depends on the mobility of the dislocations in the crystal lattice. Facilitating the dislocation motion means facilitating the deformability of steel. On the contrary, preventing the dislocation motion causes an increase in mechanical strength and hardness.

There are four methods to improve the mechanical strength of steel:

- add alloying elements (strengthening by alloying);
- Cold deformation of the metallic mass (strengthening by strain hardening);
- form precipitates inside the crystal lattice (strengthening by precipitation);
- reduce the mean grain size (strengthening by refining).

All these mechanisms increase the hardness, yield strength, and ultimate tensile strength of the steel creating obstacles to the dislocation motion.

4.2 Strengthening by solid solution

The strengthening mechanism by alloying is based on the existence of point defects in the lattice, in particular, the substitutional atoms and the interstitial atoms.

Foreign atoms always generate a perturbation in the crystal lattice creating a local stress field. This phenomenon creates an obstacle to the dislocation motion as shown in Figure 4.1.

The actual increase in strength of the metallic mass depends on both the amount of the alloying element in solution and its atomic size, that is, on the greater or lesser disruption action that a foreign atom creates in the iron lattice[1] (Figure 4.2).

[1] *The abnormality due to the presence of foreign (substitutional or interstitial) atoms in the lattice is of electromagnetic nature. It depends to the electronic configuration that is different for each chemical element and not to the size of foreign atoms with respect to iron atoms.*

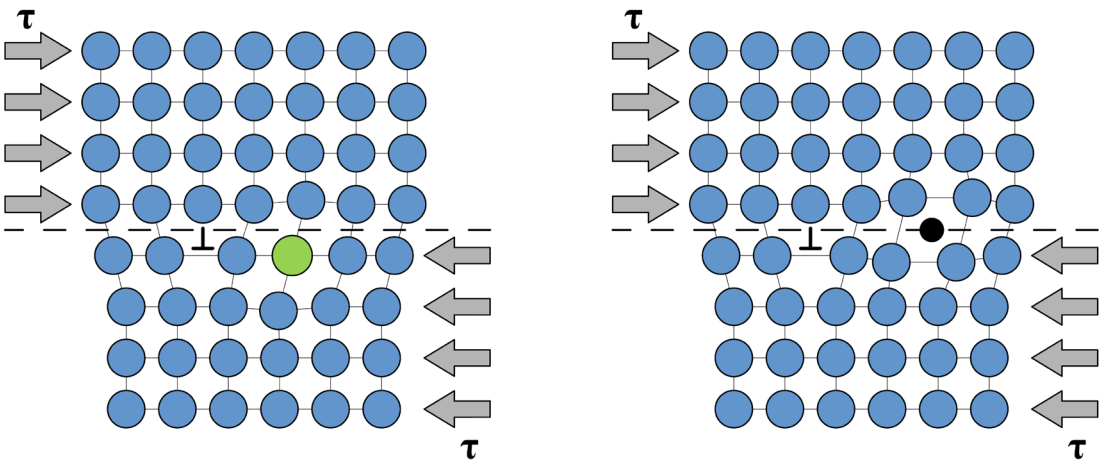

Figure 4.1 - The effect of substitutional atoms (left) and interstitial atoms (right) on the dislocation motion.

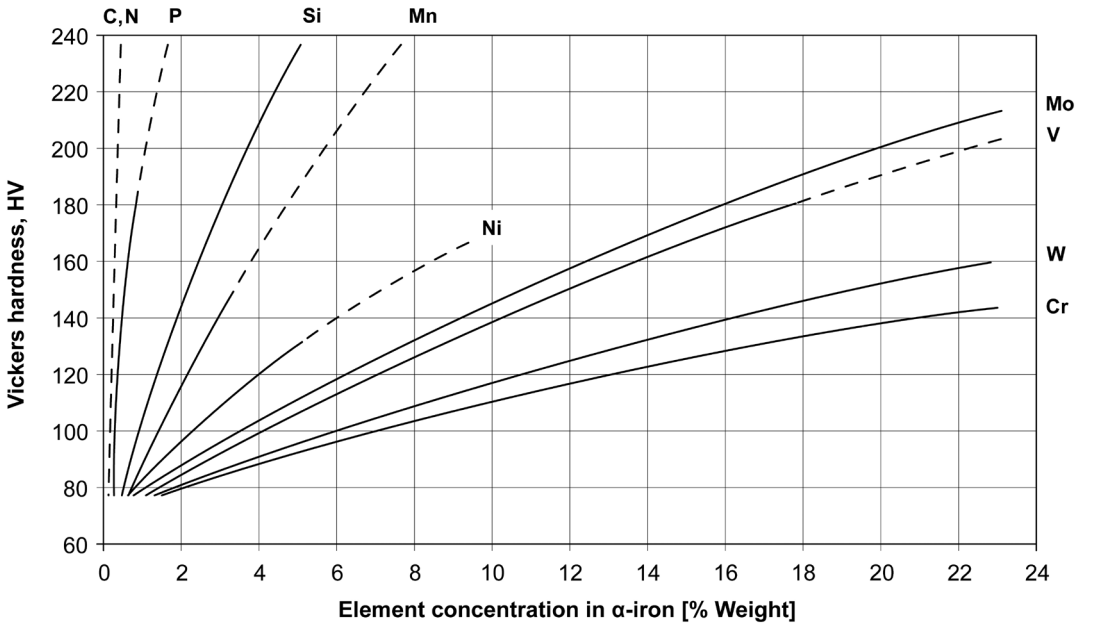

Figure 4.2 - The effect of substitutional and interstitial atoms on the hardness of α-iron lattice [from Bain and Paxton 1966].

In carbon steel and special steel, the greatest increase of strength is due to interstitial elements, i.e. carbon or nitrogen. Instead, substitutional elements are less effective. The effect of the interstitial atoms is more consistent because the strengthening of the metallic matrix is related to a greater perturbation induced by small foreign atom that enters the interstitial sites. Different is the case of the substitutional atoms which simply replace the iron atoms in their positions of equilibrium.

4.2 Strengthening by strain hardening

If a metal or alloy is subjected to cold deformation[2], it is normal to observe an increase in its strengthening characteristics (hardness, yield strength, and ultimate tensile strength). The higher is the degree of cold deformation, the greater the strengthening, that is, the increase in mechanical strength. Conversely, as the deformation increases, the residual ductility of the metallic mass decreases progressively. Cold deformation also modifies the shape and size of the crystalline grain, which is crushed and elongated in the direction of the main deformation.

This phenomenon is called strain hardening and occurs in all those cases where the shape and size of the metallic mass is modified through cold deformation. Typical technologies that cause a significant level of cold work are cold rolling, cold extrusion, drawing, deep drawing, and bending[3] (Figure 4.3).

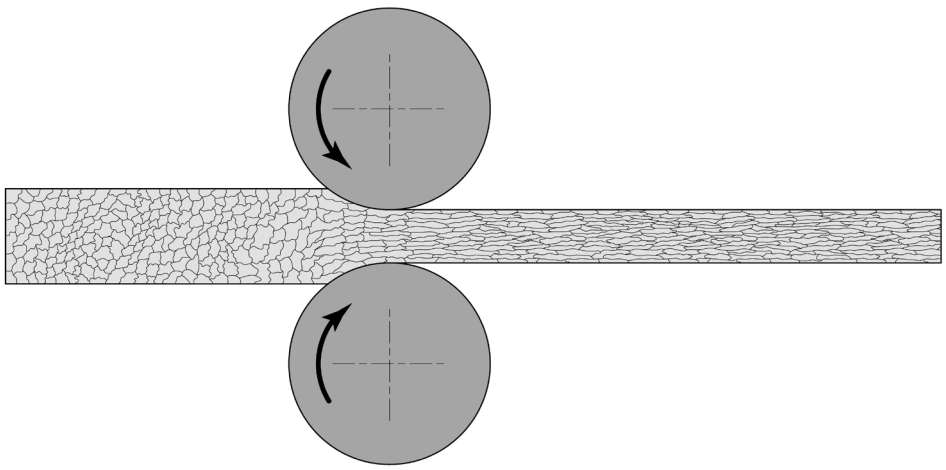

Figure 4.3 - The effect of cold rolling on the microstructure of the metallic mass.

[2] A deformation process is said to be cold if the metallic mass is permanently modified when operating at room temperature or slightly higher. Many texts indicate 1/3 of the melting temperature in Kelvin degrees as the limit. In the case of low carbon steel, this value is equal to approximately 300°C.

[3] The term "cold" is indicated in cases where a misunderstanding might arise. For example for rolling and extrusion the term "cold" is specified while drawing or banding are generically indicated because usually work at room temperature or slightly above.

The amount of strain hardening, is defined by the reduction of the section of the semi-finished product *S%*. The initial section is called A_0 and the final section is called A_f, while *S%* is equal to:

$$S\% = \frac{A_0 - A_f}{A_0} \cdot 100 \quad [4.1]$$

Figure 4.4 shows the effects of cold deformation in a low carbon steel.

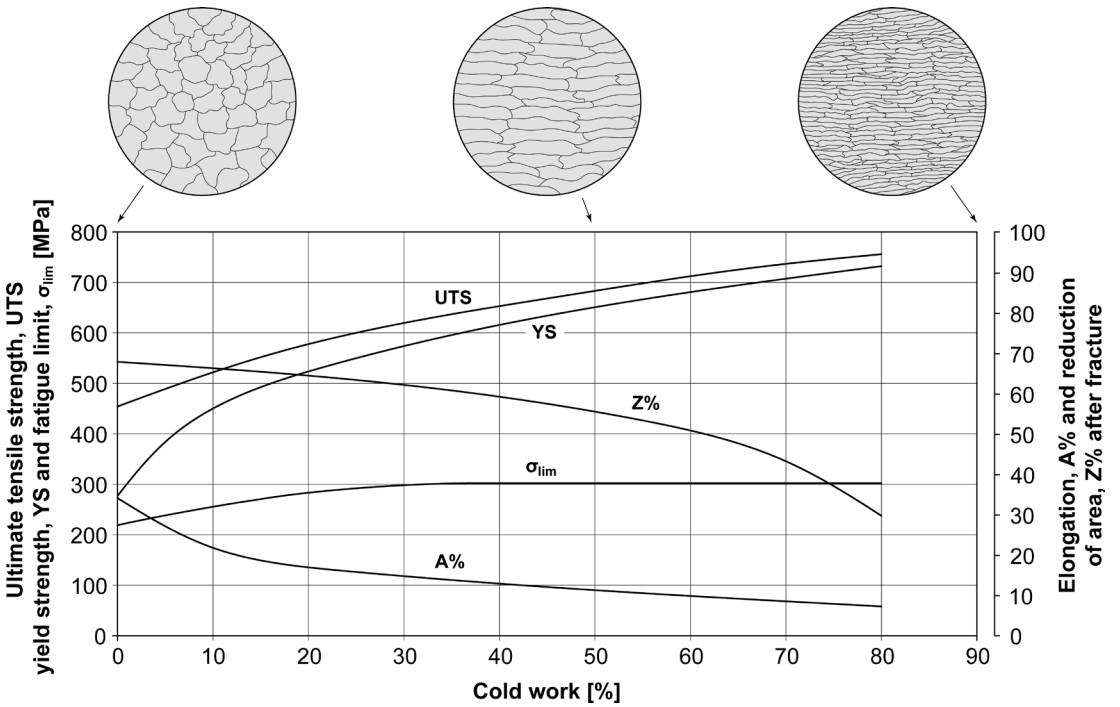

Figure 4.4 - The effect of strain hardening on the strengthening and deformability of an EN C15 steel with a pearlitic-ferritic structure [from Dieter 1988].

The efficiency of the process is not only a function of the strain hardening level, but it also depends on the type of steel structure.

Residual stresses are mechanical stresses that remain in the component when the external forces used to deform it have been eliminated. As a matter of fact, residual stresses[4] due to strain hardening are always present in cold-finished products.

[4] *Residual stresses are self-balancing stresses inside a workpiece not subjected to external forces. Typically, residual stresses are caused by plastic deformation processes (hot or cold), machinig, heat treatments, solidification of castings or welding joints. Residual stresses are difficult to evaluate and influence the behavior of mechanical components: residual stresses can add to the stresses generated during component operation and lead to component failure.*

Residual stresses are a direct consequence of the heterogeneous distribution of strain hardening in the metallic mass (Figure 4.5).

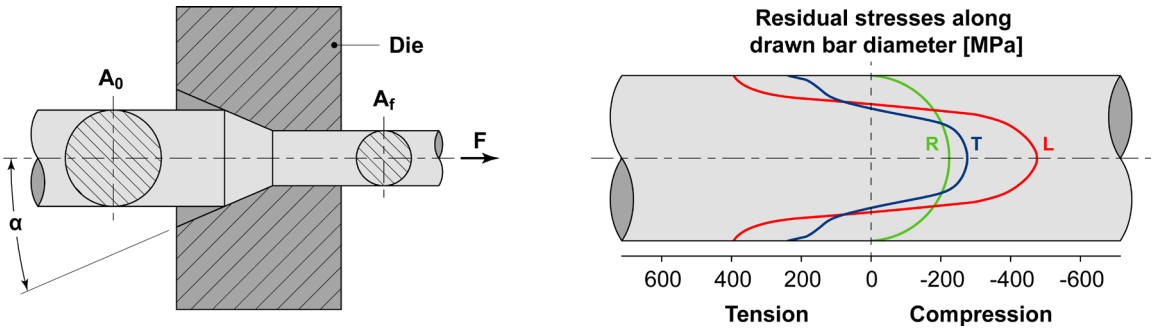

Figure 4.5 - The effect of drawing process on residual stresses of a bar of EN C45 steel (drawing angle $\alpha = 20°$; section reduction $S\% = 11.6\%$). Stresses in longitudinal *L*, radial *R* and tangential *T* direction [from Rocha et al. 2012].

Plastic deformation and strain hardening are directly related to the dislocation motion and their progressive multiplication and stacking in the crystal lattice.

It is the dislocation motion that causes their multiplication: deforming the metallic mass, that is, setting the dislocations in motion, also means increasing their number. For example, the density of dislocations in low carbon steel in the annealed state[5] is equal to 10^9 - 10^{10} m/m^3, while after strain hardening, it is in the order of 10^{16} - 10^{17} m/m^3.

The multiplication of the dislocations is understood by considering what happens, for example, to an edge dislocation when its movement is blocked at the extremities (Frank-Read mechanism). This phenomenon occurs if the line defect is anchored to obstacles, such as crystal lattice irregularities, impurities, precipitates, other dislocations, etc. In such cases, the continuous application of shear stresses produces a curvature of the advancing edge of the dislocation. In the end, the dislocation closes on itself and forms a new dislocation. As movement proceeds, there is a continuous multiplication of dislocations that increase in number as the deformation increases (Figure 4.6).

[5] *Dislocation is a line defect, measured in units of length. Therefore, in order to have a defect density, the total length of the defects must be indicated with respect to the volume.*

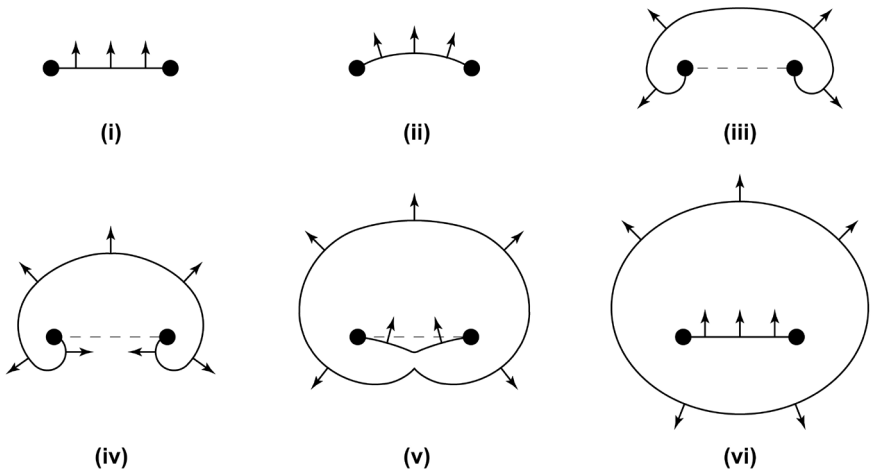

Figure 4.6 - Schematic representation of the Frank-Read Mechanism [from Campbell 2008].

The direct consequence is the creation of an ever increasing amount of obstacles to the dislocation motion. Generating new dislocations that move in every direction means forming a growing number of obstacles to their movement. By moving and multiplying, dislocations tend to obstruct each other: this progressively reduces their mobility, meaning it decreases the deformability of the metallic mass, while increasing hardness and mechanical strength.

What has been described explains what happens during the plastic deformation of a steel. The application of increasing forces is required in order to deform the metallic mass. When they are deformed, metals and alloys tend to gradually become work-hardened, that is, it is more difficult to deform them since their strength increases: this effect is due to the dislocation motion. Further deformation cause the ductile fracture of the component once the ductility of the metallic mass is exhausted.

4.3 Strengthening by precipitation

The third steel strengthening mechanism is due to nano-particles[6] of a second phase distributed in the metallic matrix.

These precipitates lead to the strengthening of steel both by hindering the dislocation motion and also by favoring their continuous multiplication. In both cases, the effect is to reduce the deformability and to increase the mechanical strength of the metal.

The mechanisms involved when the nano-particles are coherent or incoherent with the metallic matrix are different (Figure 4.7).

[6] *Particles that favor the strengthening by precipitation of metallic materials are also called dispersoids.*

If the precipitates are coherent, that is, with the same orientation of the surrounding lattice, the dislocation slows down, while it cuts in half the particle that obstructs its movement (Friedel-Fleischer effect). When the precipitates are incoherent with the lattice of the matrix, that is, they cannot be directly crossed by dislocation, both the mobility reduction of the defect and its multiplication (Orowan mechanism) are observed.
In either case precipitates reduce the dislocation motion and increase the mechanical strength of the steel.

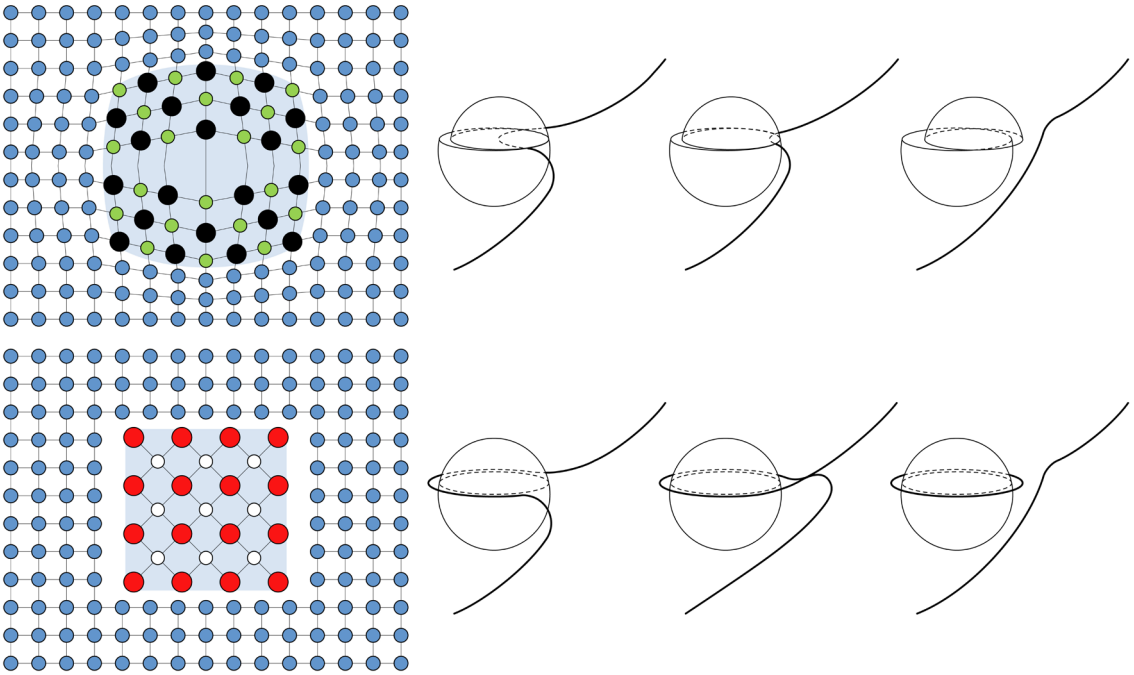

Figure 4.7 - Obstruction to dislocation motion caused by nano-particles: Friedel-Fleischer effect, in the case of coherent precipitations (above) and Orowan mechanism in the case of incoherent precipitates (below) [from Gerold 1979].

Phenomena of this type are observed in steel with a particular chemical composition, that is, if there are alloying elements present, such as titanium, vanadium, and niobium in a very small quantity (0.05-0.15%)[7]. During the hot working of semi-finished products, these chemical elements form very fine precipitates[8], which block the dislocation motion (Figure 4.8).

[7] *Steels of this type are also called micro-alloyed steels or HSLA: High-Strength Low-Alloy (Steel).*

[8] *Micro-alloyed steels include niobium carbides and niobium carbonitrides, Nb_4C_3 and Nb(C, N), vanadium nitrides and vanadium carbides, VN and V_4C_3, titanium carbides, TiC. These precipitates are formed during hot working deformation of coils, plates, bars, forged components, and so on.*

For these materials, the increase of the ultimate tensile strength ($\Delta\sigma_m$ in MPa), caused by nano-particles precipitation, can be estimated with the Ashby-Orowan formula:

$$\Delta\sigma_m = \frac{A \cdot \sqrt{V_f}}{\bar{d}} \ln\left(B \cdot \bar{d}\right) \quad [4.2]$$

A and B are two constants that depend on the material, V_f the volumetric fraction of the nano-particles, and $\bar{d}$ their average diameter in μm[9]. As is evident in equation 4.2, the finer the nano-particles and the greater is their volumetric fraction, the more effective is strenghtening by precipitation (optimum size is in the order of 5-30nm).

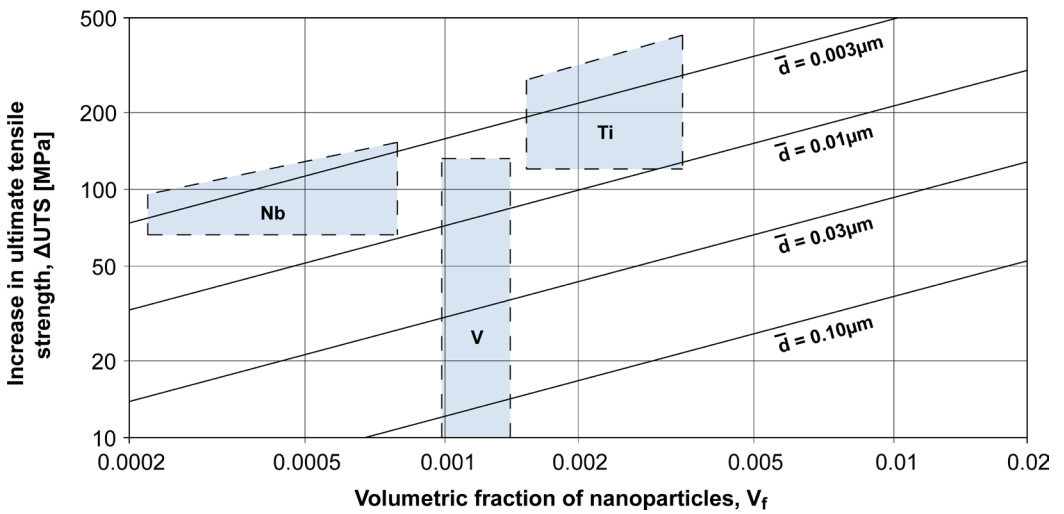

Figure 4.8 - The effect of the volumetric fraction of nano-particles , V_f , and their average size , $\bar{d}$, on strengthening by precipitation. Comparison of the Ashby-Orowan model (continuous lines) and the experimental results on High Strength Low Alloy Steel (colored areas) [from Ginzburg 2005].

4.5 Strengthening by grain refinement

The fourth strengthening mechanism is grain refinement: the grain boundaries are one of the most effective obstacles for the dislocation motion. Steel with many grain boundaries per unit of volume, that is, with small grains, has a mechanical strength, higher than steel with coarse grain.

[9] *In the case of HSLA steels, A is equal to 5.9, while B is 4000 [Ginzburg 2005].*

As seen previously in Chapter 2, the dislocations do not move randomly within the grain, but they always follow the lattice orientation. Since each grain has a uniformly arranged lattice, the path of the dislocations is defined and delimited by the grain boundaries. Therefore, the dislocations stop their movement (Figure 4.9) once they have reached the grain boundary where there is a progressive build-up of defects.

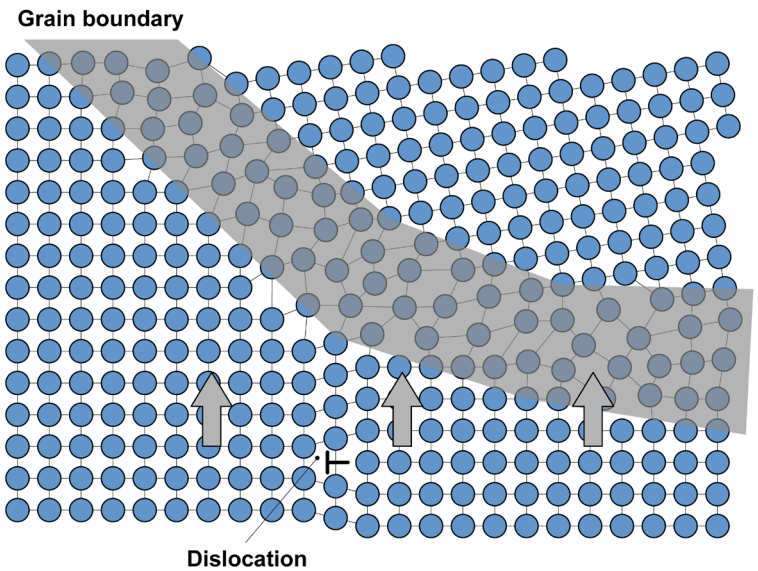

Figure 4.9 - The effect of grain boundary on dislocation motion.

Therefore, the mean grain size has important implications on the mechanical strength of steel and metal alloys. A decrease in the mean grain size creates more grain boundaries, that is, more obstacles for the dislocation motion. This condition reduces the deformability and increases the mechanical strength of steel. If, instead, the crystalline grain is coarse, that is, there are few grain boundaries, the mean free path of dislocations is large. Consequently, deformability is facilitated and mechanical strength is low (Figure 4.10).

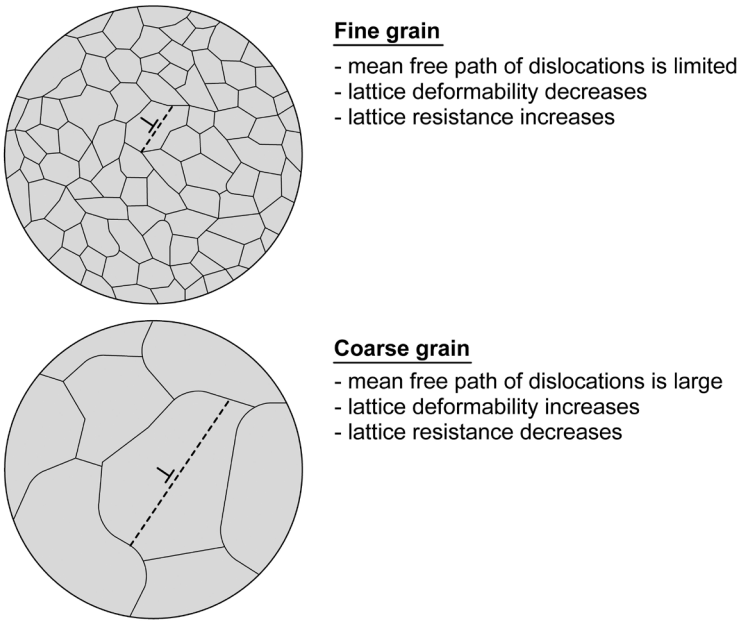

Figure 4.10 - The effect of mean grain size on mechanical strength and deformability of a metal.

There is an experimental correlation, called Hall-Petch's relation, between yield strength and mean grain size. The relation is expressed by the following formula:

$$\sigma_{YS} = \sigma_0 + kd^{-1/2} \quad [4.3]$$

where σ_{YS} is the yield strength, k is a coefficient that depends on the material (called Hall-Petch constant), σ_0 is the minimum stress required to trigger the dislocation motion, and d is the average diameter of a crystalline grain[10]. Figure 4.11 shows the graphic representation of Equation 4.3.

Even if, theoretically, an infinite increase in strength could be obtained by decreasing the mean grain size to nanometric values ($d \longrightarrow 0$), actually, the Hall-Petch's relation is valid only up to grain size of 10μm. Below these values the yield strength begins to diminish since the deformation mechanism is no longer ruled by the dislocation motion but by the sliding of the grain boundaries.

[10] *In the case of low carbon steel σ_0, it is equal to 70MPa, while k is 0.74MPa $\sqrt{m}$ [Smith & Hashemi 2006].*

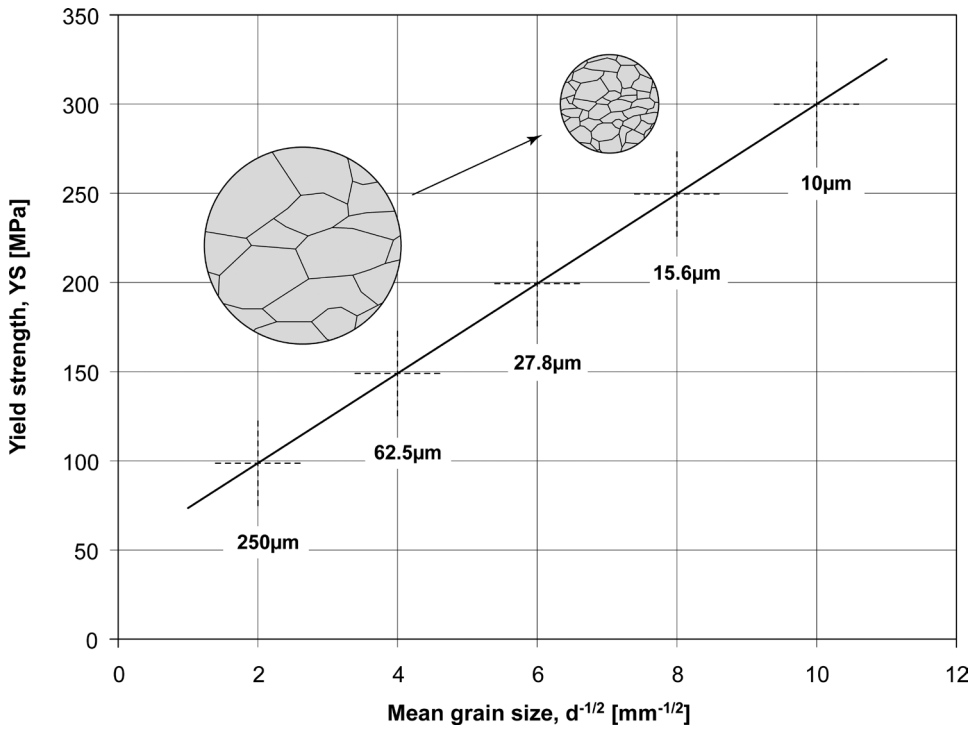

Figure 4.11 - Hall-Petch's relation for low carbon steels [from Campbell 2008].

4.5 Recovery, recrystallisation and grain growth

Let us now see what happens if a heat treatment is performed on a semi-finished product that has been strengthened by one or more of the mechanisms previously discussed.

Three metallurgic phenomena can be observed if the metallic mass is exposed to high temperature (Figure 4.12):

- recovery,
- recrystallisation,
- grain growth.

Recovery

Cold deformation occurs mainly due to the motion and multiplication of the dislocations. At the same time, crystalline grains are extended in the direction of the deformation and residual stresses originate in the semi-finished product. These phenomena accumulates a large amount of mechanical energy in the material, inducing thermodynamic instability in the lattice. When the metallic mass is warmed up at temperatures below the minimum recrystallisation temperature[11], there is a progressive redistribution of the mechanical energy accumulated in the system during plastic deformation.

[11] *For the definition of the recrystallisation temperature, see the next point of this paragraph.*

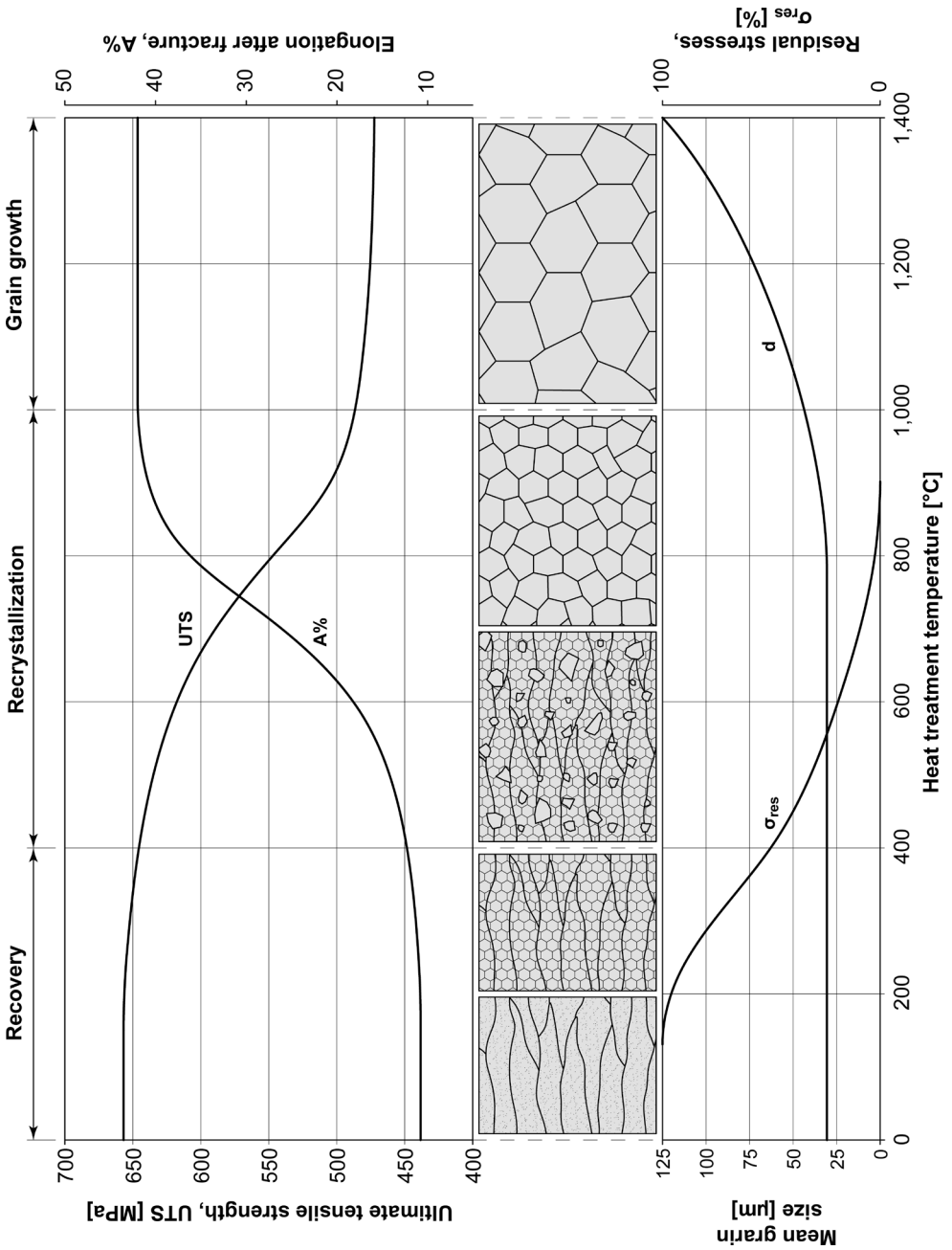

Figure 4.12 - Schematic representation of the microstructural and mechanical evolution of a strain hardened EN C15 steel, subjected to heat treatment (recovery, recrystallisation, and grain growth phenomena).

The phenomenon occurs because at these temperatures atoms diffuse from high energy positions to positions of equilibrium. This phenomenon favors a reassembly of the mechanical stresses in crystal lattices, inducing a more stable thermodynamic state than strain hardened material.

Recovery causes a significant reduction in the dislocation density through the reorganization of the crystal lattice (Figure 4.13). The main phenomena involved in recovery are: annihilation (cancellation of two opposing dislocations), polygonization, and formation of sub-grains (transformation of a curved grain caused by strain hardening in two polygonal sub-grains), and dislocation climb (progressive climb over an obstacle).
Recovery do not change significantly the mechanical strength of steel, even if the decreasing of the residual stresses improves fatigue strength and physical properties (for example, electrical and heat conductivity).

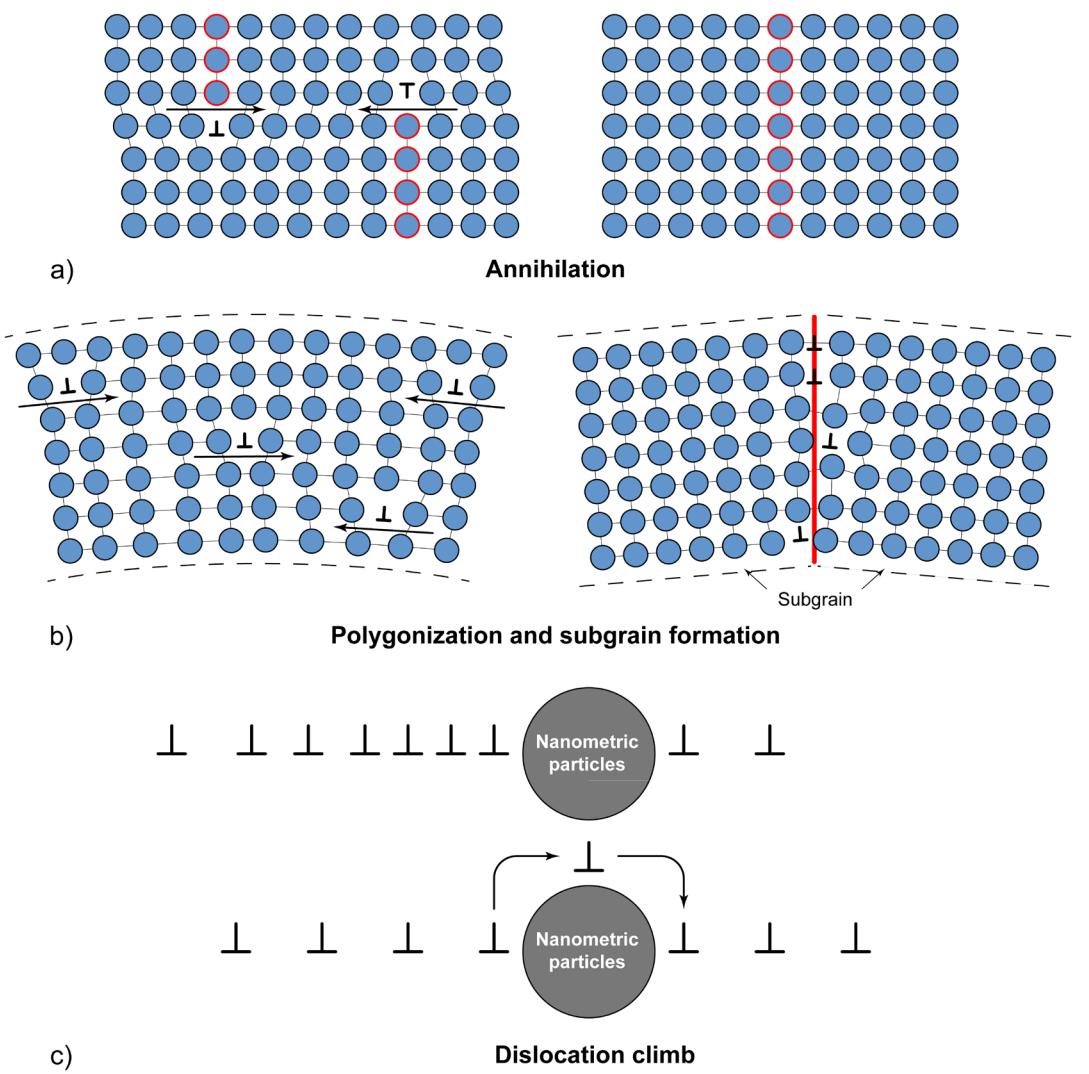

Figure 4.13 - Schematic representation of lattice phenomena that cause recovery: a) annihilation of dislocations; b) polygonization and formation of sub-grains; c) dislocation climb.

Recrystallisation

The recrystallisation phenomenon occurs if the heat treatment temperature exceeds a minimum threshold. Recrystallisation is due to a nucleation and growth mechanism activated by the mechanical energy stored in the metal mass and the increase in temperature. During recrystallisation, the cold deformed grains are transformed into new homogeneous grains without residual stresses and strain hardening, which completely replace the hardened microstructure. Therefore, at the end of recrystallisation process the microstructure completely recovers its original levels of deformability (Figure 4.14).

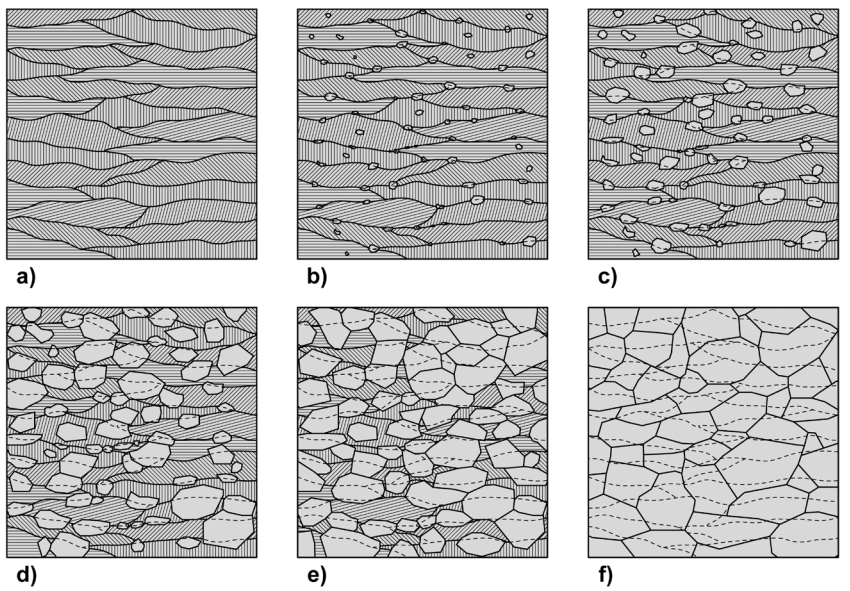

Figure 4.14 - Recrystallisation phases in steel: a) metal in the strain hardened state; b) recrystallisation with formation of new grains; (c-e) growth of new grains at the expense of the original structure; f) completed recrystallisation [from Higgins 1993].

Recrystallisation is controlled through various parameters: process temperature, chemical composition of the metal alloy, degree of strain hardening and mean size of the original grains.
The minimum recrystallisation temperature, T_r, is in the order of 0.4-0.5 of material melting point expressed in Kelvin[12]. If temperature increases, the rate of recrystallisation also increases.

[12] *The recrystallisation temperature is the minimum temperature that, after one hour of time, causes complete transformation of the strain hardened grains into new homogeneous and equally-sized crystalline grains.*

In pure metals, T_r is low: ARMCO iron, for example, recrystallises at about 400°C. The presence of atoms in solid solution (even if in a limited quantity) increases the recrystallisation temperature by many degrees: in low carbon steel T_r, it is in the order of 500°-550°C.

On the contrary, the recrystallisation temperature gradually decreases as the strain hardening increases. It should also be noted that a minimum level of cold deformation (5-10%) is required for recrystallisation to occur. Finally, consider the effect of the mean size of the original grains. Recystallisation is faster in fine-grain materials as compared to coarse-grain materials: if the starting microstructure is very work-hardened, the size of the grains at the end of recrystallisation is smaller than the undeformed materials, which have coarser crystalline grains.

Grain growth

The increase in heat treatment temperature causes the progressive enlargement of the grain size. Some crystalline grains, in order to further reduce their energy level, increase in size at the expense of adjacent grains. Consequently, the grains are coarser than those optained after recrystallisation.

The driving force of the growth is the surface energy of the grains, proportional to the total surface of the grains. During grain growth, the polycrystalline structure evolves in the direction that leads to a decrease in the surface energy of the system, i.e. a reduction in the total surface of the grain boundaries. This condition occurs if the holding temperature is sufficiently high or if the holding time is sufficiently prolonged, to favor the diffusion movement of the atoms. In this way several crystalline grains grow homogeneously, at the expense of the surrounding ones (Figure 4.15).

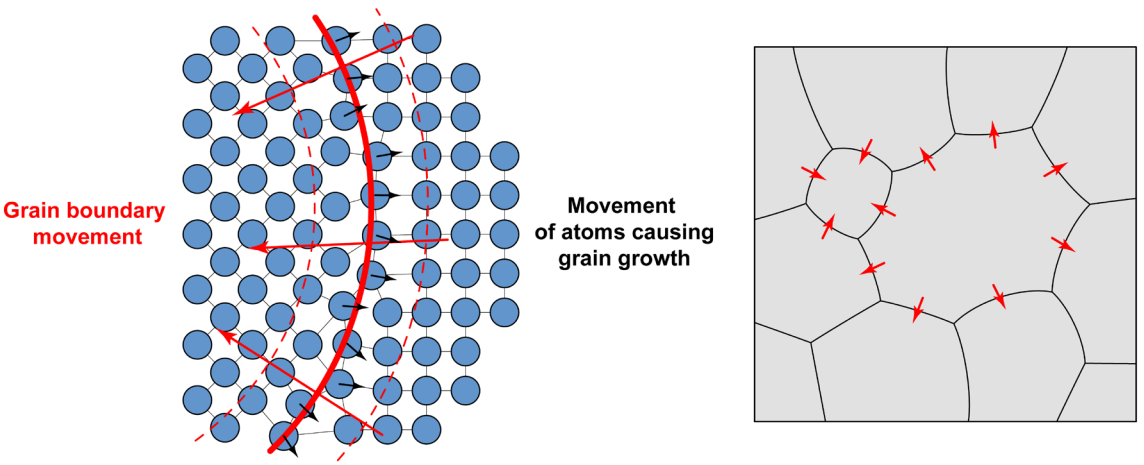

Figure 4.15 - Shematic representation of the grain growth mechanism [from Singh 1999].

Grain growth in a metallic mass may be continuous or discontinuous[13].
In the first case, all the growing crystallites increase in size homogeneously. In the second case, the growth occurs only in some points of the microstructure, with the formation of abnormal grains at the expense of the surrounding ones that remain small in size (Figure 4.16).

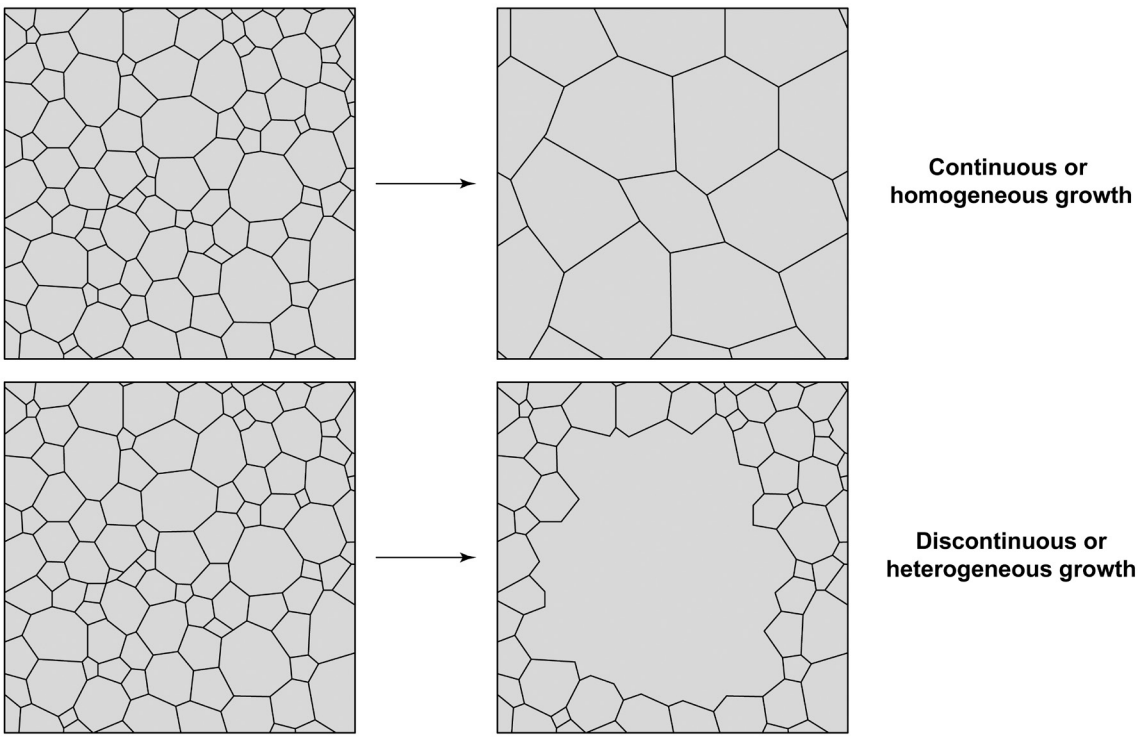

Figure 4.16 - Example of crystallite growth: a) continuous growth; b) discontinuous growth [from Thompson 1985].

The phenomenon of discontinuous growth occurs when normal recrystallisation is inhibited by very small particles. A typical case is killed steel, where small aluminum oxides (Al_2O_3) and/or small nitrides (AlN), force the crystalline grains to remain within limited sizes. However, if the heating temperature is very high or the holding time is prolonged the secondary particles begin to coalesce or even dissolve in some areas. The crystalline grain explosion occurs in these points, while the surrounding grains remain small because their growth is inhibited by the inclusions still present (Figure 4.17).

[13] *These two methods are also called primary (or continuous) growth and secondary (or discontinuous) growth.*

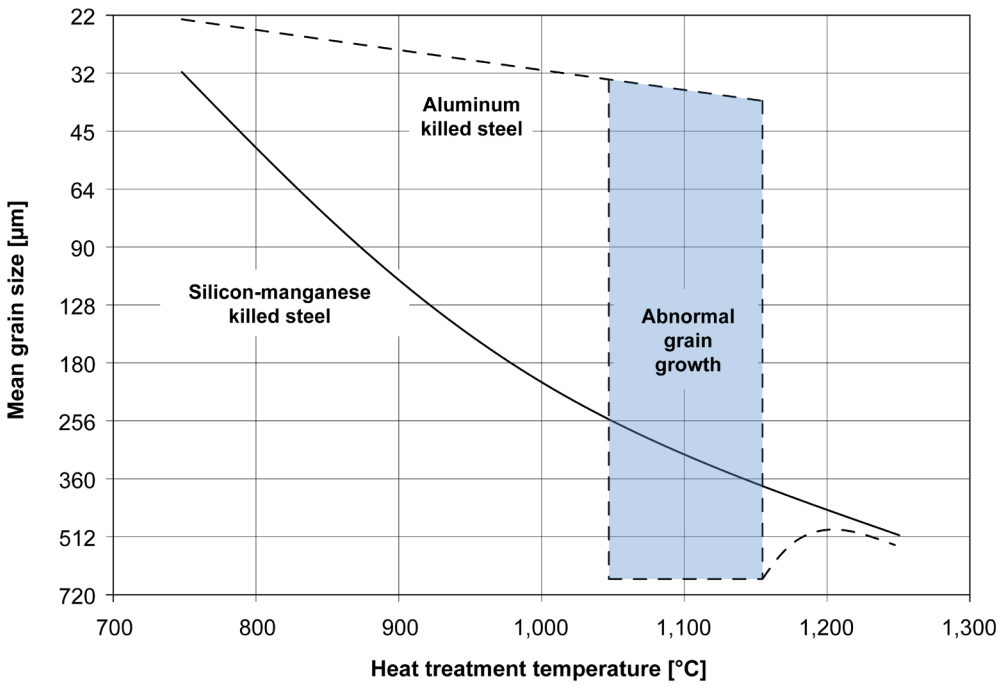

Figure 4.17 - The effect of temperature on continuous or discontinuous grain growth for silicon-manganese killed steel and aluminum killed steel [extracted from Gladman 2004].

5. PHASE DIAGRAMS

5.1 Phase diagrams for pure substances

A phase is defined as any portion of a chemical system that is homogeneous in chemical composition, state of aggregation, pressure, and temperature.

To understand the concept of phase, consider the case of a glass of water at atmospheric pressure (1 atm) and room temperature (20°C). In this situation, the water in the glass is completely liquid, is homogeneous in temperature and pressure, and its chemical composition is constant because it is a pure substance: all the water present in the glass is, therefore, a single phase. Something similar is obtained if the temperature is set at -5°C and the pressure remains atmospheric: the iced water in the glass is a single phase. The two situations described above can be replicated infinitely by changing the temperature and pressure values from time to time. It is, therefore, possible to define all the conditions in which the water is aggregated in a solid, liquid, or gaseous form. Figure 5.1 shows a graphic representation of what is experimentally obtained.

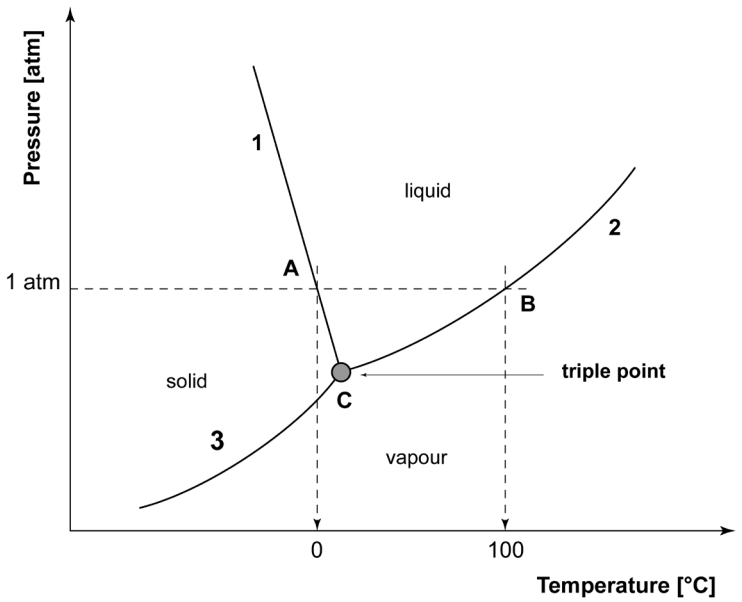

Figure 5.1 - Phase diagram for pure water: points, *A* and *B*, are the solidification temperature and the boiling temperature at atmospheric pressure, *C*, the triple point.

Figure 5.1 is a typical phase diagram for a pure substance, that is, a graph that represents the phases of the system in conditions of thermodynamic equilibrium, when temperature and pressure vary. Remember that any chemical system is defined in thermodynamic equilibrium if all the thermodynamic variables that

contribute to describing it (pressure, temperature, and chemical composition) are indicated in a completed manner and do not change over time. In the case of water, the chemical composition is constant and, therefore, only the pressure and temperature may vary.

Curve 1 in Figure 5.1 indicates the equilibrium between the solid and the liquid, that is, the condition where solidification occurs at cooling and melting occurs at heating. Along this line, there are two distinct phases (solid phase and liquid phase) corresponding to the two different aggregation states of the system.

Similarly, curve 2 and curve 3 show the equilibrium between liquid and vapour (condensation/evaporation) and between solid and vapor (deposition/sublimation).

Considering, for example, pure water at atmospheric pressure, solidification/melting occurs at 0°C (point A) and condensation/evaporation at 100°C (point B). If the pressure is modified (increased or decreased), the aggregation state transition temperatures also change. Furthermore, water, like many pure substances, has a triple point (point C), that is, a point where the three aggregation states (liquid phase, solid phase, and gaseous phase) coexist: this point is defined by a single pressure and temperature value ($p = 4.58$mmHg; $T = 0.01$°C).

The pure iron phase diagram, shown in Figure 5.2, is similar to the water phase diagram. Note that, in this case, as is typical of metals, the axes are reversed: abscissa for the pressure, ordinate for the temperature.

The fields of iron in vapour state, liquid state, and solid state are also on the diagram in Figure 5.2. It is interesting to note that, for the solid state, the allotropic transformation temperatures are also indicated: α-iron (B.C.C.), γ-iron (F.C.C.), and δ-iron (B.C.C.).

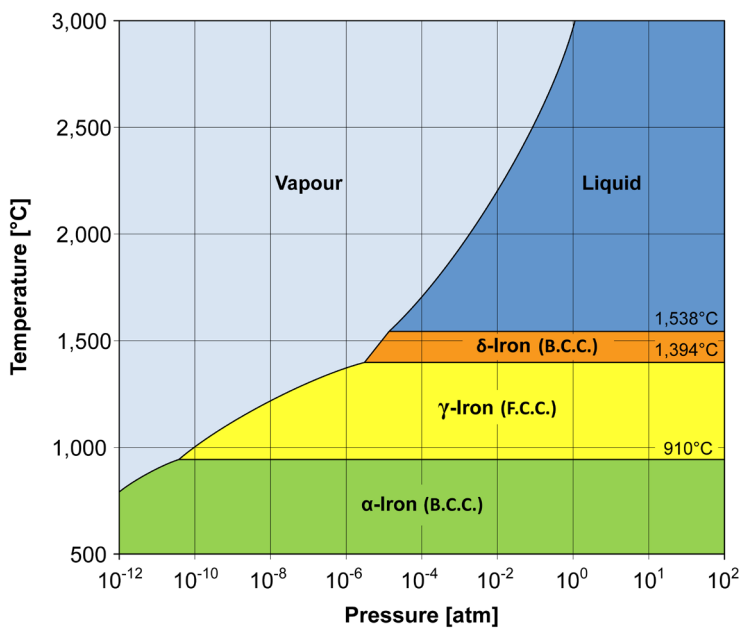

Figure 5.2 - Pure iron phase diagram.

5.2 The Gibbs Phase Rule

Before proceeding further with phase diagrams, you need to introduce a very important rule related to the systems of equilibrium: this is the so-called "Gibbs Phase Rule"[1].It allows to predict the equilibrium state of an homogeneous or heterogeneous chemical system (as, for example, a phase diagram) when there is a change in temperature, pressure, and concentration of the individual chemical species[2] that form the phases of the system.

The Phase Rule is expressed as follows:

$$V = C_i + M - F \qquad [5.1]$$

where V is the variance, C_i is the number of independent chemical components, M is the number of efficient physical factors, and F is the number of phases.

Let us see the meaning of the various parameters of equation 5.1.

The variance, or number of degrees of freedom of the system, is the number of independent variables (pressure, temperature, and concentration of chemical species present in each single phase), which can be arbitrarily chosen, for which the other variables also assume well-determined values.

The independent chemical components, C_i , are the chemical species needed to uniquely identify the composition of all the phases that form the system. C_i is obtained from the following relation:

$$C_i = C_t - r \qquad [5.2]$$

where C_t is the total number of chemical species in the system (total chemical components), while r represents the number of reversible reactions that bind these chemical species and the stoichiometric constraints between substances that form each phase[3].

The number of efficient physical factors, M, that is, the physical parameters that have an effect on changing the equilibrium of the system, is equal to two: temperature and pressure. However, it should be noted that in many applications involving metals and metal alloys, the pressure is constant and is equal to the atmospheric pressure.

---

[1] Josiah Willard Gibbs, an American Chemical Engineer, is one of the founders of thermodynamics and modern chemistry-physics. His main contribution is related to the definition of free enthalpy, (commonly known as Gibbs free energy) which allows to predict the spontaneity of a chemical reaction. He is also known for the Phase Rule which was developed in 1876.

[2] The term, "chemical species", is used to define a generic chemical substance, regardless of the number of atoms or molecules that constitute it. A chemical species can be defined only if the nature, proportion, and disposition of the chemical elements that constitute it are known. Examples of chemical species are simple substances, chemical compounds, reagents, products, and intermediates of any chemical reaction. Phases and mixtures, on the other hand, cannot be considered chemical species, since more than one chemical species of a different nature can coexist within them.

[3] Take, for example, the dissociation reaction for calcium carbonate: $CaCO_{3\,(s)} \leftrightarrow CaO_{\,(s)} + CO_{2\,(g)}$.The total chemical components are 3 ($CaCO_{3\,(s)}$, $CaO_{\,(s)}$, $CO_{2\,(g)}$), there is a single chemical reaction, and there are no stoichiometric constraints between $CaO_{(s)}$ and $CO_{2\,(g)}$. The independent chemical components are, therefore, equal to 2 (C_i= 3-1 = 2).To define the composition of the three phases that make up the system, two chemical species must, therefore, be chosen, for example $CaO_{(s)}$ and $CO_{2\,(g)}$.

Consequently, for metals and metal alloys, M, it is always equal to one.
Finally, the number of phases F: this represents the number of portions of the system with the same of chemical composition, aggregation state, pressure, and temperature.

Let us now apply the Gibbs Phase Rule to the case of the water phase diagram (Figure 5.1). Regardless of the pressure and temperature values, there is always only one independent chemical component, $C_i = 1$, since water is a pure substance.
Let us also assume that the chosen temperature and pressure values define a generic point in a one-phase field (liquid, solid, or gaseous): in these areas, the number of efficient physical factors, M, is equal to two (pressure and temperature) and the phase, F, is one. Therefore, the calculation of variance, V, becomes:

$$V = 1 + 2 - 1 = 2$$

This shows how one-phase fields are characterized by two degrees of freedom ($V = 2$). There are two parameters (specifically pressure and temperature) that can be altered within certain limits, without altering the equilibrium of the system (water remains in the same phase: liquid, solid, or gaseous).
Always with reference to Figure 5.1, let us now consider the case of the curves marked by numbers 1, 2, and 3. These lines represent the temperature and pressure conditions in which the system changes its state, that is, where two phases coexist ($F = 2$). According to the Gibbs Phase Rule:

$$V = 1 + 2 - 2 = 1$$

This means that it is possible to vary the temperature (or pressure) and, as a result, the value of the pressure (or temperature) that describes that particular condition is uniquely defined. There is only one degree of freedom of the indipendent variables (pressure, temperature) so that the two states of aggregation coexist simultaneously.
Finally, let us look at the triple point case C where all three phases are present ($F = 3$). The variance of the system is:

$$V = 1 + 2 - 3 = 0$$

Since the variance is zero, the system has no degree of freedom. Therefore, only one condition of independent variables (pressure, temperature) allows the system to have three phases in equilibrium ($p = 4.58$mmHg; $T = 0.01$°C). Similar conclusions can be reached by applying the Gibbs Phase Rule to pure iron phase diagram in Figure 5.2.

5.3 Binary phase diagrams for metal alloys

Phase diagrams for metal alloys, in their simplest formulation, are characterized by two chemical elements, generally indicated as A and B. This is why they are called binary phase diagrams.

The diagrams show the temperature in ordinate and the chemical composition of the alloy in abscissa. The pressure is a variable that is normally not considered because in many applications it is constant and is equal to the atmospheric pressure. Therefore, the system at equilibrium is completely described if temperature and chemical composition of the phases are defined.

Furthermore, in currently used phase diagrams, temperature is limited to the condition where the system is completely in a liquid phase.The vapor phase is not usually indicated.

In order to better understand the concepts set out above, let us consider the example of two liquids that are perfectly soluble between themselves: water and mint syrup (Figure 5.3).

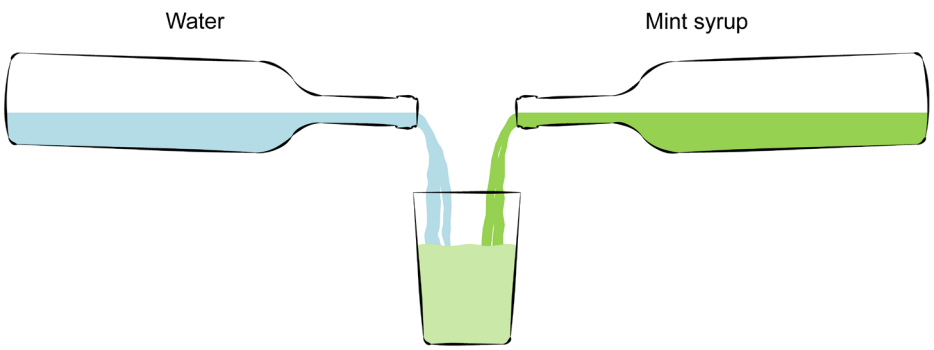

Figure 5.3 - Liquid solution between water and mint syrup: the two liquids are perfectly soluble.

By mixing water and mint syrup in a glass, a homogeneous liquid solution is obtained. As is well-known, water and mint syrup are perfectly soluble and, depending on the relative quantities, a drink that is more or less rich in mint syrup will be obtained.The color of the beverage is also an index of the greater or lesser presence of the two substances: the greater the amount of mint syrup is used, the greener the color of the liquid will be.

The system obtained is homogeneous: the temperature is well-defined and the amount of water and mint syrup is defined; the liquid solution has, at any point, the same chemical composition, aggregation state, pressure, and temperature. Therefore the system consists of a single phase, that is, it is a one-phase system.

The terms of the problem do not change if the temperature is changed: by cooling to a temperature below 0°C, the system solidifies and, the more mint is used, the greener the popsicle will be.

The mint popsicle is also an homogeneous solid system (it is a single phase) because it has the same chemical compostion state of aggregation, pressure, and temperature at all points.
In several cases, something analogous also occurs for metals.
Consider gold and silver. If they are mixed together in a crucible and then solidified, the two metals behave exactly like water and mint syrup. Both in their liquid state and in their solid state, gold and silver are perfectly soluble with each other. The liquid solution between gold and silver is homogeneous and solidification occurs with the formation of an homogeneous system.The metal alloy obtained is a solid substitutional solution[4] in which the gold lattice is partially replaced by silver atoms[5].
Even a gold-silver alloy, like the mint popsicle, has a color that varies between bright yellow (color of gold) and brilliant metallic gray (color of silver), depending on the quantity of the two metals. The aptitude of the gold-silver alloy to form homogeneous solid solutions is not an isolated case. For example, copper-nickel, molybdenum-niobium, niobium-tantalum, and silver-palladium alloys have a similar behavior.
Figure 5.4 shows the graphic representation of the concepts set out above: this is the phase diagram for gold-silver. The temperature is in ordinate, while the chemical composition of the alloy is in abscissa as a percentage in weight of silver. The percentage in weight of gold is, obviously, the complement to one hundred.

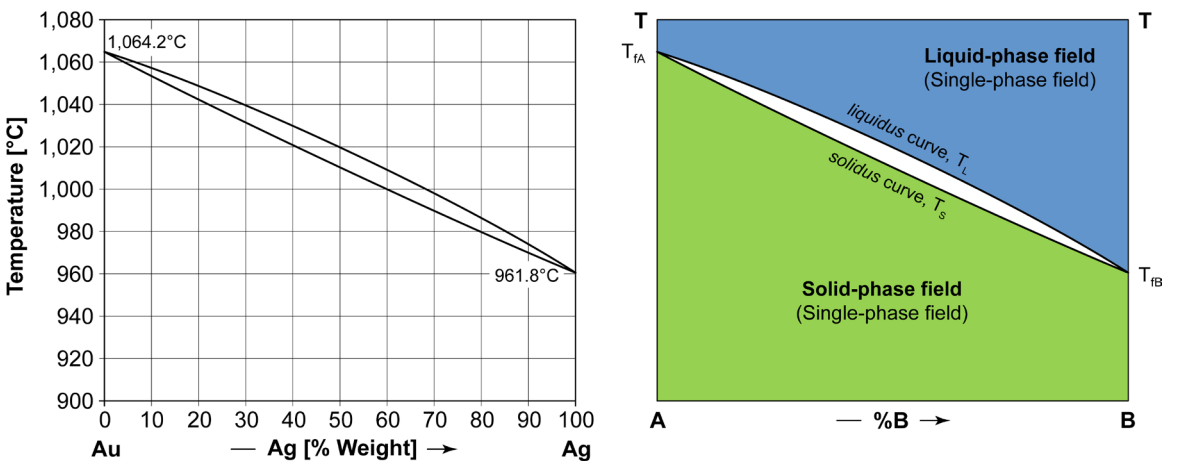

Figure 5.4 - Gold-silver phase diagram (*Au-Ag*) [from ASM-H.3 1992] and its schematic representation.

[4] *See Paragraph 2.3 of Chapter 2.*

[5] *Both gold and silver have a body-centered cubic lattice: gold has an atomic radius of 0.144nm, silver of 0.153nm.*

Figure 5.4 shows the gold-silver phase diagram: the one-phase fields of the homogeneous liquid phase (blue) and the homogeneous solid phase (green) are highlighted in color.
The diagram indicates the melting point of gold (T_{fA}) along the left vertical axis and the melting point of silver (T_{fB}) along the right vertical axis. There are also two lines called "liquidus" and "solidus" that connect T_{fA} with T_{fB}: these lines delimit the field (white color) where the alloy solidifies. Above the liquidus line (T_L), the system is completely in liquid phase[6]; under the solidus line (T_S), the system is completely in solid phase. Between liquidus and solidus lines, the system consists of two phases, since both the liquid and the solid phase coexist.

Let us apply the Gibbs Phase Rule to the binary phase diagram of Figure 5.4. Equation 5.1 is always valid, i.e:

$$V = C_i + M - F$$

In case of binary metal alloys, the number of independent chemical components, C_i, is always equal to 2, since the total chemical components are 2 (A and B[7]) and, between them, no reversible reactions or stoichiometric constraints exist ($C_i = 2 - 0 = 2$). The efficient physical factor is only one: temperature ($M = 1$). In order to define the variance value V, you need to establish the number of phases in the system:

$$V = C_i + M - F = 2 + 1 - F$$

If temperature and chemical composition detect a point in a single-phase field (blue or green color), variance is equal to two ($V = 2 + 1 - 1 = 2$). If, however, it falls within the two-phase field (white color), the variance is equal to one ($V = 2 + 1 - 2 = 1$).
This result is always valid for all binary metal alloys: one-phase fields have always $V = 2$, and two-phase fields have always $V = 1$.

[6] *Except for special cases, the two elements, A and B, are completely soluble at liquid state.*

[7] *The generic solid solution between A and B cannot be considered a chemical species because it does not have a well-defined "chemical nature" and cannot be described by a chemical formula. A solid solution is, in fact, an homogeneous mixture in which one or more chemical species are uniformly mixed, so that the solution has the same composition at each point.*

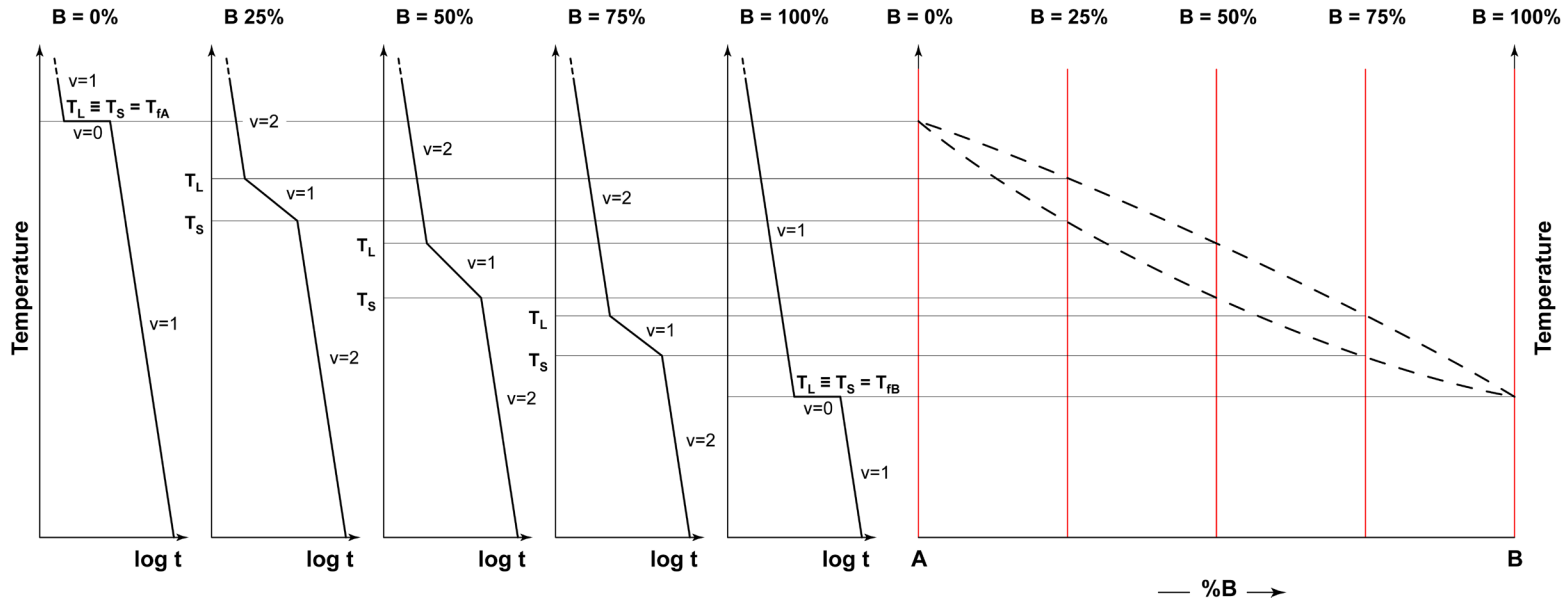

Figure 5.5 - Schematic representation of the construction method of a binary phase diagram.

5.4 Equilibrium cooling curves for binary alloys

The binary phase diagram in Figure 5.4 is obtained experimentally starting from the equilibrium cooling curves[8] that can be traced considering alloys with an increasing content of *B*. Figure 5.5 shows the trend of these curves[9] on a temperature - logarithm of time diagram and the construction method of the phase diagram.

Above T_L (system in completely liquid phase) or below T_S (system in completely solid phase), the cooling curves are all almost parallel: this means that the cooling rate is similar. This result depends to the homogeneous aggregation state (all liquid or all solid) of the system. In these cases, the cooling rate is expressed by the equation:

$$Q_s = c \cdot m \cdot \Delta T \qquad [5.3]$$

where the amount of heat extracted from the system, Q_s, is equal to the specific heat of the substance, *c*, times the mass of the system, *m*, times the temperature variation.

Heat, Q_s, calculated with equation 5.3, is called sensible heat[10] and represents the heat transferred by the chemical system when no phase transformations occurring. Note that the specific heat, *c*, varies with temperature but, both for the liquid state and the solid state, it is of the same magnitude. In the case of iron, the specific heat in a liquid state (melting point) is 0.82 kJ /kg · K, while in a solid state (room temperature) it is 0.45 kJ /kg · K.

On the contrary between T_L and T_S the slope of the cooling curve is lower. This phenomenon is typical of any phase transition (in this case from liquid to solid) and is common to most alloys[11].

To pass from T_L to T_S you need to subtract the so-called "latent heat of solidification", Q_l[12], in addition to the sensible heat Q_s.

---

[8] With reference to the equilibrium transformations, see note 13 of Chapter 1.

[9] Cooling curves are quite similar to those shown for pure iron in Figure 1.8 even if only the cooling phase is shown for binary phase diagram.

[10] The sensible term is related to the possibility to appreciate the heat extracted from the system.

[11] Eutectic composition alloys are an exception to this rule. To this regard, see Paragraph 5.9.

[12] Latent heat is called latent solidification/melting heat or latent evaporation/condensation heat in relation to the type of change in state.

The latent heat of solidification, Q_l, is a quantity of heat that varies from one chemical species to another and is proportional to the mass of the system according to the relation:

$$Q_l = \lambda \cdot m \quad [5.4]$$

where λ is the latent specific heat and m the mass of the chemical system. Q_l represents the amount of energy that, when it is subtracted from a liquid system, it causes solidification at a constant temperature. The effect of heat subtraction from the system does not induce a decrease in temperature but a transformation of the physical state of the matter through the re-aggregation of the atoms (transition from liquid to solid)[13]. For iron, the specific latent heat λ is equal to 272kJ /kg: as can be seen, the value of λ is some orders of magnitude greater than the value of the specific sensible heat, c.

The set of concepts previously expressed can be summarized as follows:
a) you need to subtract sensible heat Q_s to cool the system at temperatures higher than T_L or less than T_S;
b) you need to subtract both sensible heat Q_s and latent heat Q_l to cool the system at temperatures between T_L and T_S.
Consequently, the cooling rate is faster in case a) than in case b), since the amount of heat to be subtracted is less: Q_s in case a) and $Q_s + Q_l$ in case b). Therefore, if the temperatures are higher than T_L or less than T_S, the slope of the cooling curve is higher than in the portion between T_L and T_S.

Pure metals A ($B = 0\%$) and B ($B = 100\%$) show different cooling curves. As long as pure metal (A or B) is liquid ($T > T_L \equiv T_S$) or solid ($T < T_L \equiv T_S$), the slope of the cooling curve is the same of a completely liquid or completely solid system. In fact you only need to subtract the sensible heat Q_s.
However, thermostatation of the system occurs at the solidification temperature for a certain length of time, that is, until the transition to a state (in this case, from liquid to solid) has occurred. This phenomenon is typical of all pure substances: solidification occurs at a well-defined temperature and not in a thermal range, as is normal for most metal alloys.

Finally, a consideration relevant to the variance V of the system.

[13] In addition to latent solidification/melting heat, there is also latent condensation/evaporation heat that refers to the transition from vapor state to a liquid state, and vice versa. Latent condensation/evaporation heat is of little interest to metallic alloys and is normally not mentioned.

Since the phase diagram is binary, the independent chemical components, C_i, are 2. The efficient physical factor, M, is only the temperature[14], and the phases, F, can be read on the phase diagram. Therefore, the following occurs:

- for temperatures greater than T_L or less than T_S, ($F = 1$): $V = C_i + M - F = 2 + 1 - 1 = 2$,
- for temperatures between T_L and T_S, ($F = 2$): $V = C_i + M - F = 2 + 1 - 2 = 1$.

Also in this case, the pure metal A and pure metal B [15] are exceptions. At temperatures greater than $T_L \equiv T_S$ or less than $T_L \equiv T_s$, the variance is equal to 1 ($V = C_i + M - F = 1 + 1 - 1 = 1$) while, during the liquid-solid state transition ($T = T_L \equiv T_S$) the result is $V = C_i + M - F = 1 + 1 - 2 = 0$ with consequent thermostatation of the system as long as solidification is completed.

5.5 Complete solid solution phase diagram

The binary phase diagram shown in Figure 5.4 is a classic complete solid solution diagram.
To understand its usefulness, we study, as an example, the case of an alloy containing 30% B (Figure 5.6) indicated by the vertical axis that passes through 30% B.
The points of intersection of the vertical line at 30% B, with liquidus and solidus lines, represent the starting and ending temperature for the alloy solidification interval (i.e. approximately 1,040°C and 1,030°C[16]).

To establish the phases on the diagram, you need to draw a horizontal line perpendicular to the vertical line indicating the chemical composition in correspondence of the selected temperature: the point of intersection between the two straight lines represents the chemical system. If this point falls in the field of existence of a single phase, the system is a one-phase system, otherwise, it is a two-phase system.
Figure 5.7 shows the schematic representation of a complete solid solution phase diagram: let us consider three points: X, Y, and Z at temperatures T_X, T_Y and T_Z for the alloy at 30% B.

[14] *See Paragraph 5.2 of this chapter.*

[15] *In the case of pure substances $C_i = 1$.*

[16] *Refer to Figure 5.4.*

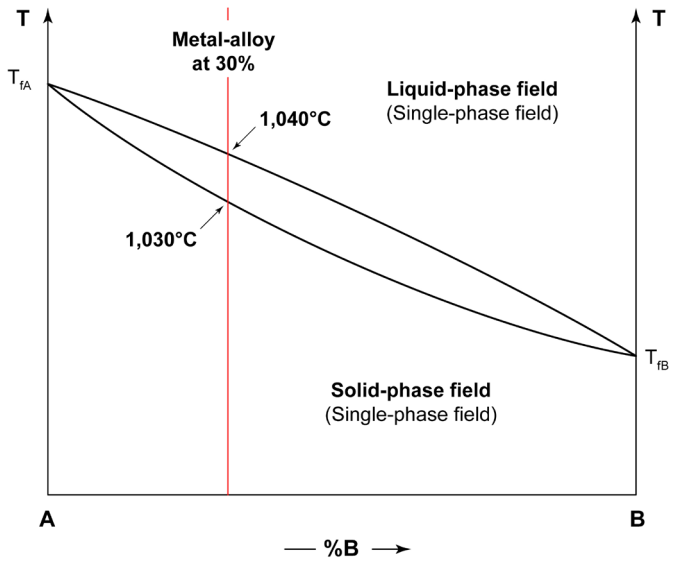

Figure 5.6 - Schematic representation of a generic complete solid solution phase diagram and graphic representation of an alloy at 30% *B* and at 70% *A*.

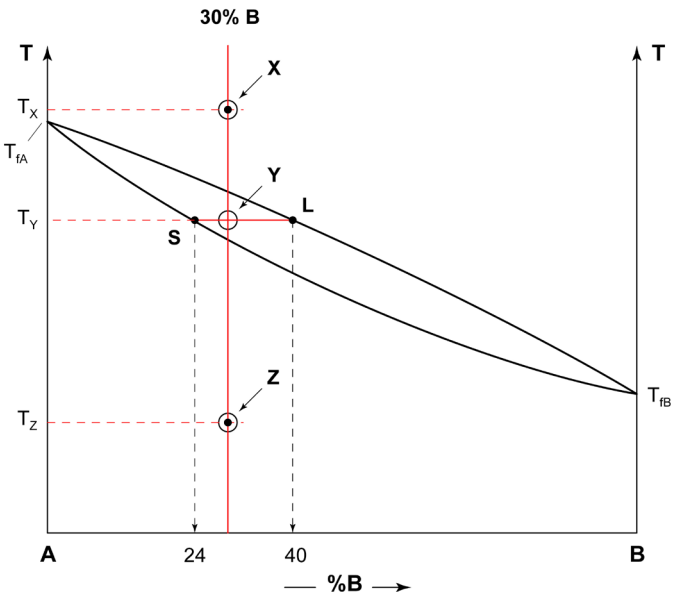

Figure 5.7 - Schematic representation of a generic complete solid solution phase diagram and graphic representation of an alloy at 30% *B*: position of points *X*, *Y* and *Z* at temperatures T_X, T_Y and T_Z.

The chemical system, i.e. the intersection of the two straight lines, is indicated by an empty circle (○), while the phase is represented by a full dot (•). Since both point X and point Z fall within one-phase fields, the full dot coincides with the circle: the system at point X consists of an homogeneous liquid (one phase), while at the point Z it consists of an homogeneous solid (one phase).

Conversely, point Y lies within the two-phase field between the lines of liquidus and solidus. To find the phases present at temperature T_Y, you need to move along the horizontal line traced in correspondence of T_Y until it meets the one-phase fields of the liquid L and solid S. Therefore, at temperature T_Y, there will be two phases: phase L (liquid) and phase S (solid).The chemical system is always indicated by an empty circle (point Y) in correspondence of the intersection between the vertical line of the alloy at 30% B and the horizontal line passing through T_Y. Instead, the two phases, that is, the two full dots (L and S) are positioned where the two one-phase fields are delimited by the liquidus and solidus lines. The field between these two lines is, therefore, a two-phase field.

5.6 Chemical composition of the phases

Phase diagrams are useful to define the chemical composition of the phases starting from the chemical composition of the alloy and the temperature.

The chemical composition of a phase can be easily determined: you need to descend vertically from the full dot and read the value of the chemical composition on the abscissa axis.

Let's look at a simple example. Take in consideration Figure 5.7 and focus on point X at temperature T_X.

The system has a chemical composition equal to 30% B and 70% A. The only phase present at that temperature is the liquid phase, which has a chemical composition equal to 30% B and 70% A. The system coincides totally with the only phase present and, therefore, the system and phase have the same chemical composition (the empty circle ○ and the full dot • coincide). Similar conclusions also apply to point Z.

The chemical system described by Y (empty circle) has a chemical composition equal to 30% B but the two phases, L and S (full dots), have a different chemical composition. Liquid phase L has a composition equal to 40% B and 60% A, while the solid phase S has a composition equal to 24% B and 76% A: the empty circle (○) and the two full dots (•) no longer coincide.

5.7 The lever rule

The number of phases at a given temperature can also be calculated through the phase diagram.

The problem does not arise when the system is one-phase (Figure 5.7): the system consists 100% of a single phase at points X and Z: at T_X, the system is entirely in an homogeneous liquid phase; whilst at T_Z, it is entirely in an homogeneous solid phase.

The problem arises when the system has two phases, such as at temperature T_Y. At T_Y, the chemical composition of the system and of the individual phases is known (see Paragraph 5.6 above), but it does not seem possible to determine how much of the system is already solid and how much is still liquid.

The so-called "lever rule" is used to obtain this data. This is a simple mathematical relationship based on the principle of mass conservation. Starting from the assumption that, in a two-phase system, the sum of the phases is always equal to 100%, the lever rule states that the quantity of the two phases (Q_L and Q_S) is inversely proportional to the distance from the point of equilibrium of the system.

This is an application of Archimede's Law of the first type Lever. The system represents the fulcrum (the position of the circle ○), while the quantity of the phases are the weights at the two ends (the full dots •) positioned at a distance that guarantees their balance (Figure 5.8).

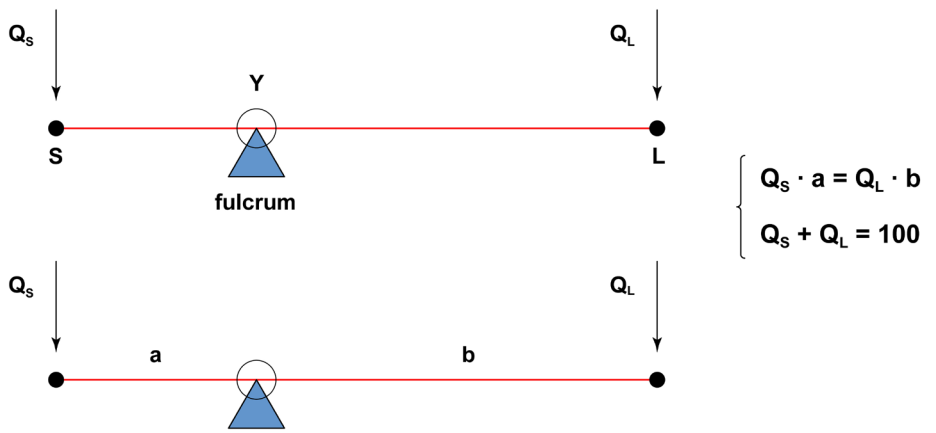

Figure 5.8 – Schematic representation of the lever rule: Q_S and Q_L represent the quantities of the solid phase S and the liquid phase L, point Y is the point of equilibrium of the system.

Segment $\overline{SY}$ is called a, and segment $\overline{YL}$ is called b; the quantity of the solid phase Q_S and the quantity of the liquid phase Q_L can be calculated using the following formulas:

$$Q_S = \frac{b}{a+b} \cdot 100\% \qquad Q_L = \frac{a}{a+b} \cdot 100\% \qquad [5.5]$$

Therefore at temperature T_Y, Q_S and Q_L are equal to:

$$Q_S = \frac{40-30}{40-24} \cdot 100 = 62.5\% \qquad Q_L = \frac{30-24}{40-24} \cdot 100 = 37.5\%$$

Therefore, at temperature T_γ, the quantity of the solid phase is 62.5%, while the quantity of the phase that is still liquid is 37.5%.

5.8 Phases and structural constituents (or microstructures)

Another important element to be taken into account is the distinction between phases and structural constituents.

The phase is a portion of a chemical system with the same chemical composition, state of aggregation, pressure and temperature, whilst the structural constituent (or microstructure) is an aggregation of one or more phases within an homogeneous or heterogeneous crystalline grain[17].

Let us take into account the simple case of the complete solid solution phase diagram. Let us suppose to observe the solidification process under a microscope.

The system solidifies in the form of single phase homogeneous crystals following the nucleation and growth mechanism[18].

Figure 5.9 shows a schematic representation of the solidification process. Note that all the grains are homogeneous and equal to each other: the phase is only one (green) but is repeated identically in the various crystalline grains. Therefore, the microstructure can be described as green homogeneous crystalline grains.

5.9 Eutectic phase digram

Not all metallic alloys are formed from chemical elements that have a complete solubility at a solid state. In many cases, the two elements, A and B can only be mixed together up to a certain content. A solubility gap occurs beyond this limit and, for example, an eutectic horizontal may appear on the phase diagram. Examples of metal alloys with partial solubility in the solid state and eutectic transformation are aluminum-silicon, iron-carbon, copper-silver, and lead-tin alloys (Figure 5.10).

[17] In the complete solid solution phase diagram the difference between phase and microstructure may not seem relevant. In this case, there is a perfect identity between the phase and the structural constituent. However, keep in mind that this distinction becomes fundamental in the case of complex structural constituents (with heterogeneous crystalline grains), such as those of the iron-carbon phase diagram.

[18] To this respect, see what is described in Paragraph 2.7 of Chapter 2.

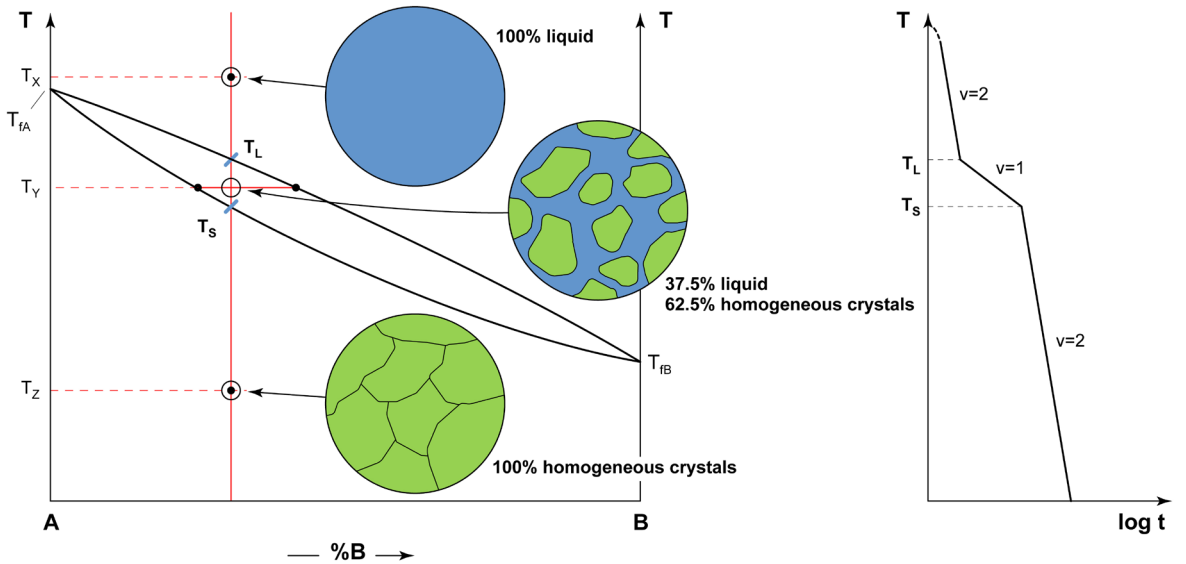

Figura 5.9 – Schematic representation of a generic complete solid solution phase diagram. Graphic representation of an alloy at 30% B and its equilibrium cooling curve.

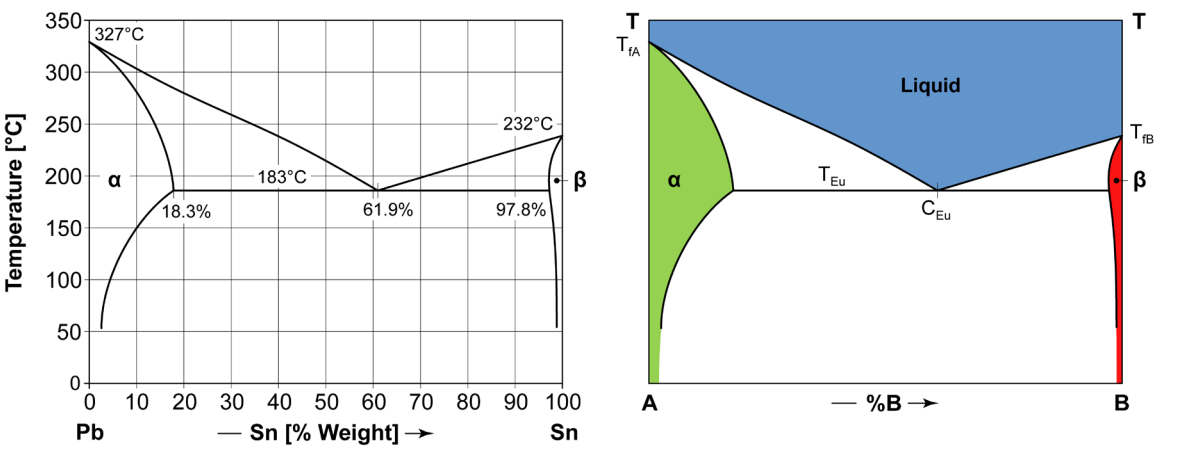

Figure 5.10 - Lead-tin phase diagram (*Pb-Sn*) [from ASM-H.3 1992] and its schematic representation.

Let us see now the schematic rapresentation of the phase diagram shown in Figure 5.10. The melting temperature of lead (T_{fA}= 327°C) is placed along the left vertical axis, and the melting temperature of tin (T_{fB} = 232°C) along the right vertical axis. The horizontal line at temperature T_{Eu} is called eutectic horizontal (183°C), while C_{Eu} indicates the composition of the eutectic alloy (61.9% *B*).

The one-phase field of the liquid (blue) is in the upper part of the diagram, while the one-phase fields of the two solid phases are indicated near the right and left vertical axes: (i) to the left, colored green, the phase rich in *A*, (ii) to the right, colored red, the phase rich in *B*.

The two solid state one-phase fields are indicated by the Greek letters α (α-phase rich in *A*) and β (β-phase rich in *B*). The solubility between *A* and *B* is not verified for every chemical composition but is limited at a temperature-dependent interval. At the eutectic temperature, for example, the solubility limit of *B* in α-phase is 18.3%, while the solubility limit of *A* in β-phase is 2.2%[19].

Let us examine the different types of alloys that can be obtained by equilibrium cooling. For each alloy, the phases and structural constituents are evaluated at various temperatures. To this regard, we observe the diagram in Figure 5.11 (different from that of Figure 5.10): for this diagram, the eutectic composition C_{Eu} is equal to 56% *B* and the solubility limits of α-phase and β-phase are respectively between 10% and 32% *B* and between 88% and 93% *B*.

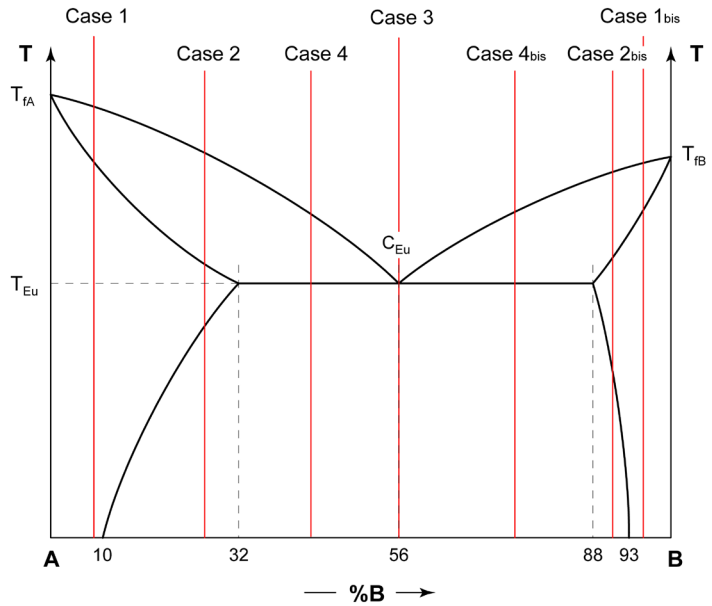

Figure 5.11 - Schematic representation of a generic eutectic phase diagram.

Case 1 (alloys with *B* < 10%)

First consider an alloy that falls completely into the α-phase field, that is, an alloy with a composition in *B* lower than the solubility limit of *B* in α-phase at room temperature (10%): this occurs if, for example, the chemical composition is equal to 8% *B* (Figure 5.12).

When solidification ends, there is complete solubility of the chemical element *B* in the lattice of α-phase.

[19] *The solubility limit of B in β-phase is equal to 97.8%, that is, 2.2% of A. Since β-phase is rich in B (from 97.8% to 100%), solubility should be expressed in terms of the content of A in β-phase.*

This condition remains unaltered until room temperature is reached. This result is perfectly consistent with what has already been observed for the complete solid solution phase diagram and, therefore, the alloy is made up of homogeneous crystalline grains of α-phase (green). The equilibrium cooling curve is also similar to that of the complete solid solution phase diagram.

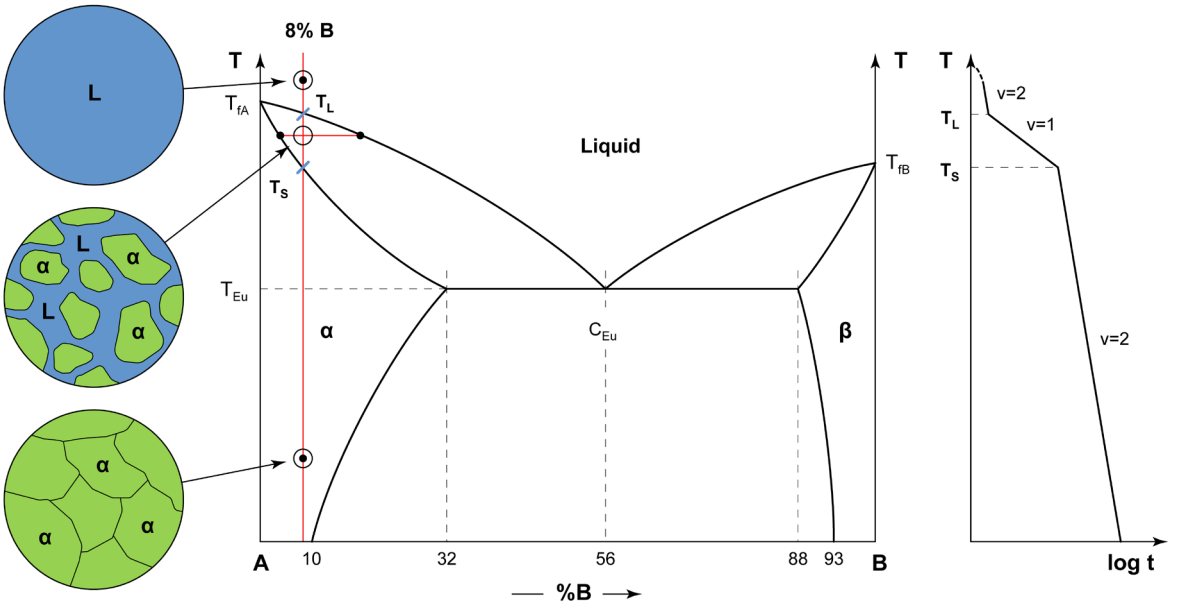

Figure 5.12 - Schematic representation of a generic eutectic phase diagram. Graphic representation of microstructure and equilibrium cooling curve of an alloy at 8% *B*.

Case 2 (alloys with 10% < *B* < 32%)

Let us now consider the alloy with a 24% *B*, that is, an alloy with a content of *B* between the solubility limit of *B* in α-phase at room temperature (10%) and the solubility limit of *B* in α-phase at eutectic temperature (32%). The proposed example is valid for any chemical composition in the interval between 10% and 32% (Figure 5.13).

In this second case, there is the important difference of the solubility limit. Up to the temperature of the solubility limit, T_{Sol}, the alloy is homogeneous and solidification takes place in the form of homogeneous crystals of α-phase, all identical to each other and green in color, similar to the alloy at 8% *B*. Below T_{Sol} the amount of *B* in excess in α-phase forms plates of β-phase at the grain boundary (red color). At room temperature, therefore, the alloy consists of homogeneous crystals of α-phase surrounded by plates of β-phase at the grain boundary.

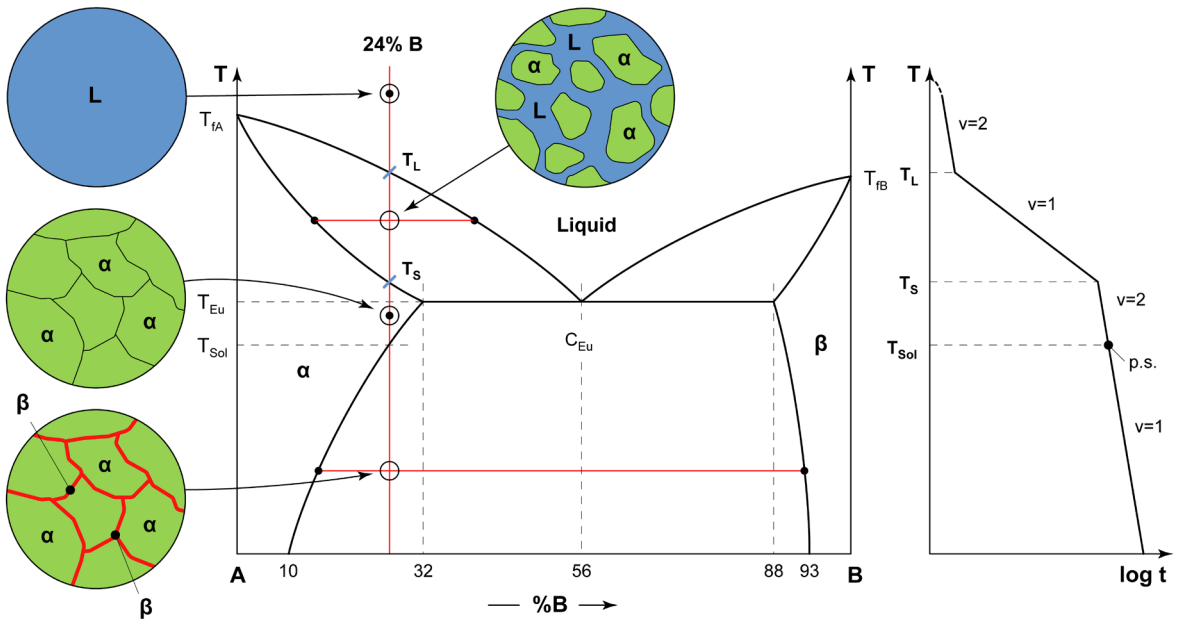

Figure 5.13 - Schematic representation of a generic eutectic phase diagram. Graphic representation of microstructure and equilibrium cooling curve of an alloy at 24% *B.*

It should be noted that the presence of a limit of solubility in metallic solid alloys is quite similar to the existence of a limit of solubility between a solute and a liquid solvent, as occurs in the case of sugar in tea. The amount of sugar that can be dissolved in a given amount of tea is limited and it depends on the temperature: the hotter the tea, the greater the amount of sugar can be dissolved. The excess sugar separates, depositing on the bottom of the container once the sugar solubility threshold in the tea is exceeded.
Something similar occurs for metallic alloys. The solubility limit of one element in one phase depends on the temperature and, once the solubility threshold is exceeded (in the case of Figure 5.13 temperature T_{Sol}), the excess of B forms plates of β-phase on grain boundary.
The quantity of the two phases at room temperature can be calculated with the lever rule. The quantity of homogeneous crystalline grains of α-phase and plates of β-phase is:

$$Q_{\alpha\, homogeneous\ crystals} = \frac{93-24}{93-10}\cdot 100 \cong 83.1\% \qquad Q_{\beta\, plates\ at\ grain\ boundary} = \frac{24-10}{93-10}\cdot 100 \cong 16.9\%$$

The cooling curve is not very different from the cases seen above (Figure 5.9 and Figure 5.12). The only difference is the discontinuity point at T_{Sol} (singular point p.s. on the equilibrium cooling curve).

The discontinuity point is due to the β-phase formation on grain boundary[20] and highlights a slight variation in slope of the equilibrium cooling curve.

Case 1bis (alloys with $\mathcal{B}$ > 93%) and 2bis (alloys with 88% < $\mathcal{B}$ < 93%)

Similar conclusions to case 1 and case 2 are obtained for the alloys that fall in the field of β-phase. The behavior of alloys with $\mathcal{B}$ > 93% is similar to those of alloys with $\mathcal{B}$ < 10%, with the difference that phases β and α are inverted. Similarly, the solidification method for alloys with 88% < $\mathcal{B}$ < 93% is similar to that of alloys with 10% < $\mathcal{B}$ < 32% (but always with inverted phases).

In the case, for example, of an alloy with 95% of $\mathcal{B}$ at room temperature (Figure 5.14), the microstructure is totally formed of homogeneous grains of β-phase (red color). On the other hand, for an alloy with 90% of $\mathcal{B}$ (Figure 5.15) the microstructure is formed of homogeneous crystals of β-phase (red color) surrounded by plates on the grain boundary of α-phase (green color).

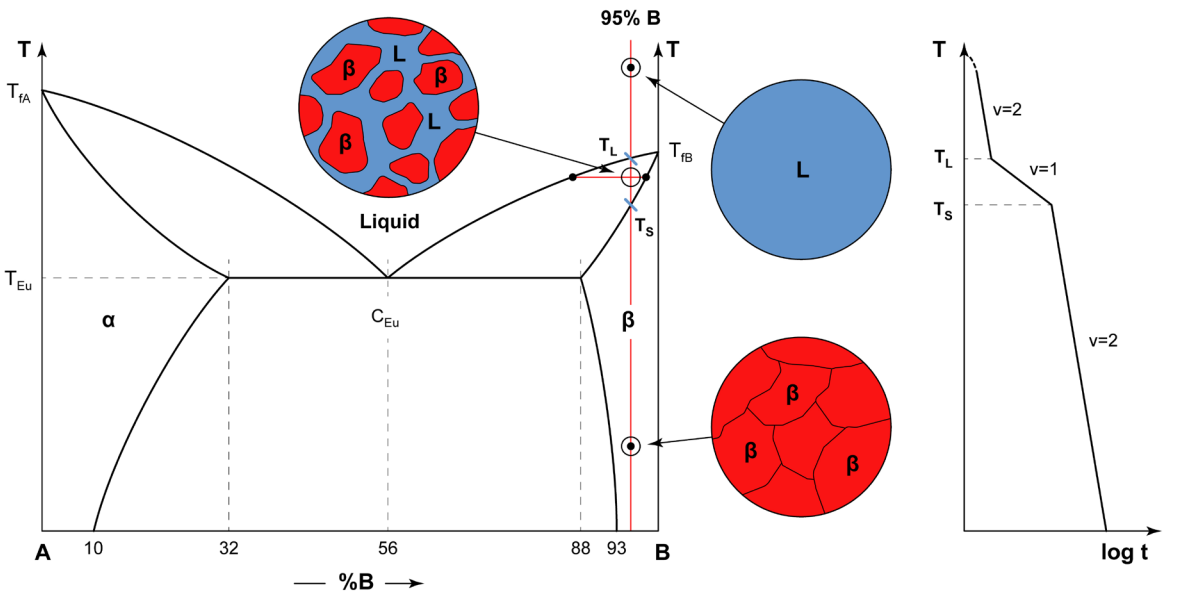

Figure 5.14 - Schematic representation of a generic eutectic phase diagram. Graphic representation of microstructure and equilibrium cooling curve of an alloy at 95% $\mathcal{B}$.

[20] *Since the passage is from a one-phase system (homogeneous crystals of α-phase) to a two-phase system (homogeneous crystals of α-phase and plates of β-phase), the value of the specific sensible heat , c , changes minimally and produce a slight variation in slope of the equilibrium cooling curve. The varation is not graphically evident and it is common practice to indicate a singular point on the equilibrium cooling curve.*

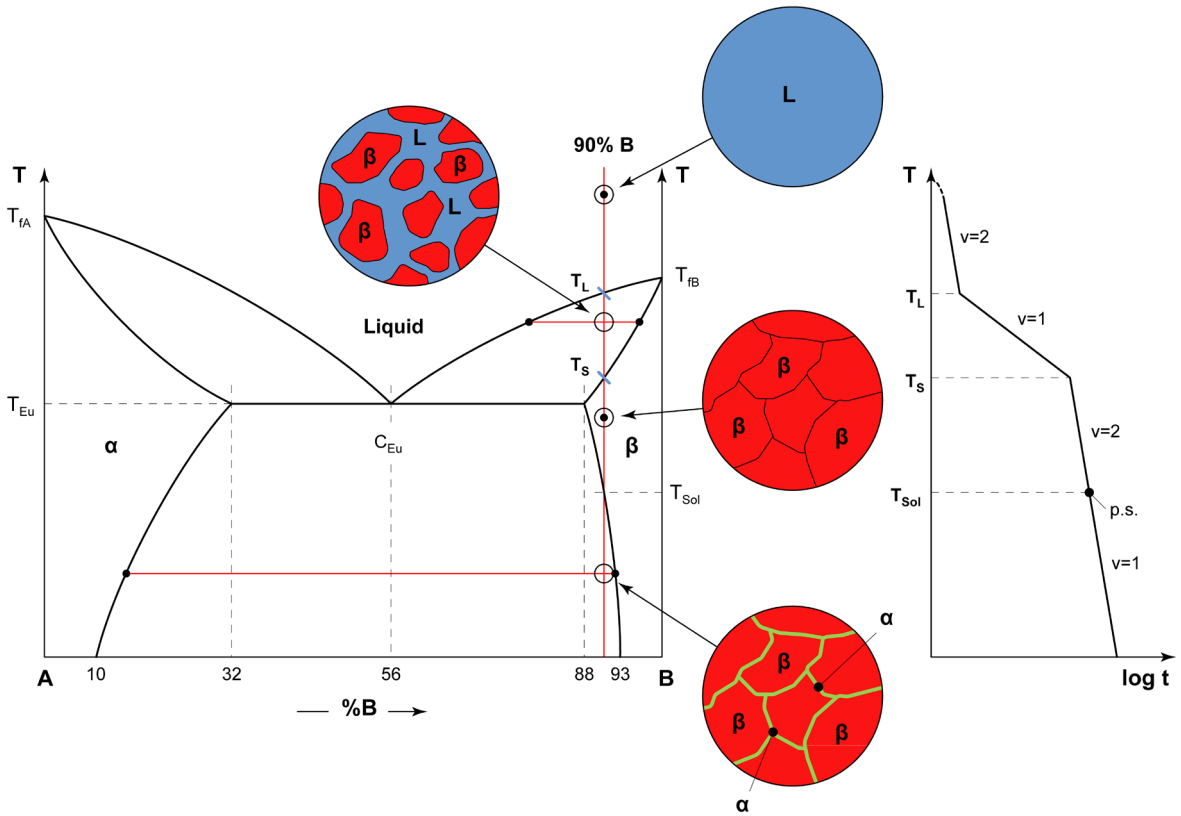

Figure 5.15 - Schematic representation of a generic eutectic phase diagram. Graphic representation of microstructure and equilibrium cooling curve of an alloy at 90% *B*.

Case 3 (eutectic alloy, *B* = 56%)

Now, let us consider what happens when the alloy intercepts the eutectic horizontal at T_{Eu} during solidification, that is, when the amount of *B* is between 32% and 88%. The eutectic horizontal has a peculiarity: it represents the lowest temperature at which alloy solidification can take place[21].

Let us first examine the eutectic composition alloy C_{Eu} (*B* = 56%): the various stages of solidification are shown in Figure 5.16.

[21] *The term, "eutectic", derives from the Greek, "eútēktos", which means "easy melting" and indicates that an eutectic alloy melts at a lower temperature as compared to its alloying elements.*

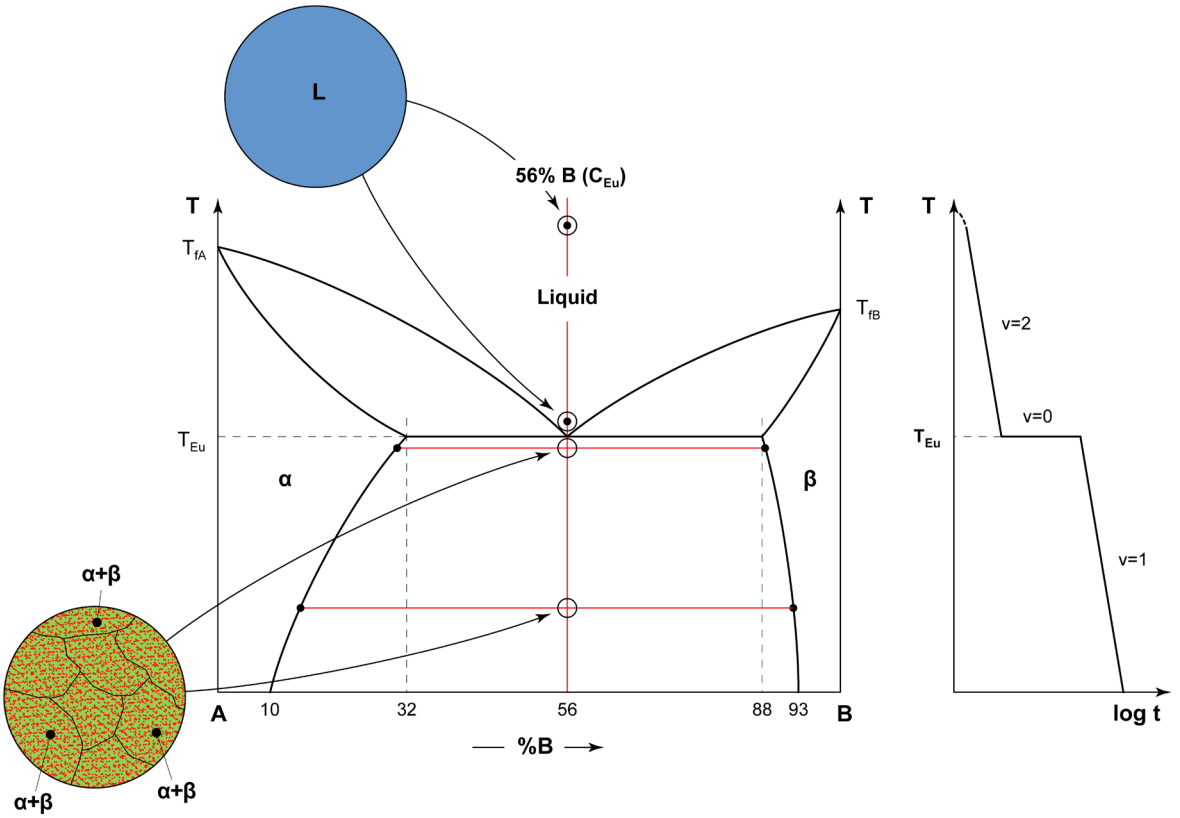

Figure 5.16 - Schematic representation of a generic eutectic phase diagram. Graphic representation of microstructure and equilibrium cooling curve of an alloy at 56% *B*.

The system is completely liquid up to an infinitesimal of a degree above the eutectic temperature. Therefore, once T_{Eu} is reached, the alloy solidifies and, through nucleation and growth, forms a crystalline structure characterized by α and β phases. At the temperature of a infinitesimal degree below T_{Eu} the system is completely in solid phase.

The microstructure obtained through this method of solidification is called eutectic structure. In the eutectic microstructure the two phases, α and β, are not separated into homogeneous grains but are connected to each other within each single grain. Therefore, heterogeneous crystalline grains of α and β phases are formed. As shown in Figure 5.17, the eutectic structure may have a lamellar (the most typical), globular, or acicular shape, depending on the alloy.

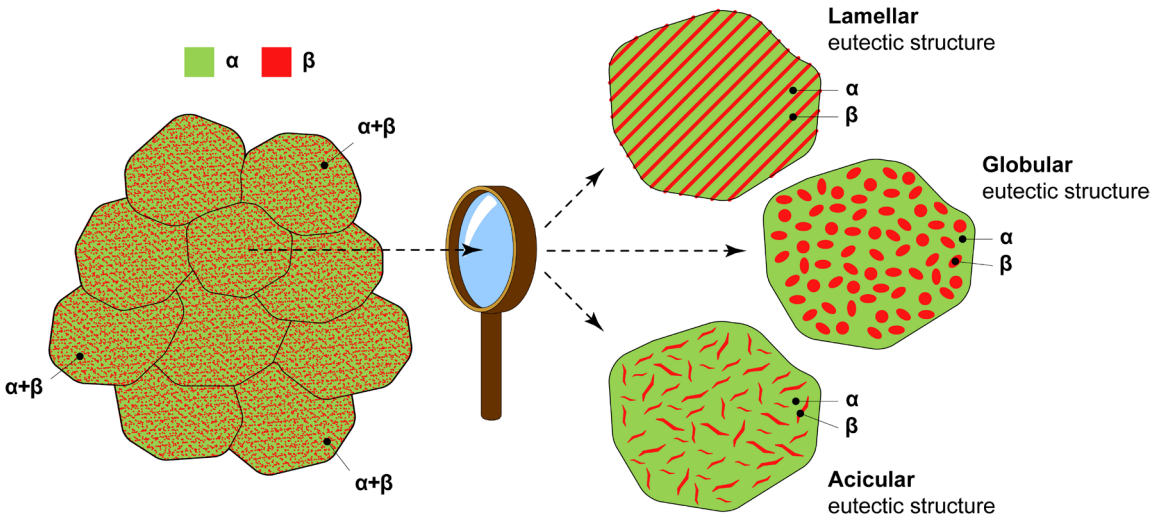

Figure 5.17 - Graphic representation of the eutectic microstructures.

An infinitesimal of a degree below T_{Eu}, the alloy at 56% B is made up of 100% eutectic crystals. The amount of the two phases within the eutectic grains can be calculated with the lever rule. The result is:

$$Q_{\alpha\, in\ eutectic\ crystals} = \frac{88-56}{88-32}\cdot 100 \cong 57.1\% \qquad Q_{\beta in\ eutectic\ crystals} = \frac{56-32}{88-32}\cdot 100 \cong 42.9\%$$

Therefore, if the eutectic crystals have a lamellar nature, the 57.1% of the lamellae is formed by α-phase and 42.9% by β-phase.

In the transition from eutectic temperature to room temperature, there is a change in the solubility of B in α-phase (that goes from 32% to 10%) and of A in β-phase (that goes from 12% to 7%). Consequently, there is a variation in the amount of the two phases in the eutectic crystals. At room temperature, the lever rule gives the following result:

$$Q_{\alpha\, in\ eutectic\ crystals} = \frac{93-56}{93-10}\cdot 100 \cong 44.6\% \qquad Q_{\beta in\ eutectic\ crystals} = \frac{56-10}{93-10}\cdot 100 \cong 55.4\%$$

At room temperature the system is always comprised of 100% lamellar crystals but the amount of the phases is slightly different: 44.6% α and 55.4% β.

During the eutectic transformation, the equilibrium cooling curve undergoes a substantial modification. Thermostatation always occurs at the eutectic horizontal while at temperatures above or below T_{Eu} the cooling law follows a well-known trend[22].

[22] *The trend of the cooling curves above and below the eutectic horizontal is similar to that observed for chemical systems with homogeneous aggregation state (all liquid or all solid).*

Thermostatation depends to the variance value that equals[23]:

$$V = C_i + M - F = 2 + 1 - 3 = 0$$

which implies maintaining the temperature at constant levels until solidification is complete (the system has no degree of freedom). An isothermal arrest is typical of all eutectic horizontal and is similar to what occurs during the solidification of pure metals (Figure 5.5).

Case 4 (hypoeutectic alloys with 32% < *B* < 56%) and Case 4bis (hypereutectic alloys with 56% < *B* < 88%)[24]

We come now to the case of hypoeutectic and hypereutectic alloys. We first see the evolution of the hypoeutectic alloy at 40% *B* during equilibrium cooling (Figure 5.18).

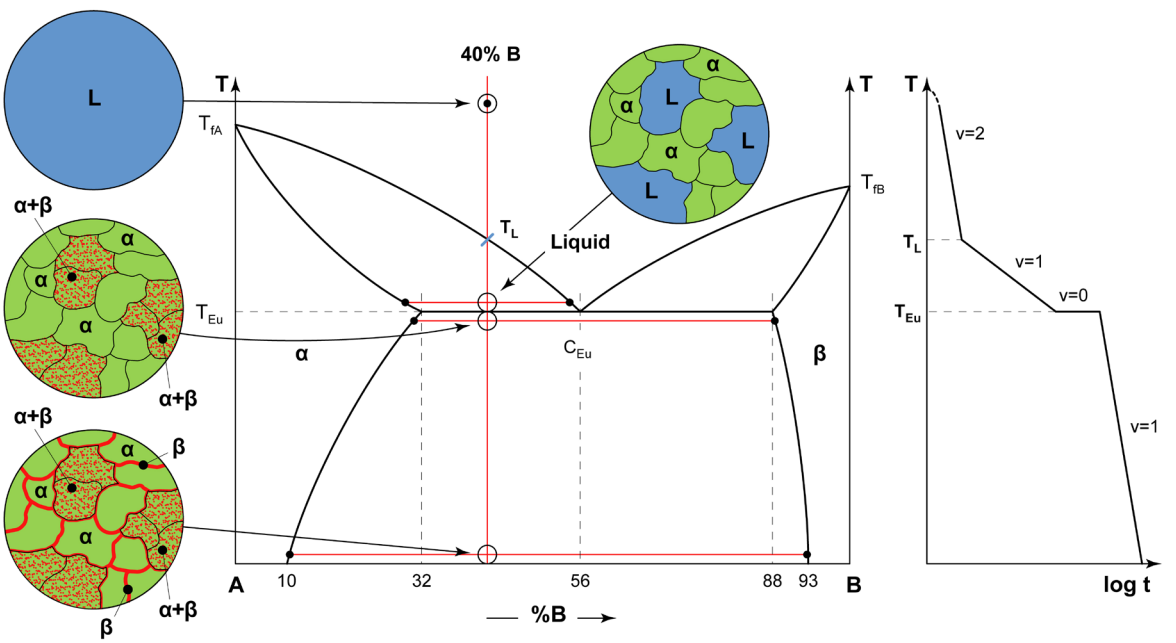

Figure 5.18 - Schematic representation of a generic eutectic phase diagram. Graphic representation of microstructure and equilibrium cooling curve of an alloy at 40% *B*.

[23] *Note that, during solidification, three phases coexist: α-phase, β-phase, and liquid.*

[24] *The prefixes "hypo" and "hyper" derive from Greek and are often used to indicate lower or higher conditions to a level considered normal. In this case, the reference is the eutectic alloy.*

The alloy in Figure 5.18 has a content 60% of A that is, greater than the content of A in the eutectic alloy (44% of A and 56% of B). Therefore, before the eutectic transformation at T_{Eu} occurs, the alloy must change its chemical composition and reduce the amount of A in excess. This phenomenon occurs during the initial phase of solidification, between temperatures T_L and T_{Eu}, when a solid fraction of homogeneous crystals of α-phase (i.e. the phase rich in A) separates from the liquid. Consequently, after reaching an infinitesimal of a degree above the eutectic temperature, the system is partially formed by the homogeneous crystals of α-phase and the liquid that has reached the composition C_{Eu}[25].

The eutectic transformation occurs at T_{Eu} and involves only the liquid that forms the eutectic microstructure. After the eutectic transformation, the system is comprised of homogeneous grains of α-phase formed between T_L and T_{Eu} and eutectic grains of α-phase and β-phase, formed from the liquid at T_{Eu}.

Let us calculate, using the lever rule, the phases present upstream and downstream of the eutectic temperature. At an infinitesimal of a degree above T_{Eu}, the result is equal to:

$$Q_\alpha = \frac{56-40}{56-32} \cdot 100 \cong 66.7\% \qquad Q_{liquid} = \frac{40-32}{56-32} \cdot 100 \cong 33.3\%$$

where the α-phase is in homogeneous crystals.

Since the eutectic transformation involves only the liquid, the quantities of structural constituents downstream of T_{Eu} are:

- 66.7% of homogeneous crystals of α-phase;
- 33.3% of eutectic crystals of α+β phases.

At an infinitesimal of a degree below T_{Eu}, the result is the following:

$$Q_\alpha = \frac{88-40}{88-32} \cdot 100 \cong 85.7\% \qquad Q_\beta = \frac{40-32}{88-32} \cdot 100 \cong 14.3\%$$

The quantities of α and β phases, represent the totality of the phases at that temperature (i.e. an infinitesimal of a degree below T_{Eu}).Therefore, at the end of the eutectic transformation, the distribution of the phases in the two structural constituents is:

- 66.7% of homogeneous crystals (66.7% of α-phase);
- 33.3% of eutectic crystals containing 19%[26] of α-phase and 14.3% of β-phase[27].

---

[25] *The crystalline grains that separate from the liquid before the eutectic transformation are also called pro-eutectic crystals.*

[26] *α-phase, in the eutectic structural constituent (19%), is obtained as the difference between the total of α-phase calculated at an infinitesimal of a degree below T_{Eu} (85.7%) less the part of α-phase that is already present in homogeneous crystals (66.7%). This calculation can be performed because the lever rule allows to calculate the totality of the phases at a given temperature.*

[27] *All the quantities of the phases calculated with the lever rule refer to the totality of the chemical system and not to the individual structural constituents.*

Finally, in the transition from the eutectic temperature to room temperature, there is a change in the solubility of B in α-phase and of A in β-phase which produces a double variation of the structure:

- homogeneous crystals of α-phase form plates of β-phase on the grain boundary (as was observed for the alloy in Figure 5.13);
- the amount of the two phases in the eutectic grains changes (as was observed for the alloy in Figure 5.16).

Therefore, at room temperature, the alloy at 40% B is comprised of:

- homogeneous crystals of α-phase,
- plates of β-phase at the grain boundary of the homogeneous crystals of α-phase,
- eutectic crystals of α + β phases.

For this condition (room temperature), the calculation of the phases amount within structural constituents was omitted: this calculation presents some issues that are out of the discussion of this text.

It is now important to discuss the equilibrium cooling curve of the alloy at 40% B: this brings together, in a single graph, the characteristics that have already been examined for the alloy at 24% B (Figure 5.13) and the alloy at 56% B (Figure 5.16).

Above T_L the equilibrium cooling curve is equal to that of a system at a liquid state ($V = 2$), then an initial solidification occurs with the formation of homogeneous crystals of α-phase between T_L and T_{Eu}. In this area, the phases are 2 ($V = 1$), and the slope of the equilibrium cooling curve becomes lower.

At T_{Eu}, variance becomes nil ($V = 0$) and thermostatation occurs until solidification is completed. Subsequently, the alloy cools down to room temperature with a slope similar to that at the liquid state (the system is completely at a solid state). Note that the variance in this latter area is 1 ($V = 1$) because the α and β phases[28] are simultaneously present.

The case of hypereutectic alloys is similar to that of hypoeutectic alloys, making sure to invert the phases of the system. Consider, for example, the generic hypereutectic alloy at 70% of B (Figure 5.19).

The only difference with hypoeutectic alloys is the excess of B as compared to the eutectic alloy (70% B in the hypereutectic alloy against 56% of B of the eutectic alloy). Consequently, during solidification, the system between T_L and T_{Eu} separates the homogeneous crystals of β-phase (the phase rich in B) to give origin, to a liquid of eutectic composition at T_{Eu}.

[28] This specification is rather important because underlines that the slope of the equilibrium cooling curve should never correlated to the variance value. The case of Figure 5.18 is symbolic: the equilibium cooling curve has the same slope when the system is completely liquid or completely solid, but in the first case the variance value is two and in the second case the variance value is one.

At T_{Eu}, liquid is transformed into the eutectic microstructure, while the homogeneous crystals of β-phase remain unchanged.

Finally, during equilibrium cooling to room temperature, homogeneous crystals of β-phase form plates on the grain boundaries and lamellae of α and β phases modify its relative quantities within the eutectic grains.

At room temperature, a generic hypereutectic alloy has the following microstructures:

- homogeneous crystals of β-phase,
- plates of α-phase at the grain boundary of the homogeneous crystals of β-phase,
- eutectic crystals of α + β phases.

The equilibrium cooling curve is equal to that of the hypoeutectic alloy at 40% of *B*.

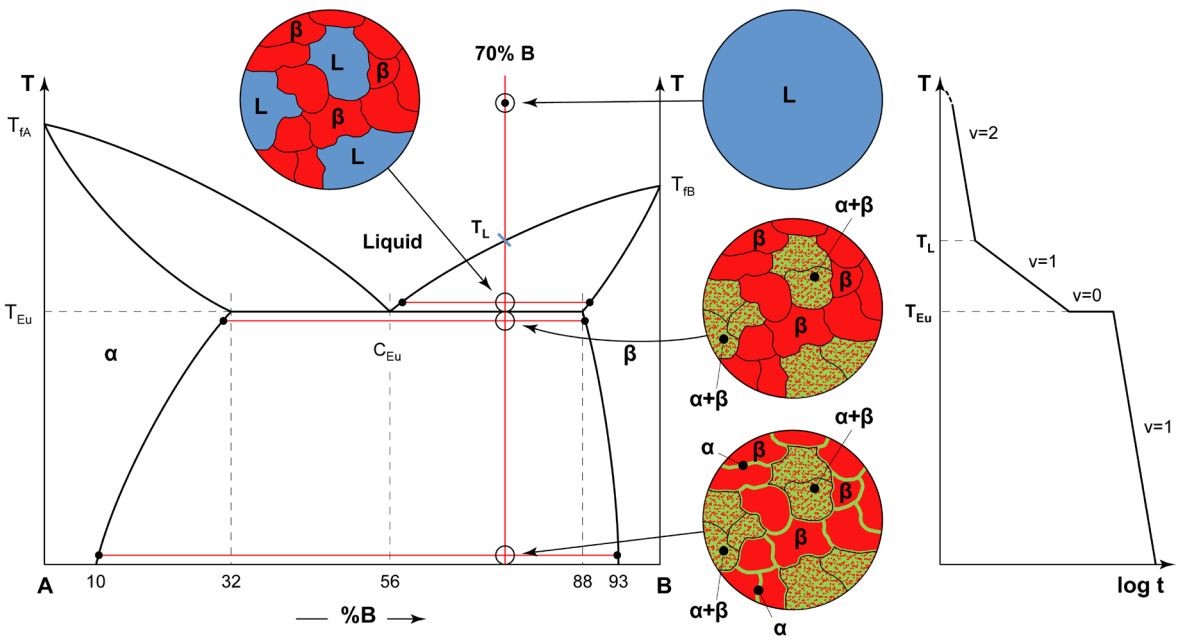

Figure 5.19 - Schematic representation of a generic eutectic phase diagram. Graphic representation of microstructure and equilibrium cooling curve of an alloy at 70% *B*.

5.10 Peritectic phase diagram

In diagrams of partial solubility at solid state, the so-called "peritectic transformation" may be present, as an alternative to the eutectic transformation. Examples of metal alloys with peritectic transformation are copper-zinc, iron-carbon, and platinum-silver alloys (Figure 5.20).

The schematic representation in Figure 5.20 shows the one-phase field of the liquid at the top of the diagram (blue color). The one-phase field of the solid phases are also indicated to the left, α-phase rich in *A* (green color), and to the right, β-phase rich in *B* (red color). Horizontal line at temperature T_{Pe} is called peritectic horizontal (1186°C), while C_{Pe} is the alloy of peritectic composition (44.7%).

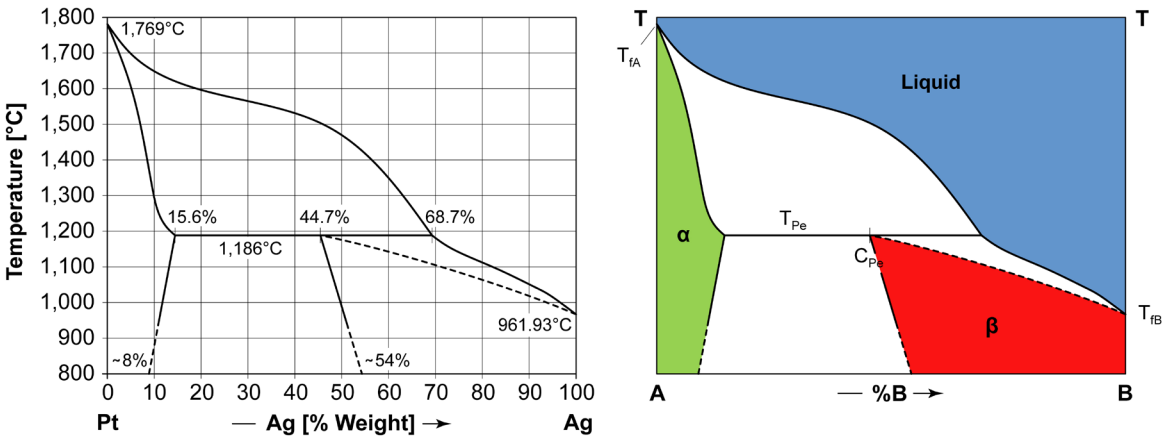

Figura 5.20 – Platinum-silver (*Pt-Ag*) phase diagram [from ASM-H.3 1992] and its schematic representation.

Let us now examine the different types of alloys that can be obtained by equilibrium cooling. For each alloy, the phases and structural constituents are evaluated at the various temperatures. To this regard, observe the diagram in Figure 5.21 (different from that of Figure 5.20). For this diagram, the peritectic composition C_{Pe} is equal to 57% *B* and the solubility limits are between 4% and 12% *B* for α-phase and between 52% and 57% *B* for β-phase.

Case 1 (alloys with $B < 4\%$)

Alloys with a content of *B* less than 4% do not intercept the peritectic horizontal: their equilibrium cooling curves are quite similar to that of Figure 5.12 (Case 1 of the eutectic phase diagram).

Case 2 (alloys with $4\% < B < 12\%$)

Alloys with a content of *B* between 4% and 12% also do not intercept the peritectic horizontal: their equilibrium cooling curves are quite similar to that of Figure 5.13 (Case 2 of the eutectic phase diagram).

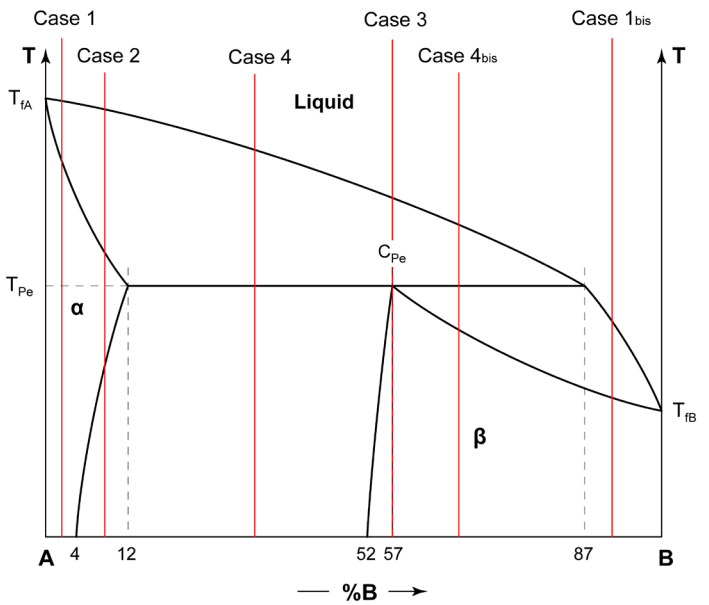

Figure 5.21 - Schematic representation of a generic peritectic phase diagram.

Case 1bis (alloys with $B > 87\%$)

Alloys with a content of B greater than 87% also do not intercept the peritectic line: their equilibrium cooling curves are quite similar to that of Figure 5.14 (Case 1bis of the eutectic phase diagram).

Case 3 (peritectic alloy with $B = 57\%$)

The first case refers to the peritectic alloy with $B = 57\%$ (Figure 5.22).

The alloy begins to solidify starting from temperature T_L with the formation of homogeneous crystals of α-phase. Solidification continues to an infinitesimal of a degree above T_{Pe}; at this temperature the system is comprised of homogeneous crystals of α-phase and liquid, their quantities can be calculated with the lever rule:

$$Q_\alpha = \frac{87-57}{87-12} \cdot 100 \cong 40\% \qquad Q_{liquid} = \frac{57-12}{87-12} \cdot 100 \cong 60\%$$

The peritectic transformation occurs at T_{Pe}, similar to a sort of "chemical reaction" between reagents and products[29]. Liquid and α-phase in homogeneous crystals act as reagents that give origin, as a product, to β-phase in homogeneous crystals. In summary, we have:

$$liquid + \alpha \rightarrow \beta$$

[29] *No chemical reaction occurs during the peritectic transformation: this concept has been only used to point out that phases and structural constituents before the peritectic transformation have nothing in common with phases and structural constituents after the transformation.*

It should be noted that the microstructure formed during peritectic transformation is always composed of homogeneous crystals.

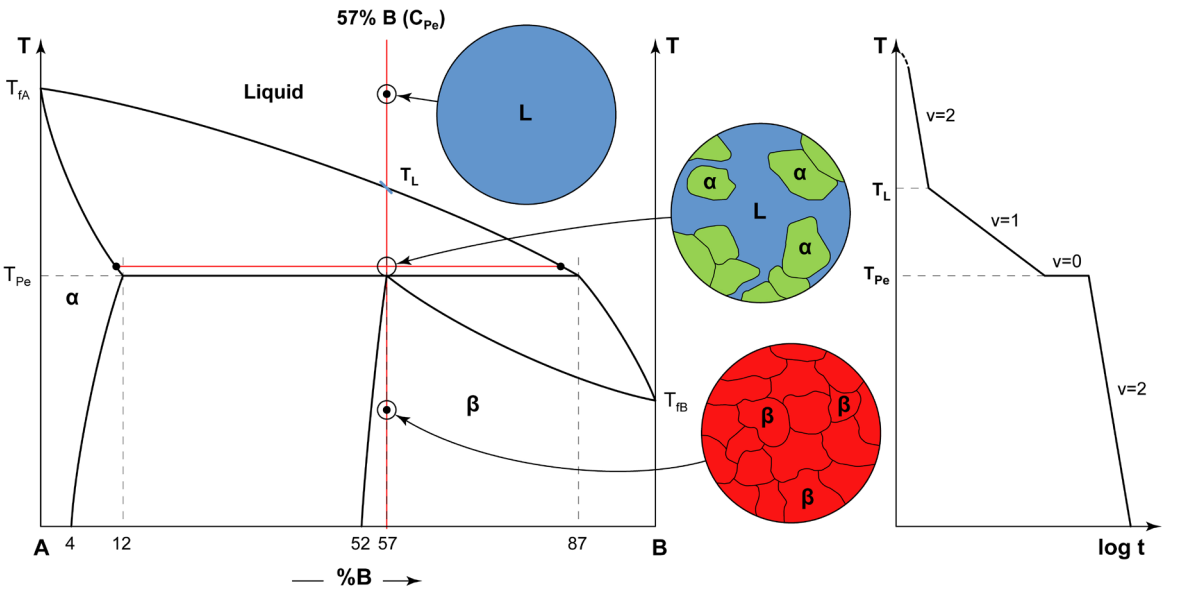

Figure 5.22 - Schematic representation of a generic peritectic phase diagram. Graphic representation of microstructure and equilibrium cooling curve of an alloy at 57% *B*.

The equilibrium cooling curve is similar to that of the alloys in Figure 5.18 or 5.19. Above T_L, the equilibrium cooling curve is typical of a liquid state system ($V = 2$). Subsequently, between T_L and T_P, there is partial solidification ($V = 1$): the cooling curve slope becomes lower, due to the latent heat of solidification Q_l. At peritectic temperature T_{Pe}, the variance is:

$$V = C_i + M - F = 2 + 1 - 3 = 0$$

and temperature stops until solidification is completed. Finally, when the system is completely solid, the alloy cools down to room temperature, with a cooling rate equal to that in the liquid state.

Case 4 (alloy with 12% < *B* < 52%)[30]

We consider the chemical composition at 32% *B* (Figure 5.23). As in the previous case, the alloy starts solidifying at T_L, forming homogeneous crystals of α-phase. Their amount increases until the peritectic horizontal is reached. Upstream of T_{Pe}, the amount of the two phases is:

$$Q_\alpha = \frac{87-32}{87-12} \cdot 100 \cong 73.3\% \qquad Q_{liquid} = \frac{32-12}{87-12} \cdot 100 \cong 26.7\%$$

while downstream, the system is formed by both α-phase and by β-phase in the following quantities:

$$Q_\alpha = \frac{57-32}{57-12} \cdot 100 \cong 55.6\% \qquad Q_\beta = \frac{32-12}{57-12} \cdot 100 \cong 44.4\%$$

The peritectic transformation can be schematized as follows:

$$liquid + \alpha \rightarrow \alpha + \beta$$

where solid α and β phases are both in homogeneous crystals.

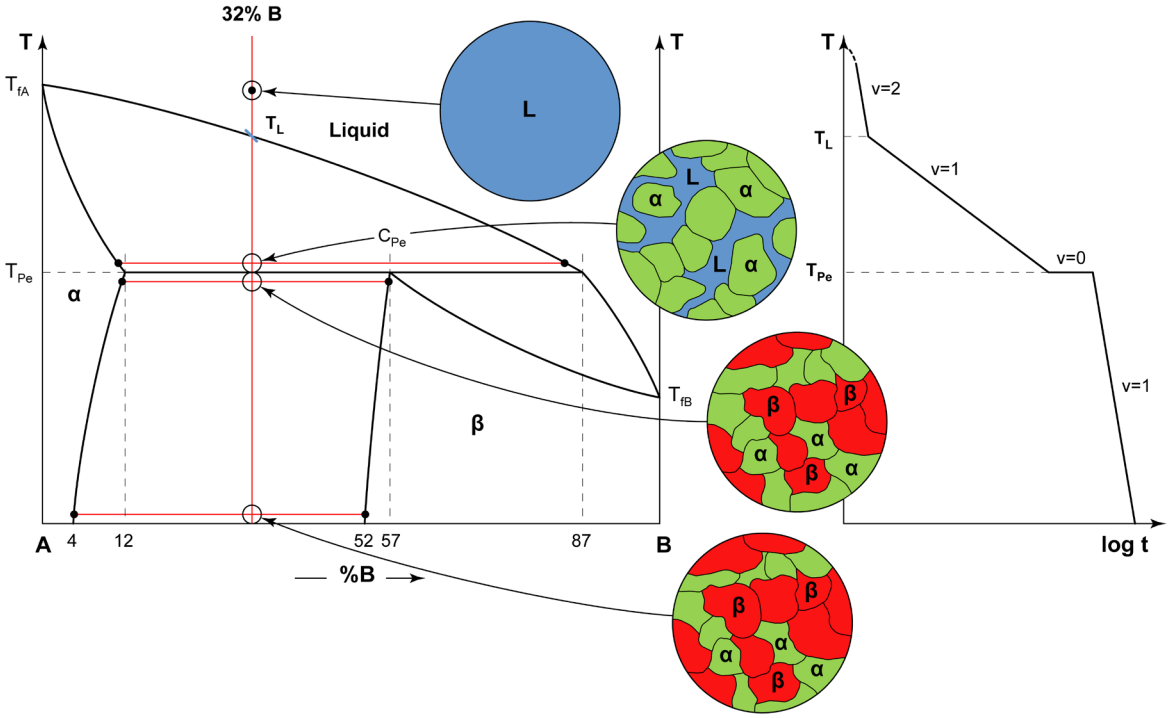

Figure 5.23 - Schematic representation of a generic peritectic phase diagram. Graphic representation of microstructure and equilibrium cooling curve of an alloy at 32% *B*.

[30] *In the case of the peritectic horizontal, the prefixes, hypo- and hyper-, are not used to indicate chemical composition alloys that are lower or greater than the peritectic value.*

Solubility variation of α and β phases is observed from peritectic temperature to room temperature. In this case, since both phases are present at T_{Pe}, no new phase is formed. The quantities of the phases at room temperature are equal to:

$$Q_\alpha = \frac{52-32}{52-4} \cdot 100 \cong 41.7\% \qquad Q_\beta = \frac{32-4}{52-4} \cdot 100 \cong 58.3\%$$

The amount of the two structures at room temperature (homogeneous crystals of α-phase and homogeneous crystals of β-phase) is slightly different from what is calculated downstream T_{Pe}.
The equilibrium cooling curve is similar to that of Case 3[31].

Case 4bis (alloy with 57% < *B* < 87%)

The alloy used as reference has 70% *B* (Figure 5.24).
The alloy begins to solidify starting from temperature T_L with the formation of homogeneous crystals of α-phase. An infinitesimal of a degree above T_{Pe}, the amount of liquid and of α-phase in homogeneous crystals is:

$$Q_\alpha = \frac{87-70}{87-12} \cdot 100 \cong 22.7\% \qquad Q_{liquid} = \frac{70-12}{87-12} \cdot 100 \cong 77.3\%$$

Peritectic transformation occurs at T_{Pe}. Liquid and homogeneous crystals of α-phase give origin to liquid and homogeneous crystals of β-phase, according to "reaction":

$$liquid + \alpha \rightarrow liquid + \beta$$

Once the peritetic transformation has ended the system is still partially liquid. As a result of the cooling, the alloy completes its solidification at temperature T_S in the form of homogeneous crystals of β-phase.

The equilibrium cooling curve shows a thermostatation at the peritectic temperature.

Between T_L - T_{Pe} and T_{Pe}-T_S, the slope of equilibrium cooling curve is similar and it is lower than the slope observed for temperature above T_L or below T_S. The change in slope betwen T_L - T_{Pe} and T_{Pe}-T_S is due to latent heat, Q_l.

[31] *Downstream of T_{Pe}, the equilibrium cooling curve has the same pattern for both Case 3 and Case 4, since the system is completely solid. The variance change, V = 2 in case 3 and V = 1 in case 4, has no effect on the slope of the equilibrium cooling curve.*

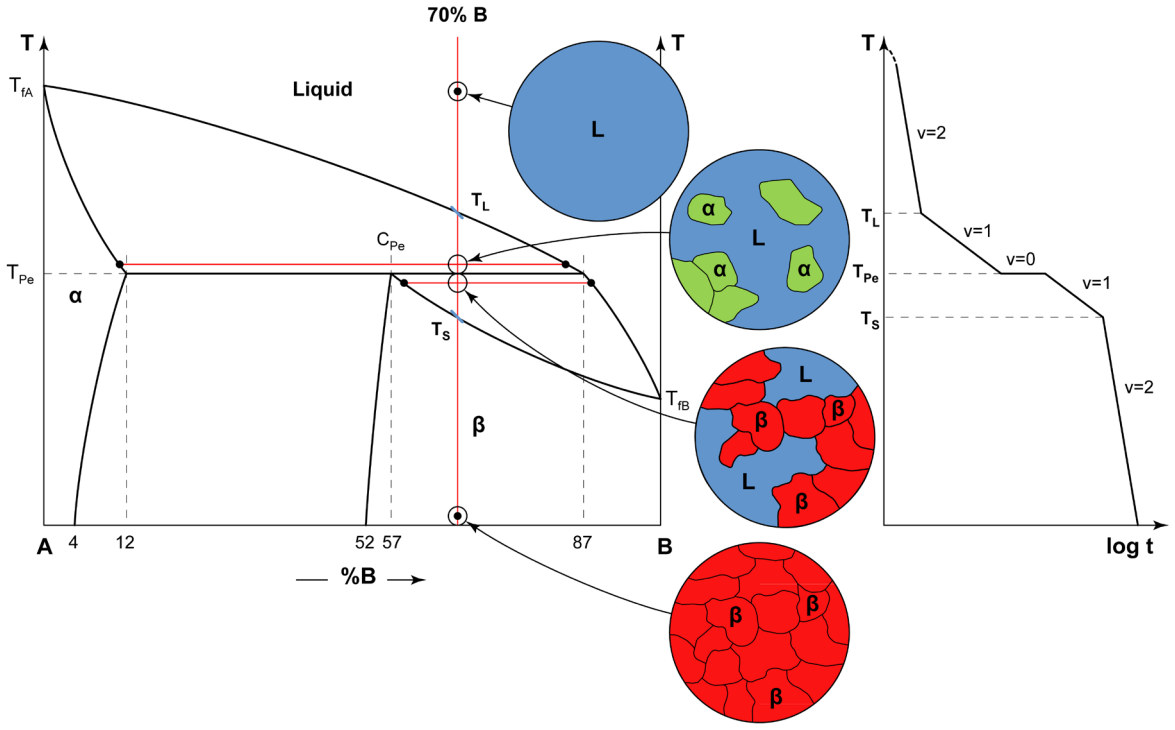

Figure 5.24 - Schematic representation of a generic peritectic phase diagram. Graphic representation of microstructure and equilibrium cooling curve of an alloy at 70% *B*.

5.11 Intermediate phases

Often, binary phase diagram are more complex than those seen in previous paragraphs: they normally highlight various structural transformations, not just one[32]. These structural transformations are related to phases of an intermediate chemical composition between pure metal *A* and pure metal *B*[33].

A typical example is the copper-zinc phase diagram (Figure 5.25). In addition to the liquid phase (blue), α-phase (green, rich in copper) and η-phase (red, rich in zinc) there are also β, γ, δ and ε phases (all represented in yellow): these intermediate phases have different chemical composition, depending on the temperature and derive from various peritectic transformations.

[32] *The phase diagrams studied in the previous paragraphs have always considered a single structural transformation (eutectic or peritectic).*

[33] *The phase diagrams studied in the previous paragraphs have always considered the existence of a single solid phase (diagram of complete solubility at solid state) or of two solid phases (diagram of partial solubility at solid state), respectively rich in metal A (α-phase) and metal B (β-phase).*

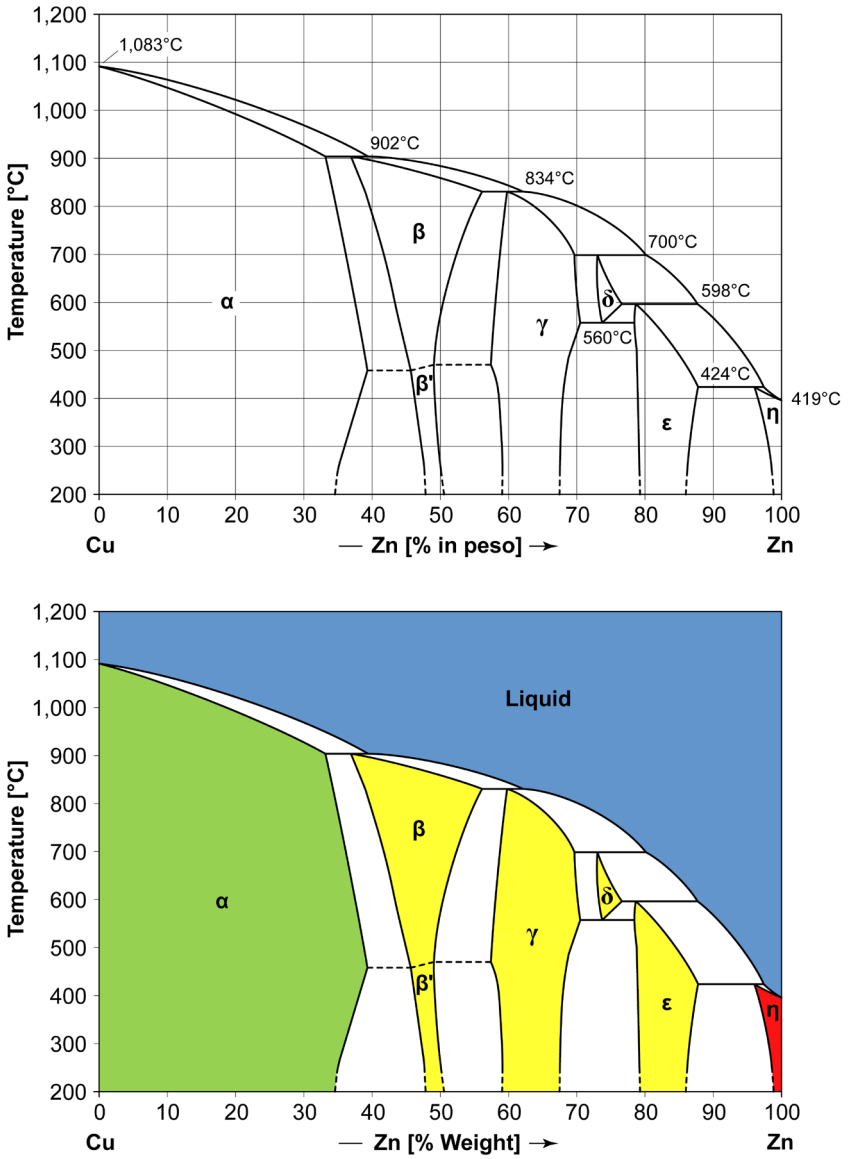

Figure 5.25 - The copper-zinc phase diagram (*Cu-Zn*) [from ASM-H.3 1992] and its schematic representation.

On the contrary when the chemical composition of the intermediate phases is uniquely defined, we speak of compounds (intermetallic or interstitial[34]). These are represented on the phase diagram by a vertical line in correspondence of the stoichiometric chemical composition of the compound. A typical example is the magnesium-lead phase diagram (Figure 5.26).

[34] *To this regard, see Paragraph 2.3 of Chapter 2.*

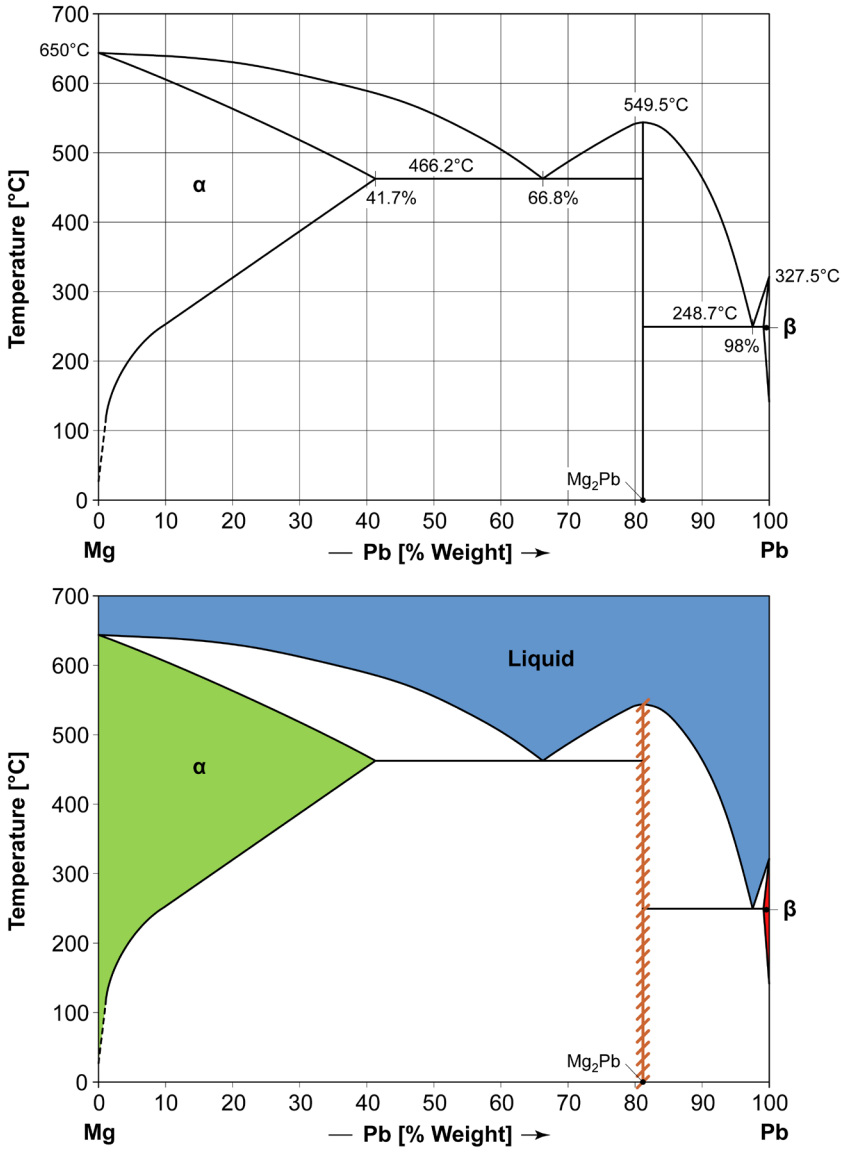

Figure 5.26 - Magnesium-lead phase diagram (*Mg-Pb*) [from ASM-H.3 1992] and its schematic representation.

In the *Mg-Pb* phase diagram Mg_2Pb exists from room temperature to melting temperature (549.5°C) and it is limited to the single vertical line containing 81% of lead (outlined in light brown).

Phase Mg_2Pb is properly called an intermetallic compound, since it consists of two metallic elements (*Mg* and *Pb*) in specific stoichiometric ratios (two magnesium and one lead atom).

The intermetallic compound Mg_2Pb also acts as a limit between two eutectic horizontal lines, one on the left (466.2°C) and the other on the right (248.7°C) of the vertical line at 81%.

The presence of a compound (intermetallic or interstitial) does not modify the considerations regarding the quantitative evaluations of the phase diagram in Figure 5.26 (chemical composition, Gibbs Phase Rule, lever rule, structural constituents, etc.): the compound Mg_2Pb is considered as a one-phase field whose area is reduced to a vertical line.

Figure 5.27 shows the solidification of a hypoeutectic alloy with 52% lead. As can be seen, the structural constituents are similar to those of the alloy in Figure 5.18, where the β-phase is replaced by intermetallic compound Mg_2Pb.

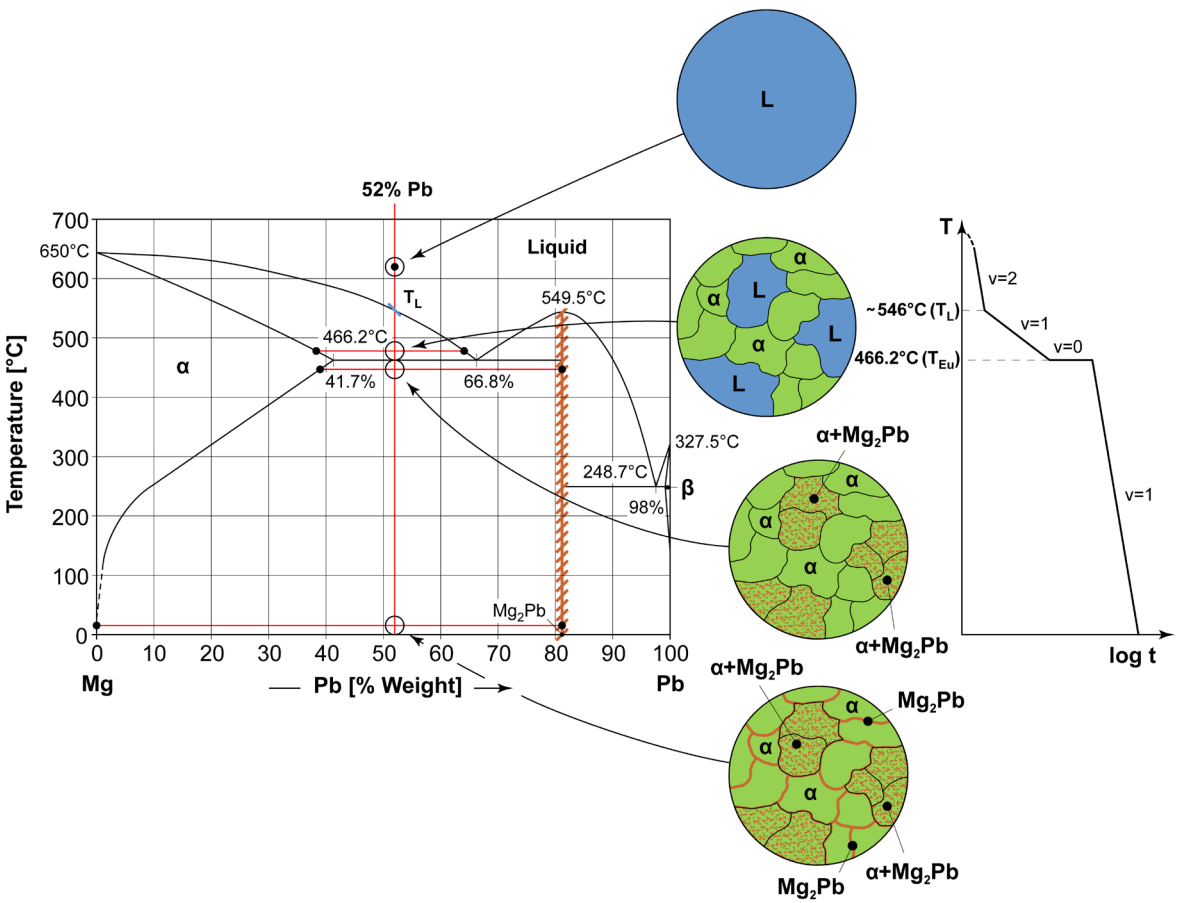

Figure 5.27 - Magnesium-lead phase diagram (*Mg-Pb*) [from ASM-H.3 1992] and schematic representation of the equilibrium cooling curve of an alloy with 52% lead.

5.12 Solid state transformations

The eutectic and peritectic transformations are not exclusive to liquid phase, but they can also occur in the solid state.

If they occur at a solid state, they are called eutectoid or peritectoid transformations: the only difference is the aggregation state of the phase undergoing transformation, which is in a solid state rather than in a liquid state. Consider the example in Figure 5.28 that shows two simple phase diagrams arranged one over the other.

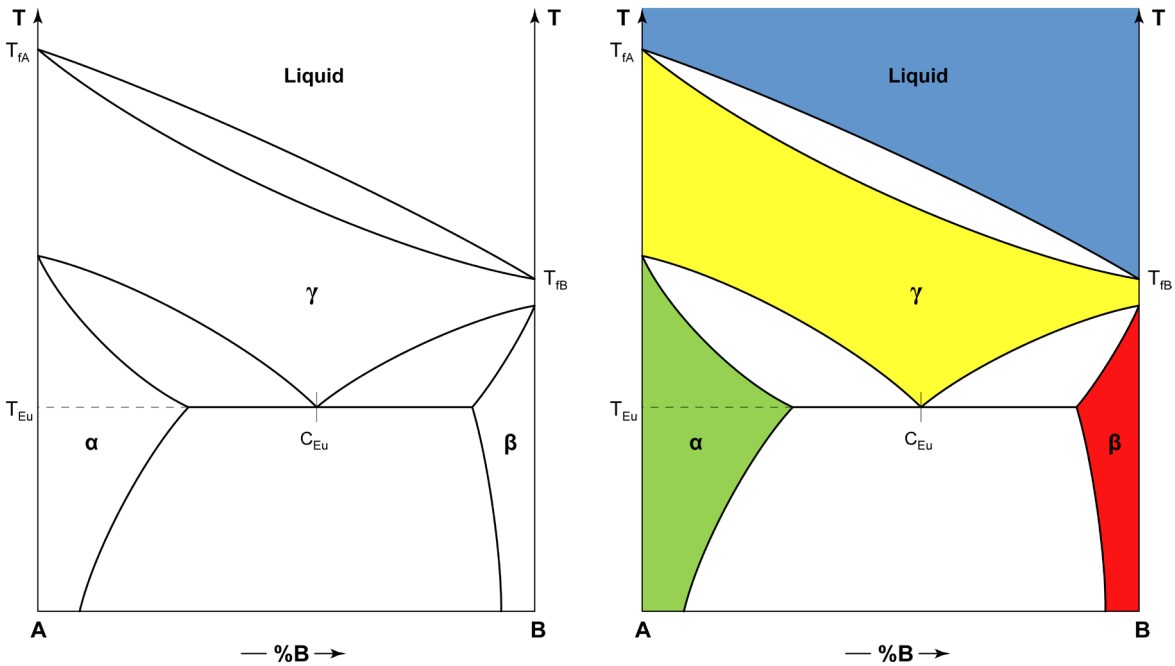

Figure 5.28 - Generic binary phase diagram with an eutectoid transformation.

This diagram is elementary and derives from what is seen on simple phase diagrams.

Considering a generic alloy at 70% *B* (Figure 5.29), that is, an hypereutectoid alloy[35]. Solidification always occurs with the formation of homogeneous crystals of γ-phase (yellow) which undergo a partial transformation in homogeneous crystals of β-phase (red) during cooling. An eutectoid transformation, similar to the eutectic transformation in Figure 5.19 occurs at T_{Eu}: in case of eutectic horizontal, the transformation occurs on liquid, while in case of eutectoid horizontal the transformation occurs, on the solid state γ-phase. The eutectoid transformation is, therefore, analogous to the eutectic transformation, even if it involves the solid state γ-phase and not the liquid.

[35] *There are also hypoeutectoid and hypereutectoid alloys in addition to hypoeutectic and hypereutectic ones.*

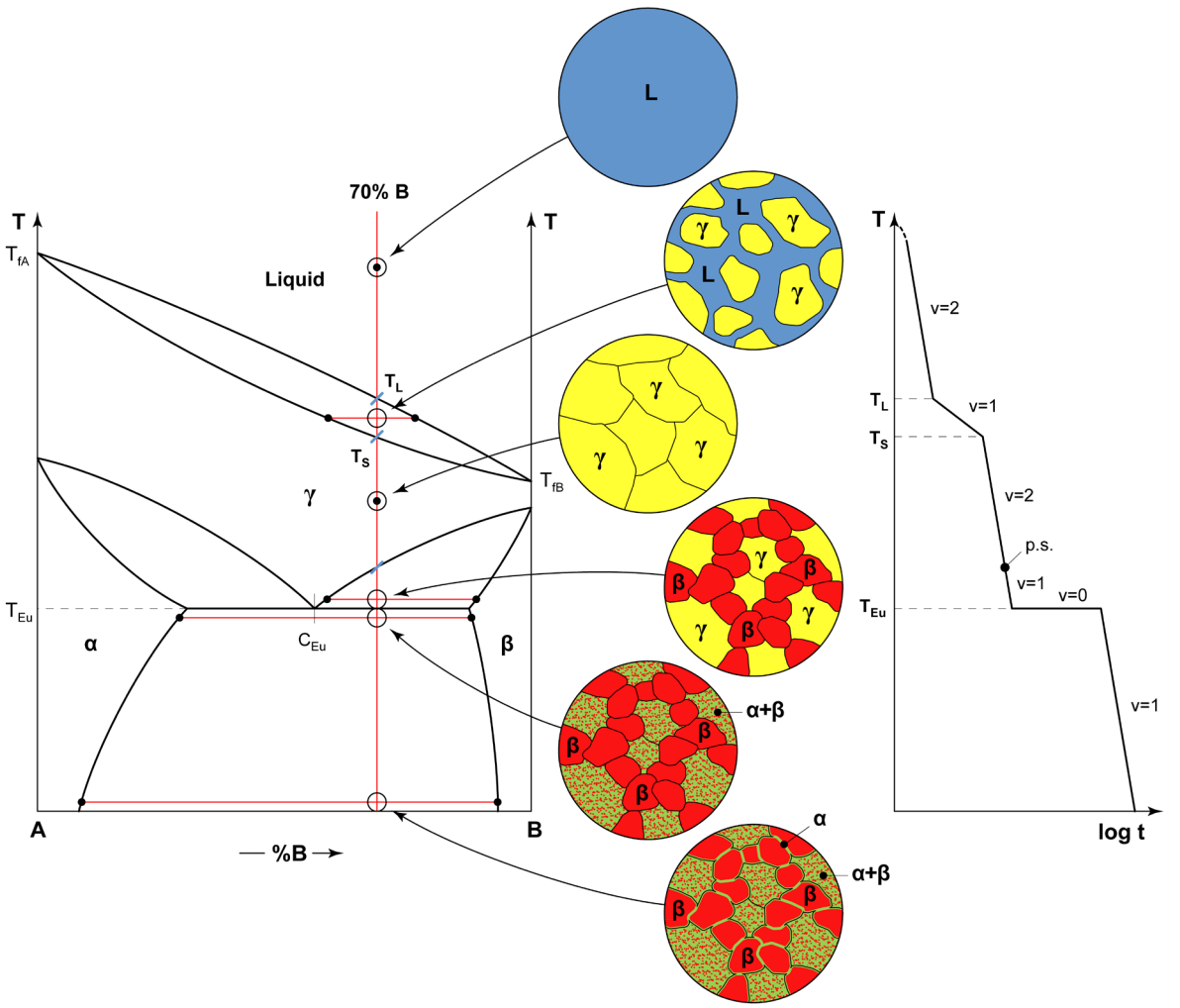

Figure 5.29 - Generic binary phase diagram with an eutectoid transformation and schematic representation of the equilibrium cooling curve of an alloy at 70% *B*.

The eutectoid transformation forms a lamellar structure:

$$liquid \rightarrow \alpha_{lamellar} + \beta_{lamellar} \ \ (eutectic\ transformation)$$
$$phase\ \gamma \rightarrow \alpha_{lamellar} + \beta_{lamellar} \ \ (eutectoid\ transformation)$$

The result of a peritectoid transformation is:

$$liquid + \alpha \rightarrow \beta_{homogeneous\ crystals} \ \ (peritectic\ transformation)$$
$$\alpha + \gamma \rightarrow \beta_{homogeneous\ crystals} \ (peritectoid\ transformation)$$

Figure 5.30 shows the set of liquid state and solid state transformations in phase diagrams.

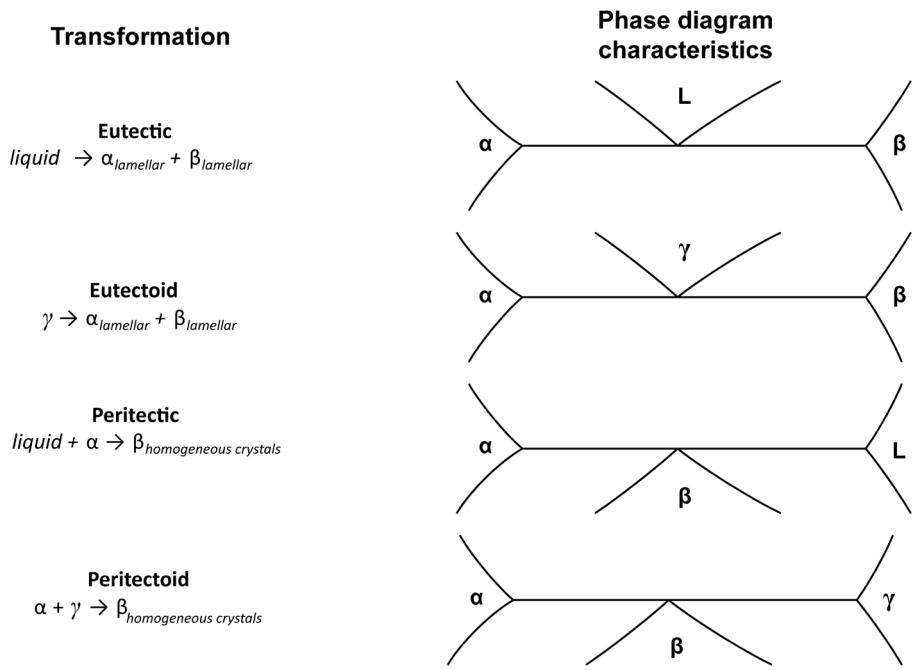

Figure 5.30 - Example of liquid state (eutectic and peritectic) and solid state (eutectoid and peritectoid) transformations in phase diagrams.

6. IRON-CARBON PHASE DIAGRAM (*Fe-C*)

6.1 Why is the *Fe-C* phase diagram required?

The starting point for the study of steel is the iron-carbon phase diagram (Figure 6.1) which shows the phases[1] of the alloy under conditions of thermodynamic equilibrium as temperature[2] and carbon content changes.

The *Fe-C* phase diagram has three structural transformations ($V = 0$): peritectic transformation at 1,495°C, eutectic transformation at 1,148°C, and eutectoid transformation at 727°C.

In addition to the liquid, the one-phase fields of the *Fe-C* phase diagram are four:

- α-phase (light green) at the bottom left of the diagram, from 912°C up to room temperature. α-phase has a very limited amplitude and a maximum carbon solubility of 0.02% at 727°C;
- γ-phase (yellow) between 1,394°C and 912°C. γ-phase has a large extension on the diagram and a maximum carbon solubility of 2.11% at 1,148°C;
- δ-phase (light brown) at top left on the diagram, between melting temperature at 1,538°C and 1,394°C. δ-phasea has a very limited amplitude and a maximum carbon solubility of 0.09% at 1,495°C;
- Fe_3C phase (red), on the vertical axis to the right of the diagram. Fe_3C phase has constant carbon composition of 6.69%, from melting temperature to room temperature.

Conventionally, the *Fe-C* alloys are divided into steel and cast iron: steel, if carbon is less than 2.11%, cast iron if higher.

The *Fe-C* phase diagram has several peculiarities. It is limited at 6.69% carbon, i.e. the stoichiometric percentage of carbon in iron carbide (Fe_3C). Beyond this value, the alloys that do not have any practical use, since the excess carbon separates from the iron in the form of graphite.

Another peculiarity is related to the solubility of iron and carbon in the liquid state: it is assumed that carbon is soluble in the liquid throughout the entire extension of the phase diagram. Practically, however, the solubility of carbon in iron is limited to about 5%[3]. This is why the liquidus curve, at the top right in the *Fe-C* phase diagram, is indicated with a dotted line.

Finally, iron carbide (Fe_3C) is a metastable compound, i.e. non-stable: it tends to decompose into iron and graphite carbon (g) according to the reaction [6.1]:

$$Fe_3C \rightarrow 3Fe + C_{(g)} \quad [6.1]$$

[1] *For the phase definition, see paragraph 5.1 of Chapter 5.*

[2] *As already observed in Chapter 5, the cooling rate of an alloy on the phase diagram is always very slow (equilibrium cooling). This allows the system, at each infinitesimal variation in temperature, to return to equilibrium, that is, to uniformize the temperature and the chemical composition of the phases at all points of the system (see also note 13 of Chapter 1).*

[3] *Over 5%, carbon separates from the liquid in the form of graphite.*

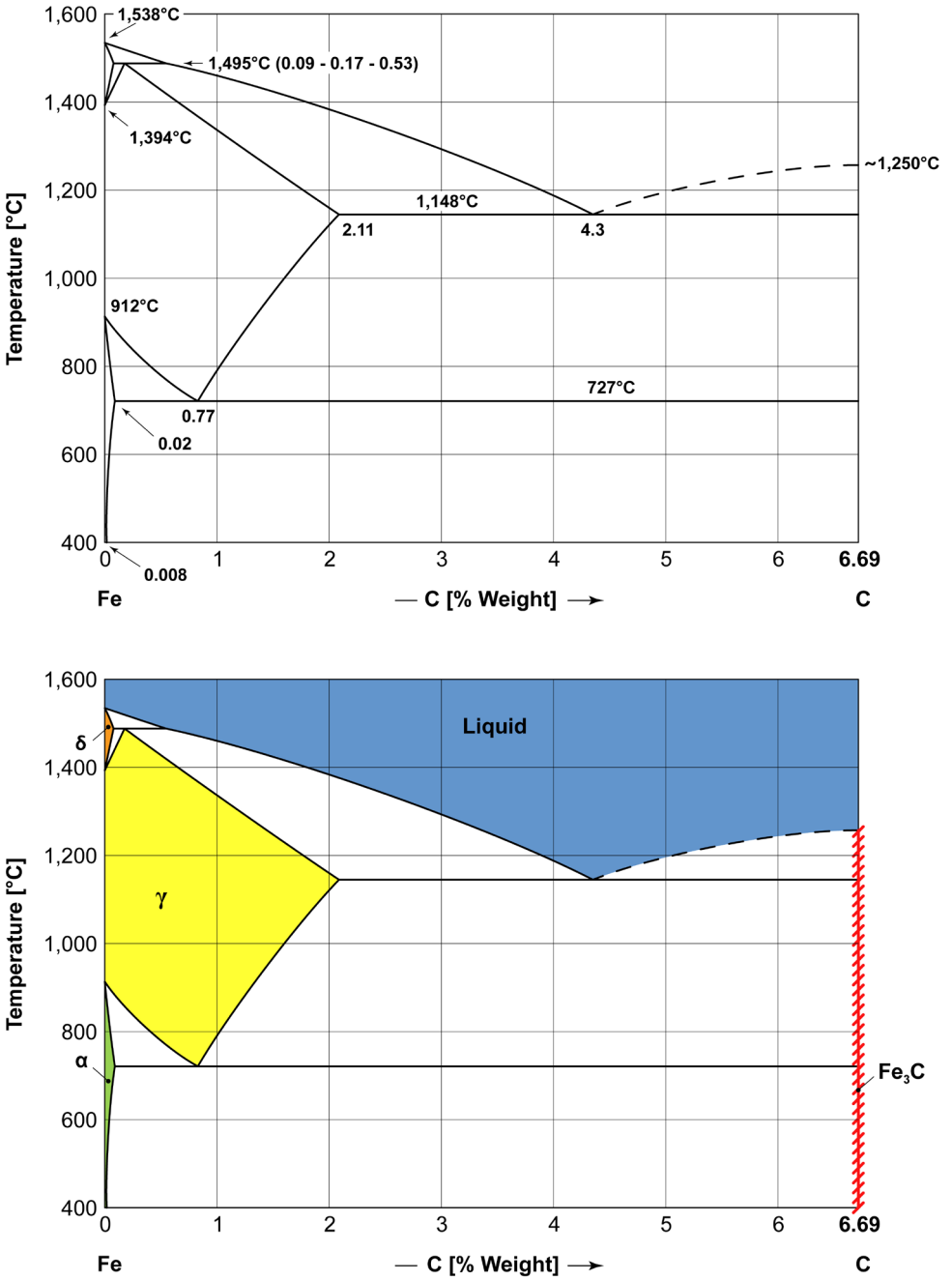

Figura 6.1 – *Fe-C* phase diagram. The one-phase fields are highlighted with different colors [from ASM-H.3 1992].

Since the decomposition of iron carbide takes place over a very long period of time, the reaction [6.1] can be neglected. This is particularly true for steel and for cooling rate used in industrial applications. However, graphite is to be considered for cast iron, especially in case of elements that promote graphitization.

6.2 Eutectoid, hypoeutectoid, and hypereutectoid steel

The cooling of *Fe-C* alloys can be studied by dividing the different types of steel into two families:

- hypoeutectoid steel, if $C < 0.77\%$,
- hypereutectoid steel, if $C > 0.77\%$,

since steel with $C = 0.77\%$ is the eutectoid alloy that divides the two families.

Case 1: Eutectoid steel ($C = 0.77\%$)

Let us first consider the case of eutectoid steel ($C = 0.77\%$) and study the trend of its phases during equilibrium cooling, from melting to room temperature, as provided by the *Fe-C* phase diagram (Figure 6.2). Initial solidification occurs between T_L and T_S (temperature of liquidus and solidus) and involves the formation of homogeneous crystals of γ-phase. Subsequently the alloy undergoes the eutectoid transformation at 727°C. The eutectoid transformation is similar to the eutectic one, already described in Chapter 5. The only difference is related to the phase that is transformed: during the eutectic, it is the liquid phase while, during the eutectoid, it is the γ-phase at solid state.

The eutectoid of the *Fe-C* phase diagram is particular and always involves the transformation of homogeneous crystals of γ-phase in crystals of lamellar nature, with alternating lamellae of α and Fe_3C phases.

Therefore, at an infinitesimal of a degree less than 727°C, the structure of eutectoid steel consists of 100% of crystals with alternating lamellae of α-phase and of Fe_3C phase (Figure 6.3).

During the final cooling, from the eutectoid temperature to room temperature, the system is always composed of 100% of lamellar crystals.

The quantity of the two phases (α and Fe_3C) at 20°C can be calculated with the lever rule[4]:

$$Q_\alpha = \frac{6.69 - 0.77}{6.69 - 0.008} \cdot 100 \cong 88.6\% \qquad Q_{Fe_3C} = \frac{0.77 - 0.008}{6.69 - 0.008} \cdot 100 \cong 11.4\%$$

[4] *At 727°C the quantity of α-phase is ~88,8% and the amount of Fe_3C phase is ~11,2%. The difference compared to the same quantities calculated at 20°C depends on the variation of carbon solubility in α-phase.*

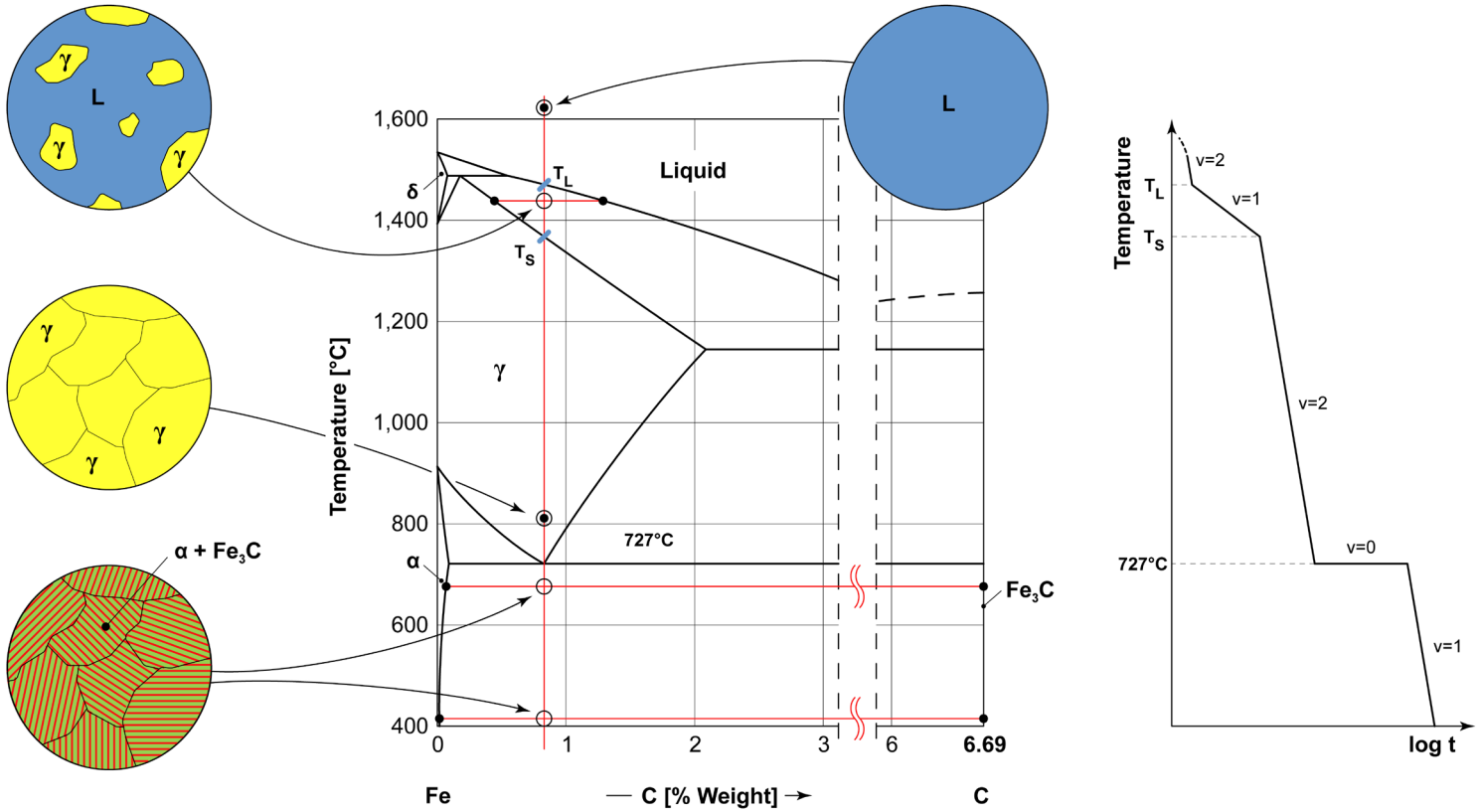

Figure 6.2 - *Fe-C* phase diagram. Graphic representation of microstructure and equilibrium cooling curve of an eutectoid steel ($C = 0{,}77\%$).

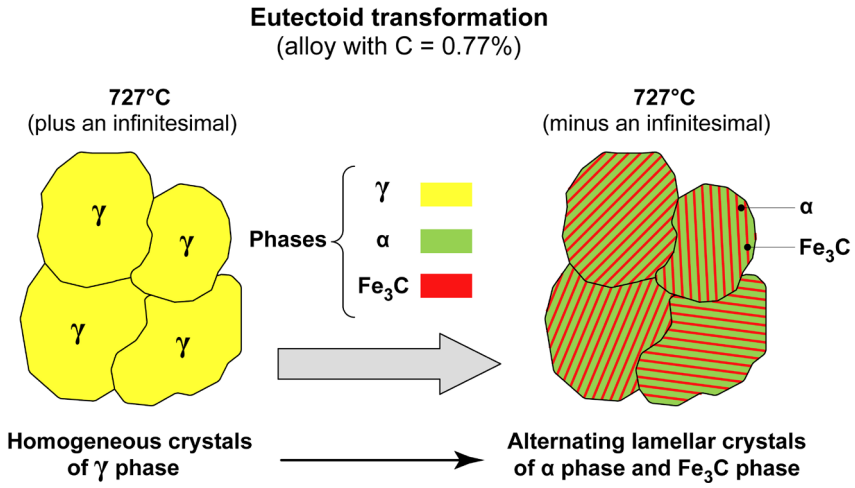

Figure 6.3 - Graphic representation of the eutectoid transformation of the alloy with $C = 0.77\%$.

Case 2: Hypoeutectoid steel ($0.02\% < C < 0.77\%$)

Let us now consider the case of hypoeutectoid steel, i.e. *Fe-C* alloys with carbon contents less than 0.77% (Figure 6.4).

A generic hypoeutectoid steel, during solidification between T_L and T_S, crosses the area of the peritectic horizontal at 1,495°C. In particular:

- alloys with $0.02\% < C < 0.09\%$ solidify in homogeneous crystals of δ-phase and then turn completely into homogeneous crystals of γ-phase;
- alloys with $0.09\% < C < 0.53\%$ undergo a peritectic transformation and, then give rise to a system of homogeneous crystals of γ-phase;
- alloys with $0.53\% < C < 0.77\%$ solidify in homogeneous crystals of γ-phase.

As can be observed, below a certain temperature level, the system is entirely formed of homogeneous crystals of γ-phase. Consider, for example, what happens to any hypoeutectoid alloy at 1,300°C: from that temperature[5] and up to temperature T_1, the system consists of 100% of homogeneous crystals of γ-phase.

[5] *Hypoeutectoid alloys consist of homogeneous crystals of γ-phase, even for temperatures above 1,300°C. The numeric indication of 1,300°C has no specific value: it is only a purely indicative value (it could also be 1,200°C or 1,350°C) to make the reader aware that the system is fully in γ-phase for a wide temperature range.*

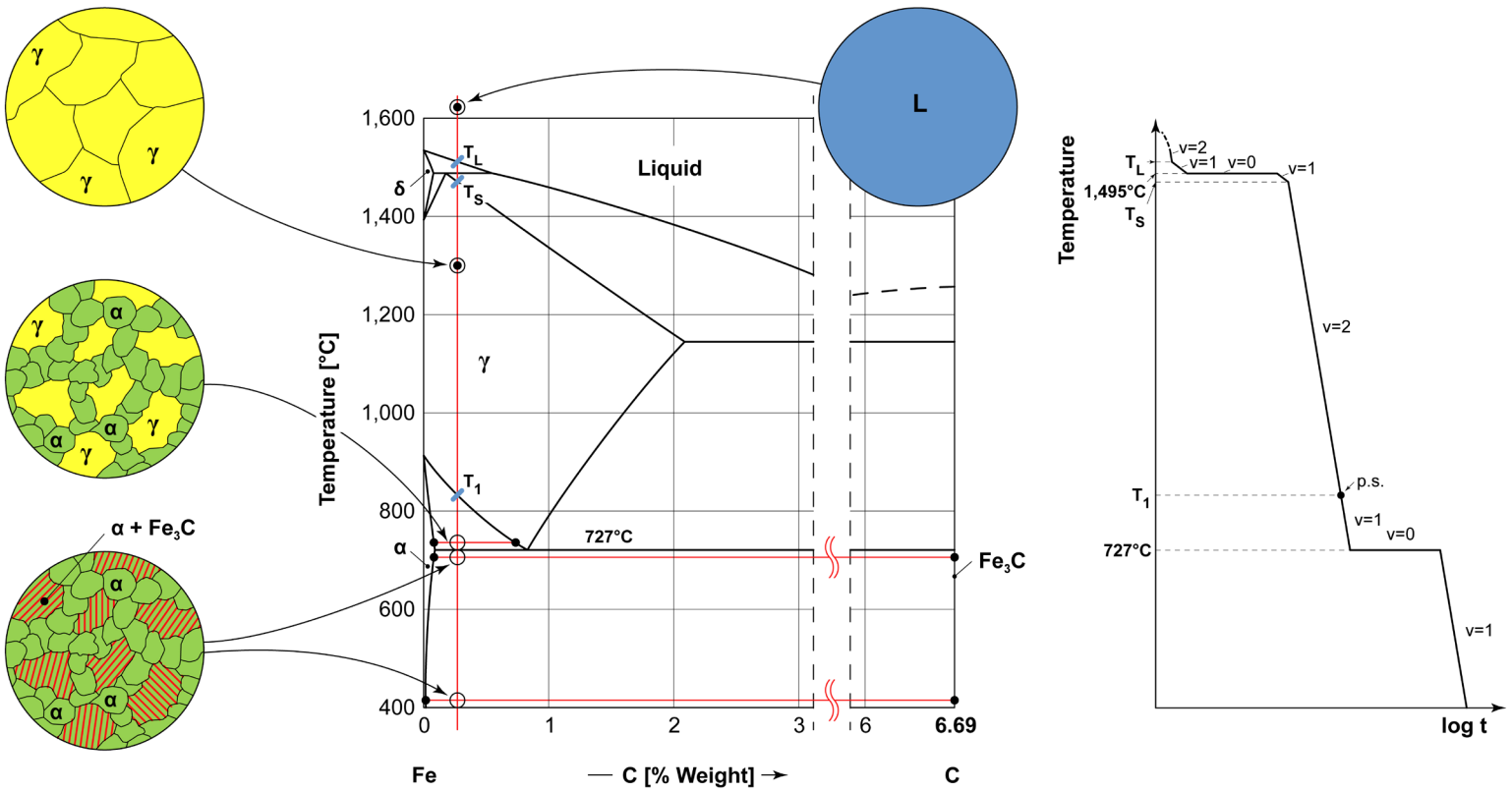

Figure 6.4 - *Fe-C* phase diagram. Graphic representation of microstructure and equilibrium cooling curve of a generic hypoeutectoid steel.

To understand the transformations that occur at the eutectoid horizontal, you need to consider, what we have seen for steel with $C = 0.77\%$.

The hypoeutectoid alloy has carbon contents lower than 0.77%; consequently its iron content is greater than alloy with $C = 0.77\%$. Therefore, before the eutectoid transformation can take place, the alloy must reduce the excess iron between T_1 and 727°C, and it forms α-phase in homogeneous crystals.

An infinitesimal of a degree above 727°C, that is, a moment before the eutectoid transformation begins, the alloy is composed of homogeneous crystals of α-phase and homogeneous crystals of γ-phase.

The greater is the amount of homogeneous crystals of α-phase, the lower is the percentage of carbon in the alloy. For $C = 0.02\%$ you have 100% of homogeneous crystals of α-phase, while for $C = 0.77\%$, the quantity of α-phase in homogeneous crystals is zero (eutectoid alloy). At intermediate chemical compositions, homogeneous crystals of α-phase is inversely proportional to the carbon content.

At 727°C, as is typical for all alloys in the *Fe-C* phase diagram, the homogeneous crystals of γ-phase transform into lamellar crystals composed of alternating layers of α-phase and Fe_3C phase; on the contrary homogeneous crystals of α-phase remains unchanged (Figure 6.5).

Finally, during very slow cooling to room temperature, the structure does not undergo significant modifications and remains comprised of homogeneous crystals of α-phase and lamellar eutectoid crystals[6].

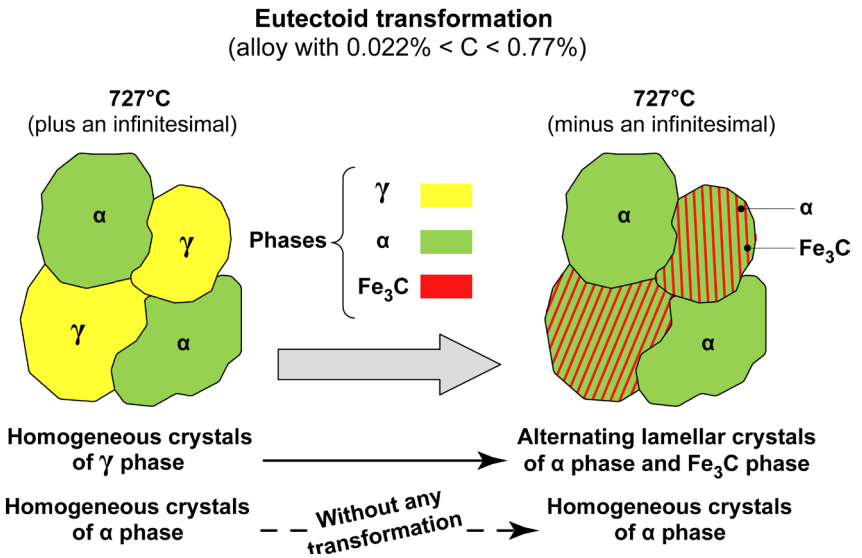

Figure 6.5 - Graphic representation of the eutectoid transformation of a generic hypoeutectoid alloy ($0.02\% < C < 0.77\%$).

[6] *During cooling from 727°C to 20°C, hypoeutectoid alloys form plates of phase Fe_3C on the grain boundary of homogeneous crystals of α-phase. Plate formation is due to the solubility variation of carbon in α-phase. However, the quantity is very limited (less than 0.3%) and can practically be neglected.*

Case 3 Hypereutectoid steel (0.77% < C < 2.11%)

Lastly, the case of steel with a carbon content greater than 0.77%. Hypereutectoid steel forms homogeneous crystals of γ-phase without crossing the peritectic horizontal at 1495°C or the eutectic horizontal at 1148°C (Figure 6.6).

This steel family has a higher carbon content than eutectoid steel. Therefore, before the eutectoid transformation occurs, excess carbon is reduced between T_1 and 727°C, forming plates of Fe_3C phase on the grain boundary of homogeneous crystals of γ-phase.
The higher the carbon content, the greater the quantity of plates on the grain boundary. The maximum amount of plates on the grain boundary is for the alloy with $C = 2.11\%$. The result is equal to:

$$Q_{Fe_3C} = \frac{2.11 - 0.77}{6.69 - 0.77} \cdot 100 \cong 22.6\% \qquad Q_{\gamma} = \frac{6.69 - 2.11}{6.69 - 0.77} \cdot 100 \cong 77.4\%$$

The amount of plates of Fe_3C phase is between 22.6%, for the alloy with 2.11% carbon, and 0%, for the alloy with 0.77% carbon.
The transformation of the homogeneous grains of γ-phase to lamellar grains composed of alternating layers of α-phase and Fe_3C phase, takes place at the eutectoid temperature; F_3C phase, previously deposited on the grain boundary, does not undergo any change (Figure 6.7).
Lastly, during the very slow cooling to room temperature, the structure does not undergo any further change.

6.3 Structural constituents of the *Fe-C* phase diagram

The study of equilibrium cooling of the *Fe-C* alloys allows to determine phases and microstructures in equilibrium at each temperatures.

With reference to steel, there are three types of microstructures[7]:
- homogeneous grains,
- lamellar grains,
- plates on grain boundary,

formed by the phases shown by *Fe-C* phase diagram (γ, α and/or Fe_3C phases).

[7] *In metallurgy, the terms "crystals", "grains" and "crystalline grains" are used indistinctly and interchangeably.*

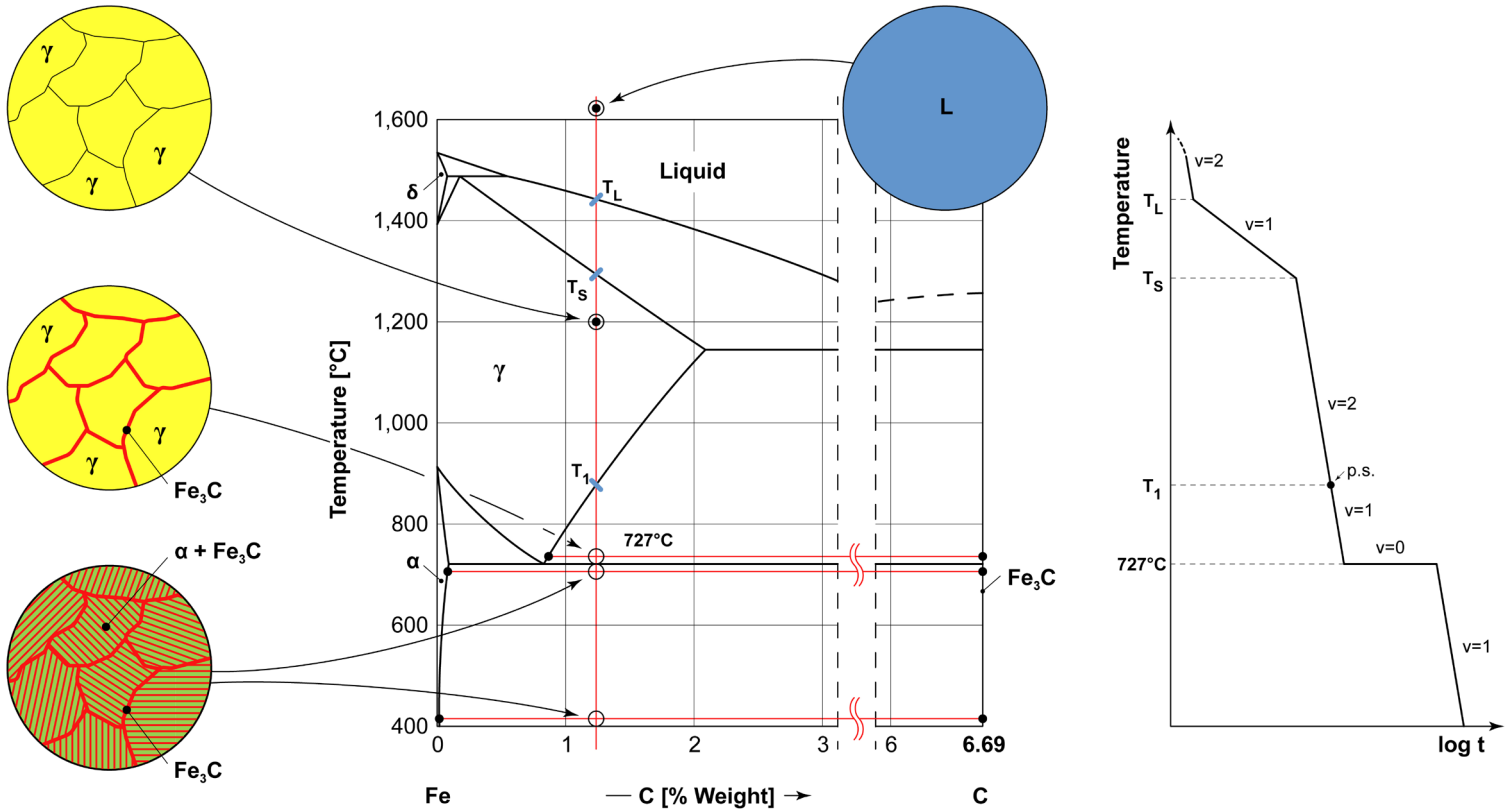

Figure 6.6 - *Fe-C* phase diagram. Graphic representation of microstructure and equilibrium cooling curve of a generic hypereutectoid steel.

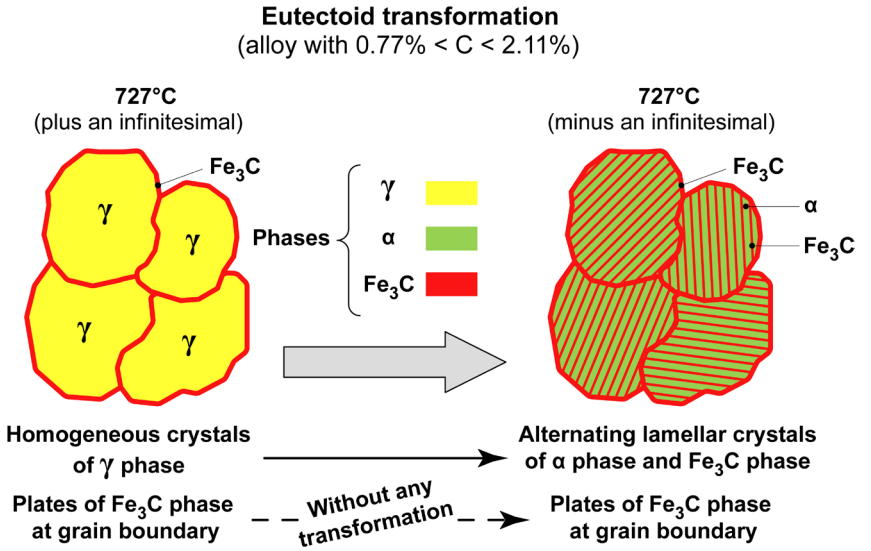

Figure 6.7 - Graphic representation of the eutectoid transformation of a generic hypereutectoid alloy ($0.77\% < C < 2.11\%$).

Conventionally, phases and microstructures of steel[8], are indicated with a specific denomination:

- austenite with reference to homogeneous grains of γ-phase;
- ferrite (or α-ferrite[9]) with reference to homogeneous grains of α-phase;
- pearlite with reference to lamellar grains composed of alternating layers of α-phase and Fe_3C phase;
- cementite with reference to plates of Fe_3C phase at the grain boundary of homogeneous crystals or lamellar crystals.

As it is well understood, it is much easier to speak of ferrite and pearlite rather than microstructures with homogeneous grains of α-phase and alternating lamellar grains of α-phase and of Fe_3C phase.

It is also important to remember that microstructure of the *Fe-C* phase diagram are always comprised of one or more phases, aggregated in a particular form. For example, ferrite is not simply α-phase but it is α-phase aggregated in the form of homogeneous crystals.

[8] *In metallurgy, the terms "structures", "microstructures" and "structural constituents" are used interchangeably.*

[9] *The therm α-ferrite is used to distinguish this microstructure from δ-ferrite, which exists near the melting temperatures, for alloy with very low carbon. In particular, α-ferrite consists of homogeneous crystals of α-phase, while δ-ferrite consists of homogeneous crystals of δ-phase. The term used to define the structure is the same (ferrite) because the crystal lattice is body-centered cubic and the aggregation is in homogeneous crystals for both phases (α and δ).*

The distinction is not just formal: α-phase, in fact, is not present only in homogeneous grains but also in the form of lamellae in pearlite grains. In the latter case, however, it is not possible to speak of lamellar ferrite (erroneous term) but of α-phase in lamellae, aggregated to the Fe_3C phase in lamellae[10].

Therefore, for the three families of steel described above, at 20°C and in conditions of thermodynamic equilibrium, the microstructures are:

- eutectoid steel ($C = 0.77\%$): pearlite,
- hypoeutectoid steel ($0.02\% < C < 0.77\%$): ferrite and pearlite (the quantities of the two microstructures are function of the carbon content),
- hypereutectoid steel ($0.77\% < C < 2.11\%$): pearlite and cementite (the quantities of the two microstructures are function of the carbon content).

The amounts of the microstructures can be calculated with the lever rule. The result is shown in Figure 6.8.

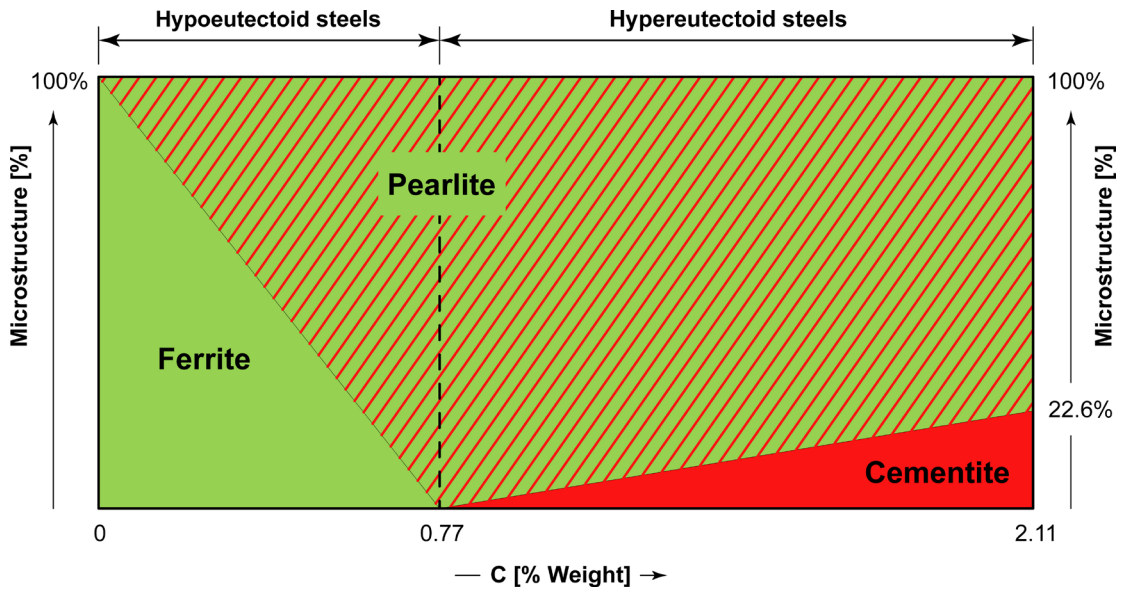

Figure 6.8 - The effect of carbon content on steel microstructure at room temperature.

[10] The distinction between phases and microstructures is very important. Unfortunately, in many books, it is written that pearlite is a lamellar aggregate of ferrite and cementite. This definition is incorrect, since a microstructure (pearlite) cannot be described as an aggregate of two other microstructures (ferrite and cementite). Pearlite is a structural constituent and it must be defined by one or more phases, aggregated according to a certain method. For this reason, pearlite is an aggregate in lamellar crystals composed of alternating layers of α-phase and Fe_3C phase. Similarly, ferrite is an aggregate in homogeneous crystals of α-phase, while cementite is Fe_3C phase in the form of plates on the grain boundary.

6.4 Critical points of the *Fe-C* phase diagram

As seen in the previous paragraph, steel undergoes an important transformation at the solid state: γ-phase, turns completely into α-phase and Fe_3C phase. This important phenomenon must be taken into account when explaining the microstructural changes that occur during industrial heat treatments[11].

The critical points indicate the trasformation of γ-phase and are defined according to the carbon content (Figure 6.9)[12]:

- critical point A_3: points on the *Fe-C* diagram where γ-phase in homogeneous crystals (austenite) transforms into α-phase in homogeneous crystals or, more simply, where austenite transforms into ferrite;
- critical point A_1: points of the *Fe-C* diagram where γ-phase in homogeneous crystals (austenite) transforms into lamellar crystals composed of alternating layers of α-phase and Fe_3C phase or, more simply, where austenite becomes pearlite;
- critical point A_{cm}: points on the *Fe-C* diagram where γ-phase in homogeneous crystals (austenite) transforms into Fe_3C phase in plates on the grain boundary, or, more simply, where austenite transforms into cementite.

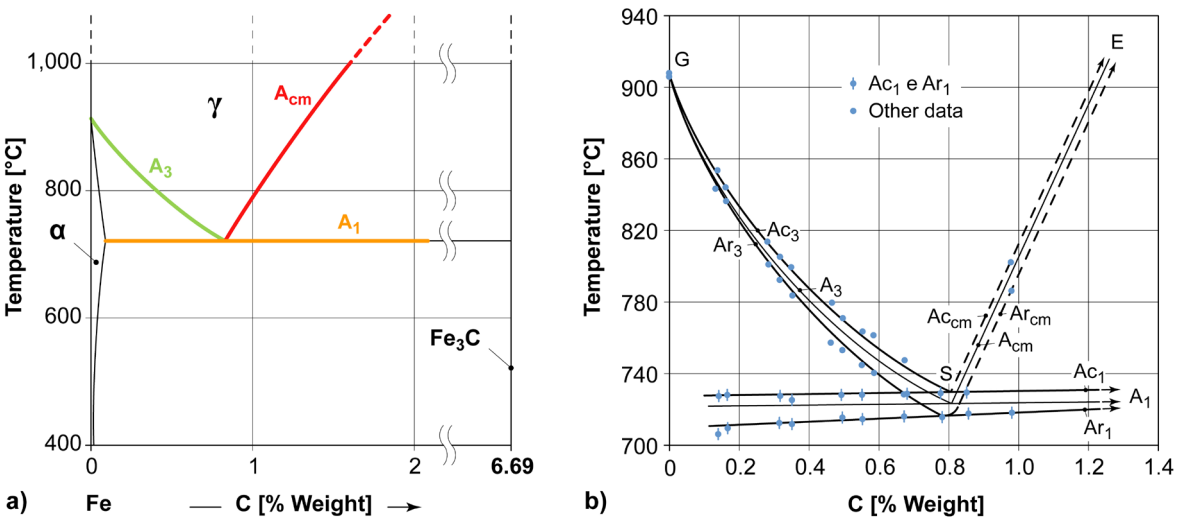

Figure 6.9 - Critical points of the *Fe-C* phase diagram: a) definition of critical points; b) real position of critical points at equilibrium, heating, and cooling [from Bain and Paxton 1966].

[11] *The transformation of austenite is typical of steels and explains the ability of steel to form different mechanical/metallurgical properties, in relation to the heat treatment performed. Other alloys, such as aluminum alloys or copper alloys, do not have this characteristic.*

[12] *Critical points are always designated by the letter A (arrêter) followed by a number (1, 2, 3, 4) or letters (cm).*

The critical points are determined in conditions of thermodynamic equilibrium and, therefore, letter *e* (A_{e1}, A_{e3}, A_{ecm}) should always be present in their description. Nevertheless letter *e* is often omitted.
Critical points can also be measured in conditions of non-equilibrium, i.e. in conditions of continuous heating or cooling: in these cases are used letter *c* (A_{c1}, A_{c3}, A_{ccm}) or letter *r* (A_{r1}, A_{r3}, A_{rcm})[13]. The position of the critical points at heating (A_c) or at cooling (A_r) is different from equilibrium (A_e). The different position depends to the thermal hysteresis of the system when the condition of equilibrium is missing. Thermal hysteresis causes an increase in critical points with respect to equilibrium in the heating phase, or a decrease in the cooling phase.
Critical points are useful for describing the transformations of steel without indicate the temperature. Considering, for example, an hypereutectoid steel, it can be stated that austenite begins to transform into cementite at the temperature of A_{cm}. Therefore, at temperature of A_{c1}, the remaining austenite transforms into pearlite.

6.5 The effect of alloying elements

All types of steel, even the most commonly used, is not simply iron and carbon. In addition to carbon, there are always other alloying elements: sometimes as residue of the steel production process, other times because they are added to obtain specific properties.
In all types of steel, for example, traces of silicon and manganese are always detectable, both used in steel making due to the elimination of harmful chemical species[14]. Sulfur and phosphorus are also systematically present as residue of the iron ore used as raw material.
Finally, manganese, chromium, nickel, molybdenum, vanadium, and silicon can be found as specially added alloying elements.
Steel alloying elements cause substantial changes to the *Fe-C* phase diagram. Their effect can be classified into two categories:

- austenitizing chemical elements,
- ferritizing chemical elements.

The first group includes manganese (*Mn*), nickel (*Ni*), carbon (*C*), nitrogen (*N*), copper (*Cu*): these are called austenitizing because they tend to expand γ-phase field and close α-phase field of the *Fe-C* diagram (Figure 6.10).

[13] In practice, only the critical points measured in condition of continuous heating are always used, i.e. A_{c1} and A_{c3}. Critical point A_{ccm} is, however, only indicated as A_{cm}.

[14] Silicon and manganese are used to neutralize oxygen. Manganese, in combination with calcium, favors the separation of sulfur present in the liquid steel bath. Oxygen and sulfur are two harmful chemical elements for steel, since they induce a significant reduction of impact strength and fracture toughness.

Ferritizing elements (Figure 6.10), such as titanium (*Ti*), chromium (*Cr*), molybdenum (*Mo*), vanadium (*V*), silicon (*Si*), tungsten (*W*), aluminum (*Al*) boron (*B*), tantalum (*Ta*), and niobium (*Nb*). Have opposite effects (contraction of γ-phase field and expansion of α-phase field).

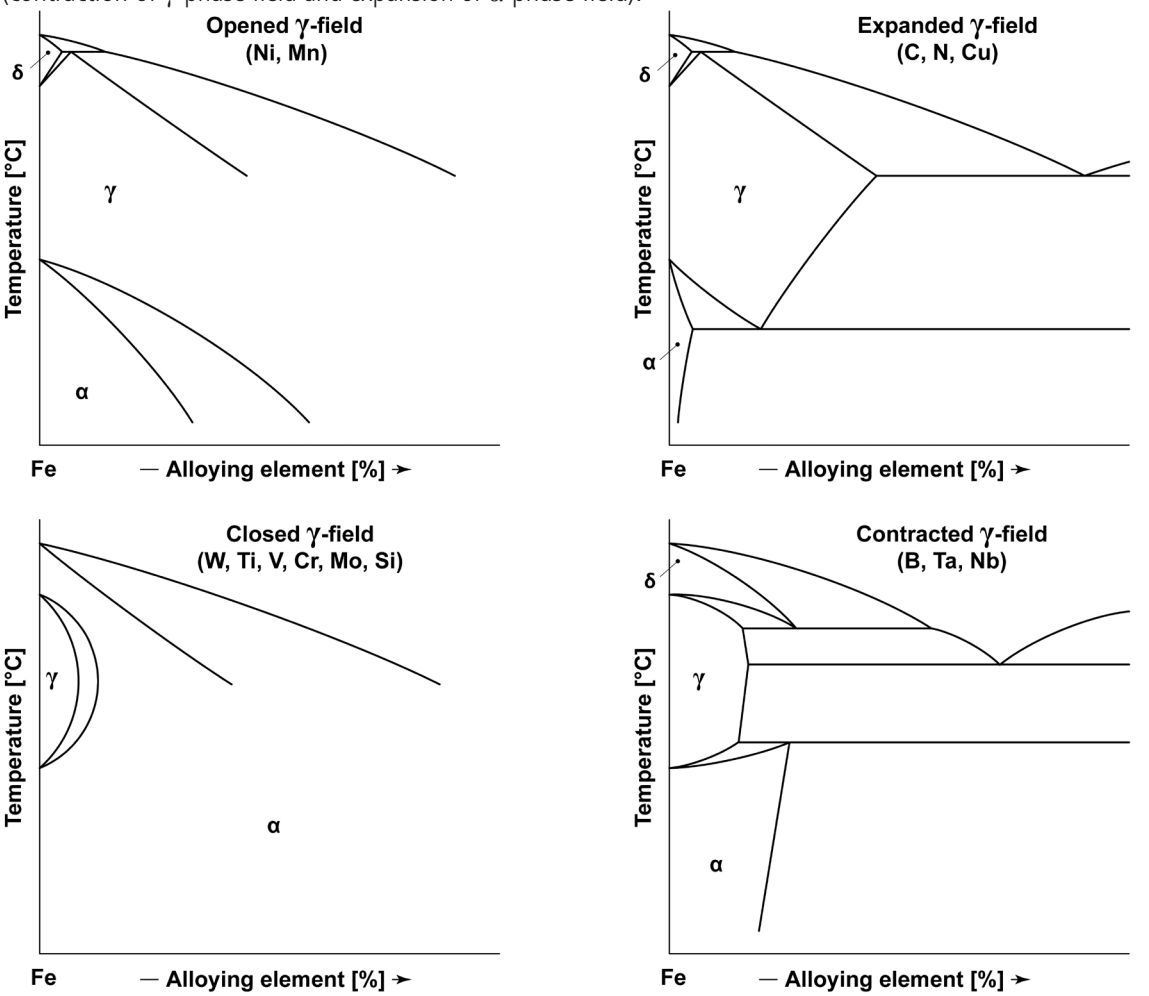

Figura 6.10 - Schematic representation of the types of phase diagrams that iron forms with austenitizing and ferittizing alloying elements [from Bain and Paxton 1966].

The austenitizing or ferritizing action of the alloying elements is not only function of the alloying elements content, but it also depends on the alloying elements type (Figure 6.11). For example, the ferritizing effect of titanium is much higher than chromium: 0.8% titanium is enough to close the γ-phase field almost completely while, with 5% chromium, γ-phase field is only slightly narrower.

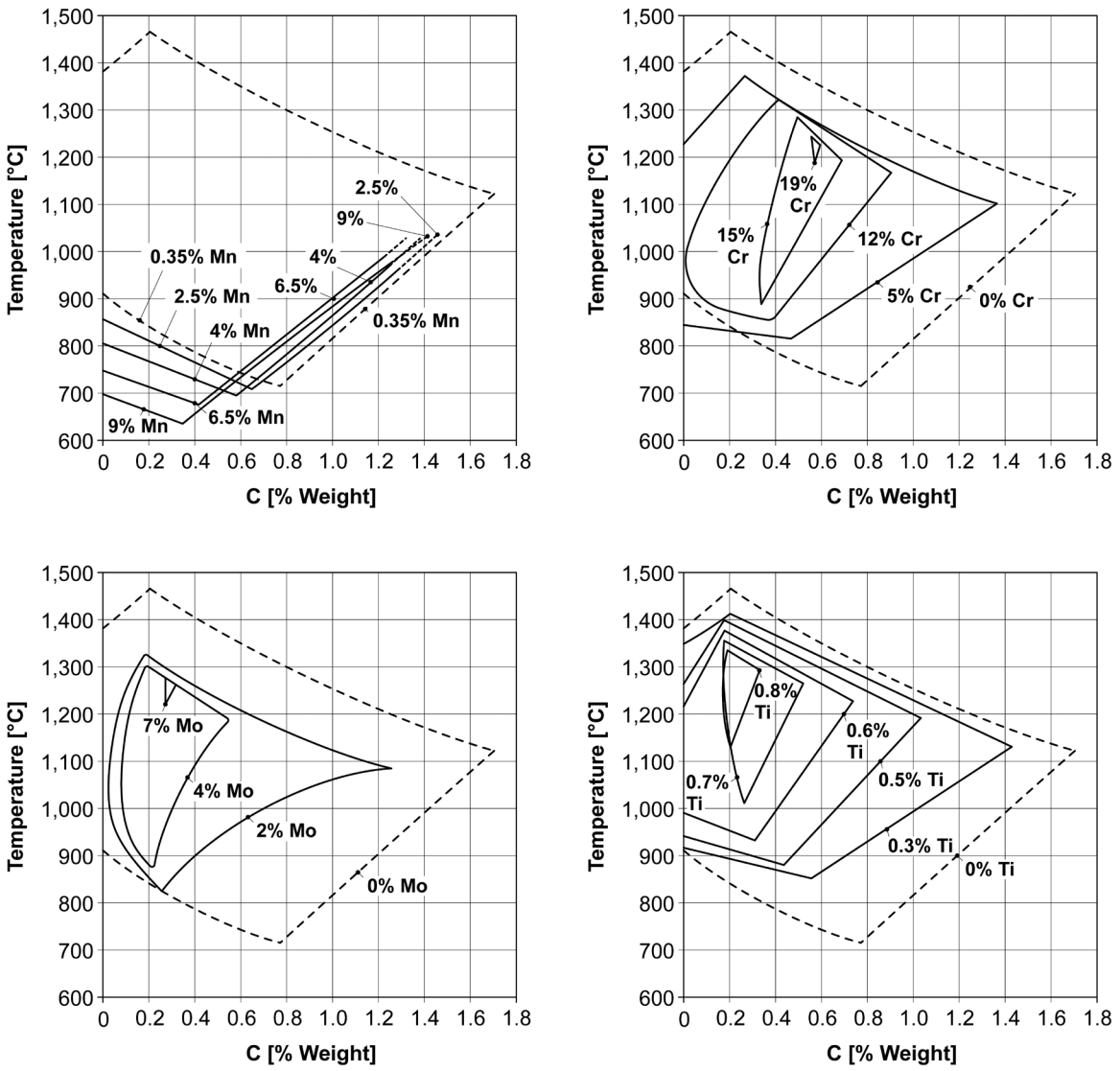

Figure 6.11 - The effect of manganese, chromium, molybdenum, and titanium on amplitude of γ-phase field of the *Fe-C* phase diagram [from ASM-H.4 1991].

The alloying elements can raise (ferritizing elements) or lower (austenitizing elements) the eutectoid temperature. On the contrary, the carbon content of the eutectoid alloy (that for *Fe-C* equals 0.77%) is always reduced by the addition of any alloying element (Figure 6.12).

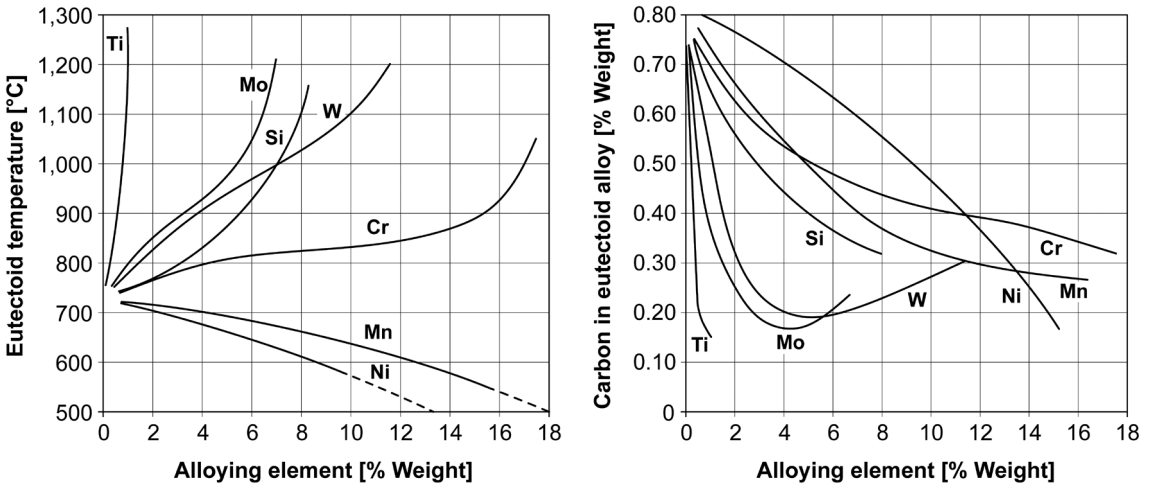

Figure 6.12 - The effect of alloying elements on the eutectoid temperature and on the carbon content of the eutectoid steel [from Bain and Paxton 1966].

The critical point temperatures, can be calculated through various empirical formulas. The most commonly used are listed in [Andrews 1965], valid for low alloy steel with $C < 0.6\%$ [6.2; 6.3]:

$$Ae_1[°C] = 723 - 10.7Mn - 16.9Ni + 29.1Si + 16.9Cr + 290As + 6.38W \quad [6.2]$$

$$Ae_3[°C] = 910 - 203\sqrt{C} - 30Mn + 44.7Si - 15.2Ni - 11Cr - 700P + 31.5Mo + 104V - 20Cu + 460Al + 13.1W + 120As \quad [6.3]$$

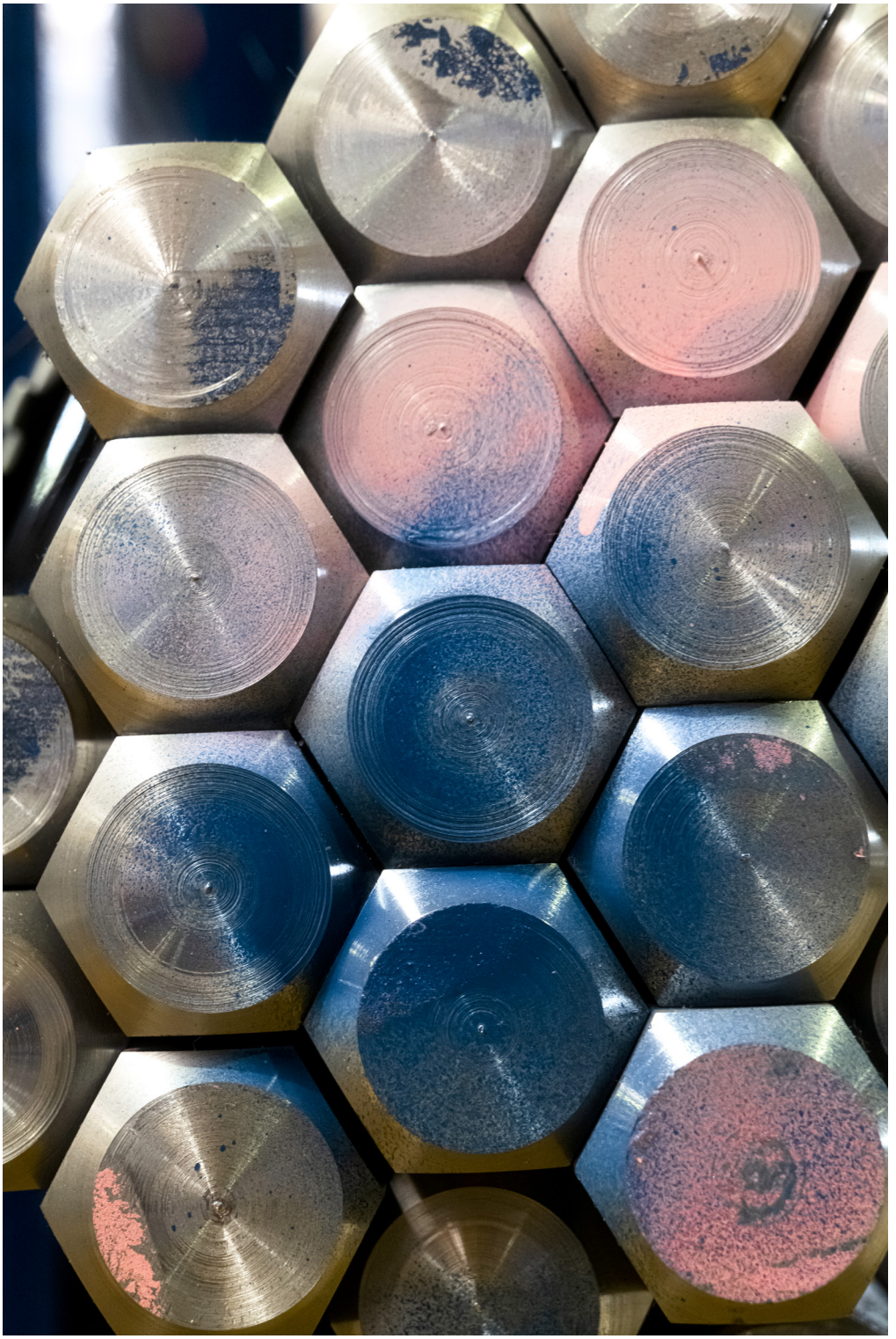

7. T.T.T. AND C.C.T. DIAGRAMS

7.1 What are the T.T.T. and C.C.T. diagrams?

The *Fe-C* phase diagram is very important because it provides information regarding the steel microstructures in conditions of thermodynamic equilibrium, i.e. the microstructures at the end of equilibrium cooling.

In industrial practice, however, the cooling curves used for heat treatments are different from equilibrium cooling[1]: only a very slow cooling in the furnace can be generally assimilated to equilibrium cooling.

When cooling curves are different from equilibrium cooling, it is no longer possible to refer to the *Fe-C* phase diagram and, to predict the microstructures at the end of the heat treatment, other diagrams are needed. To solve the problem of austenite transformations under conditions of non-equilibrium, there are two types of diagrams: the isothermal transformation diagrams and the continuous cooling diagrams. These diagrams show the austenite transformations and the microstructure at the end of the heat treatment in relation to cooling curves. Usually, these diagrams show the temperature in ordinate and the logarithmic scale of time in abscissa[2].

Normally, the isothermal transformation diagrams and the continuous cooling diagrams are simply called T.T.T. diagrams (Time Temperature Transformations) and C.C.T. diagrams (Continuous Cooling Transformations).

7.2 Bain's Experiences. T.T.T. diagram and C.C.T. diagram for eutectoid steel.

The T.T.T. and C.C.T. diagrams were originally developed in the 1930s by E. C. Bain[3] and E. S. Davenport. Later, these diagrams were corrected by M. Cohen, who indicated the martensitic transformation.

The T.T.T. and C.C.T. diagrams are born on the evidence that, according to the cooling curve, austenite can form:

- structures such as ferrite, pearlite, and cementite, as typical for *Fe-C* phase diagram;
- new structures such as bainite and martensite, not present on the *Fe-C*.

[1] *Keep in mind that, during the actual heat treatments, the heating curves are also different from equilibrium heating.*

[2] *The logarithmic scale of time is a mathematical operator used to reduce the extension of the abscissa.*

[3] *Edgar Collins Bain (1891-1971), American chemist and metallurgist (BSc and MSc from Ohio State University). He interrupted his PhD to work at the Goodrich Company. After a short pause in the American Army's technical department (Sub-liutenant at the Chemical Warfare Service), in 1919 he joined the General Electric Company, dealing with the use of X-rays in metallurgy. In 1924, he moved to the laboratories of Union Carbide and Carbon Corporation. From 1928 until his retirement in 1957, he worked for the US Steel Corporation in Pittsburgh, Pennsylvania. Famous worldwide for his research in the field of steel heat treatments and the effect of alloying elements, Bain is also remembered for having discovered bainite.*

Case 1 (T.T.T. diagram for eutectoid steel)

The simplest example refers to eutectoid steel ($C = 0.77\%$). In this steel, if you consider the *Fe-C* phase diagram, austenite transforms completely into pearlite.

Let us see, however, what transformations occur if the same alloy is subjected to an actual cooling curve.

First consider the case of an isothermal cooling curve (Figure 7.1).

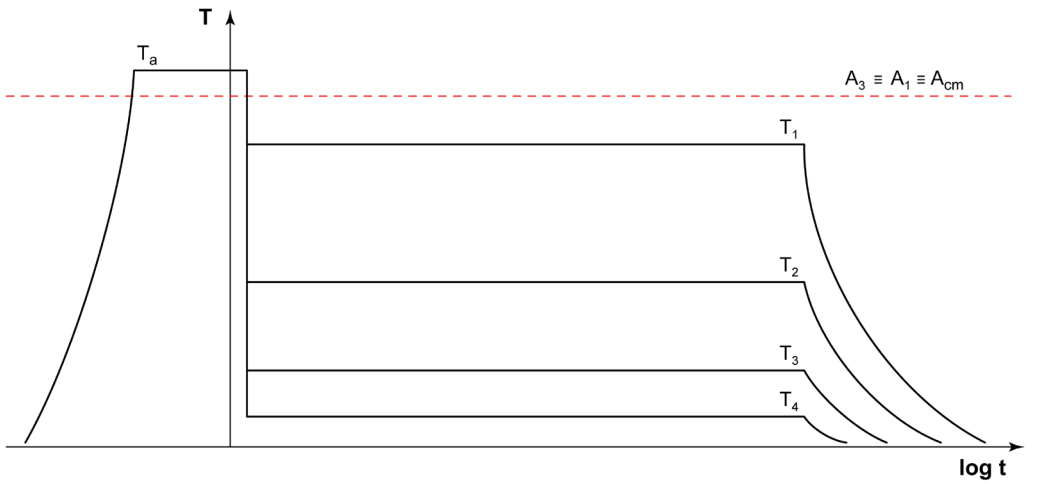

Figure 7.1 - Schematic representation of isothermal cooling curves (T_1, T_2, T_3 or T_4).

The alloy is heated above the critical point[4], in order to have the complete transformation of the microstructure into austenite (temperature T_a). After a certain period of time in the austenitic field, steel is cooled sharply to a given temperature (in this case, T_1, T_2, T_3 or T_4). The temperature is then kept constant (isothermal holding), in order to evaluate the structural changes that steel undergoes over time.

At the end, the system is air cooled to room temperature.

The idea behind this particular cooling method is quite simple. After austenitization, a rapid cooling of the steel is required, in order to have non-equilibrium conditions in the system and to prevent the transformation into pearlite at 727°C, as expected by the *Fe-C* phase diagram. Rapid cooling freezes the austenitic microstructure and brings it virtually unchanged to temperature T_1, T_2, T_3 or T_4. At these temperatures, we want to observe the microstructures and the time when the transformation begins and ends[5].

[4] As seen in Chapter 6, an eutectoid steel has only one critical point ($A_3 \equiv A_1 \equiv A_{cm}$) that, in conditions of equilibrium, corresponds to 727°C.

[5] The isothermal cooling method is sometimes also used in the industrial field, as is the case, for example, of isothermal annealing (Chapter 10).

The isothermal transformation curves of austenite for steel with $C = 0.77\%$ is shown in Figure 7.2: it is the so-called "T.T.T. diagram"[6] for eutectoid steel.

The graph shows two red curves in the form of C joined at the bottom with two red horizontal lines defined by the letters M_s and M_f. The first C and the horizontal line at M_s represent the beginning of the transformation of the austenite, while the second C and the horizontal line at M_f represent the end of the transformation of austentite into a new microstructure.

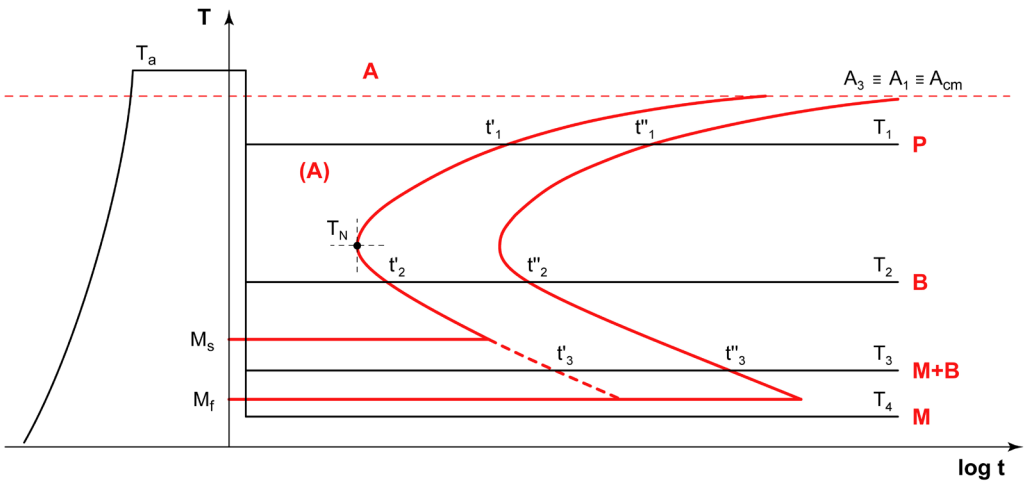

Figure 7.2 - The T.T.T. diagram (red lines) for eutectoid steel; the cooling curves are black.

Consider the trajectory characterized by isotherm T_1 (in black). Above the critical point, steel has a stable austenitic microstructure (letter A). As a result of rapid cooling up to T_1 austentite becomes unstable (letter A in parentheses), i.e. it is in thermodynamic conditions that allow its transformation.

At temperature T_1, the austenite transformation is not immediate but occurs with a certain delay: it begins at time t'_1 (first curve at C, red) and ends with time t''_1 (second curve at C, red). Similar for the isotherm at T_2 (in black), where austenite begins to transform at t'_2 and ends at t''_2.

As can be observed in Figure 7.2, the C curves have a nose shape, that is, they show a temperature T_N, that minimized the starting time of the austentite transformation. This temperature is very important for defining the final microstructure of the steel: above T_N, austentite transforms into pearlite (letter P), instead, under T_N, the transformation forms a different microstructure called bainite (letter B). Bainite is a non-equilibrium microstructure because it does not exist on the *Fe-C* phase diagram. In conclusion: at temperature T_1, 100% of austenite becomes 100% of pearlite. At temperature T_2, 100% of austenite turns into 100% of bainite.

[6] *The T.T.T. diagrams are also called C curves or S curves due to their shape.*

Let us now examine the last two isothermal trajectories (T_3 and T_4), simply starting from T_4.
The isotherm at T_4 (in black) intercepts the field limited by the two red horizontal lines M_s and M_f (i.e. martensite *start* and martensites *finish*) during the initial cooling. This is the area of transformation of austenite into martensite.
Martensite is a steel microstructure, not present on the *Fe-C* phase diagram, that is, a non-equilibrium microstructure. In summary, at the end of the isotherm T_4, the microstructure is completely martensitic. It should be noted that the transformation of austenite into martensite is completed when the initial cooling curve meets the horizontal line M_f. The isothermal holding at T_4 is non influential to the microstructural changes.
A little more complex is the case of the isotherm at T_3. The cooling curve (in black) initially intercepts the field limited by the red horizontal line of M_s without arriving to M_f. In this area, the microstructure is only partially transformed into martensite, while there is still a certain amount of austenite. Subsequently, the isotherm at T_3 crosses the red dotted line. Here, at point t'_3, begins the modification of austenite in bainite, which ends in t''_3. The final microstructure consists of martensite and bainite.

Case 2 (C.C.T. diagram for eutectoid steel)

Now observe what occurs for eutectoid steel ($C = 0.77\%$) subjected to continuous cooling.
Let us first consider the cooling curve. After heating and holding at T_a, steel is subjected to continuous cooling (according to trajectories T_1, T_2, T_3 or T_4). The cooling curves are very different with respect to the isothermal cooling. This time, the temperature varies continuously from the austenitization temperature (T_a) to room temperature, according to different cooling curves that become more and more rapid (from T_1 to T_4)[7].

[7] *The anisothermal cooling method is the most common in industrial heat treatments. Steel components cooled in a furnance, in air, in oil, or in water are subjected to anisothermal cooling (Chapter 10).*

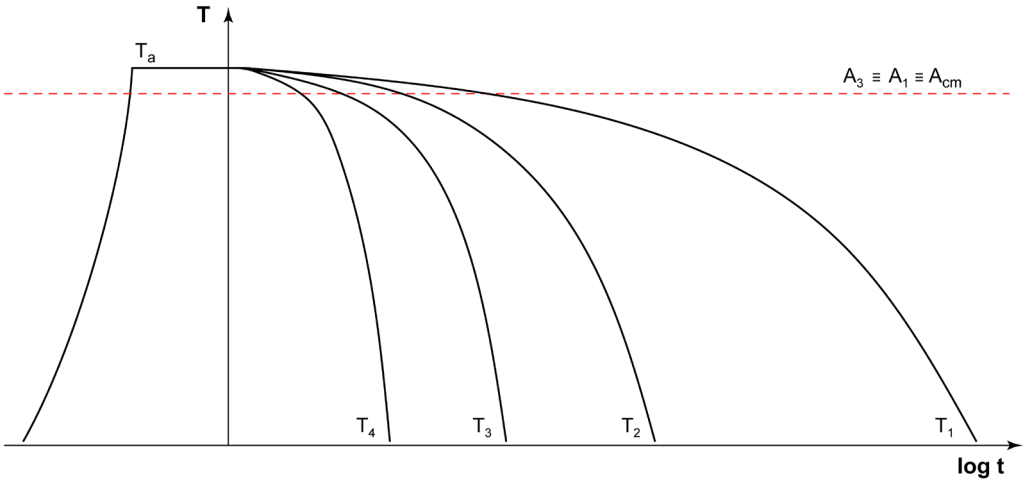

Figure 7.3 - Schematic representation of continuous cooling curves (T_1, T_2, T_3 or T_4).

Figure 7.4 shows a schematic representation of C.C.T. diagram for eutectoid steel (red lines).

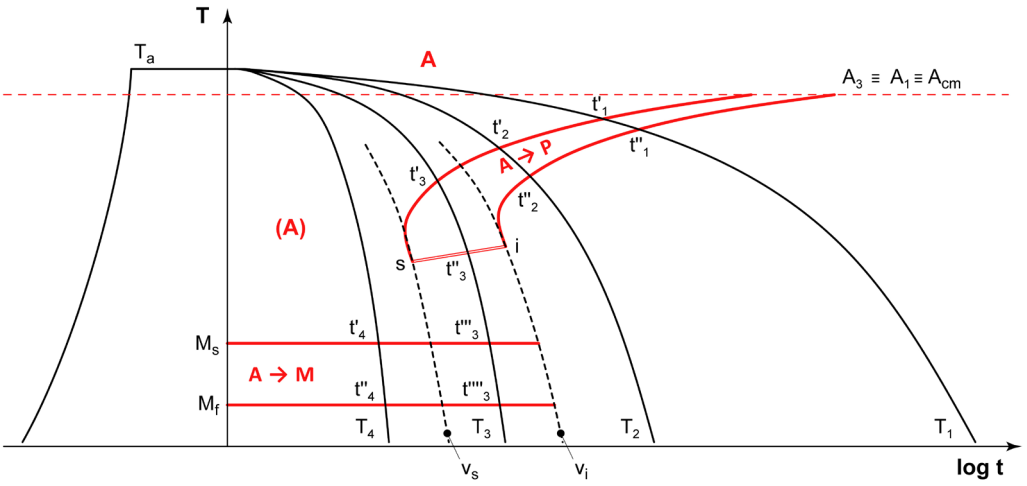

Figure 7.4 - C.C.T. diagram (red lines) for eutectoid steel; the cooling curves are black.

Following the cooling curve T_1, austenite begins to transform at time t'_1 and ends at time t''_1, transforming completely into pearlite.
The trajectory described by T_2 is similar to that of T_1, which intercepts the same field as the previous one. Also in this case, the austenite forms 100% of pearlite between t'_2 and t''_2.
A bit more complex is the cooling curve indicated with T_3. At t'_3 austenite begins to transform into pearlite.

This transformation ends at t''_3, when only a part of the austenite is transformed. The austenite not yet transformed becomes martensite, due to the cooling between M_s ed M_f (from time t'''_3 to time t''''_3). The amount of pearlite and martensite is due to the cooling rate.

The closer the trajectory T_3 approaches i, the greater the amount of pearlite and the lesser the amount of martensite; conversely if T_3 is close to s[8]. The double thin red line, found between s and i in Figure 7.4, is an area of arrest for the austenite transformation. On the contrary, the other red curves of the diagram are drawn with thick lines, since they represent the beginning and end of the austentite transformations.

In the case of the cooling curve indicated by t'_4 austenite transforms completely into martensite when it crosses the two horizontal lines (M_s and M_f) between t'_4 and t''_4.

The cooling curve passing through s is the slowest one that forms only martensite[9]. Similarly the cooling curve passing through i is the fastest cooling curve that forms only pearlite[10].

7.3 T.T.T. diagrams and C.C.T. diagrams for hypoeutectoid steels

After the case of eutectoid steel, you need to consider a hypoeutectic steel subjected to isothermal (T.T.T. diagrams) or continuous (C.C.T. diagrams) cooling.

The typical diagrams are shown in Figures 7.5 and 7.6. As you can see, the two diagrams are very similar to those of eutectoid steel. The only differences are related to the fields of transformation of austenite into ferrite (both in T.T.T. and C.C.T. diagrams) and the presence of the so-called "bainitic island" (only for C.C.T. diagrams).

[8] If trajectory T_3 passes through i, the system forms 100% of pearlite, instead if trajectory T_3 passes trough s, the system forms 100% of martensite.

[9] If the cooling curve has a slower rate, system forms other microstructures in addition to martensite.

[10] The concept of higher or lower critical rate is not related to the value of the cooling rate but by the shape of the curve. For example, the curve for lower critical rate (v_i) for a eutectoid steel is the fastest cooling curve that forms 100% of pearlite: this curve is positioned on the temperature-time axis, lower and to the left with respect to the other cooling curves that form 100% of pearlite.

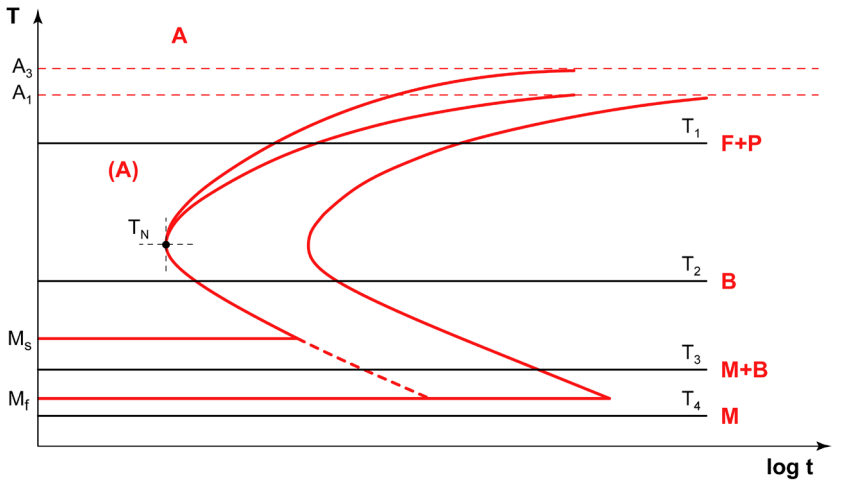

Figure 7.5 - Example of a T.T.T. diagram for a generic hypoeutectoid steel ($C < 0.77\%$).

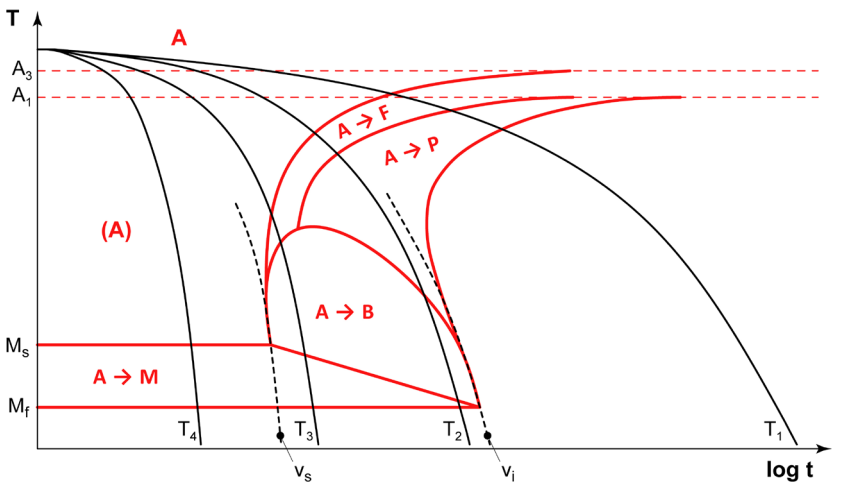

Figure 7.6 - Example of a C.C.T. diagram for a generic hypoeutectoid steel ($C < 0.77\%$).

Let us now consider four isothermal cooling curves on the T.T.T. diagram in Figure 7.5. The result is:

- at the end of the horizontal line at T_1, the microstructure is ferritic-pearlitic;
- at the end of the horizontal line at T_2, the microstructure is bainitic;
- at the end of the horizontal line at T_3, the microstructure is martensitic-bainitic;
- at the end of the horizontal line at T_4, the microstructure is martensitic.

Similarly, for the four continuous cooling curves of the generic C.C.T. diagram in Figure 7.6, the result is:

- at the end of cooling curve T_1, the microstructure is made up of ferrite and pearlite;
- at the end of cooling curve T_2, the microstructure is made up of ferrite, pearlite, bainite, and martensite;
- at the end of cooling curve T_3, the microstructure is made up of ferrite, bainite, and martensite;
- at the end of cooling curve T_4, the microstructure is made up of martensite.

Also in this case the curves indicated with v_s and v_i, represent two limit conditions: v_s is the slower cooling rate that forms only the martensitic microstructure; v_i is the fastest cooling rate that forms only ferrite and pearlite.

The Figures 7.5 and 7.6 show schematic representations of T.T.T. and C.C.T. diagrams. In a real case, there are only one T.T.T. diagram and only one C.C.T. diagram for each steel.
In particular, the shape and position of the T.T.T. and C.C.T. diagrams varies with various parameters. The addition of alloying elements, including carbon, causes a delay in the austenite transformation. Consequently, the higher the amount of alloying elements, the more the T.T.T. and C.C.T. diagrams[11] move down and to the right. Similar effects are caused by the increase in austenitization time and the austenitization temperature[12] (Figure 7.7).
The forward shift of the T.T.T. and C.C.T. diagrams explains why it is easier to form martensite in steel containing alloying elements in addition to carbon.
Figures 7.8 to 7.10 show some examples of real T.T.T. and C.C.T. diagrams for hypoeutectoid steels.
In this regard, it is interesting to note how the real T.T.T. and C.C.T. diagrams show many useful informations to evaluate microstructures and their characteristics at the end of the heat treatment.
All T.T.T. diagrams show the hardness value on the right and vertically. In many cases, the percentage of microstructure is also indicated. For example, in Figure 7.8 the isothermal cooling curve at 600°C forms 25% ferrite and 75% pearlite with hardness of 29HRC (number inside the circle). Similarly, in Figure 7.10, the isothermal cooling curve at 400°C forms 100% bainite with hardness of 40HRC.
The C.C.T. diagrams show similar informations. In this case, the hardness values are reported at the end of the cooling curves.

[11] *An exception to this general rule is cobalt, which moves T.T.T. and C.C.T. diagrams to the top and left.*

[12] *An increase in austenitization time and austenitization temperature causes an increase of the mean grain size and a delay of the austenite transformation.*

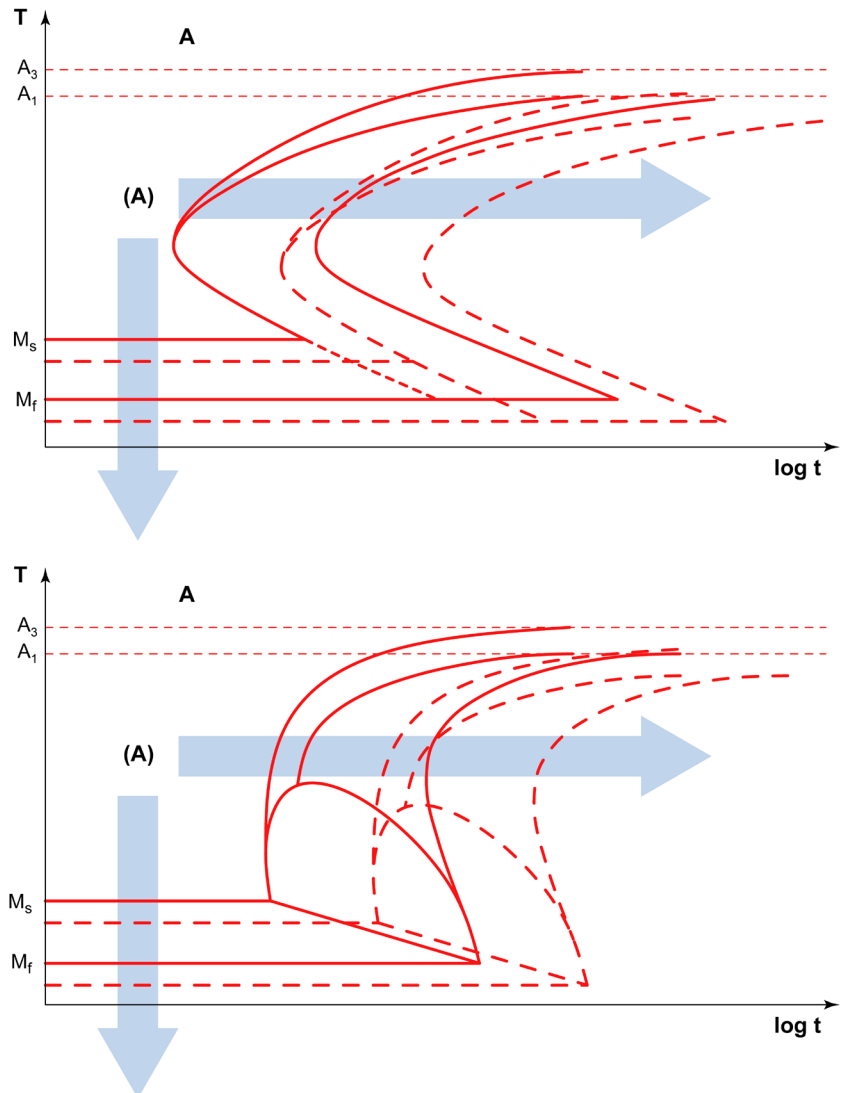

Figure 7.7 - Example of the shift of T.T.T. (top) C.C.T. (bottom) diagrams caused by the addition of alloying elements or the increase in the austenitization temperature and/or austenitization time.

For example, in Figure 7.9, the slowest cooling curve forms a microstructure with 40% ferrite, 60% pearlite and hardness of 200HV. The slowest and the fastest cooling curve in Figure 7.10 instead form 2% of ferrite and 98% pearlite (22HRC), and 100% martenstite (57HRC) respectively[13].

[13] *A three-digit hardness value refers to Vickers hardness scale (HV), while a two-digit hardness value refers to Rockwell C hardness scale (HRC).*

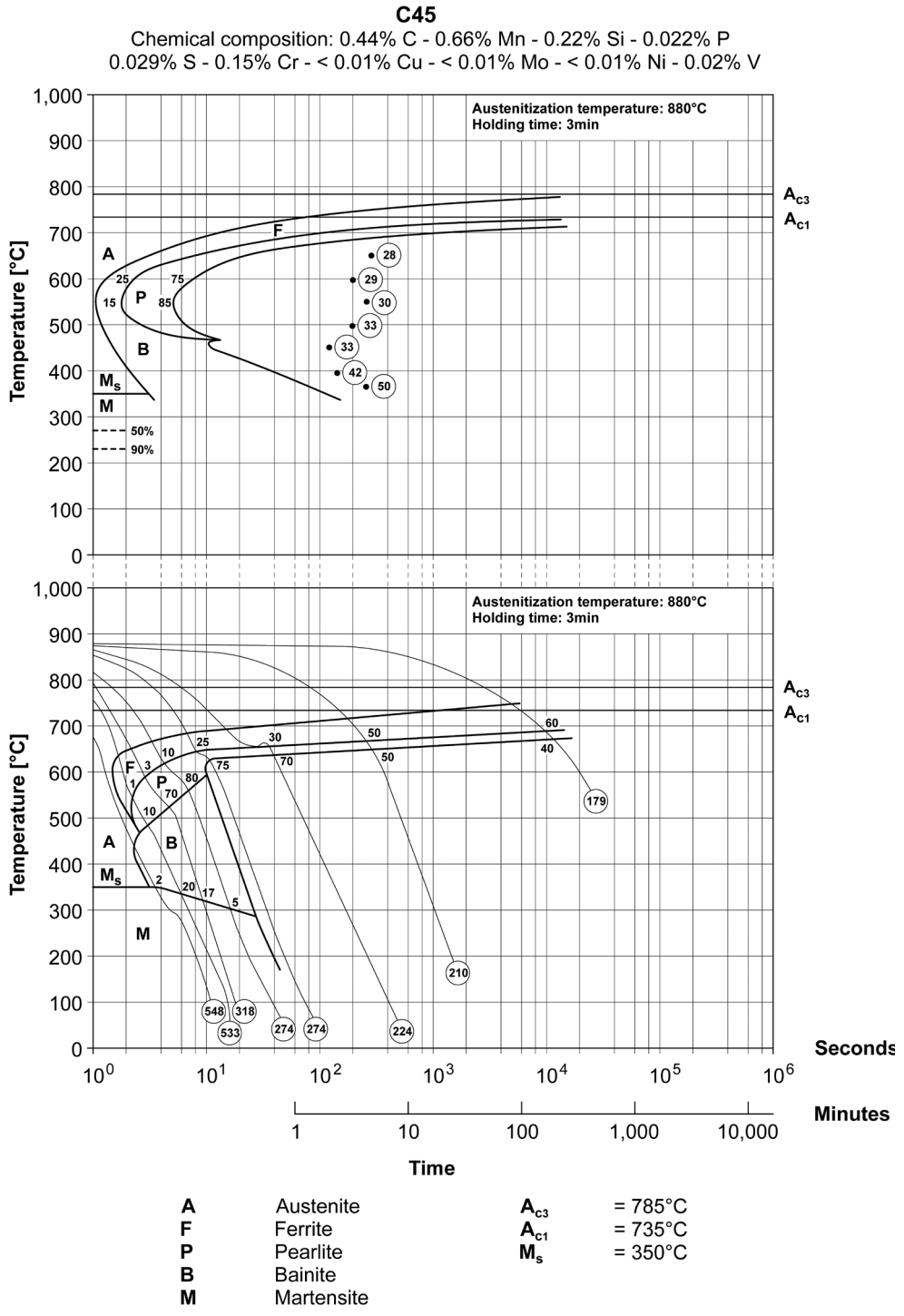

Figure 7.8 - T.T.T. and C.C.T. diagrams for EN C45 steel (0.44%C; 0.22%Si; 0.66%Mn; 0.022%P; 0.029%S; 0.15%Cr; 0.02%V - austenitized at 880°C for 3 minutes) [from Wever et al.1954/56/58].

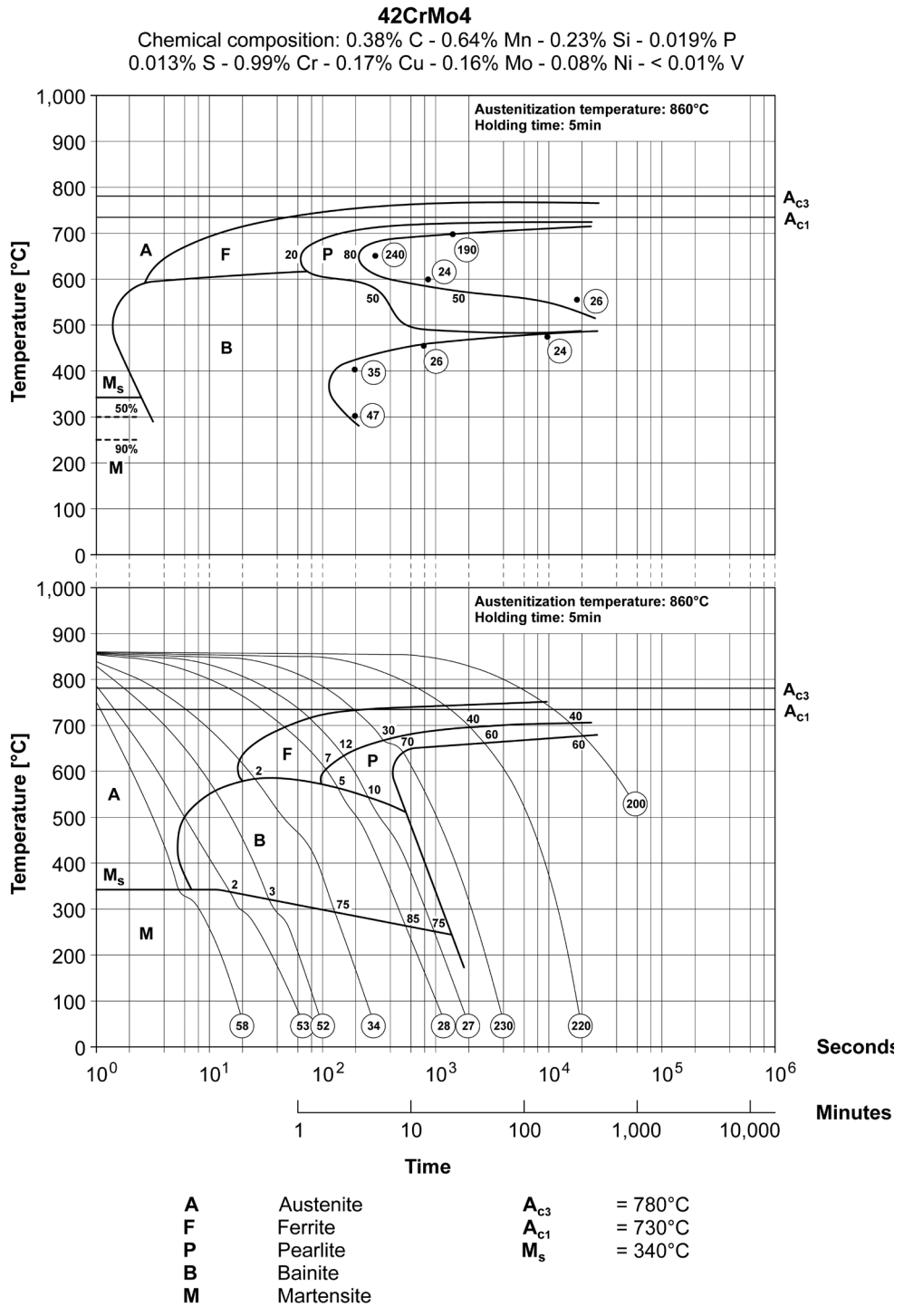

Figure 7.9 - T.T.T. and C.C.T. diagrams for EN 42CrMo4 steel (0.38%C; 0.23%Si; 0.64%Mn; 0.019%P; 0.013%S; 0.99%Cr; 0.08%Ni; 0.16%Mo; 0.17%Cu < 0.01%V - austenitized at 860°C for 5 minutes) [from Wever et al.1954/56/58].

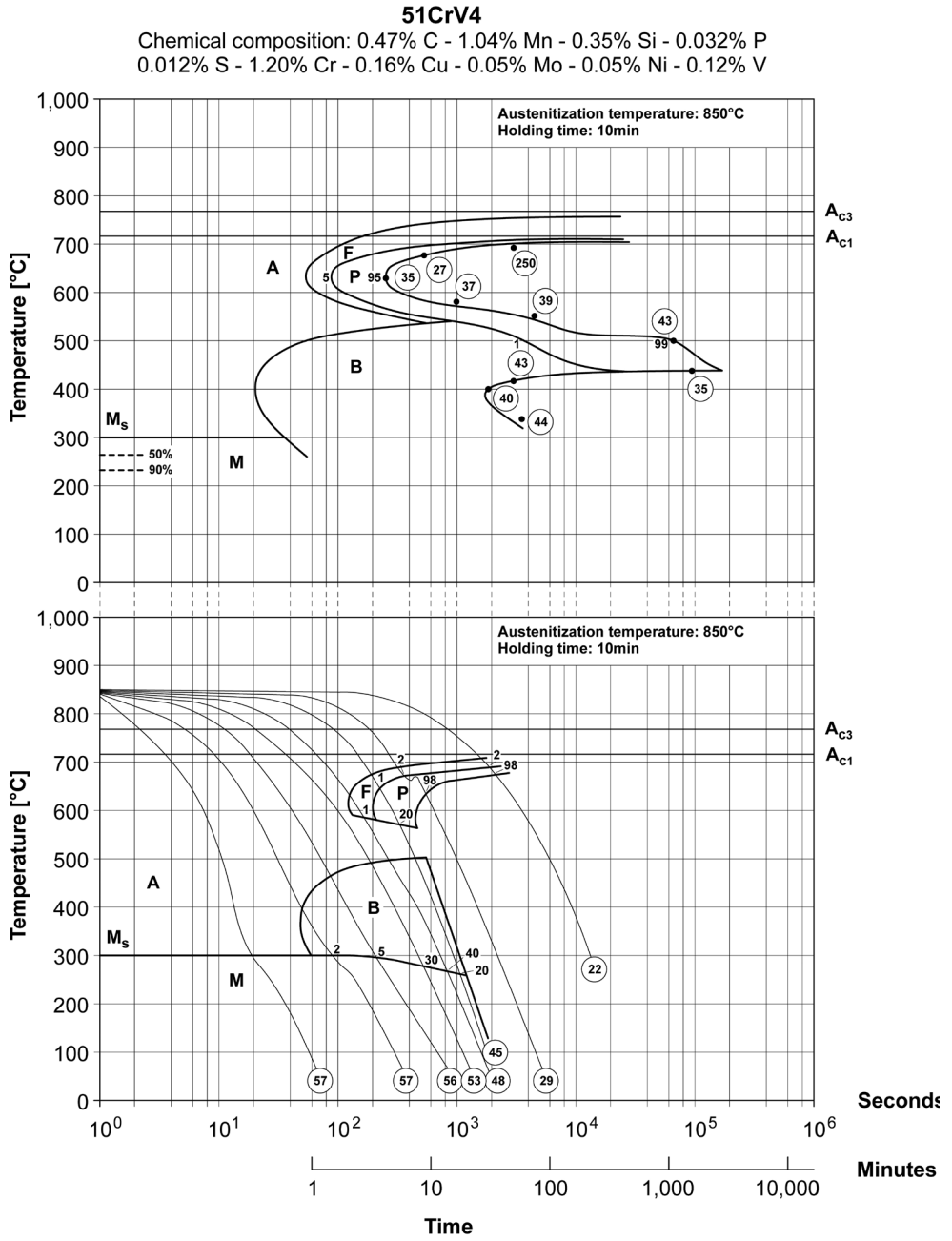

Figure 7.10 - T.T.T. and C.C.T. diagrams for EN 51CrV4 steel (0.47%C; 0.35%Si; 1.04%Mn; 0.032%P; 0.012%S; 1.20%Cr; 0.05%Ni; 0.05%Mo; 0.16%Cu, 0.12%V - austenitized at 850°C for 10 minutes) [from Wever et al.1954/56/58].

7.4 T.T.T. diagrams and C.C.T. diagrams for hypereutectic steels

Let us now consider a generic hypereutectoid steel: typical T.T.T. and C.C.T. diagrams are shown in Figures 7.11 and 7.12.

The shape of the diagrams does not change with respect to hypoeutectoid steel. The only changes are the critical point at the highest temperature that becomes A_{cm} and the transformation into cementite/carbide (C) instead of ferrite.

For the four isothermal cooling curves on the T.T.T. diagram in Figure 7.11, the result is:

- at the end of the horizontal line at T_1, the microstructure is made up of cementite and pearlite;
- at the end of the horizontal line at T_2, the microstructure is made up of bainite;
- at the end of the horizontal line at T_3, the microstructure is made up of martensite and bainite;
- at the end of the horizontal line at T_4, the microstructure is made up of martensite.

while for the four continuous cooling curves on the C.C.T. diagram in Figure 7.12, the result is:

- at the end of cooling curve T_1, the microstructure is made up of cementite and pearlite;
- at the end of cooling curve T_2, the microstructure is made up of ferrite, pearlite, bainite, and martensite;
- at the end of cooling curve T_3, the microstructure is made up of cementite, bainite, and martensite;
- at the end of cooling curve T_4, the microstructure is made up of martensite.

The cooling curve indicated by v_s has the same meaning as in Paragraph 7.3, while v_i is the fastest cooling curve that forms only pearlite and cementite.

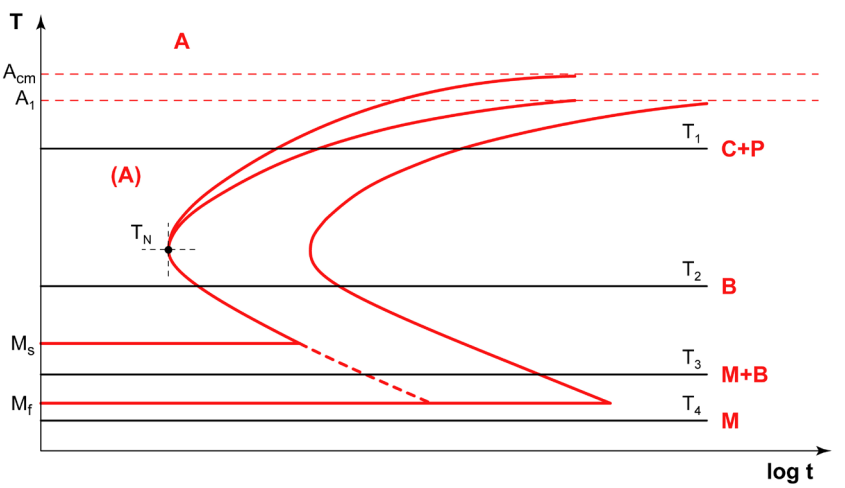

Figure 7.11 - Example of T.T.T. diagram for a generic hypereutectoid steel ($C > 0.77\%$).

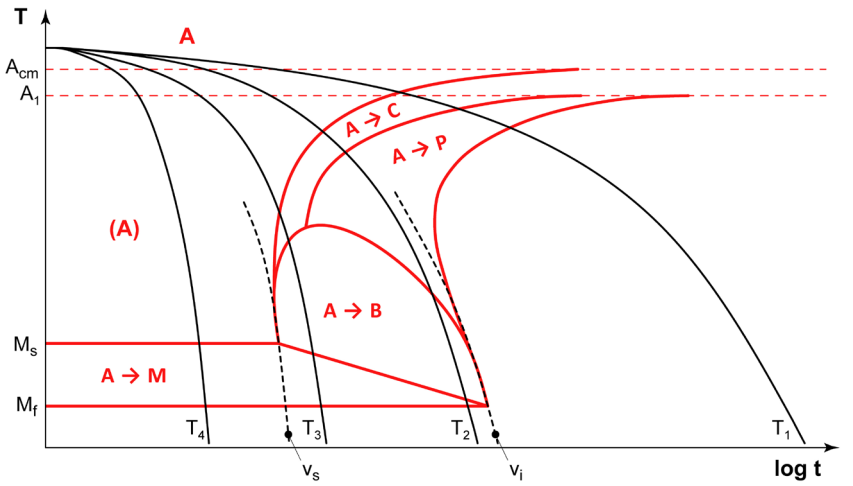

Figure 7.12 - Example of the C.C.T. diagram for a generic hypereutectoid steel ($C > 0.77\%$).

The Figures 7.11 and 7.12 show schematic representations of T.T.T. and C.C.T. diagrams. Two real examples of T.T.T. and C.C.T. diagrams for hypereutectic steel are shown in Figures 7.13 and 7.14. The wording $A + C$ indicates that a certain amount of carbides is always present.

Also in the case of hypereutectoid steel, the alloying elements, as well as the increase in austenitization time and/or austenitization temperature cause a shift to the right and bottom of the T.T.T. and C.C.T. diagrams, i.e. a delay in the austenite transformation.

7.5 Absence of martensite finish, M_f on T.T.T. and C.C.T. diagrams.

The horizontal line of martensite finish, M_f, is not usually present in real T.T.T. and C.C.T. diagrams, especially in the case of high carbon content or low alloy steel. In fact, in these types of steel M_f are near or below room temperature.

The addition of carbon and other alloying elements leads to a gradual lowering of the horizontal lines of M_s and M_f (Figure 7.15). For this reason, in the case of hypoeutectoid and hypereutectoid steels, it is normal not to find the indication M_f (Figures 7.8, 7.9, 7.10, 7.13, and 7.14). In these cases, if M_f is absent and if the cooling curve forms martensite, a certain amount of non-transformed austenite is normal. The indication RA[14] at the end of the cooling curves, followed by a number, indicates the quantity of non-transformed austenite, known as retained austenite.

[14] *Retained Austenite.*

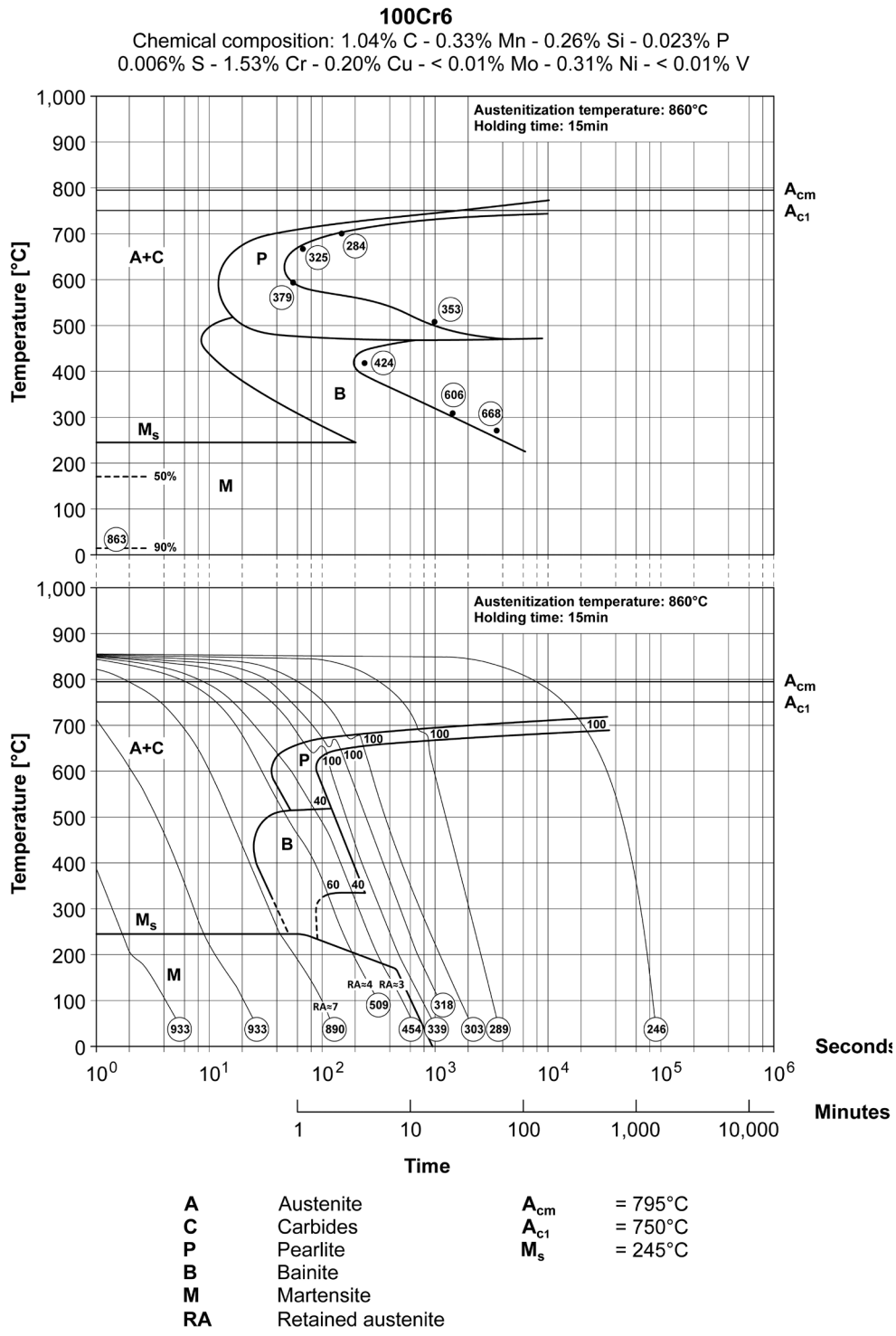

Figure 7.13 - T.T.T. and C.C.T. diagrams for EN 100Cr6 steel (1.04%C; 0.26%Si; 0.33%Mn; 0.023%P; 0.006%S; 1.53%Cr; 0.20%Cu; 0.31%Ni; < 0, 01%Mo; < 0.01%V - austenitized at 860°C for 15 minutes) [from Wever et al.1954/56/58].

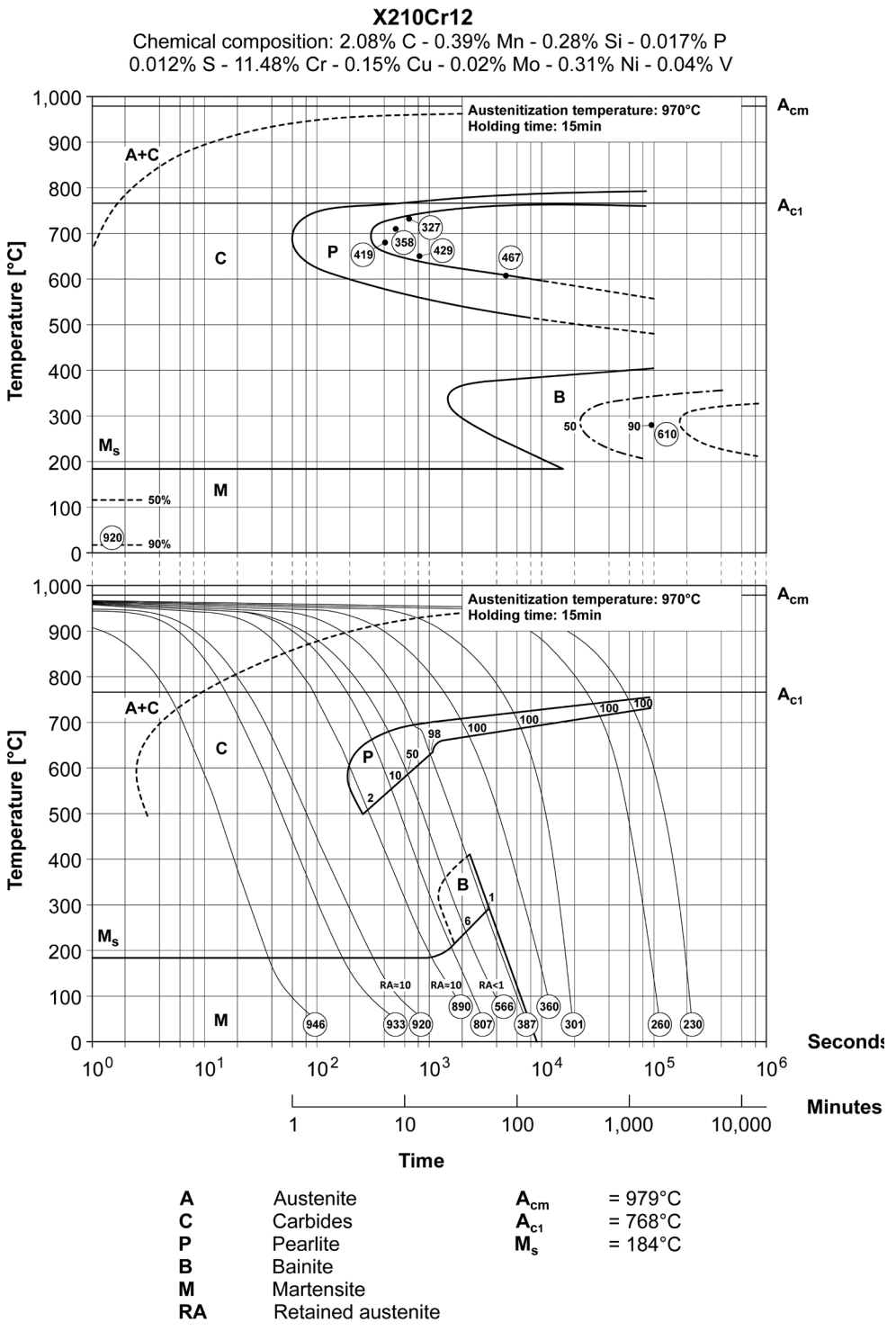

Figure 7.14 - T.T.T. and C.C.T. diagrams for EN X210Cr12 steel (2.08%C; 0.28%Si; 0.39%Mn; 0.017%P; 0.012%S; 11.48%Cr; 0.31%Ni; 0.02%Mo; 0.15%Cu: 0.04%V - austenitized at 970°C for 15 minutes) [from Wever et al.1954/56/58].

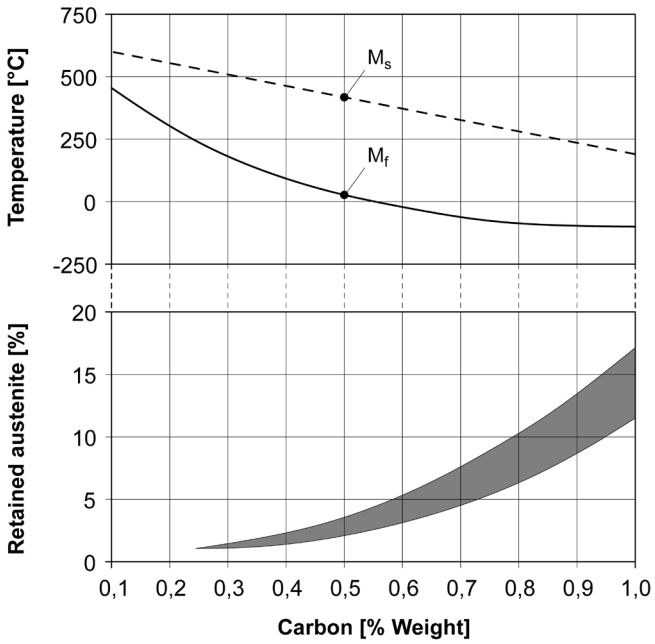

Figure 7.15 - The effect of carbon on the amount of retained austenite at room temperature and on the downward shift of the M_s and M_f temperatures [from Totten 2006].

The retained austenite is due to the rapid cooling. Various empirical formulas estimate the shift of M_s and M_f caused by alloying elements. A simplified formula is that proposed by [Steven and Haynes 1956]:

$$M_s = 561 - 474C - 33Mn - 17Cr - 17Ni - 21Mo \quad [7.1]$$

$$M_{10} = M_s - 18 \quad [7.2]$$

$$M_{50} = M_s - 85 \quad [7.3]$$

$$M_{90} = M_s - 185 \quad [7.4]$$

$$M_f = M_{100} = M_s - 387 \quad [7.5]$$

M_x is a temperature in Celsius degrees and it indicates the volumetric fraction x of martensite transformed at a given tempeature (for example, at temperature M_{50}, the 50% of austenite is already transformed into martensite). The equations from 7.1 to 7.5 demonstrate that retained austenite cannot be avoided, not even for medium carbon steel (for example, C40 steel); in fact for these steels the value of M_f is approximately -30°C.

8. STEEL MICROSTRUCTURES

8.1 Equilibrium microstructures and non-equilibrium microstructures

The *Fe-C* phase diagram and T.T.T. or C.C.T. diagrams highlight how steel may have different microstructures: this characteristic depends on both the chemical composition and the cooling methods.

Downstream of solidification or as a result of heating process, steel, always passes through the field of γ-phase. Therefore at these temperatures, the microstructure is austenitic. If subjected to a slow equilibrium cooling, austenite transforms into:

- pearlite if steel is eutectoid ($C = 0.77\%$);
- ferrite and pearlite if steel is hypoeutectoid ($0\% < C < 0.77\%$);
- pearlite and cementite if steel is hypereutectoid ($0.77\% < C < 2.11\%$).

On the other hand, after non-equilibrium cooling, the same austenite transforms into:

- pearlite, bainite and/or martensite if steel is eutectoid;
- ferrite, pearlite, bainite and/or martensite if steel is hypoeutectoid;
- cementite, pearlite, bainite and/or martensite if steel is hypereutectoid[1].

In general, the microstructures formed during equilibrium cooling are microstructures of equilibrium, while the microstructures formed during non-equilibrium cooling are microstructures of non-equilibrium.

This classification is important because ferrite, pearlite, and cementite are often referred to as equilibrium microstructures and bainite and martensite as non-equilibrium microstructures.

While in the case of bainite and martensite, the definition is certainly correct (bainite and martensite are always non-equilibrium microstructures), for other microstructures, the definition is not correct. For example, ferritic-pearlitic microstructures can be formed in conditions of equilibrium (as a result of a very slow cooling, as provided by the *Fe-C* phase diagram), or in conditions of non-equilibrium (as a result of cooling according to T.T.T. or C.C.T. diagrams). This is similar for cementite and pearlite microstructures.

[1] *For a description of the microstructures formed after non-equilibrium cooling, see Chapter 7. The list of the microstructures is only an example. As a matter of fact, a hypereutectoid steel can form cementite-pearlite or cementite-pearlite-bainite or cementite-pearlite-bainite-martensite or bainite-martensite or only martensite, in relation to the cooling curve. Finally, do not forget that the formation of retained austenite is also possible.*

A more appropriate classification of steel microstructures refers to austenite transformation mechanisms. In this case, we speak of:

- microstructures that are formed from austenite through nucleation and growth mechanisms due to carbon diffusion;
- microstructures that are formed from austenite through instantaneous transformation without carbon diffusion.

The first group refers to the transformation of austenite into pearlite, ferrite, cementitite or bainite[2]. The second refers to the transformation of austenite into martensite.

8.2 Transformations through nucleation and growth

As seen in the previous paragraph, ferrite, pearlite, cementite, and bainite are microstructures formed through nucleation and growth from austenite, due to carbon diffusion[3].

Figure 8.1 shows a schematic representation of the nucleation and growth mechanism of the new microstructures at the expense of the original austenitic microstructure.

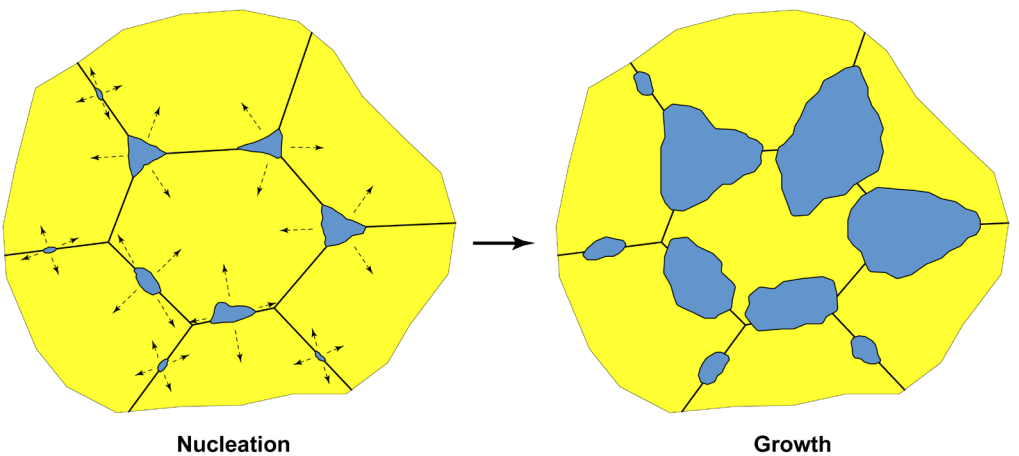

Figure 8.1 - Example of the nucleation and growth mechanism of steel microstructures. The yellow grains represent the original microstructure (austenite), instead the blue grains represent the new microstructure (pearlite, ferrite, cementite or bainite).

[2] To avoid confusion, the metallurgical theory of bainitic transformation as a diffusional transformation was preferred (diffusive theory). There is also a second theory, called displacive theory, for the transformation of bainite: in this case the transformation follow a mechanism similar to that of the martensitic transformation.

[3] Austenite is also a microstructure formed through nucleation and growth. Austenite nucleates and grows starting from liquid and/or from homogeneous crystals of δ-phase, in relation to the carbon content of steel. The mechanism is described in Paragraph 2.7 of Chapter 2.

Now let us see what happens if the number of nuclei increases or decreases.
Consider Figure 8.2: if the nucleation phase is favored, the growth is limited and the final microstructure has very fine grains. On the contrary, if few nuclei are formed, the growth is facilitated and the final microstructure has coarse grains. What happens is typical of all the microstructures formed by nucleation and growth: the more nucleation is favored, the more the final microstructure is fine-grained. The more growth is favored, the more the final microstructure is coarse-grained.

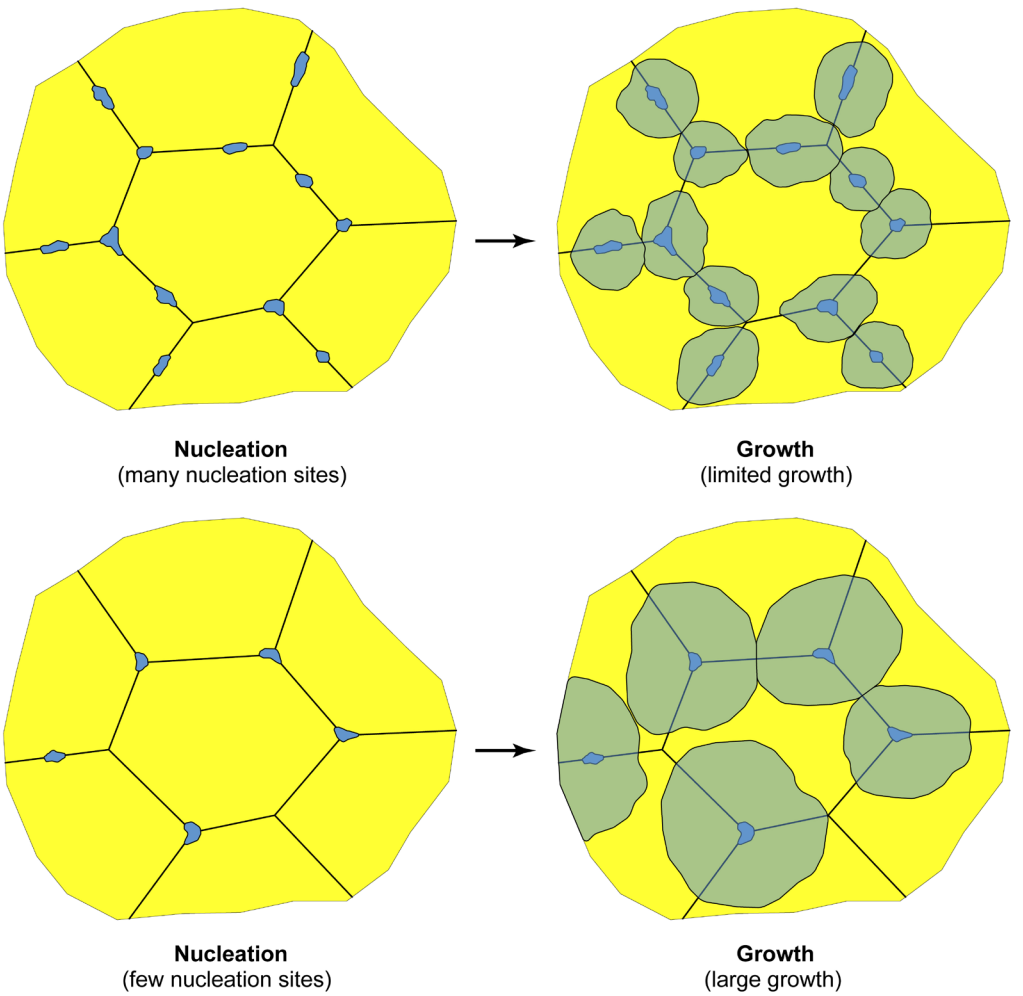

Figure 8.2 - Examples of the nucleation and growth mechanism if the nucleation is favored (at the top) or if the nucleation is limited (at the bottom). The yellow grains represent the original microstructure (austenite), instead the blue grains represents the new microstructure (pearlite, ferrite, cementite or bainite).

The microstructural transformations through nucleation and growth mechanism always depend on the temperature: austenite transformation at high temperature is dominated by growth (carbon diffuses faster) whilst nucleation predominates when temperature decreases (carbon diffuses more slowly).

Taking into account the same microstructure that forms from austenite:

- the final microstructure is finer if it nucleates and grows at a low temperature,
- the final microstructure is coarser if it nucleates and grows at high temperatures.

Observe, for example, the case of transformation through the nucleation and growth of pearlite (Figure 8.3): at high temperatures, close to 700°C growth is prevalent ($V_G > V_N$), while at lower temperatures, such as at 600°C, nucleation prevails ($V_N > V_G$)[4].

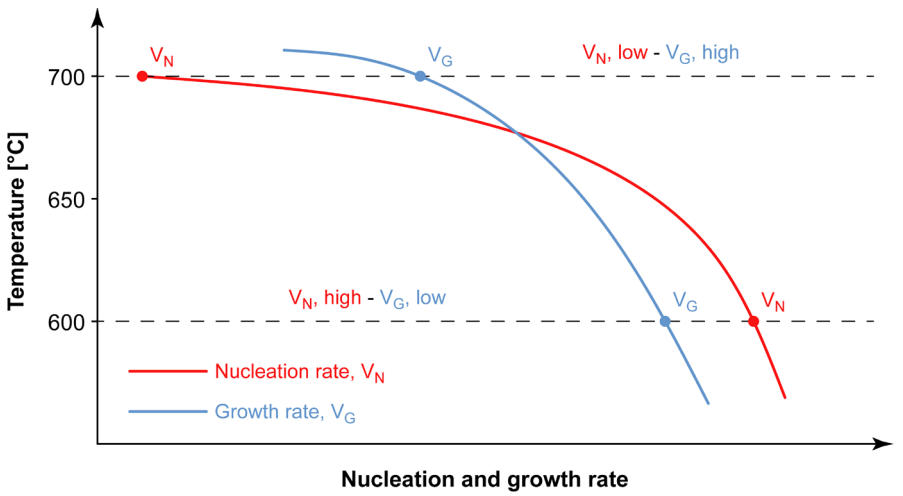

Figure 8.3 - Correlation between temperature and nucleation rate V_N or growth rate V_G of the austenite-pearlite transformation.

[4] *Both the rate of nucleation and the rate of growth, increase when temperature decreases. What is important is whether one or the other predominates. The example has a general validity (transformation of austenite into pearlite, ferrite, cementite, and bainite) even if it refers to the nucleation/growth of pearlite.*

8.3 Pearlite

Let us consider the austenite-pearlite transformation[5] governed by carbon diffusion and the nucleation and growth phenomena. Pearlite (lamellar grains composed of alternating layers of α-phase and Fe_3C phase) is formed from austentite (homogenous grains of γ-phase) when, as predicted by the *Fe-C* phase diagram or by the T.T.T./C.C.T. diagrams, γ-phase must transform into α-phase and Fe_3C phase. As long as the system is in γ-phase, carbon is in solid solution in the iron lattice. When the transformation from γ-phase to α-phase must occurs, the solubility of carbon is reduced drastically and Fe_3C phase must be formed. In fact, the diffusion of carbon atoms cause their concentration in several areas (lamellae of Fe_3C phase) and their depletion in other areas (lamellae of α-phase).

If the transformation occurs at high temperature, carbon diffuses from wide areas of γ-lattice (large-scale diffusion) and the lamellae of Fe_3C phase and of α-phase have a large size. If, however, the transformation takes place at a low temperature, carbon has a more limited diffusion path (short-range diffusion) and the lamellae of Fe_3C phase and of α-phase have a smaller size.

In the first case, the final microstructure consists of coarse pearlite colonies. In the latter case, however, the final microstructure is comprised of fine pearlite colonies (Figure 8.4).

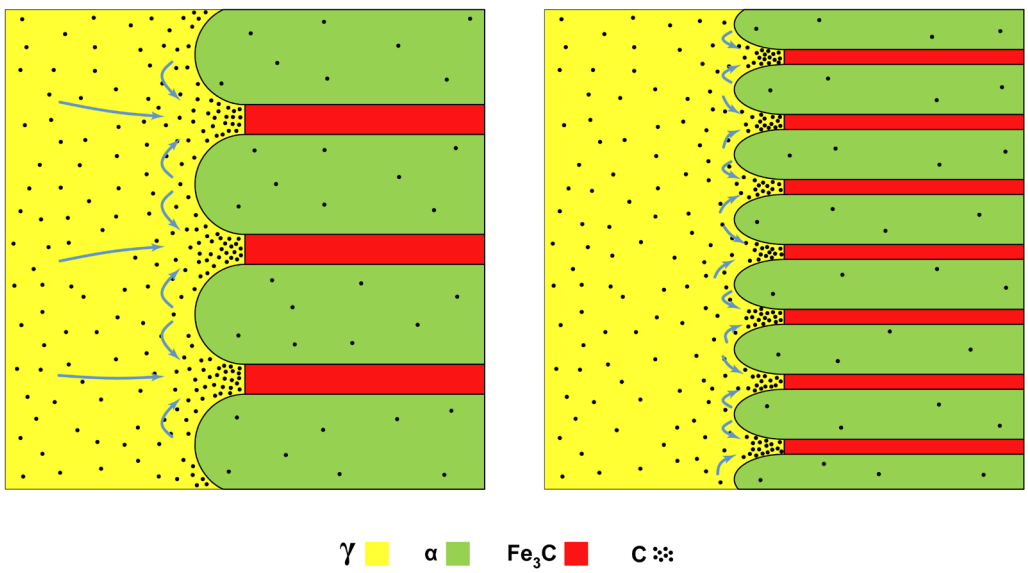

Figure 8.4 - Graphic representation of the nucleation and growth mechanisms of pearlite colonies: high-temperature transformation (to the left) and low-temperature transformation (to the right).

The pearlite colonies develop from the grain boundaries of the homogeneous crystals of γ-phase. The competitive growth of the various colonies leads to the formation of colonies of different sizes.

[5] *The transformation of austenite into pearlite occurs at eutectoid temperature for equilibrium cooling (Fe-C phase diagram) or during non-equilibrium cooling (T.T.T. or C.C.T. diagrams) when the cooling conditions are such as to trigger it.*

Considering the transformation of a single grain of austenite, the greater the number of nucleation sites, the greater the number of pearlite colonies.
On the contrary, if the nucleation sites are few, the growth of pearlitic colonies is large (Figure 8.5).

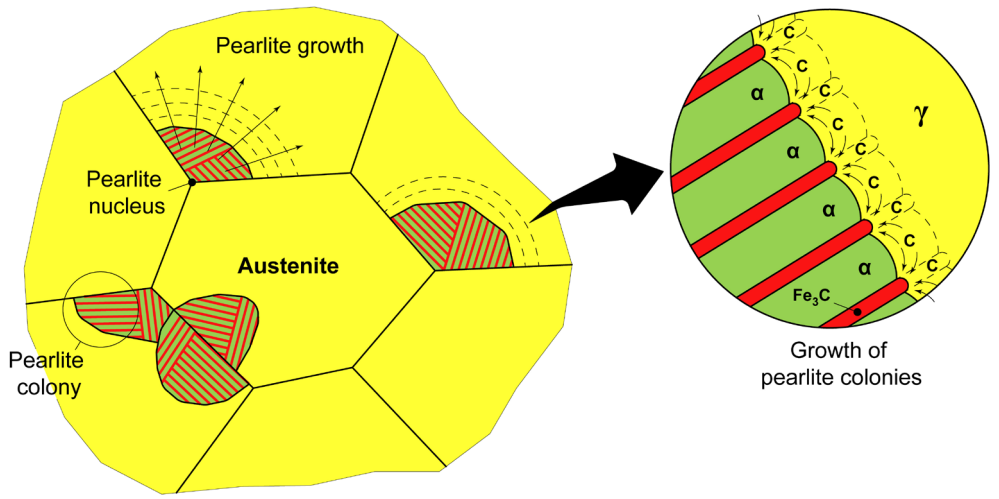

Figure 8.5 - Graphic representation of the nucleation and growth mechanisms of pearlite colonies [from Campbell 2008].

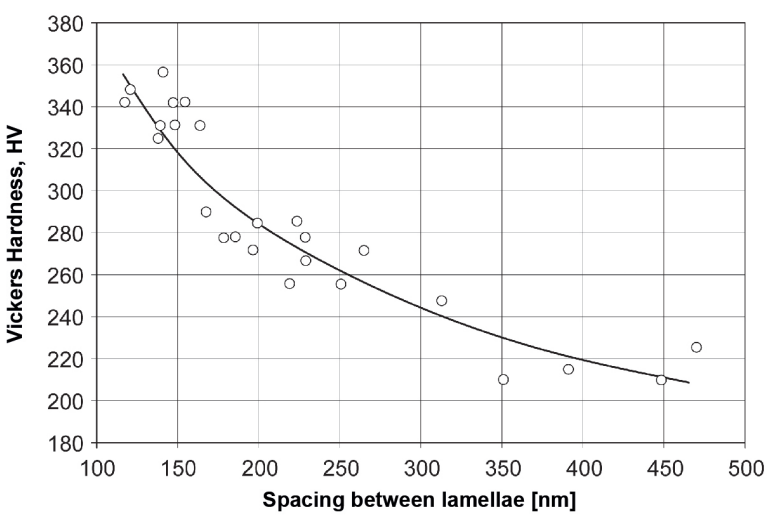

Figure 8.6 - Correlation between the spacing of pearlite lamellae and the Vickers hardness [from Clayton and Danks 1990].

In summary, if nucleation is favored, many small pearlite colonies (fine microstructure) are formed; if growth is favored, only a few pearlite colonies with large lamellae (coarse microstructure) are formed.
Typically, the hardness of pearlite in an annealed state is in the order of 200-350HV, in relation to the spacing of the lamellae: the more the lamellar microstructure is fine, the greater is the hardness (Figure 8.6).

At a metallographic level, pearlite, at least for magnifications up to 500x, has the shape of dark gray irregular grains. It is difficult to distinguish the lamellae of α-phase and the lamellae of Fe_3C phase[6] (Figure 8.7), and only with larger magnifications, for example, using scanning electron microscope, the pearlite microstructure can be easily observed (Figure 8.8).
Except for steel with eutectoid composition, the pearlitic microstructure is usually mixed with ferritic grains (hypoeutectoid steels) or cementite plates (hypereutectoid steel).

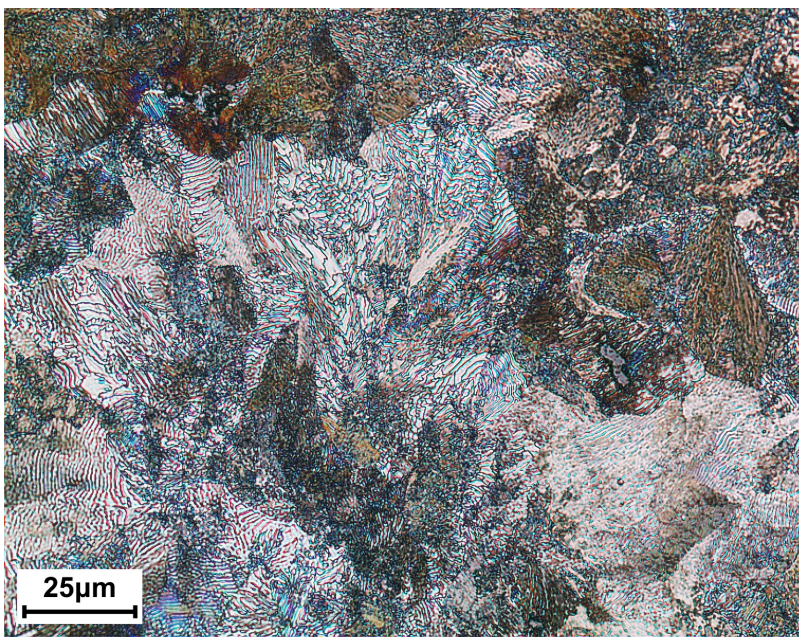

Figure 8.7 - Pearlitic microstructure of an EN R260Mn steel. Appearance under the metallographic microscope - Nital 2% etch. [Laboratories of the Department of Mechanical Engineering, Politecnico di Milano - Milano].

[6] *The typical metallographic etchant used for carbon steel is Nital 2, which is a 2% solution of nitric acid in ethyl alcohol. Nital selectively "attacks" the grain boundaries and the interface between the lamellae, leaving the other areas of the crystalline grains unaltered. This is the reason why pearlite is etched both internally and on the grain boundary assuming a typical dark gray color.*

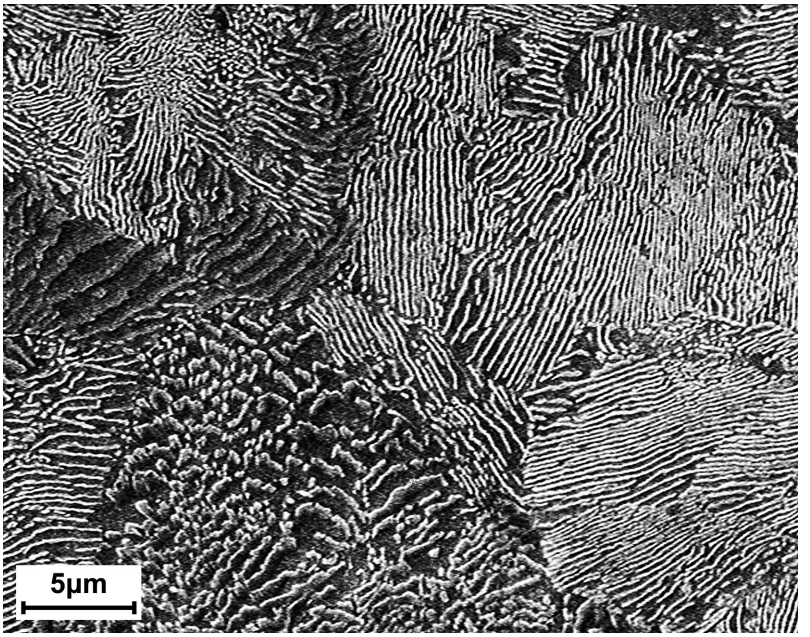

Figure 8.8 - Pearlitic microstructure of an EN R260M steel. Appearance under the scanning electron microscope - Nital 2% etch. [Laboratories of the Department of Mechanical Engineering, Politecnico di Milano - Milano].

8.4 Ferrite

For a generic hypoeutectoid steel, before the pearlitic transformation occurs, γ-phase forms homogeneous grains of α-phase, i.e. ferrite: the new microstructure originates from a variation in the solubility of carbon in γ-phase and is formed through nucleation and growth mechanism.

Ferrite nucleates on the grain boundary of the austenitic crystallites and it grows both along the grain boundaries and within the austenite grains (Figures 8.1 and 8.2).

In hypoeutectoid steel ferrite grows in combination with pearlite. The microstructure is almost all ferritic[7] only if the steel has a very low carbon content ($C < 0.02\%$).

The morphology of ferrite depends from both the cooling method, and the manufacturing process: the grains - with an irregular shape - may be equiaxed (Figure 8.9) or arranged along the maximum deformation direction (Figure 8.10).

[7] *An exception are ferritic stainless steels that, due to their high chromium content, have a completely ferritic microstructure, from melting to room temperature. Stainless steels are not part of this volume, since they have already been treated in Boniardi M., Casaroli A., Stainless Steels, Lucefin, Esine, 2014.*

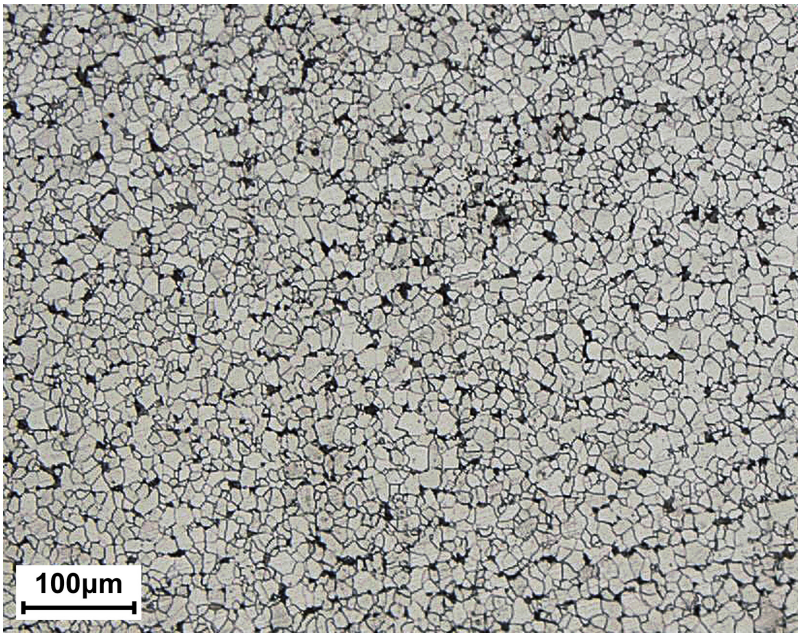

Figure 8.9 - Ferritic-pearlitic microstructure of an EN S235 steel. Appearance under the metallographic microscope - Nital 2% etch. [Exova S.r.l. Laboratories, Crema - Cremona].

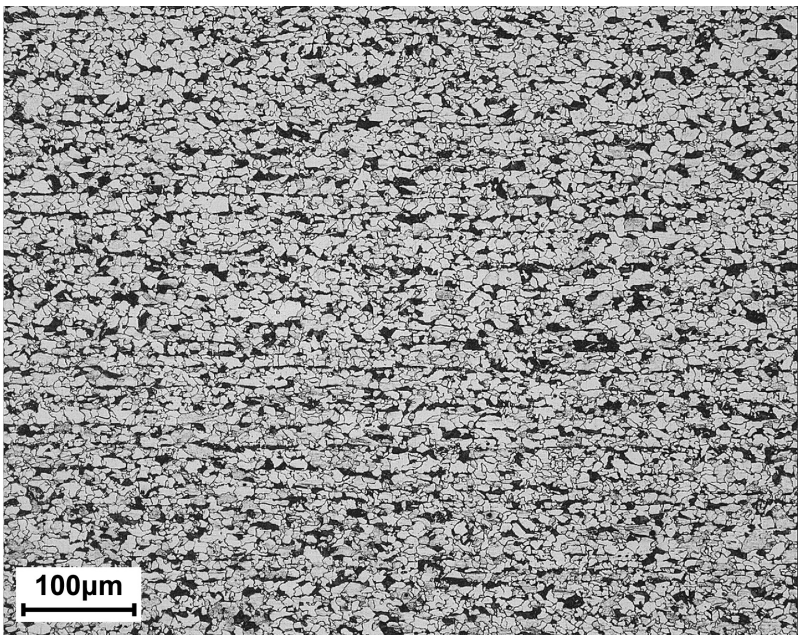

Figure 8.10 - Ferritic-pearlitic microstructure of an EN S355 steel. Appearance under the metallographic microscope - Nital 2% etch. [Exova S.r.l. Laboratories, Crema - Cremona].

In medium-carbon steels, ferrite has slightly different characteristics. Both a homogeneously distributed microstructure of pearlite and ferrite (Figure 8.11) and a microstructure where ferrite is predominantly along the grain boundary of pearlite can be observed (Figure 8.12).
In this second case, it is common to speak of proeutectoid ferrite.
Ferrite in annealed state has a very low hardness, in the order of 60-100HV, which can reach up to 250HV, only due to a significant grain refining. Under a metallographic microscope, ferrite has a white or light gray color[8].
In hypoeutectoid steel, it is also possible to observe an acicular/needle-like ferrite, called Widmanstätten's ferrite[9]. This structure is obtained by the rapid cooling of austenite from high temperatures or through the transformation of an austenitic structure with a coarse grain[10] (Figure 8.13).

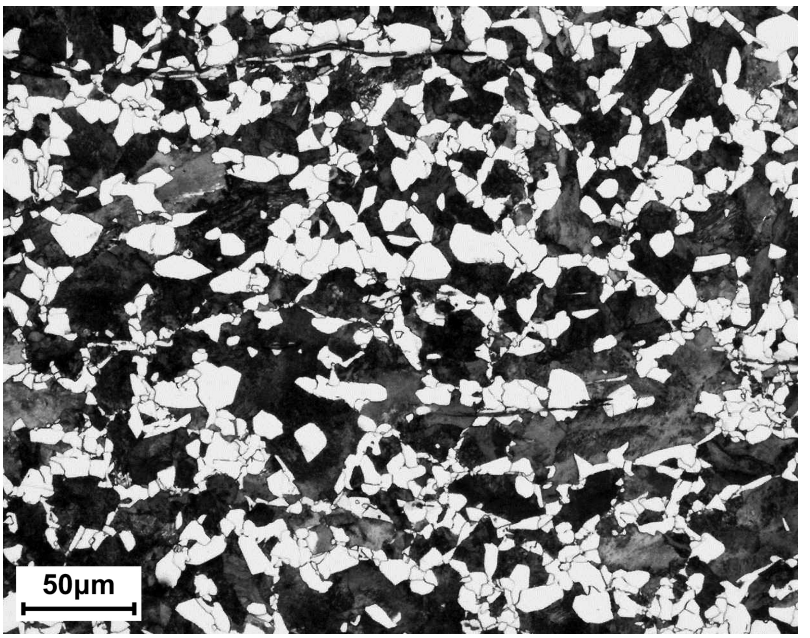

Figure 8.11 - Ferritic-pearlitic microstructure of an EN C40 steel. Appearance under the metallographic microscope - Nital 2% etch. [Omeco S.r.l. Laboratories, Monza - Monza Brianza].

[8] Nital 2 selectively "attacks" only the boundaries of the crystalline grains. For this reason, the inner part of the ferrite grains is not etched and the grains assume a typical white or light gray color.

[9] Alois von Beckh-Widmanstätten (1754-1849), Count of the Austro-Hungarian Empire, as well as typographer and scientist. He was director of the Vienna Imperial Porcelain Works. The discovery of acicular microstructures that are observed after etching with nitric acid of the polished surfaces of iron-nickel meteorites is attributed to him.

[10] Typically, Widmanstätten's ferrite is observed on medium-carbon steel workpieces forged at 1,200°-1,250°C and than air-cooled or in the Heat Affected Zone (H.A.Z.) of the welding joints of low carbon steel.

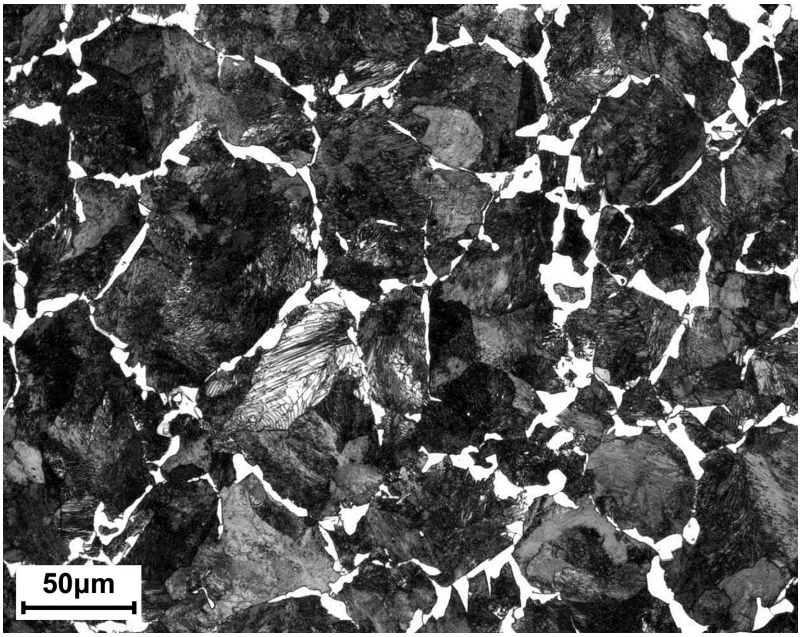

Figure 8.12 - Ferritic-pearlitic microstructure with proeutectoid ferrite of an EN C55 steel. Appearance under the metallographic microscope - Nital 2% etch. [Omeco S.r.l. Laboratories, Monza - Monza Brianza].

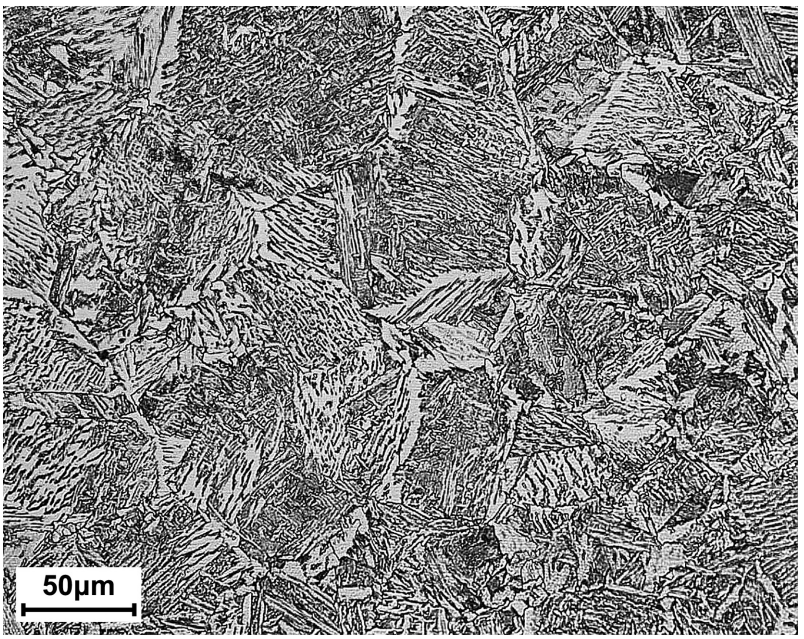

Figure 8.13 - Ferritic-pearlitic microstructure with Widmanstätten's ferrite of an ASTM F60 steel. Appearance under the metallographic microscope - Nital 2% etch. [Hammer S.r.l. Laboratories, Rho - Milano].

8.5 Cementite

Hypereutectoid steels form plates of Fe_3C phase on the grain boundary (cementite) before γ-phase transforms into pearlite. As for ferrite, the new phase originates from a variation in the solubility of carbon in γ-phase and is formed through nucleation and growth mechanisms.

Cementite nucleates and grows along the grain boundary of the austenitic grains. The term carbides is usually used instead of cementite[11] if steel contains alloying elements that reacts with carbon to form compound.

In hypereutectoid steel, cementite is present in combination with pearlite. Its name derives from the analogy with cement that holds bricks together.

Under a metallographic microscope, cementite appears whitish, since it is not attacked by the etching typically used for the metallography of steel.

The typical morphology of cementite is showed in Figure 8.14.

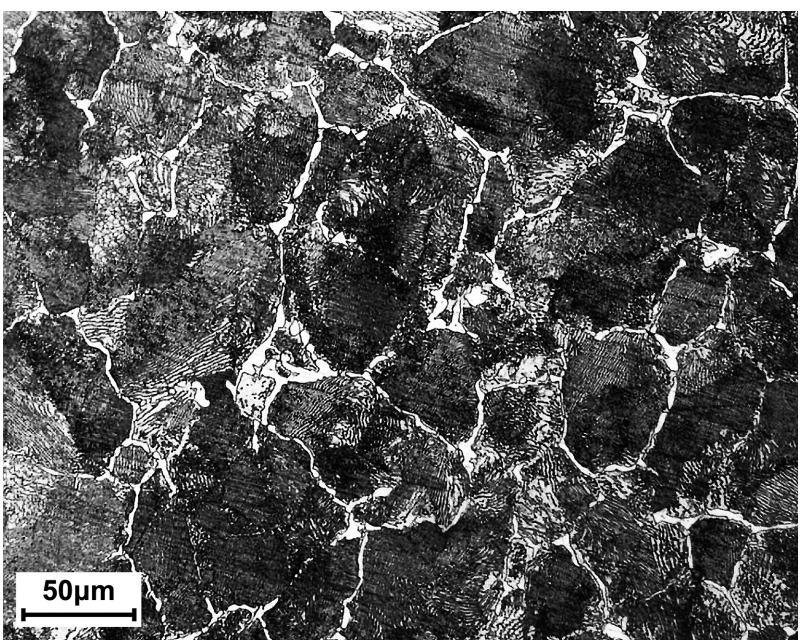

Figure 8.14 - Pearlite with cementite on the grain boundary of an EN C90 steel. Appearance under the metallographic microscope - Nital 2% etch. [Exova S.r.l. Laboratories, Crema - Cremona].

[11] This type of compound are very rich of the alloying elements (Cr, Mo, V, Ti, W, etc.). Therefore, it would be wrong to call them "cementite", a term that refers only to iron carbides (Fe_3C).

8.6 Bainite

The T.T.T. and C.C.T. diagrams highlight the existence of two microstructures not present on the *Fe-C* phase diagram: bainite and martensite.

Bainite is a very fine aggregate of α-phase and Fe_3C phase, both with an acicular morphology formed at temperatures between 250°C and 550°C. Bainite is formed from austenite under non-equilibrium conditions, both for isothermal cooling (T.T.T. diagrams) and for continuous cooling (C.C.T. diagrams).

The transformation of austenite into bainite occurs through nucleation and growth and is governed by the diffusion of carbon. In relation to the transformation temperature, we can speak of upper bainite and lower bainite (Figure 8.15).

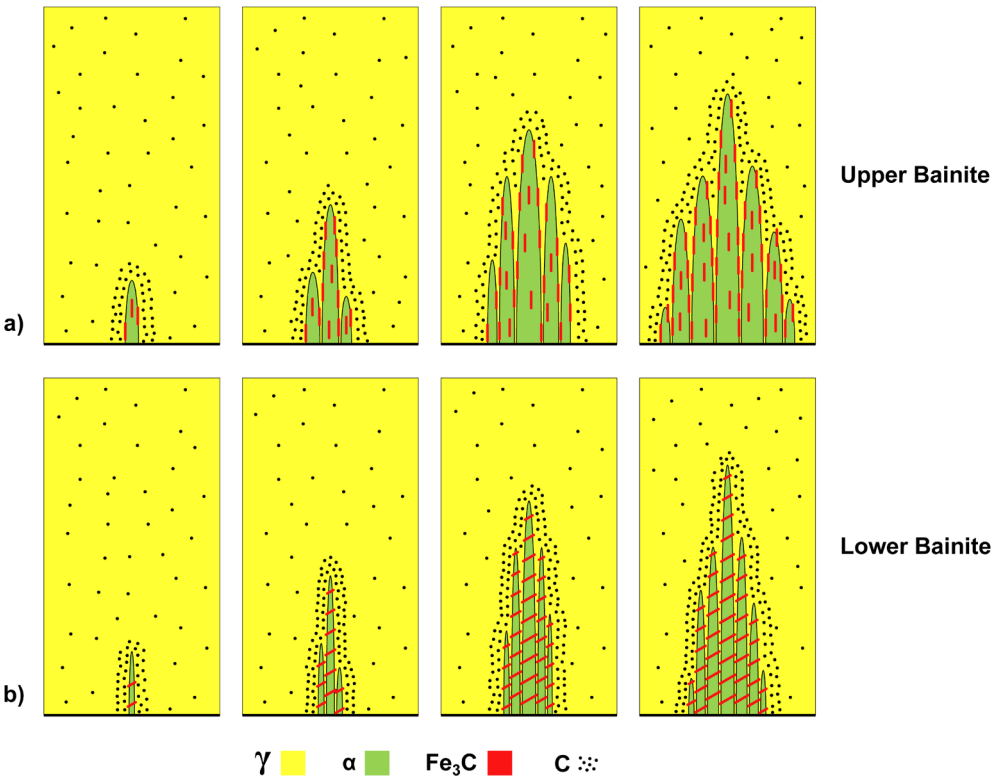

Figure 8.15 - Graphic representation of the nucleation and growth mechanisms of bainite: a) upper bainite; b) lower bainite.

Upper bainite transformation occurs between 400°C and 550°C. At these temperatures the rate of carbon diffusion is less than what occurs during the pearlitic transformation and sharp laths of α-phase surrounded by acicular plates of Fe_3C phase form from austenite grain boundary. Both laths of α-phase and acicular plates of Fe_3C phase are oriented in the same direction (Figure 8.15a).

Upper bainite is a sort of degenerated pearlite in which the lower mobility of carbon prevents deformation of lamellae (typical of pearlite) and allows the growth of lath of α-phases surrounded by acicular plate of Fe_3C phase (typical of bainite).
Lower bainite is similar to upper bainite. This is also obtained through nucleation and growth from austenite at temperatures between 250°C and 400°C. At these temperatures the mobility of carbon is further limited and the lath of α-phase are finer than the previous case, with plates of iron carbide (Fe_3C) tilted at approximately 60° with respect to the lat axis (Figure 8.15b).
The α-phase of bainite is harder than α-phase of pearlite, due to the high density of the dislocations. As a result, the hardness of bainite is greater than the hardness of pearlite and is between 300HV and 650HV (Figure 8.16).

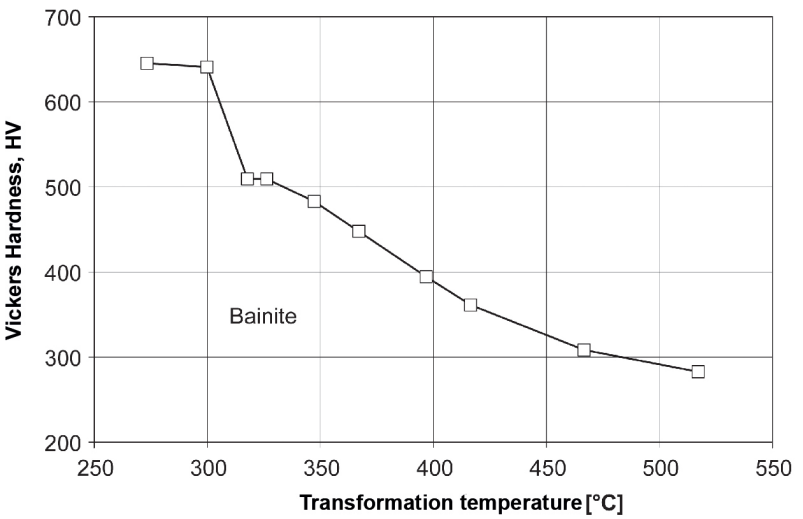

Figure 8.16 - Correlation between the isothermal transformation temperature of the bainitic microstructure and the Vickers Hardness for eutectoid steel [Ohmori and Honeycombe 1971].

Under a metallographic microscope, the acicular microstructure of bainite (Figures 8.17 and 8.18) cannot be distinguished, that is, it is not easy to observe the laths of α-phase and the acicular plates of Fe_3C phase.
Moreover, with classic metallographic techniques, lower bainite is very similar to martensite and is easily confused. The bainitic microstructure can be distinguished from the other microstructures (Figure 8.19) only through scanning electron microscope.

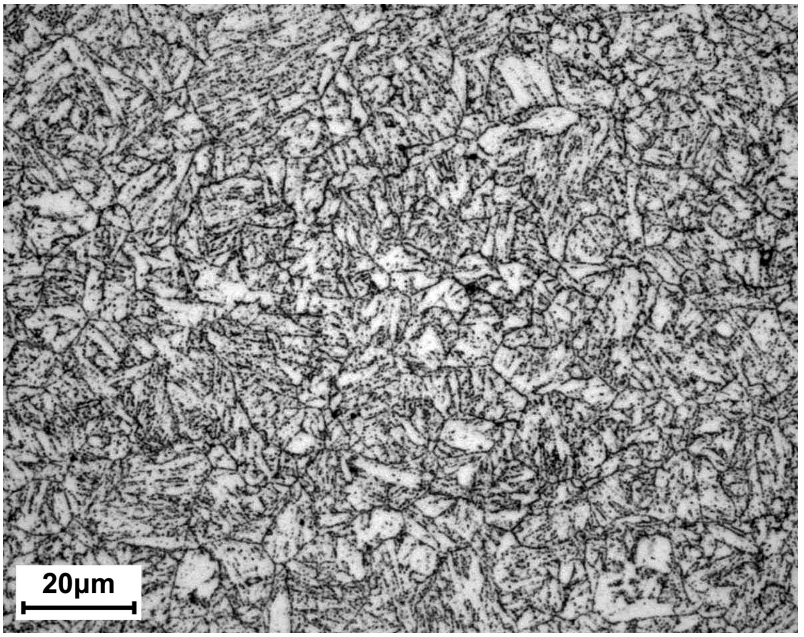

Figure 8.17 - Bainitic microstructure of an ASTM P91 / T91 (9Cr-1Mo) steel. Appearance under the metallographic microscope - Vilella etch. [Omeco S.r.l. Laboratories, Monza - Monza Brianza].

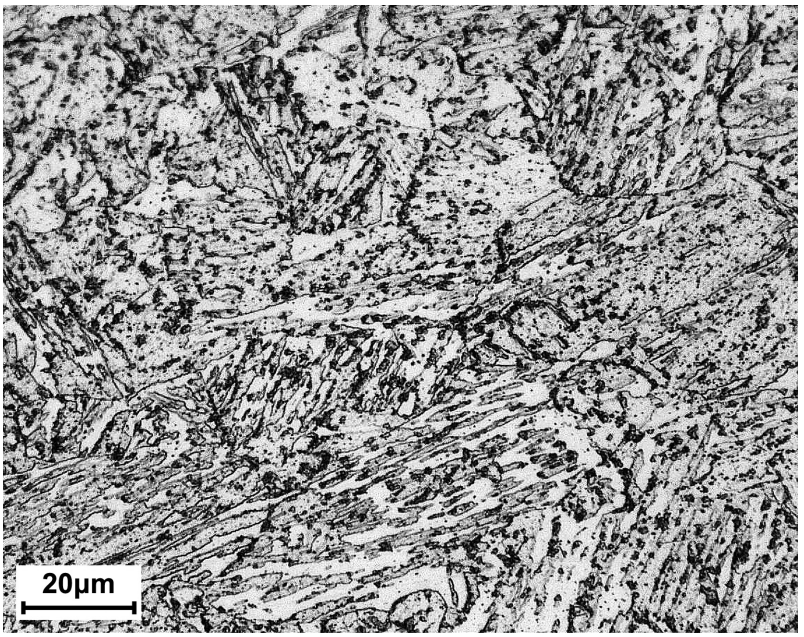

Figure 8.18 - Bainitic microstructure of an ASTM F22V steel (2.25Cr-1Mo-0.25V). Appearance under the metallographic microscope - Nital 2% etch. [Hammer S.r.l. Laboratories, Rho - Milano].

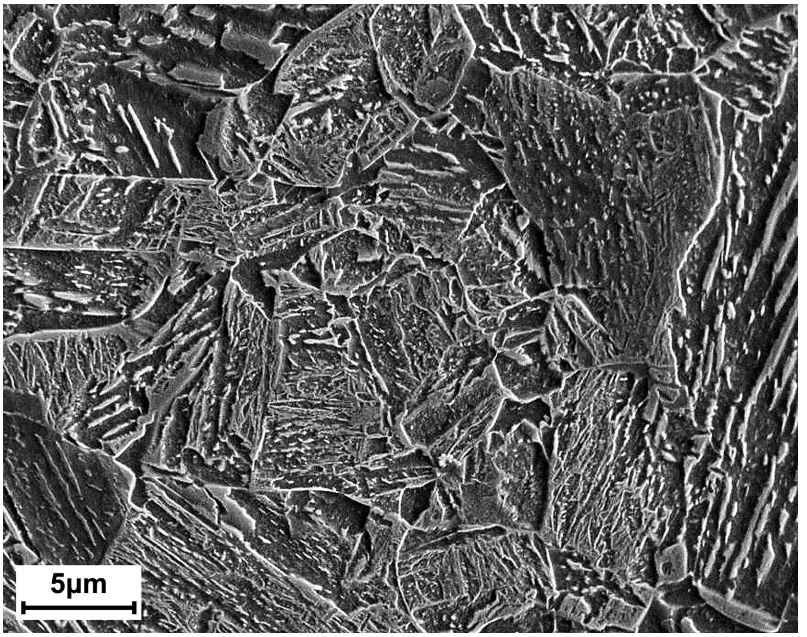

Figure 8.19 - Bainitic microstructure of an EN C75 steel. Appearance under the scanning electron microscope - Nital 2% etch. [Laboratories of the Department of Mechanical Engineering, Politecnico di Milano - Milano].

8.7 Martensite and instantaneous transformations of steel

The austenite-martensite transformation is very different from all the others observed previously. The martensite is obtained by instantaneous transformation of the austenite lattice[12], without diffusion phenomena.

The transformation from austenite to martensite is due to a rapid cooling when the cooling rate is higher than the cooling curve, v_s, on the C.C.T. diagrams.

The martensite is formed during the transformation of the F.C.C. lattice of γ-phase into the B.C.C. lattice of α-phase if carbon does not diffuse from the F.C.C. lattice, due to rapid cooling. This microstructure has a body-centered tetragonal lattice (B.C.T.) and is called α'. Since carbon does not diffuse during transformation, the martensite has the same chemical composition of the austentite.

The austenite-martensite transformation is characterized by the rearrangement of the atoms of the lattice, that is, by their repositioning through a coordinated movement.

[12] *The rate of the austenite-martensite transformation is equal to the speed of sound in steel, i.e. about 5,500 m/s.*

The phenomena involved during martensitic transformation are listed below (Figure 8.20):

- at high temperature, the austenite is stable and carbon occupies the interstitial sites of the F.C.C. lattice of γ-phase;
- if the cooling curve were slow, the carbon would spread from the F.C.C. lattice of γ-phase, forming iron carbides (Fe_3C). If the carbon were no longer present, the F.C.C. lattice of γ-phase would transform into the B.C.C. of α-phase;
- Since, however, the cooling rate is very high, carbon remains trapped in the F.C.C. lattice of γ-phase, which turns into a distorted B.C.C. lattice, called α′-phase, with a body-centered tetragonal lattice (B.C.T.).

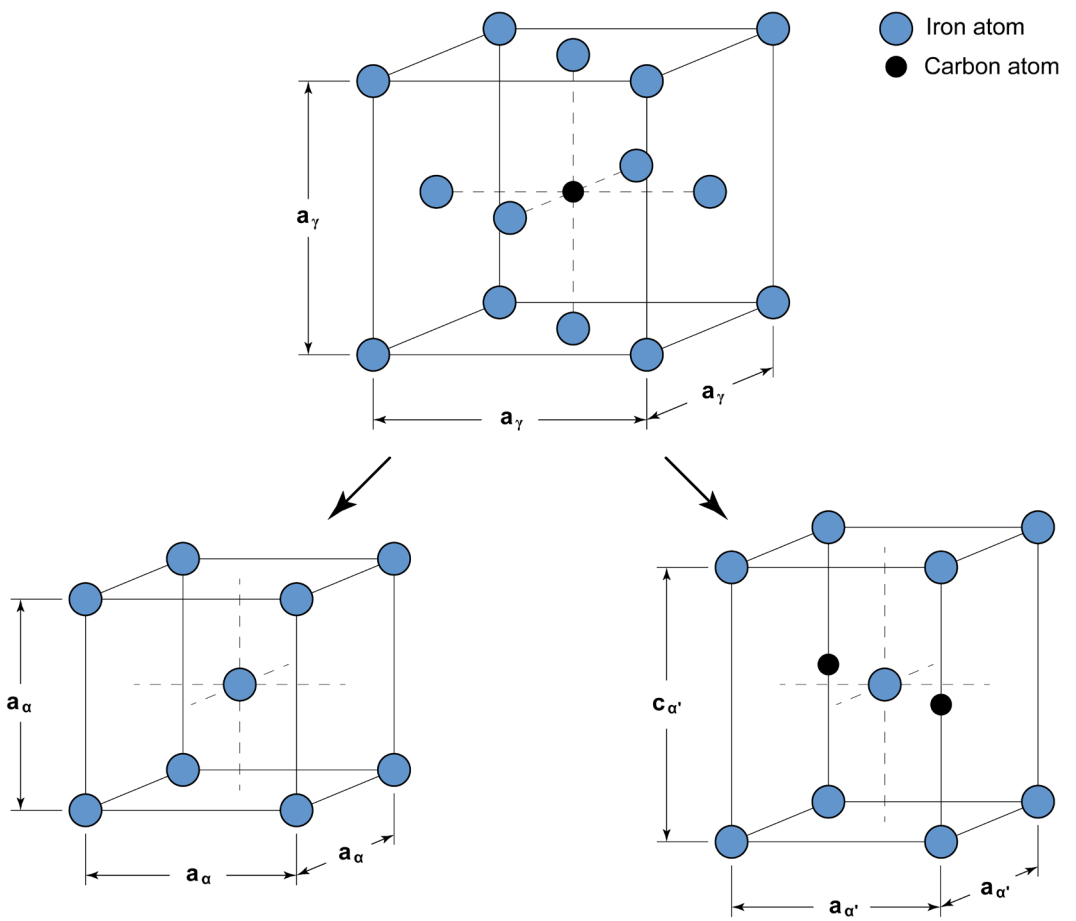

Figure 8.20 - Schematic representation of (i) the F.C.C. lattice of γ-phase of austenite, with a carbon atom in solution in the octahedral interstitial site, (ii) the B.C.C. lattice of α-phase of ferrite without carbon atoms in solution (carbon solubility is practically nil), (iii) the B.C.T. lattice of α′-phase of martensite, with carbon atoms in solution (in the same octahedral interstitial site of the F.C.C. lattice of austenite).

The B.C.T. lattice of martensite (α′-phase) is not very different from the B.C.C. lattice of ferrite (α-phase): the B.C.T. lattice is a body-centered cubic lattice elongated along one of the three directions, that is, with one of the axes of the cube ($c_{\alpha'}$) larger than the other two ($a_{\alpha'}$).
The distortion of the martensite lattice derives from the carbon atoms trapped in the cell since diffusion phenomena are inhibited due to the high cooling rate[13]. For this reason, it can be said that martensite is a ferritic microstructure oversaturated with carbon.
To explain the martensitic transformation, we usually refer to the theory proposed by Bain. Let us consider two adjacent F.C.C. cells (γ-phase), having lattice parameter a_γ: carbon atoms are dissolved within their lattice in correspondence of the octahedral interstitial site. Observing the two adjacent cells, it is easy to notice that the B.C.T. cell of martensite is already present within the original F.C.C. lattice. If the F.C.C. cell has lattice parameter a_γ, the B.C.T. has lattice parameters a_γ and $a_\gamma \cdot \frac{\sqrt{2}}{2}$ with carbon atoms arranged along the major edges (Figure 8.21).

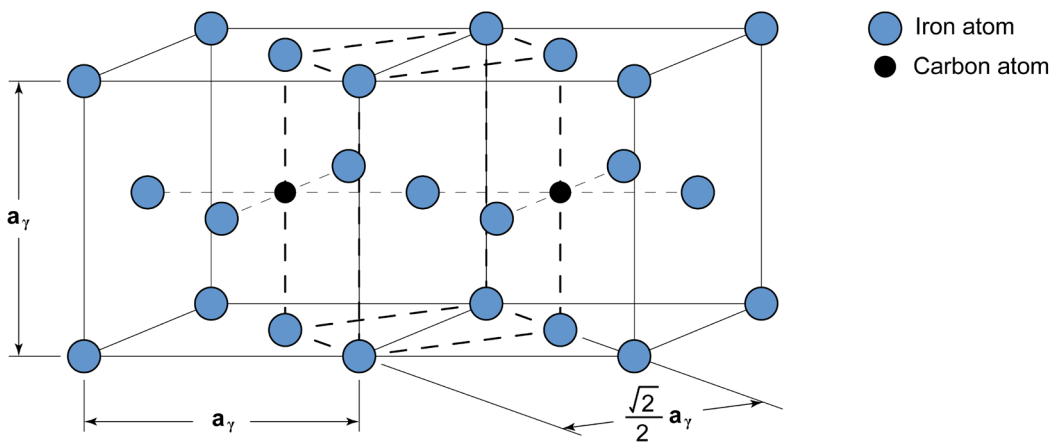

Figure 8.21 - Schematic representation of the austenite-martensite transformation. The B.C.T. cell (α′-phase) is formed during cooling due to the coordinated movement of the iron atoms.

When the F.C.C. cell of austenite cools down, it is transformed into the B.C.T. cell of martensite (α′-phase) due to the coordinated motion of the atoms of the lattice. At room temperature, the B.C.T. cell has undergone a reduction of 20% along the major edge (a_γ becomes $c_{\alpha'}$) and an expansion of 12% of the two minor edges ($\frac{\sqrt{2}}{2} \cdot a_\gamma$ become $a_{\alpha'}$).

[13] *From a statistical point of view, carbon atoms do not occupy all octahedral interstitial sites available in the F.C.C. cells of austenite. As a result, not all edges $c_{\alpha'}$ of the tetragonal cells of martensite are distorted in the same way.*

Simple geometric calculations highlight how the tetragonal cell of martensite at room temperature has a specific volume higher than the tetragonal cell within the original γ-lattice; in fact, the martensitic transformation always produces an increase of volume of about 4.3-4.5%.

The distortion of the martensite lattice depends only on the carbon content trapped inside the cell (Figure 8.22): the greater the amount of carbon, the greater the lattice distortion.

Therefore, also the hardness of martensite depends only on the carbon content and it is between 400HV and 800HV (Figure 8.23).

The only way to change hardness of the martensitic microstructure is to change the carbon content[14], i.e. change the type of steel. The martensitic microstructure has always the same hardness for the same type of steel, and it makes no sense to speak of fine or coarse martensite since the austenite-martensite transformation is instantaneous and does not occur through nucleation and growth.

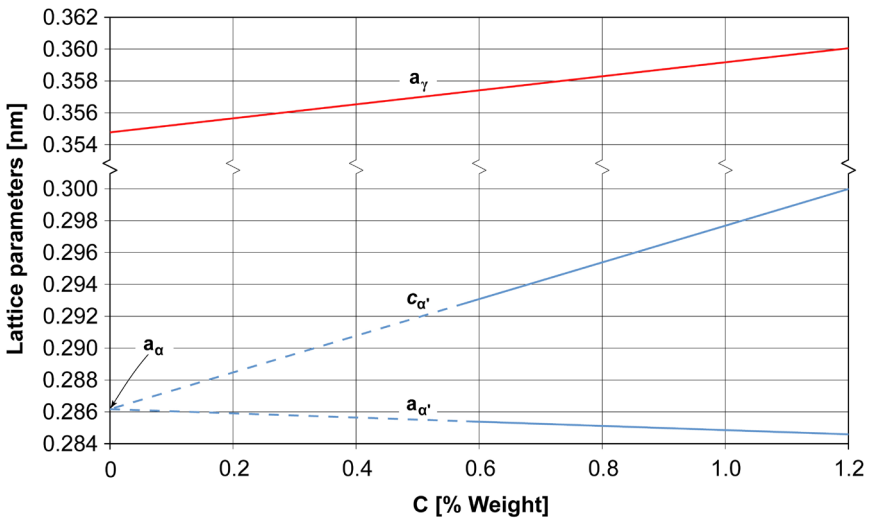

Figure 8.22 - Lattice parameters of the F.C.C. cell of γ-phase at 912°C, the B.C.C. cell of α-phase at 20°C, and the B.C.T. cell of martensite at 20°C [from Onink et al.1993 and Cheng et al.1991.

[14] *The correlation between the hardness of martensite and the carbon content is referred to as-quenched martensite. The correlation does not take into account the effect of other heat treatments (tempered martensite).*

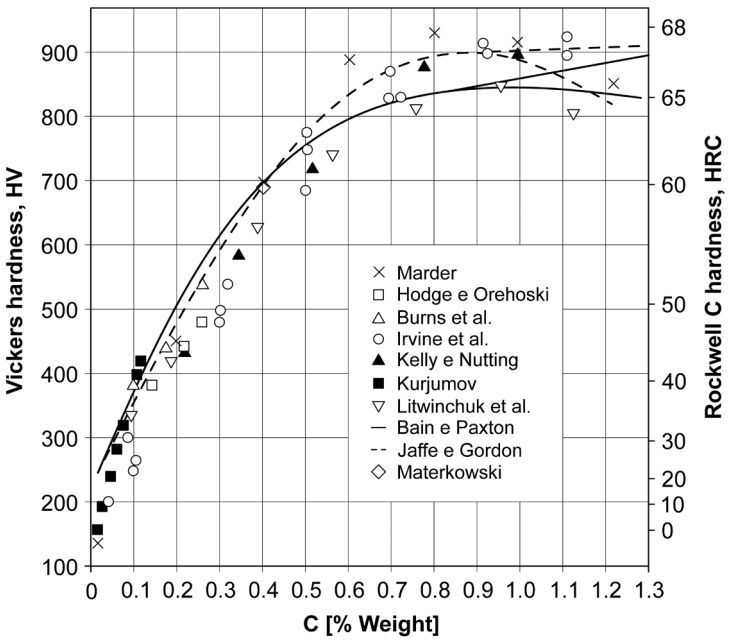

Figure 8.23 - The effect of carbon content on the hardness of as-quenched martensite [from Krauss 1980].

Under a metallographic microscope, martensite has an acicular morphology (Figure 8.24). If carbon is lower than 0.6%, the microstructure is formed of lath *(lath martensite)* ; instead, if carbon is greater than 1%, the microstructure is formed of plates *(plate martensite)*. Lastly, if carbon is between 0.6% and 1%, the microstructure is mixed. In both cases, the acicular microstructure of martensite consists of lath or plates arranged according to an equilateral triangle shape: this is the distinctive feature of the microstructure observed under a metallographic microscope (Figures 8.25 and 8.26) or under a scanning electron microscope (Figures 8.27 and 8.28).

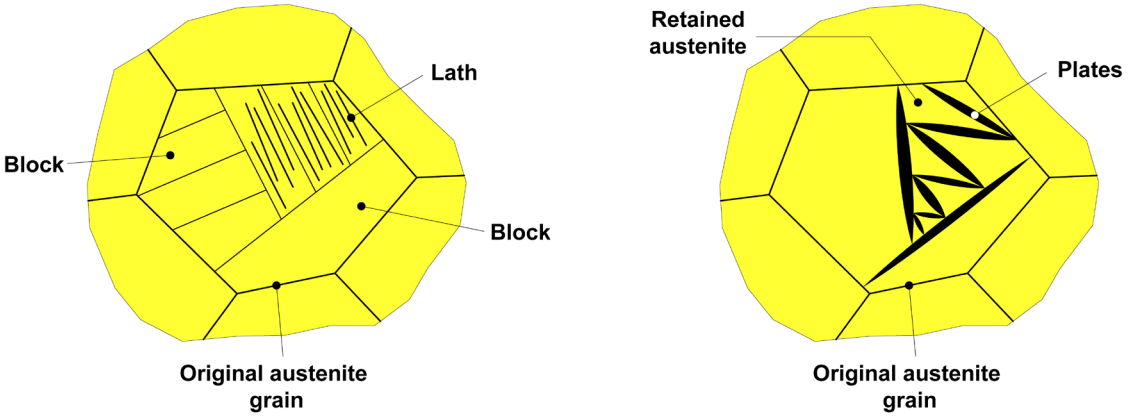

Figure 8.24 - Graphic representation of lath and plates of the martensitic microstructure [from Campbell 2008].

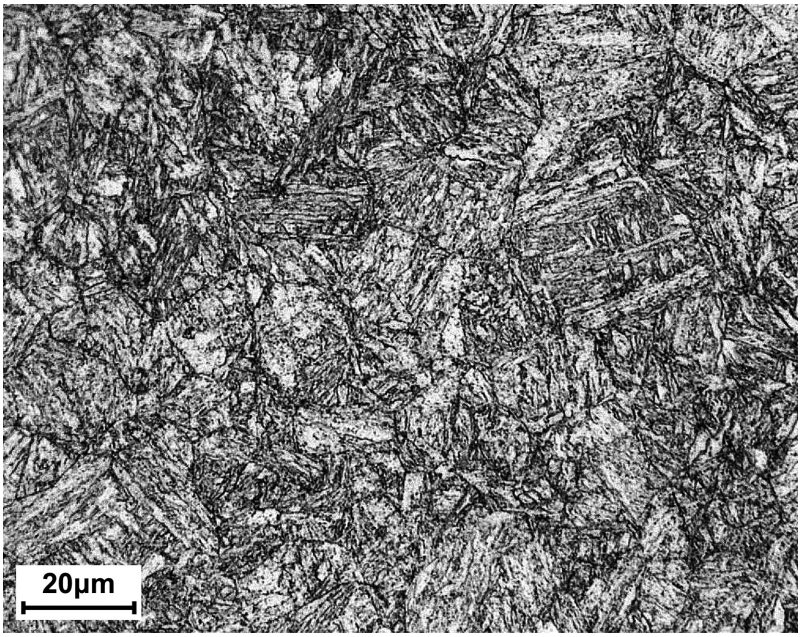

Figure 8.25 - Martensitic microstructure of an AISI 8630 steel. Appearance under the metallographic microscope - Nital 2% etch. [Hammer S.r.l. Laboratories, Rho - Milano]

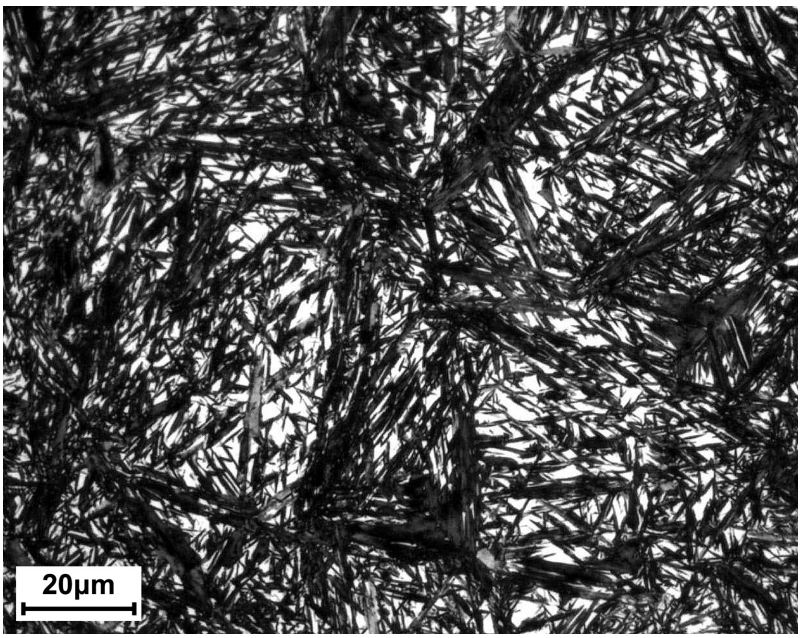

Figure 8.26 - Martensitic microstructure with retained austenite of an EN 100Cr6 steel. Appearance under the metallographic microscope - Nital 2% etch. [Omeco S.r.l. Laboratories, Monza - Monza Brianza].

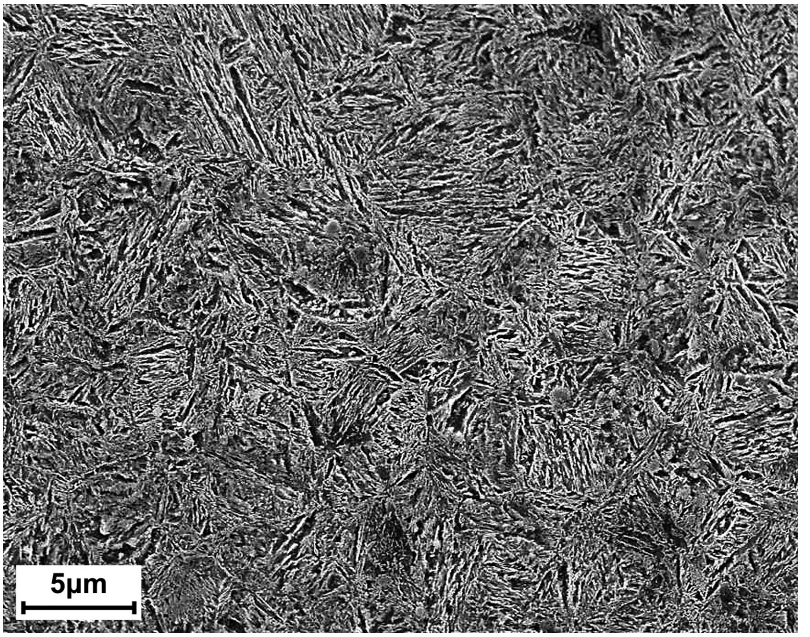

Figure 8.27 - Martensitic microstructure of an EN 42CrMo4 steel. Appearance under the scanning electron microscope - Nital 2% etch. [Laboratories of the Department of Mechanical Engineering, Politecnico di Milano - Milano].

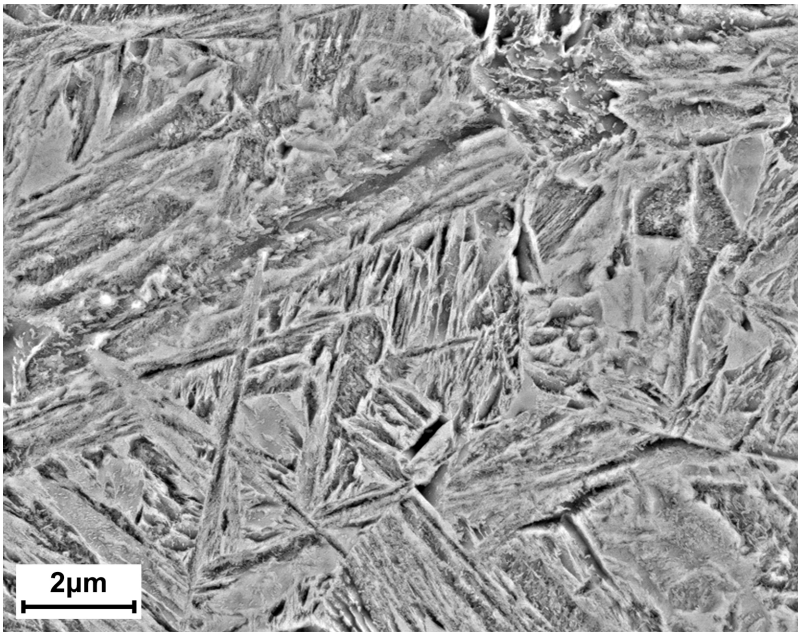

Figure 8.28 - Martensitic microstructure of an EN 34MnB5 steel. Appearance under the scanning electron microscope - Nital 2% etch. [Laboratories of the Department of Mechanical Engineering, Politecnico di Milano - Milano].

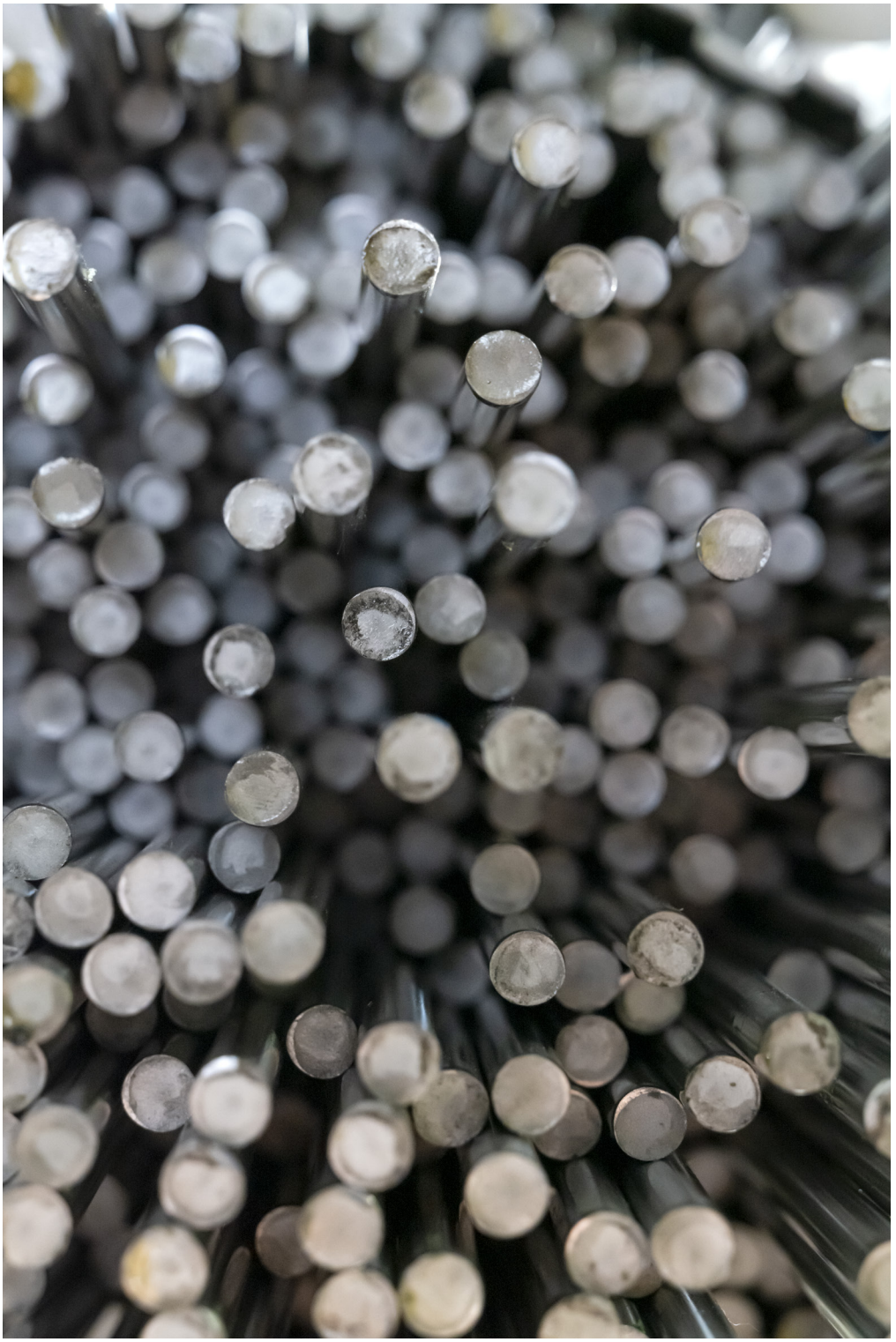

9. INDUSTRIAL HEAT TREATMENT OF STEELS

9.1 What are industrial heat treatments?

Industrial heat treatments are thermal cycles that are performed on semi-finished products or mechanical components, in order to modify the mechanical properties of the steel. An industrial heat treatment consists in heating, holding, and cooling cycles, and are normally carried out using industrial furnaces.

There are several ways to classify industrial heat treatments. The most used method is based on the holding temperature, and allows to divide the heat treatments into (Figure 9.1):

- heat treatments above critical points,
- heat treatments below critical points (sub-critical heat treatments).

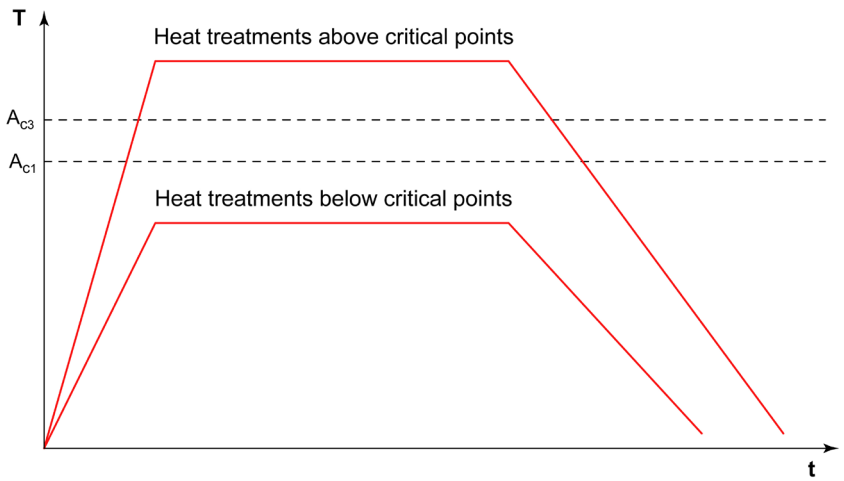

Figure 9.1 - Example of a heat treatment above or below critical points for a generic hypoeutectoid steel.

The main difference between the two types of heat treatment is related to the possibility of having or not having the transformation from γ-phase to α-phase during the heat treatment.

If the heat treatment exceeds critical points the final microstructure is different from the initial one. After the heating and holding phases, the original microstructure transforms into austenite and, during the cooling phase, the austenite forms new microstructures as a functin of the cooling rate. The morphological and mechanical properties of the microstructure are modified as well as the size of crystalline grains, level of strain hardening, level of recovery or recrystallisation, level of micro-hardness or residual stresses, etc.

If the heat treatment is sub-critical, the microstructure remains substantially unchanged; in fact, if the heating cycle is below critical points, no austenitic transformation occurs, and there is no microstructural transformation at the end of the cooling phase. Only the morphological and mechanical characteristics of the microstructure can be modified, but not the type.

9.2 Main types of heat treatments

Heat treatments above critical points are called:

- annealing,
- normalizing,
- hardening.

Annealing and normalizing produce a microstructure of ferrite and pearlite (hypoeutectoid steels) or pearlite and cementite (hypereutectoid steels) characterized by a medium/low hardness, good cold deformability and good machinability.

Instead, in the case of hardening, the objective is the opposite: to have a martensitic or bainitic/martensitic microstructure and give steel high hardness and mechanical strength.

Heat treatments below critical points are called:

- sub-critical annealing,
- tempering.

Sub-critical annealing includes various types of heat treatments, such as machinability, recrystallisation and stress-relief annealing. These heat treatments are performed when the microstructure is ferritic-pearlitic (or pearlite and cementite) and are designed to further improve machinability and reduce residual stresses caused by previous machining.

Tempering, on the other hand, is carried out on martensitic or bainitic/martensitic microstructures, to improve the impact strength and lowering residual stresses caused by the hardening process[1].

There are also two important heat treatments combination: normalizing plus annealing for machinability and hardening plus tempering.

There is another group of heat treatments in addition to those above or below critical points: surface heat treatments. These are thermal or thermo-chemical treatments that affecting only the surface and they include surface hardening, carburizing, carbonitriding, nitriding, nitrocarburizing.

Figure 9.2 shows a summary of the main types of steel heat treatments.

[1] *Another important function of tempering is to induce the transformation of retained austenite into bainite/martensite.*

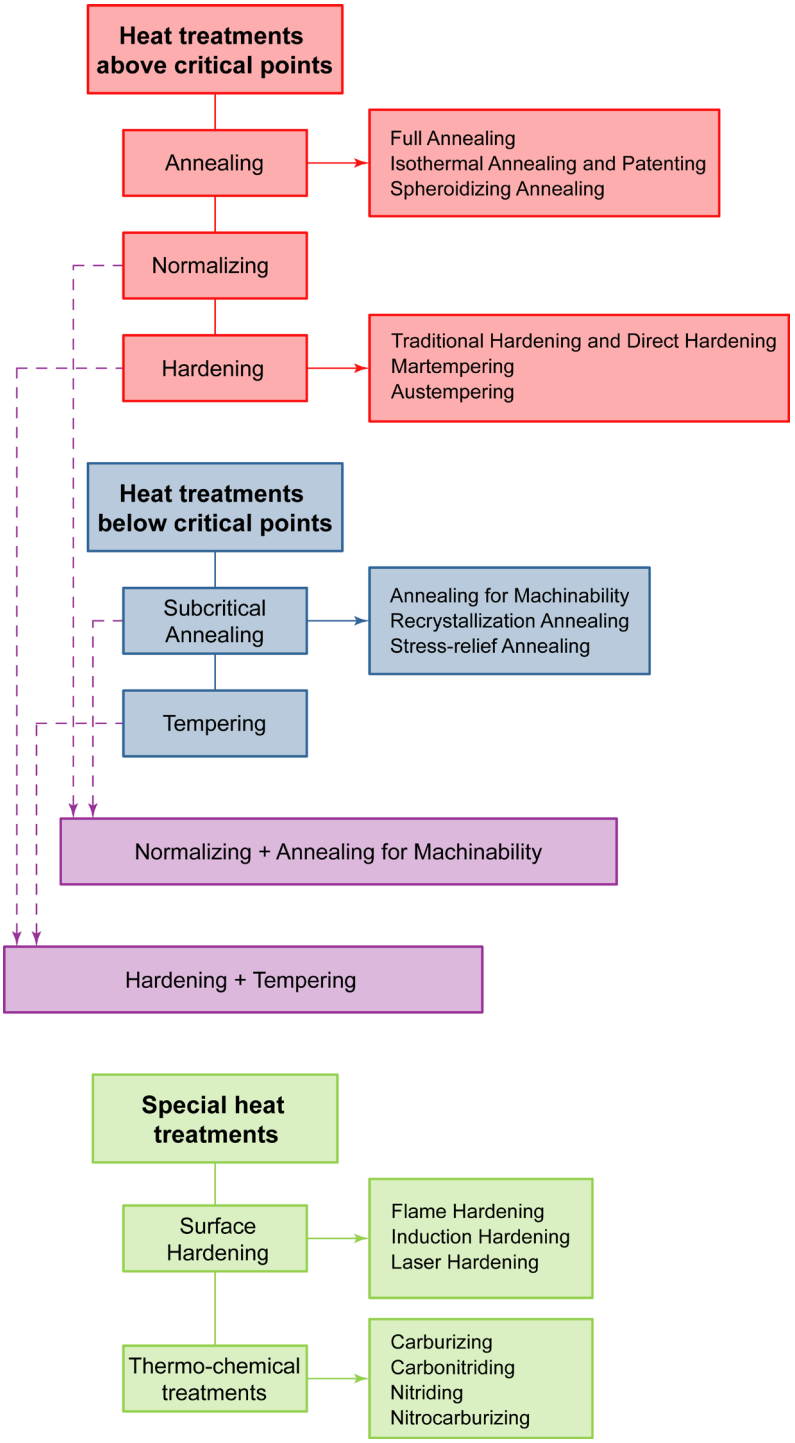

Figure 9.2 - Schematic representation of the main types of steel heat treatments.

10. HEAT TREATMENTS ABOVE CRITICAL POINTS

10.1 Common aspects of heat treatments above critical points

As seen in Chapter 9 heat treatments above critical points are annealing, normalizing, and hardening. Each of these heat traetment has three different phases: heating, soaking and cooling.

Some common aspects should be considered before proceeding further with the study of these heat treatments, in fact heating and soaking are practically identical and have similar problems.

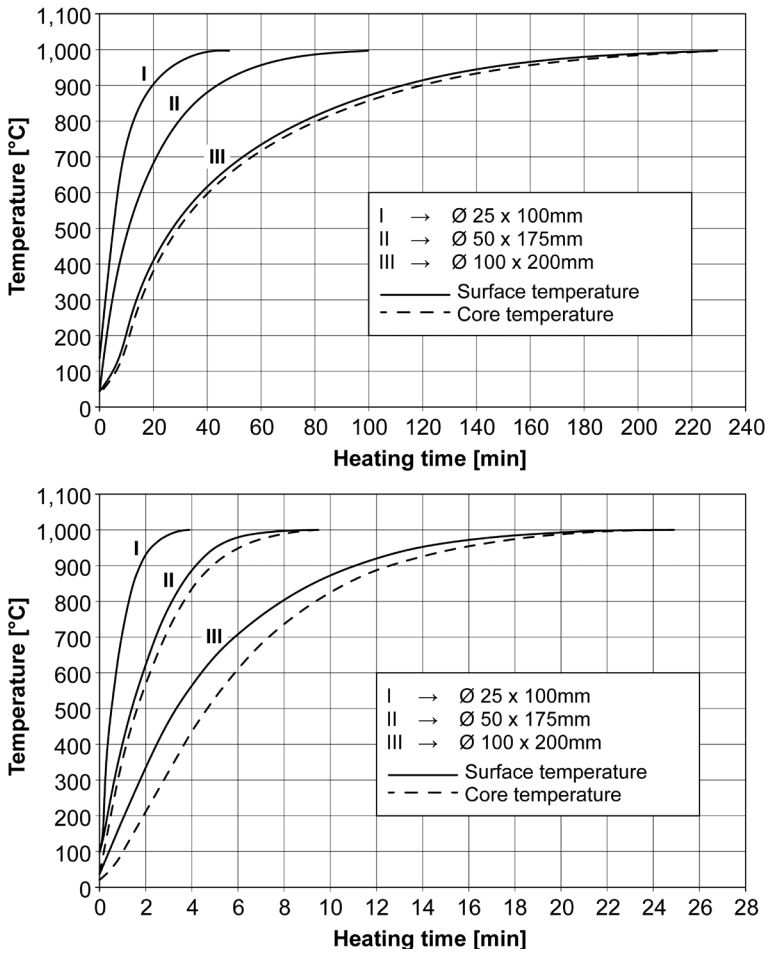

Figure 10.1 - Correlation between temperature and heating time for steel bars of different diameter and length, heated to 1,000°C in a muffle furnace (top) and in a salt bath furnace (bottom) [from Thelning 1975].

Heating

Heating can be carried out in different ways, depending on the types of industrial furnaces, the size of the workpieces, and the thermal properties of the steels.

First of all, keep in mind that the heating rate is greatly influenced by both the thermal capacity of the furnace and the geometrical characteristics of the component. The heating phase must ensure that the heat generated by the furnace heating elements equally affects all the parts of the workpieces to be heat treated (Figures 10.1 and 10.2).

Another important aspect is the furnace temperature when the workpieces are inserted inside it; in fact, the furnace can be already hot or still cold (Figure 10.3).

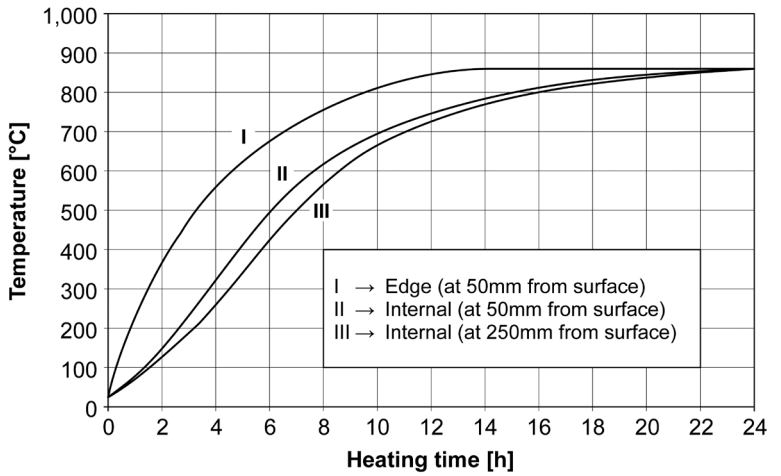

Figure 10.2 - Correlation between temperature and heating time for a 2,300x950x500mm steel plate, heated at 850°C in a muffle furnace [from Thelning 1975].

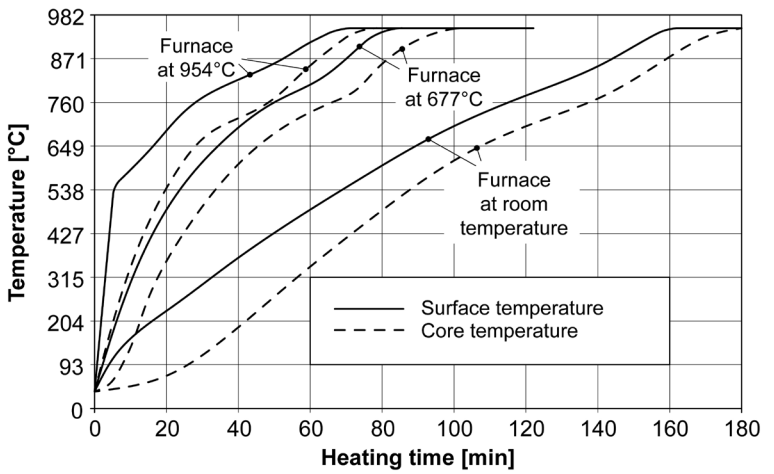

Figure 10.3 - Correlation between temperature and heating time for a 75mm thick steel plate, heated at 954°C and inserted into a cold or pre-heated muffle furnace [from Briggs 1958].

Other elements to consider are the geometry of the workpiece and the thermal conductivity of the steel[1]. In general, the time required to equalize temperature between the core and the surface increases as the size of the component increases and the thermal conductivity of the steel decreases.
If the steel conductivity is low or the component is large, the surface heat up quickly and expans, while the core remains cold and does not deform. This temperature gradient generates stresses and/or irreversible deformations that can lead to scrapping the component[2]. Consequently, a great deal of attention should be paid to the heating rate of the component to be heat treated. To this regard, Figure 10.4 shows how heating carried out with a controlled method, reduces the temperature difference between the surface and the core of the component without increasing the heating time.
Other problems are related to the oxidation and decarburization of steel, resulting in carbon depletion on the surface. This aspect is of great importance when the workpieces are not further finished on machine tools. In some cases, it is convenient to perform the heat treatment in a non-oxidizing atmosphere. Nitrogen atmosphere or mixtures of inert and reducing gases (mixtures of N_2 with CO and/or H_2) are usually used to protect components from oxidizing, during heat treatment.

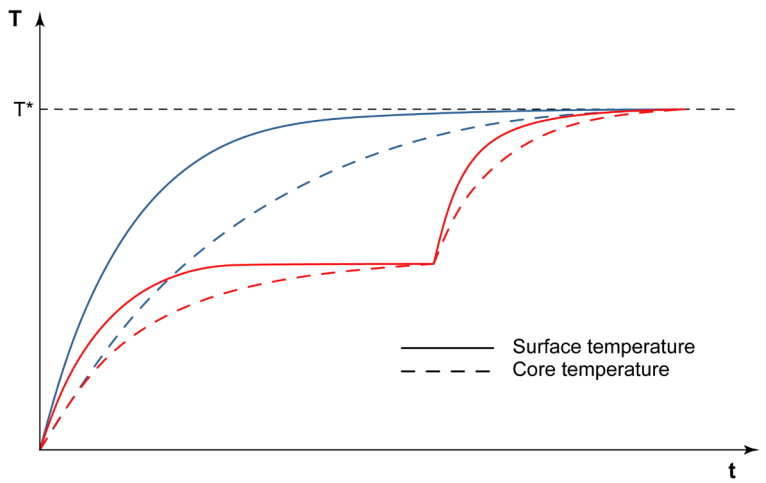

Figure 10.4 - Schematic representation of a continuous heating cycle (blue) and a step heating cycle (red): T^* is the heating temperature .

[1] *The thermal conductivity of steel, at least in first approximation, is inversely proportional to the amount of alloying elements. Materials with low thermal conductivity, therefore, belong to families of steels with high content of alloying elements, i.e. tool steels and stainless steels. These steels, especially on large-sized workpieces and/or with complex geometries, may have problems during heat treatment, both during heating and cooling.*

[2] *In addition to the dimension, even the shape of the component should not be underestimated. Very thick sections near very thin sections generate significant thermal gradient which can lead to a permanent deformation of the component during heating or cooling.*

Soaking

The soaking phase is defined by two parameters: the heat treatment temperature and the holding time. The holding temperature is defined by the type of heat treatment to be carried out, while its duration depends on the workpiece size. There are two requirements to be met during soaking.

First, the workpieces must reach thermal equilibrium, i.e., the core temperature and the surface temperature are the same. Secondly, soaking should allow for the development of the structural transformations requested by the heat treatment, such as the transformation of the original microstructure into austenite, the dissolution of carbides, the recrystallisation, the diffusion of the alloying elements, etc.

Empirical formulas can be used to estimate the holding time, i.e. the time that passes from when the furnace has reached the heating temperature until the beginning of cooling. They provide an estimate of the penetration rate of heat energy in the workpiece and are based on the principles of heat transmission in solids. If the heat treatment is carried out in air, the minimum holding time can be estimated in the range of one minute per millimeter or half an hour per inch, where the dimensional indication (millimeters or inches) refers to:

- the thickness of the section, in the case of plates with small thickness as compared to the other two sizes;
- the radius of the section, in the case of round pieces of infinite length.

For example, the soaking time of a cylindrical bar of 100mm in diameter, or a plate of 50mm in thickness, made of carbon steel and heat treated in air, is equal to one hour.

For heat treatments performed in fused salt baths, holding times are cut in half (one minute every two millimeters or fifteen minutes per inch). For high-alloy steel, such as tool steel or stainless steel, the holding times must be increased by 20%.

Please note that this rule gives good results for sections of a thickness (or radius) between 10mm and 100mm. A thickness (or radius) of less than 10mm has an holding time longer than what was calculated; on the contrary a thickness (or radius) greater than 100mm, has a shorter holding time. These empirical formulas does not take into account the thermal characteristics of the furnaces used and how the components are loaded into the furnace.

If a greater level of detail is needed, the thermal behavior of the components to be treated and the furnaces to be used can be investigated through suitable thermocouples applied to specific samples. Figure 10.5 shows an example.

10.2 Full annealing

Full annealing involves the progressive heating until a temperature of 20°-50°C above critical point A_{c3} if the steel is hypoeutectoid, or between critical point A_{c1} and critical point A_{cm} if steel is hypereutectoid (Figure 10.6).

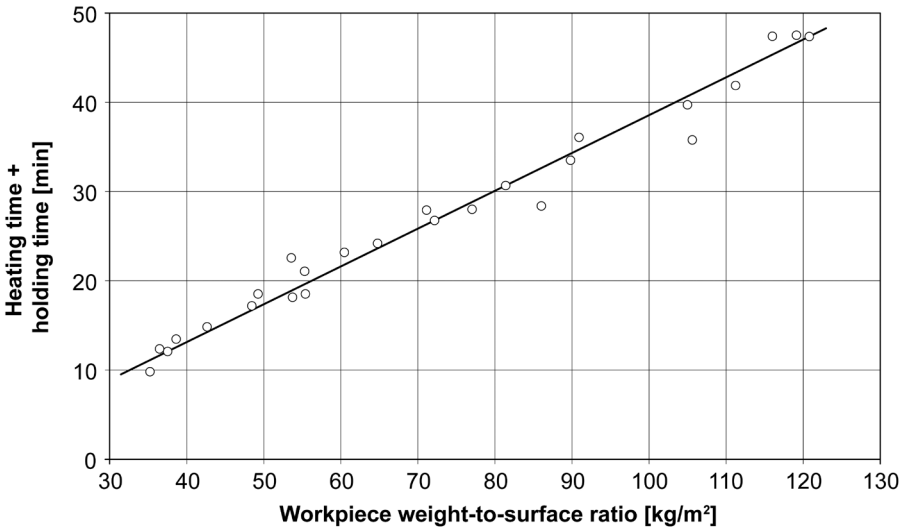

Figure 10.5 - The effect of workpiece weight/surface ratio on the heating plus holding time. This diagram is valid only for a resistance heating muffle furnace having a power of 8 kW and dimensions of 240x240x400mm [from Jost et al.1976].

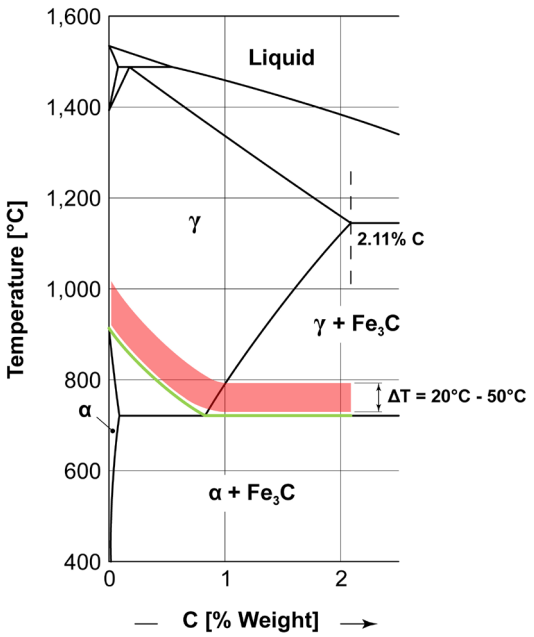

Figure 10.6 - The effect of carbon on the holding temperature for full annealing of steels (red band). The green line highlights critical points.

Soaking time should be long enough to equalize the temperature within the semi-finished product/component to be treated (Paragraph 10.1), and form austenite (if the steel is hypoeutectoid) or austenite and cementite (if the steel is hypereutectoid) in the whole component. The holding temperature varies between 760°C and 900°C, depending on steel chemical composition. Generally, it is never advisable to exceed these values because of the risk of grain growth and worsening of mechanical properties.

It is also worth mentioning a distinction between hypoeutectoid and hypereutectoid steels after the heating and soaking phase: while the first are completely austenitized, the latter, have a microstructure consisting of austenite plus carbides[3] due to the holding temperature between A_{c1} and A_{cm}. In fact, a holding temperature between A_{c1} and A_{cm} prevent the risk of grain growth or, worse, steel burning[4].

The cooling phase is very slow, in the order of 5°-30°C/hour, and is carried out in the furnace. Usually, after reaching 300°C, the workpiece is extracted from the furnace and cooled in air.

With reference to the C.C.T. diagram of a generic hypoeutectoid steel, the cooling phase can be compared to what is shown in Figure 10.7.

At the and of the annealing, a coarse microstructure of ferrite and pearlite (if the steel is hypoeutectoid), or pearlite and cementite (if the steel is hypereutectoid), is formed.

The microstructure is very homogeneous both from a chemical and morphological point-of-view, with equally-sized coarse grains. Hardness is very low and, consequently, cold deformability is high. Machinability may not be optimal due to the high level of grain growth[5].

Typically, full annealing is performed on semi-finished products obtained by forging, stamping or hot rolling, or on workpieces that require very slow cooling to form a microstructure with good machinability[6].

[3] The hypereutectoid steel has not a completely austenitic microstructure before cooling due to the holding temperatures between A_{c1} and A_{cm}.

[4] Burning is a phenomenon that occurs when the heating temperature is to high and cause the formation of liquid metal along the grain boundaries (i.e. areas with a lower melting temperature). If burning occurs, the components permanently lose their mechanical properties and they must be scrapped.

[5] Extremely coarse crystalline grains facilitate the formation of build up edge on the tool face, causing premature wear of the tool.

[6] Steel used for tools or bearings, martensitic stainless steel and air hardening steel.

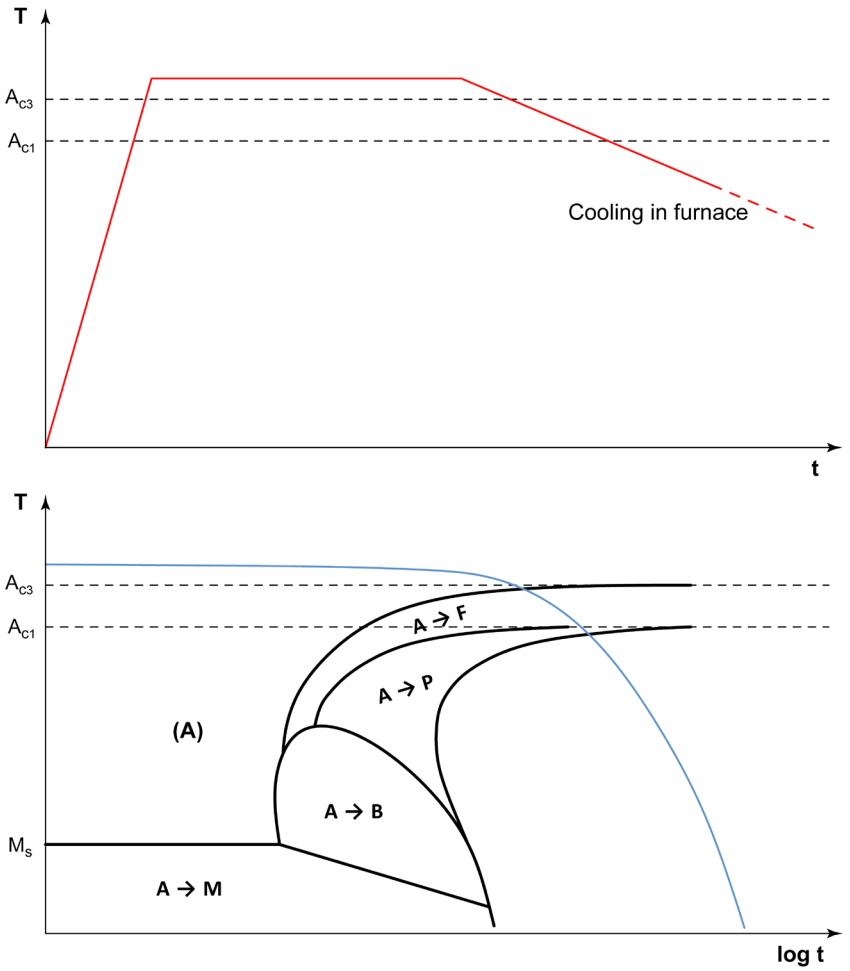

Figure 10.7 - Schematic representation of full annealing for a generic hypoeutectoid steel (on the top). The cooling curve is superimposed on the C.C.T. diagram (on the bottom).

10.3 Isothermal annealing and patenting

Full annealing is rarely performed, because of the high costs due to the extended use of the heat treatment furnace. An economical alternative is the isothermal annealing that produces results similar to full annealing. To understand what occurs during this heat treatment, see Figure 10.8.

Steel is initially heated and holded at the austenitization temperature (temperatures are the same as full annealing), therefore, a rapid cooling is carried out, in order to prevent the austenite transformation.

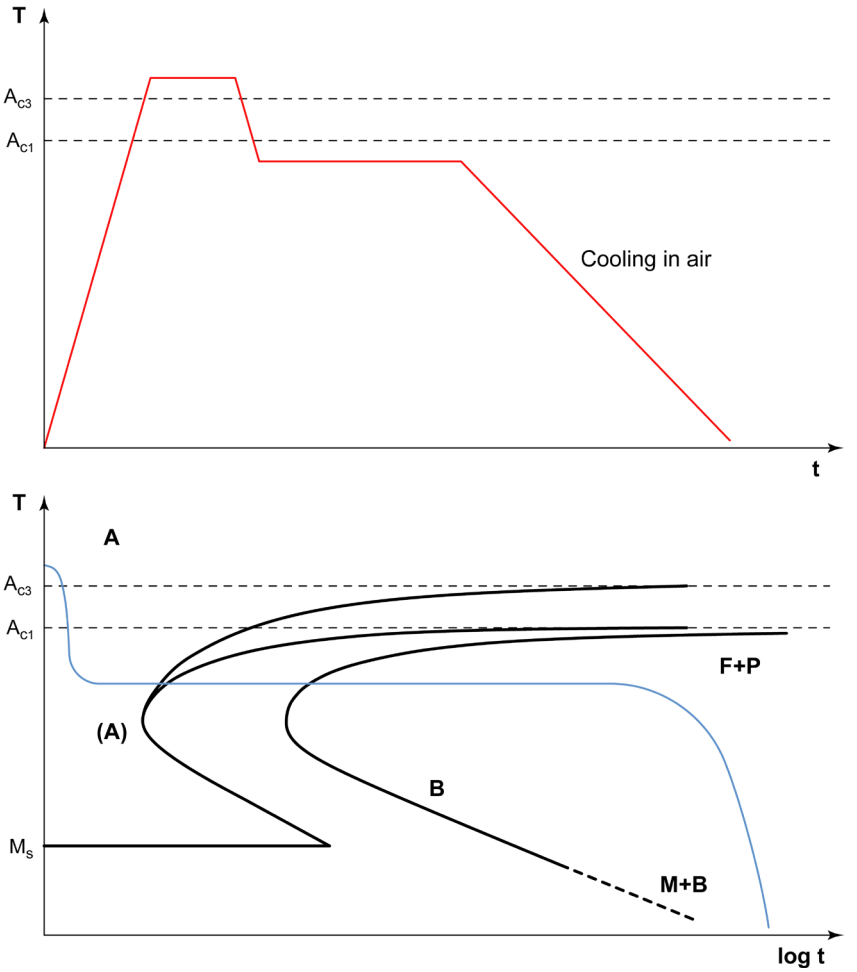

Figure 10.8 - Schematic representation of the isothermal annealing for a generic hypoeutectoid steel (on the top). The cooling curve is superimposed on the T.T.T. diagram (on the bottom).

The rapid cooling phase ends at a temperature between critical point A_{c1} and the nose of the T.T.T. diagram (indicatively at temperatures between 600°C and 700°C). The system remains at this temperature, called isothermal holding temperature, until the austenite transformation is completed.
The new microstructure is formed of ferrite and pearlite (hypoeutectoid steel). Instead, if the steel is hypereutectoid, the microstructure is formed of cementite and pearlite.
Another alternative to full annealing is spheroidizing annealing. This heat treatment can be carried out according to different methods (Figures 10.9 and 10.10).

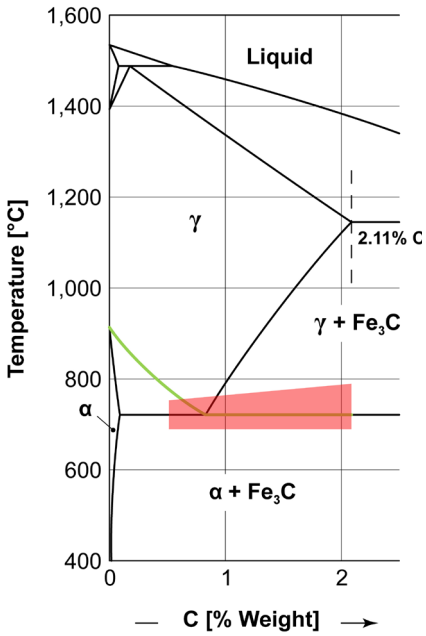

Figure 10.9 - The effect of carbon on the holding temperature for spheroidizing annealing of steels (red band). The green line highlights the critical points.

In the case of hypoeutectoid steel with a medium carbon content, the holding temperature is slightly lower than critical point A_{c1} (Figure 10.10a) and the cooling phase is carried out in the furnace (very slow cooling). Alternatively, the component may be warmed slightly above critical point A_{c1} and than gradually cooled to a temperature below the same critical point. Also in this case, the final cooling is carried out in the furnace (Figure 10.10b).

In the case of hypereutectoid or hypoeutectoid steels with high carbon content, steel is heated just above critical point A_{c1}, it is holded at that temperature for one or two hours, and then it is cooled just below the same critical point A_{c1}, for one or two hours. This sequence is then repeated two or three times.The final cooling is carried out in the furnace (Figure 10.10 c).

Spheroidizing annealing promotes carbon diffusion: at the end of the heat treatment the microstructure is globular with α-phase matrix scattered with globular shaped iron carbides. In all these cases, we speak of globular pearlitic microstructure (Figure 10.11).

Spheroidizing annealing is the typical heat treatment carried out on tool or bearing steels and, in general, on all steels with a medium-high carbon content, in order to form a microstructure with low hardness, good cold deformability, and high machinability.

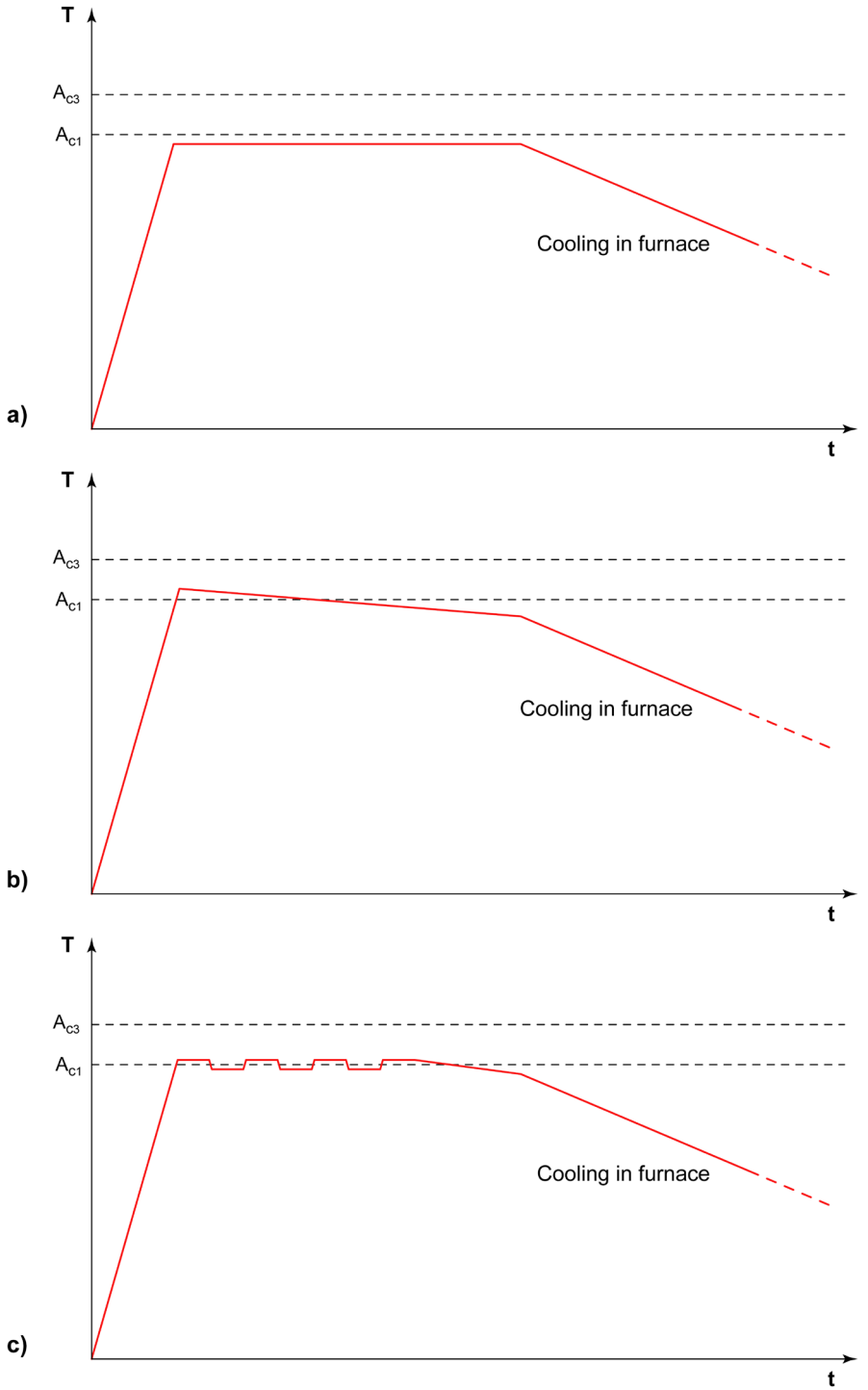

Figure 10.10 - Schematic representation of spheroidizing annealing; a) constant holding ~20°C below A_{c1}, b) heating ~10°C above A_{c1}, and very slow cooling at ~30°C under A_{c1}, c) oscillations ± 5°C around A_{c1} [from Spur and Stöferle 1980-1994].

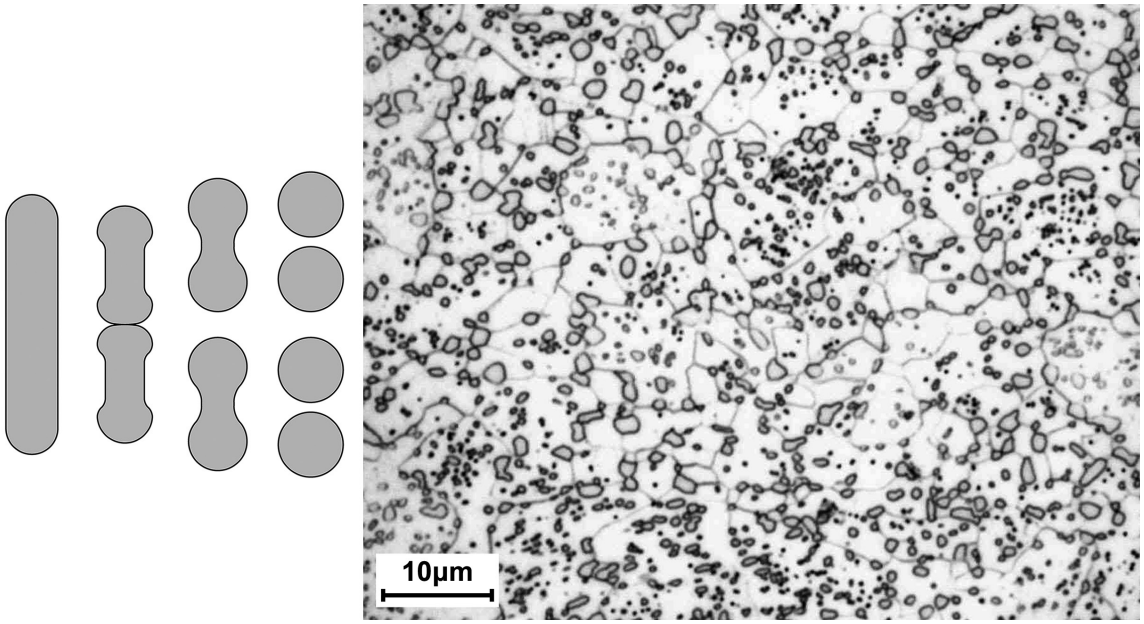

Figure 10.11 - Schematic representation of the transformation of Fe_3C phase from lamellar to globular shape during spheroidizing annealing (to the left). Globular pearlitic microstructure of an EN C67 steel (to the right). Appearance under the metallographic microscope - Nital 2% etch. [Omeco S.r.l. Laboratories, Monza - Monza Brianza].

10.4 Normalizing

Normalizing involves the progressive heating until a temperature of 40°-80°C above critical point A_{c3} if the steel is hypoeutectoid, or between critical point A_{c1} and critical point A_{cm} if the steel is hypereutectoid (Figure 10.12). Therefore, the heating temperature is between 780°C and 930°C, that is, temperatures very similar to those of full annealing.

Also the soaking phase is similar to the case of full annealing. At the end of the holding phase the microstructure consists of austenite (if the steel is hypoeutectoid) or austenite and cementite (if the steel is hypereutectoid).

Cooling is carried out by extracting the workpiece from the furnace and leaving it to air cool. The cooling rate is in the order of 10°-50°C/ min, depending both on the size of the component and the characteristics of the air flux (temperature, turbulence, etc.).

The C.C.T. diagram of Figure 10.13 shows the cooling curve during the normalizing of a generic hypoeutectoid steel. The microstructure downstream of normalizing is made up of ferrite and pearlite, if the steel is hypoeutectoid, or cementite and pearlite, if the steel is hypereutectoid. In both cases, the microstructure is homogeneous and the grains have small dimensions, smaller than those generated by full annealing.

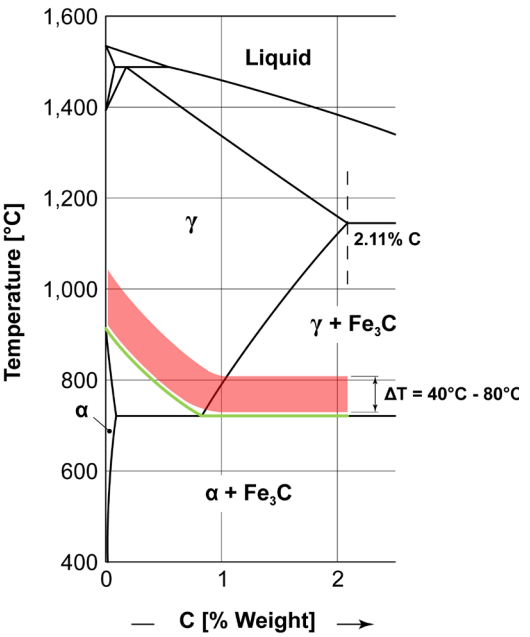

Figure 10.12 - The effect of carbon on the holding temperature for normalizing of steels (red band). The green line highlights the critical points.

Usually, normalizing produces a refining of the grain dimension[7], due to the structural transformation $\gamma \rightarrow \alpha$, and the air cooling. Normalizing removes unwanted acicular microstructures (Widmannstätten microstructures), which are typical of forging, and it reduce the amount of segregation bands, which are quite common in semi-finished products after hot working.

10.5 Hardening

The last heat treatment above critical points is hardening. Heating and soaking are identical to those already described for normalizing. The material is brought to a temperature of 40°-80°C above critical point A_{c3} if the steel is hypoeutectoid, or between the critical points A_{c1} and A_{cm} if the steel is hypereutectoid. The holding temperature is between 780°C and 930°C and the microstructure at the end of the holding phase is austenite (hypoeutectoid steels) or austenite plus carbides (hypereutectoid steels). The difference with annealing or normalizing lies in the cooling phase, which must be sufficiently rapid to form martensite. In particular, the cooling rate must be greater than the cooling curve, v_s, shown in the C.C.T. diagram[8]. At the end of the heat treatment, the microstructure is martensitic in the case of hypoeutectoid steel or martensitic plus carbides in the case of hypereutectoid steel.

[7] *Semi-finished products subjected to normalizing are tipically forged or hot-rolled workpieces.*

[8] *See Paragraphs 7.3 and 7.4 of Chapter 7.*

Cooling after hardening is normally carried out by immersing the workpiece in fluids such as water, caustic aqueous solutions, aqueous solutions of organic polymers, mineral oils. The average cooling rate on the surface of the workpieces is in the order of 200°-600°C/min and depends on the quenching medium and the size of the semi-finished product. As an alternative a salt bath or a high pressure gas stream can be used. For specific types of steels, such as air hardening steels, martensitic stainless steels and tool steels, even the air cooling can guarantee the formation of martensite. The cooling phase for a generic hypoeutectoid steel is similar to what is shown in Figure 10.14.

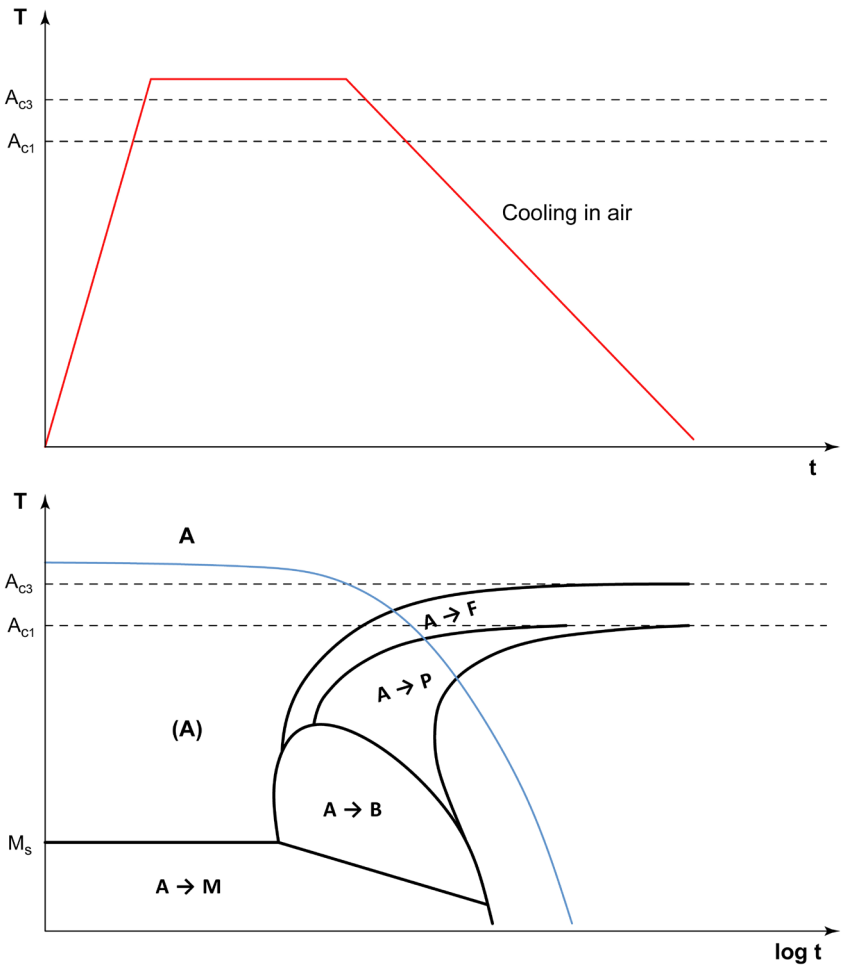

Figure 10.13- Schematic representation of normalizing for a generic hypoeutectoid steel (on the top). The cooling curve is superimposed on the C.C.T. diagram (on the bottom).

[8] *See paragraphs 7.3 and 7.4 of chapter 7.*

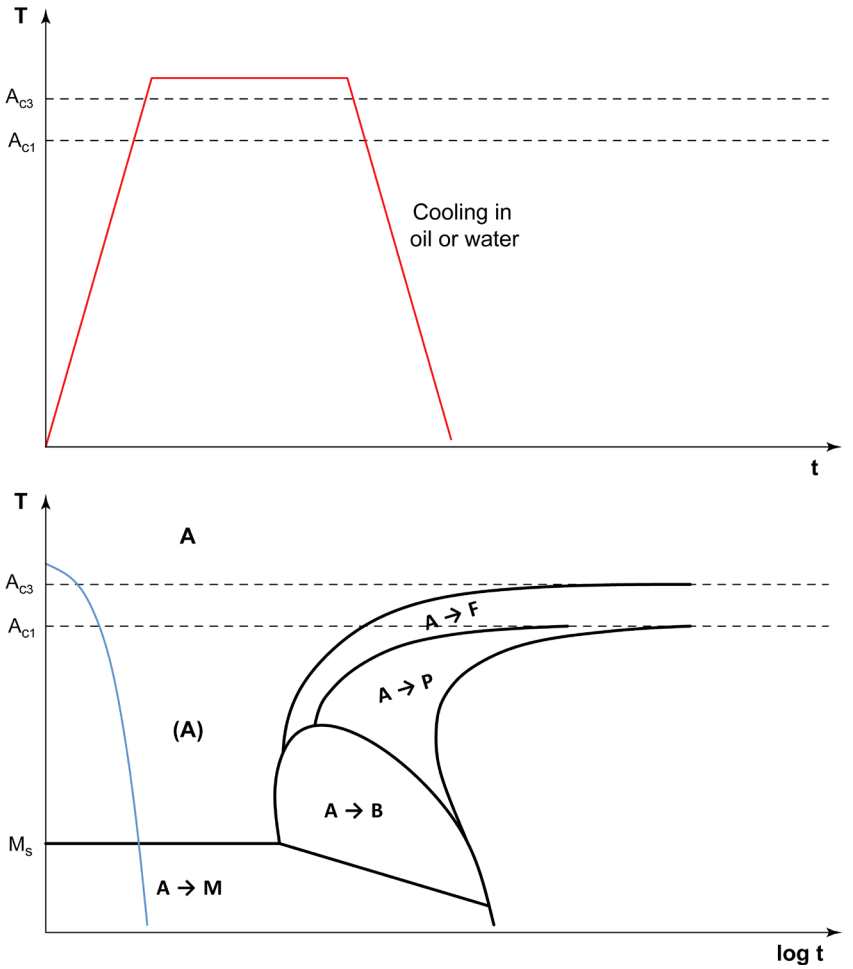

Figure 10.14 - Schematic representation of hardening for a generic hypoeutectoid steel (on the top). The cooling curve is superimposed on the C.C.T. diagram (on the bottom).

The cooling curve for hardening is not described by a specific cooling method (in furnace or in air, as in the case of full annealing or normalizing), but it is defined by the microstructure.
The purpose of hardening is to form martensite in order to increase as much as possible the mechanical properties of the steel, i.e. hardness, yield strength and ultimate tensile strength.
Hardening must be followed immediately by tempering, in order to mitigate the excessive hardness and brittleness of the martensite (Chapter 11).

10.6 Hardening and quenching media

If the quenching medium has a boiling point much lower than that of the workpiece, the cooling phase always follows three steps. Initially, the liquid evaporates instantly and forms a stable vapor layer around the component: this first stage is called the Leidenfrost phenomenon[9]. The vapor layer causes a very low cooling rate, since the heat exchange is mediated by a gaseous phase. When the temperature of the workpiece drops below a given limit threshold (called Leidenfrost temperature), the vapor layer becomes unstable. Steam bubbles begin to form on the surface of the component, and new liquid comes into contact with the hot workpiece, vaporizing immediately. This phenomenon produces extremely high cooling rates.

The third phase occurs when the temperature of the component equals the boiling point of the liquid: the component will be in constant contact with the fluid which will no longer evaporate. In this phase, the heat exchange occurs by convection between a liquid and a solid and the cooling rate becomes low, again. Figure 10.15 shows what was previously described.

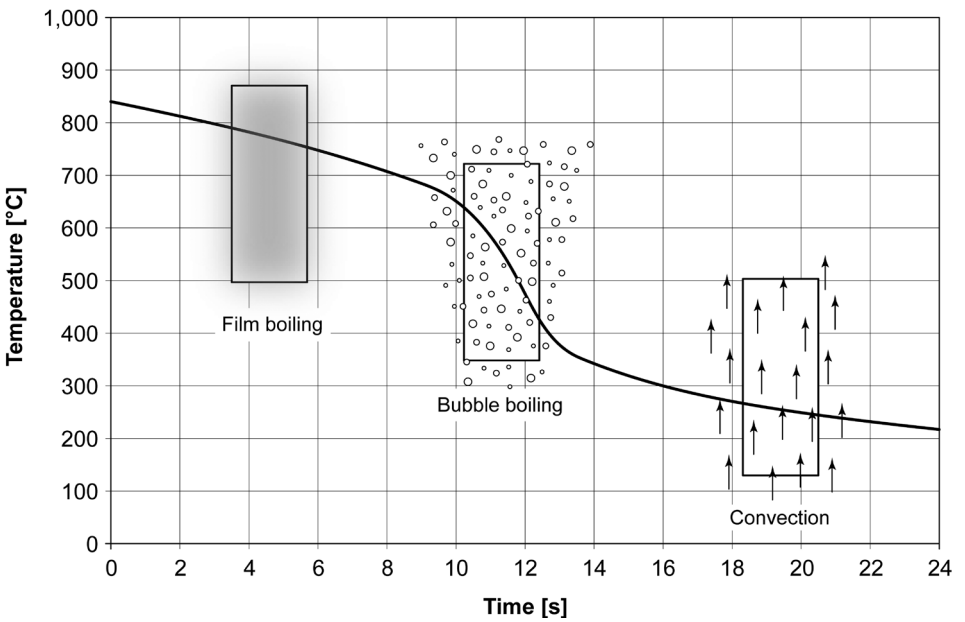

Figure 10.15 - Schematic representation of the cooling rate of a hot component immersed in a quenching medium [from ASM-H.4 1991].

[9] *The phenomenon was first described by German physician, Johann Gottlob Leidenfrost, in the book: De Aquae Communis Nonnullis Qualitatibus Tractatus, published in 1746.*

Ideally, a quenching medium should produce a very rapid cooling rate in the initial stages, when the temperature is high, and then becomes lower when approaching the austenite-martensite transformation[10]. Therefore for real fluids it is very important to raise the Leidenfrost temperature and reduce the time when the vapor forms a stable film around the workpiece.
The Figure 10.16 shows several examples of cooling curves produced by the most common quenching media.

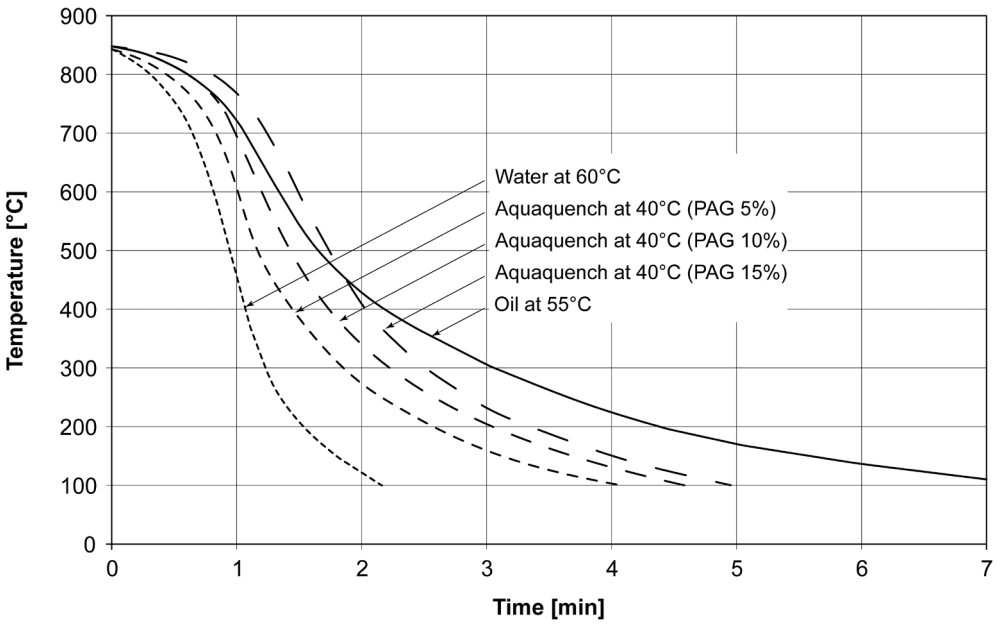

Figure 10.16 - Cooling curves produced by different quenching media as measured in the center of stainless steel bars (length: 150mm, diameter: 75mm) [from Thelning 1975].

A parameter used to simplify the behavior of the hardening fluids is the so-called "quenching intensity factor", indicated by the letter *H*, which represents the greater or lesser ability of a quenching medium to cool a steel component.
In general, the quenching intensity factor depends on the nature of the fluid: water has a higher *H* than oil which, in turn, has a higher *H* than a molten salt bath. The quenching intensity factor also depends on the fluid temperature and its level of agitation.
To exemplify all these concepts, it is useful to consider that agitated water at 20°C has a higher *H* than agitated water at 60°C or agitated oil at 20°C has a higher *H* than the still oil at 20°C.

[10] The high cooling rate at the initial stage allows to cool the metallic mass to the martensite start temperature without intersecting the transformation area of the austentite into ferrite and pearlite (hypoeutectoid steel) or into cementite and pearlite (hypereutectoid steel). Instead below M_s the cooling rate must decrease in order to reduce the residual stress caused by the martensitic transformation.

A quantitative definition of the quenching intensity factor H of a quenching medium was given by Grossman[11]:

$$H = \frac{h}{2k} \quad [10.1]$$

where h is the heat transfer coefficient of the interface between the workpiece and fluid[12] and k is the thermal conductivity of the metal mass. The experimental evaluation of H, allows to categorise the quenching media in terms of quenching intensity factor.

A fluid is considered ideal when there is no resistance to thermal exchange between the component and the quenching medium ($h \rightarrow \infty$), i.e., the surface of the workpiece is instantly brought to the temperature of the fluid. In this case the value of H is conventionally set to ∞.

In real fluids, the value of H is always lower than the ideal one and it is affected by the nature of the fluid, its temperature, and its agitation level. At room temperature and without agitation, water has a quenching intensity factor equal to 1, oil equal to 0.3, and air equal to 0.05[13]. Some examples of the quenching intensity factor are shown in Table 10.1.

Quenching medium	Temperature [°C]	Agitation [m/s]	Quenching intensity factor H [in^{-1}]
Water	32°	0 0.25 0.51 0.76	1.1 2.1 2.7 2.8
Water	55°	0 0.25 0.51 0.76	0.2 0.6 1.5 2.4
Oil for hardening	65°	0.51	0.7
Oil for rapid hardening	60°	0 0.25 0.51 0.76	0.5 1 1.1 1.5
Air	27°	0 2.54 5.08	0.05 0.06 0.08

Table 10.1: Quenching intensity factor for various quenching media.

[11] *Grossman M.A., Elements of Hardenability, American Society for Metals, Metals Park, Ohio, USA, 1952.*

[12] *The heat transfer coefficient, h, is the inverse of the resistance that the component opposes to the heat exchange with the fluid. h is defined as* $h = q/A \cdot (T_1 - T_2)$ *where q is the heat that leaves the workpiece towards the fluid, A is the surface of the workpiece,* T_1 *the temperature of the component and* T_2 *the fluid temperature. h is expressed in* W/m^2K.

[13] *The unit of measure of H expressed in the International System of Units (S.I.) is* $[m^{-1}]$. *However, the values of H are normally indicated in* $[in^{-1}]$, *following the Anglo-Saxon unit of measure used by Grossmann.*

10.7 Steel hardenability

The hardening heat treatment described in paragraphs 10.5 and 10.6 is valid for small-sized components, i.e, when the cooling rate can be considered almost identical in every point of the component.
If you consider a medium or a large sized components, instead, the surface tends to cool quite quickly due to direct contact with the quenching medium, while the core follows a lower cooling rate.
Let us try to understand the effects produced by this phenomenon on the microstructure. Suppose you want to harden a medium-sized component in oil, made with a low carbon steel (steel *A*).
We use a series of numbers, from 1 to 7, to indicate some points along the section of the component (from 1 - the surface up to 7 - the core): therefore, we superimpose the cooling curves of each point with the C.C.T. diagram and evaluate the microstructures (Figure 10.17).

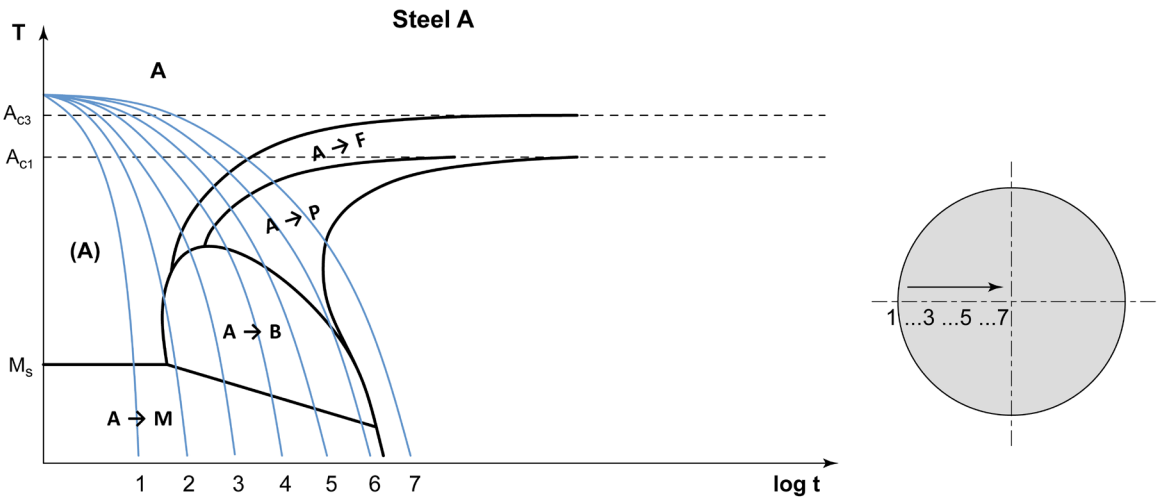

Figure 10.17 - Cooling curves for oil quenching superimposed on the C.C.T. diagram of a steel with low hardenability (low carbon steel).

The Figure 10.17 shows how only with cooling curve 1 the microstructure is completely martensitic. With cooling curves from 2 to 6, the microstructure is a mixture of bainite, ferrite, pearlite, and martensite; with curve 7 the microstructure is only ferritic-pearlitic.
Let us now evaluate what happens if we decide to harden in oil the same workpiece but made with a low alloy steel (steel *B*).
Since the component and the quenching medium have not changed, the cooling curves are virtually identical[14], instead the C.C.T. diagram is moved more downward and to the right with respect to the temperature-time axes (the steel *B* contains more alloying elements than the steel *A*).

[14] *In addition to the quenching medium and the component size, the cooling rate is also influenced by the chemical composition of the steel. However, this parameter has a very limited effect and it can be ignored.*

In this second case, cooling curves 1, 2, and 3, form only martensite, while curves from 4 to 7, also form other microstructures (Figure 10.18).

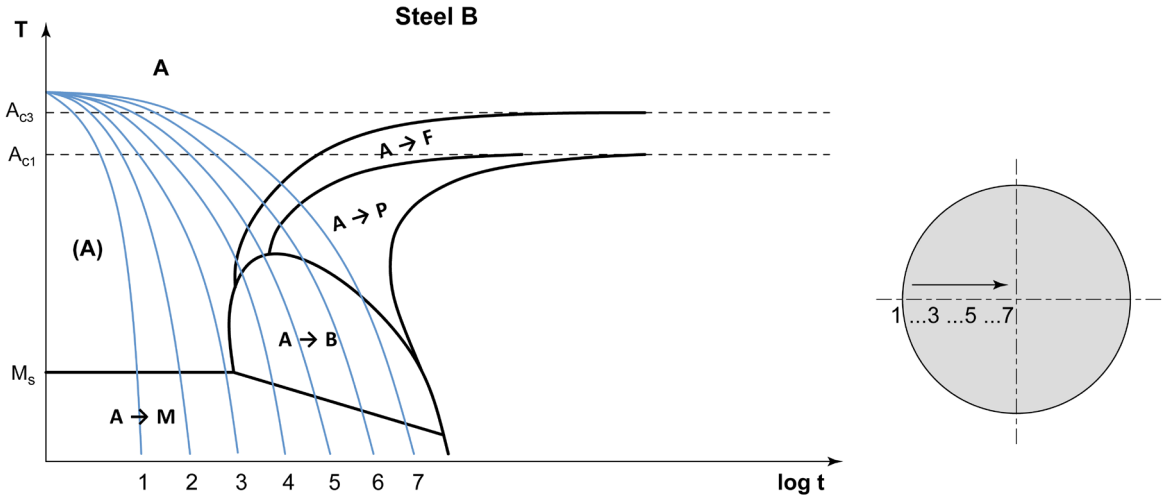

Figure 10.18 - Cooling curves for oil quenching superimposed on the C.C.T. diagram of a steel with medium hardenability (low alloy steel).

Since a given hardness is associated to each cooling curve, it is possible to trace the hardness profile along the section of the component at the end of the hardening. The result shown in Figure 10.19 highlights the importance of the chemical composition of steel: the amount of martensite and therefore the hardness profile, is different even if the two components has the same size and they are heat treated with the same quenching medium.

A typical example is shown in Figure 10.20, which shows the hardness profile along the section of round bars made of carbon steel (EN C50) or low alloy steel (EN 42CrMo4).

The ability of steel to form martensite is called hardenability. Consequently, it is common to speak of more or less hardenable steels in relation to their ability to form martensite.

Hardenability is a property that is strictly dependent on the chemical composition of the steel. Hardenability increases:

- as the amount of alloying elements, including carbon, increases,
- as the average size of the crystallite increases.

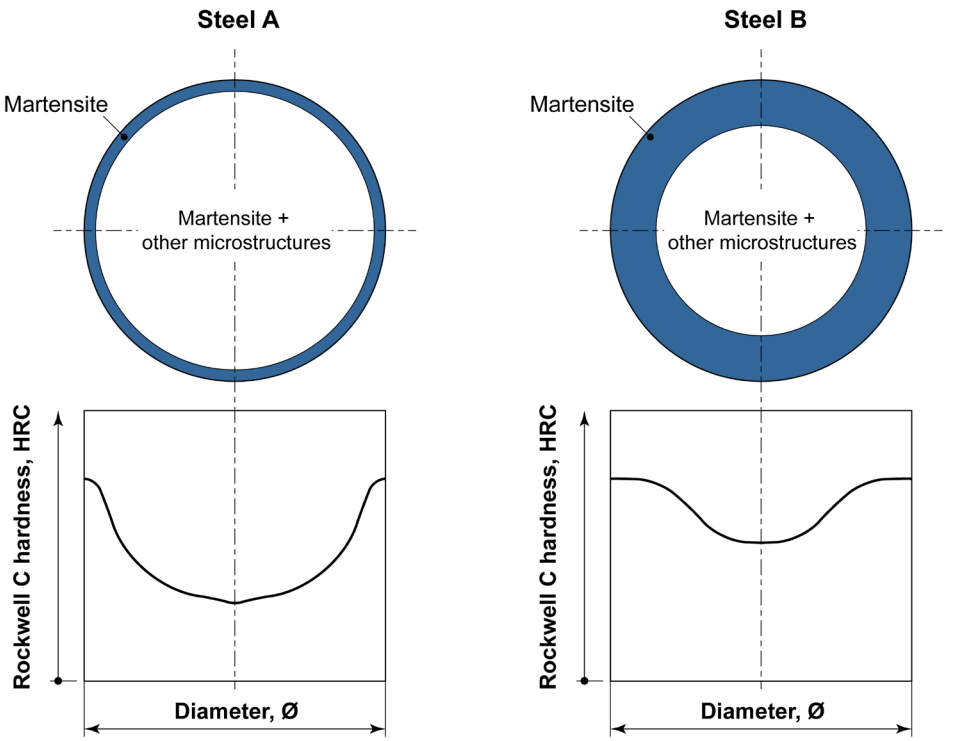

Figure 10.19 - Radial hardness profile along the section of two cylindrical bars with the same size but made of low carbon steel (steel *A*) or low alloy steel (steel *B*) and hardened in oil.

The hardenability is independent of the workpiece shape and the quenching medium. Hardenability is also an important parameter used to define the behavior of mechanical components.

A mechanical component with ideal behavior should have the same impact strength, hardness, and tensile strength throughout its section and length.

Since the homogeneity of mechanical properties depends on the steel microstructure after hardening, it is always advisable to have martensite throughout the component. In fact, martensite has two great advantages: (i) it is the microstructure with the highest mechanical strength and (ii) it has always the same hardness for a given chemical composition[15]. Therefore, where there is martensite, there is also homogeneity of mechanical behavior.

[15] *The hardness of martensite after hardening depends only on the steel carbon content.*

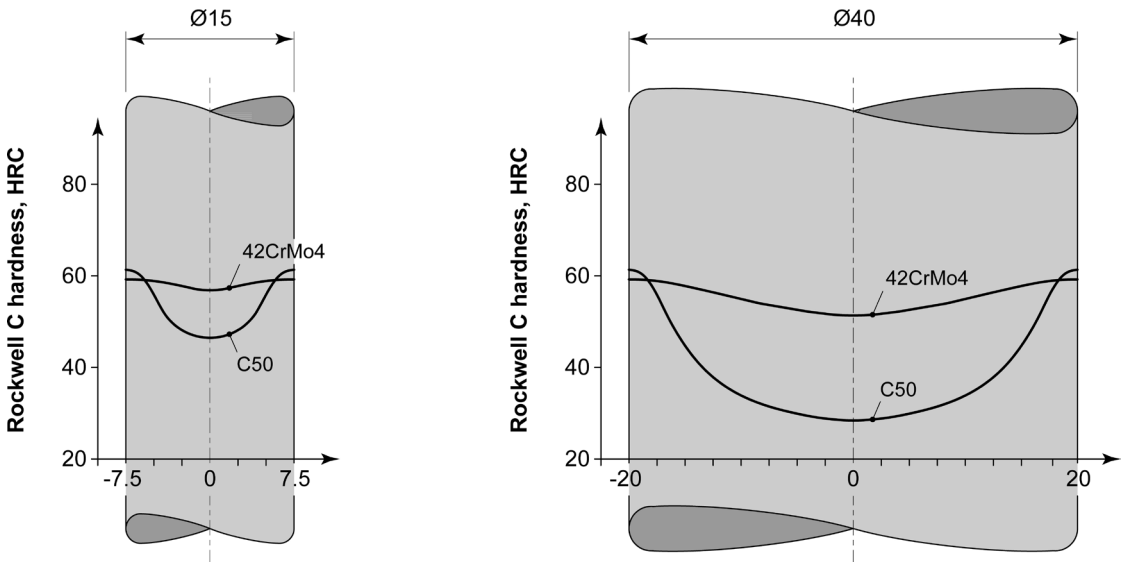

Figure 10.20 - Radial hardness profile along the section of two cylindrical bars (Ø15mm and Ø40mm) made of EN C50 or EN 42CrMo4 steel, and hardened in water at 30°C with an agitation level of 0.3 m/s [from Totten 2006].

A workpiece is completely hardened when it has the 100% of martensite in the core and, therefore, at all other points in the section. As a result, the workpiece has uniform hardness and uniform mechanical strength everywhere.
Practically, only workpieces of small size and made of steels having medium-high hardenability show uniform hardness everywhere. Nevertheless, a component is considered satisfactory if, after hardening, has an amount of martensite in the core of 50% for hardened and tempered steels, of 70% for case hardening steels, and of 80% for spring steels. As a rule of thumb, steel hardenability increases, as the component size increases.

10.8 Evaluation of steel hardenability and the Jominy test

There are many methods to quantify the hardenability of a steel: the most important is the "Jominy end-quench test", which is described by the EN-ISO 642 standard in Europe and the ASTM A 255 standard in the United States.
The samples for the Jominy test must be taken from the component to be tested. The samples must have a diameter of 25mm, a length of 100mm and a support surface at one of the two ends.

The sample is first introduced into a special ceramic jacket (in order to reduce the oxidizing effect of the atmosphere), and than is placed in a muffle furnace where it is austenitized at the desired temperature[16] for 30 minutes. Immediately after the extraction from the furnace, the sample is inserted into a perforated support and its free end, called the "quenched end", is quenched with a jet of water at a temperature of 20°C ± 5°C (Figure 10.21).

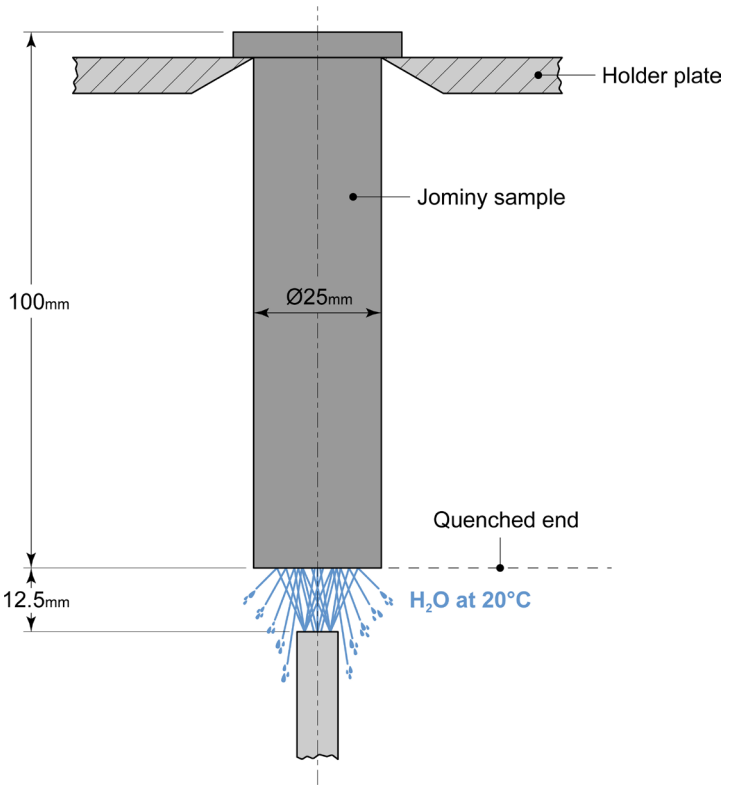

Figure 10.21 - Execution method of the Jominy test.

As a result sample undergo a cooling rate that is more rapid the closer the sample sections are to the quenched end. At the end of the test, sample is grinded along a line on the cylinder surface: the grinding depth is in the order of 0.4-0.5mm. The hardness measurements are performed on the grinded surface using a Rockwell C hardness tester, progressively moving away from the quenched end.
The so-called Jominy hardenability curve is obtained by representing the hardness values on a graph, as a function of the distance from the quenched end. Figure 10.22 shows a typical example.

[16] *It is very important to select the correct heating temperature for the Jominy end-quenched test since the austenitization phase affects the mean grain size and therefore the steel hardenability.*

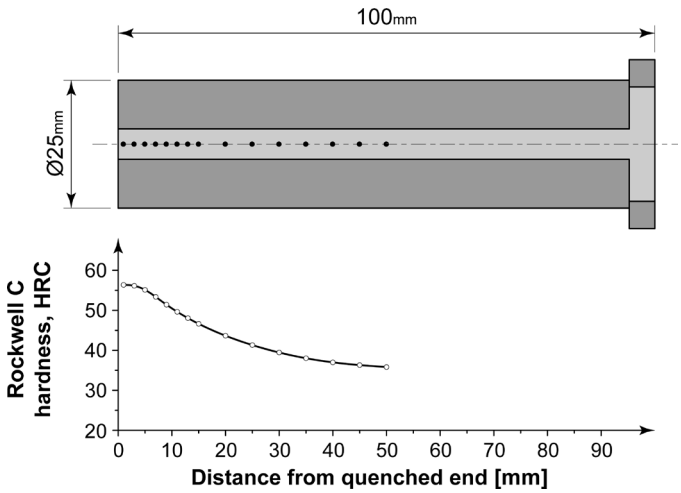

Figure 10.22 - Schematic representation of a typical Jominy hardenability curve.

For example, Figure 10.23 shows the comparison between an EN 42CrMo4 steel and an EN C50 steel. The 42CrMo4 steel has a higher hardenability than C50 steel, even if the latter shows a higher hardness on the quenched end due to its higher carbon content. Therefore, a component in 42CrMo4 steel has more homogeneous hardness along the section compared to the same component in C50 steel.

The hardness profile along the Jominy sample is similar to that of a real cylindrical component cooled in a quenching medium. The surface of the workpiece is similar to the quenched end of the Jominy sample while the core has a cooling rate that is more similar to section far from the quenched end[17].
Consequently, if the Jominy hardenability curve is flat, the microstructure along the entire section of the cylindrical component is homogeneous and there are no major variations in hardness and mechanical properties. On the contrary, if the Jominy sample shows a sharp change in hardness, the mechanical strength of the cylindrical component is higher on the surface than in the core.
Therefore large-sized components must be made of steel with a high hardenability while components with a small or medium size can also be produced using steel with lower hardenability.

[17] *However, it is important to underline that the two hardness profiles cannot be superimposed. The hardness of real workpieces must be evaluated experimentally even if the Jominy hardenability curve is similar to the hardness profile along the section of a hardened cylindrical component.*

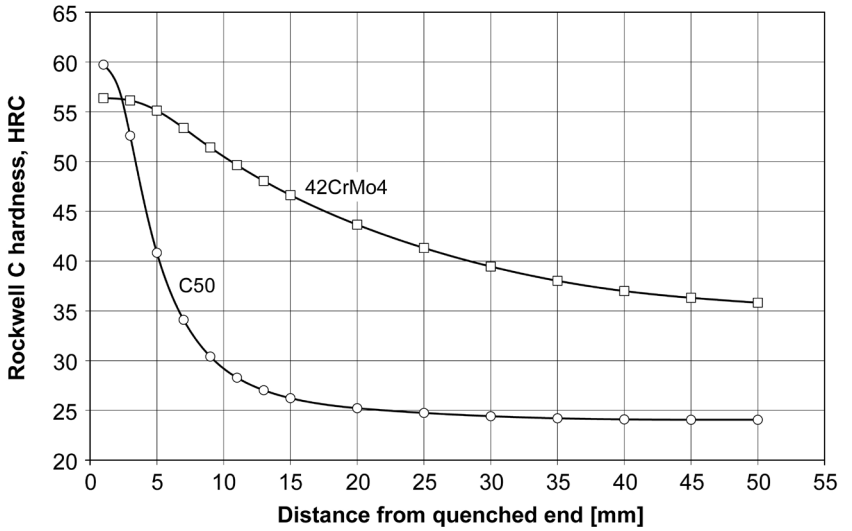

Figure 10.23 - Comparison between the Jominy hardenability curves of an EN C50 steel and an EN 42CrMo4 steel.

10.9 Hardenability and the chemical composition of steel

The hardenability is closelly related to the chemical composition of the steel. In general, the greater the amount of alloying elements, including carbon, the greater the steel hardenability.

The increase in hardenability caused by the alloying elements depends directly on the movement of the T.T.T. and C.C.T. diagrams. Since the addition of alloying elements moves the T.T.T. and C.C.T. diagrams down and to the right, it is easier to form martensite even if the cooling rate is low.

Not all alloying elements, however, have the same effect: chromium, manganese, molybdenum, and vanadium, has a major effect on hardenability while other elements such as nickel, for example, have little effect. Carbon has a mild effect on the steel hardenability, even though it is the alloying element that makes the martensite hard.

Also the mean size of the austenitic grains affects the hardenability: a coarse grain increase the hardenability while a very fine grain reduces it.

Several researchers have worked on numerical correlations between the hardenability of steel and its chemical composition. This work gave rise to several formulas to estimate the Jominy hardenability curve.

A simple example are the formulas proposed by Just[18]. These formulas allow to calculate the hardness along the Jominy sample at distance E (mm) from the quenched end as a function of the chemical composition of the steel and the mean size of the austenitic grain G[19]. At the quenched end (J_0, E = 0mm) hardness depends only on carbon content[20]. The correlation proposed by Just is [$C < 0.6\%$]:

$$J_0 = 60\sqrt{C} + 20\ HRC \quad [10.2]$$

At distance E = 1mm from the quenched end (J_1) the result is:

$$J_1 = 60\sqrt{C} + 1.6Cr + 1.5Mn + 16\ HRC \quad [10.3]$$

At distances between E = 6mm and E = 80mm from the quenched end ($J_{6\text{-}80}$), the result for many steels (hardened and tempered steel, case hardening steel, spring steel, etc.) is[21]:

$$J_{6-80} = 95\sqrt{C} - 0.0028E^2\sqrt{C} + 20Cr + 14Mn + 6Ni + 38Mo + 6Si + 39V + 96P + \\ - 0.8G - 12\sqrt{E} + 0.9E - 13\ HRC \quad [10.4]$$

If the values of $J_{6\text{-}80}$ are higher than J_0 or than J_1, $J_{6\text{-}80}$ is equal to the lowest value between J_0 and J_1. A simplified version of [10.4], valid between 6mm and 40mm for hardened and tempered steels, is:

$$J_{6-40} = 102\sqrt{C} + 22Cr + 21Mn + 7Ni + 33Mo - 15.47\sqrt{E} + 1.102E - 16\ HRC \quad [10.5]$$

another semplified version valid for case hardening steels is:

$$J_{6-40} = 74\sqrt{C} + 14Cr + 5.4Ni + 29Mo + 16Mn - 16.8\sqrt{E} + 1.386E + 7\ HRC \quad [10.6]$$

10.10 Hardenability problems for large-sized workpieces

In many cases it is useful to estimate the hardness profile produced by hardening of large-sized workpieces. In these cases, the hardness profile can be estimated using the so-called "Lamont diagrams"[22] (Figures 10.24-10.29).

---

[18] Just E., Formul der Härtbarkeit, Härterei Technische Mitteilungen, Vol.23 (2), pp. 85-100, 1968 and Just E., New Formulas for Calculating Hardenability Curves, Metal Progress, n. 11, pp. 87-88, 1969.

[19] According to the ASTM E112 standard the mean size of the austenitic grain is determined by optical microscopy (the sample is grinded and etched according to specific procedures, for example with the McQuaid-Ehn method). The mean grain size G is the number of grains n that can be observed on a surface of 25.4x25.4mm (inch²) at 100 magnifications according to the formula $n = 2^{G-1}$. G is an increasing number as the mean grain size decreases. A microstructure with a mean grain size of 5.6μm corresponds with G = 12, 11μm to G = 10, 22μm to G = 8, 45μm to G = 6, 90μm to G = 4, 180μm to G = 2. Typically, a good quality steel has a mean grain size between G = 6 and G = 10.

[20] The hardness of martensite depends only on the carbon content of steel (Paragraph 8.7 - Figure 8.23). Therefore, if the microstructure is completely martensitic, as in the case of the quenched end of the Jominy sample, the hardness is proportional to the carbon content. The alloying elements have no effect in this position of the Jominy sample.

[21] Just's formulas are valid within very broad chemical composition limits (C < 0.6%, Cr < 2%, Mn < 2%, Ni < 4%, Mo < 0.5%, V < 0.2%).

[22] Lamont J.L., How to Estimate Hardening Depth in Bars, Iron Age, vol. 152, pp. 64-70, 1943.

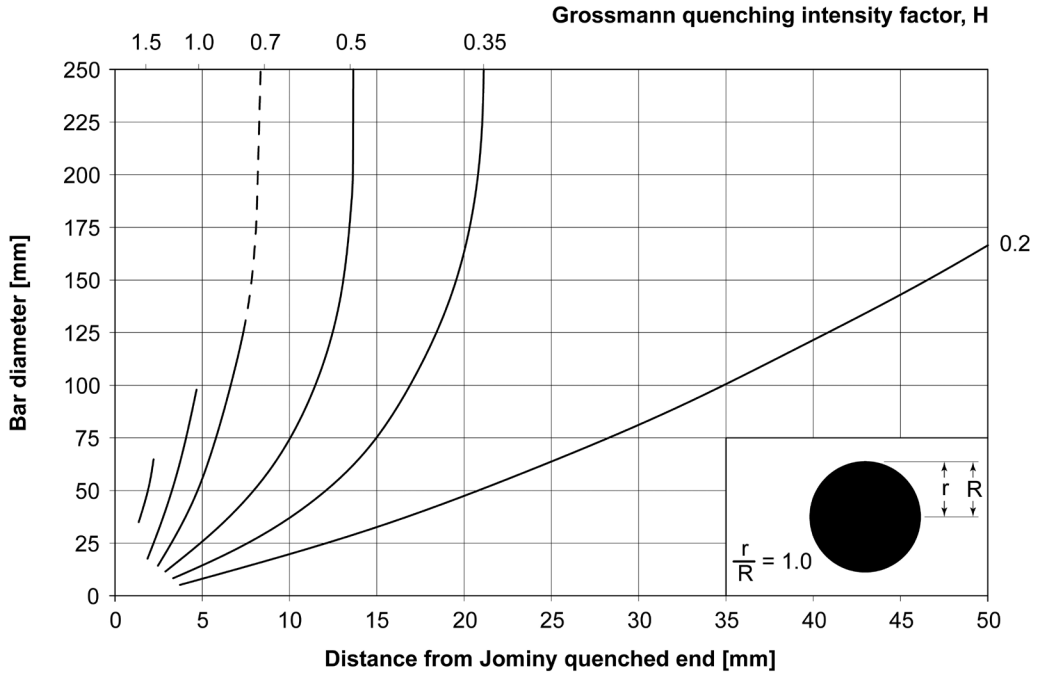

Figure 10.24 - Lamont diagram for points located at distance $r = R$ from the center of the bar with radius R [from Lamont 1943].

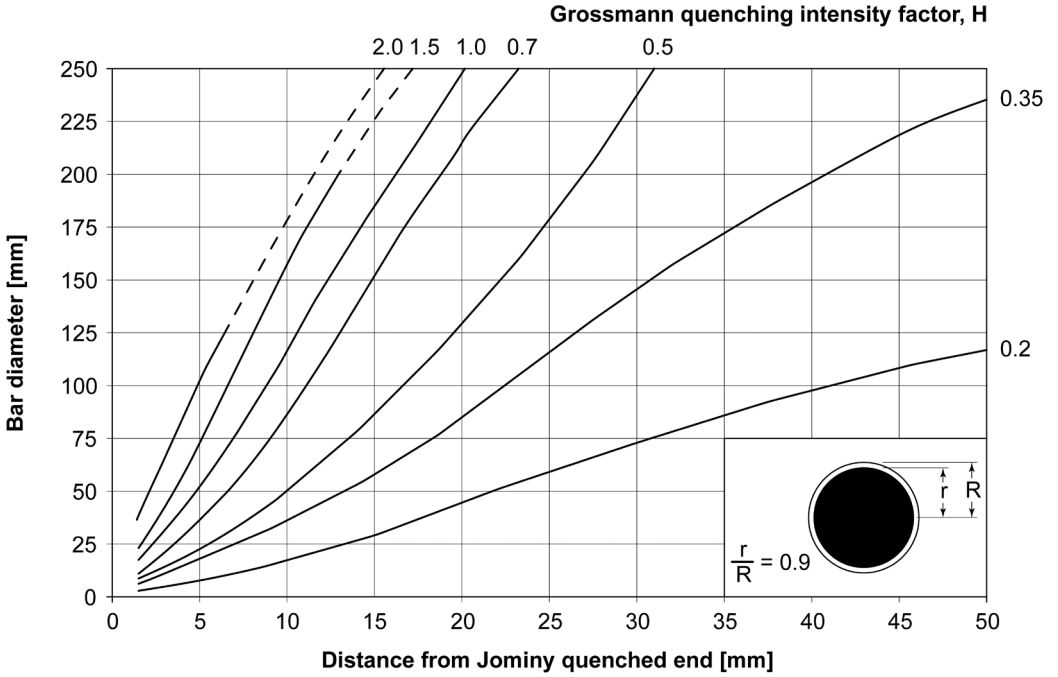

Figure 10.25 - Lamont diagram for points located at distance $r = 0.9 \cdot R$ from the center of the bar with radius R [from Lamont 1943].

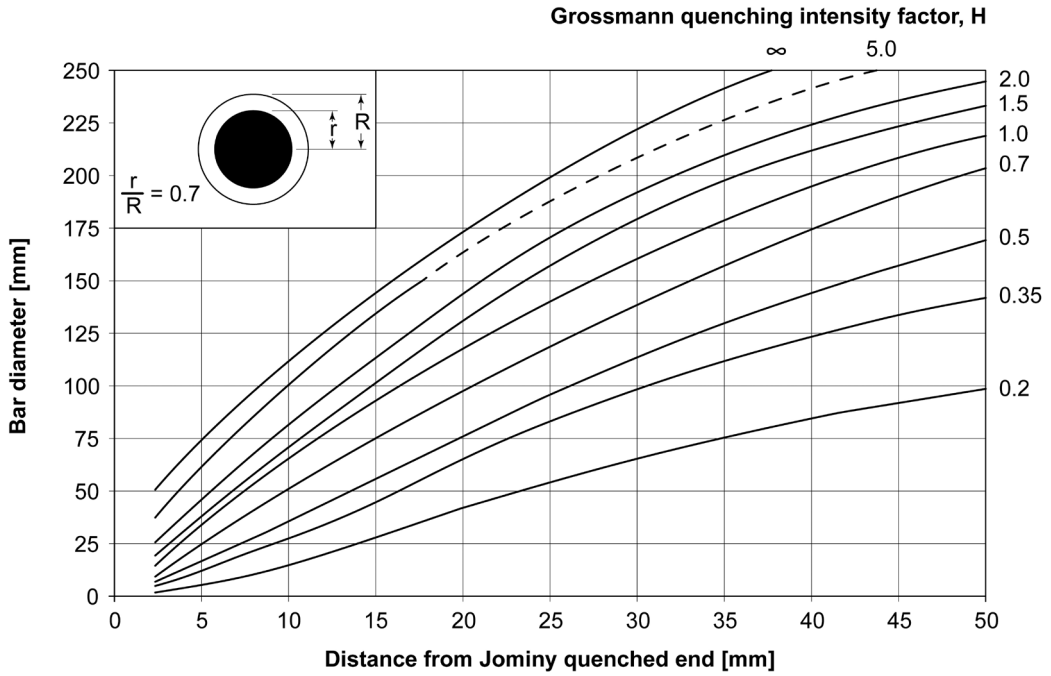

Figure 10.26 - Lamont diagram for points located at distance $r = 0.7 \cdot R$ from the center of the bar with radius R [from Lamont 1943].

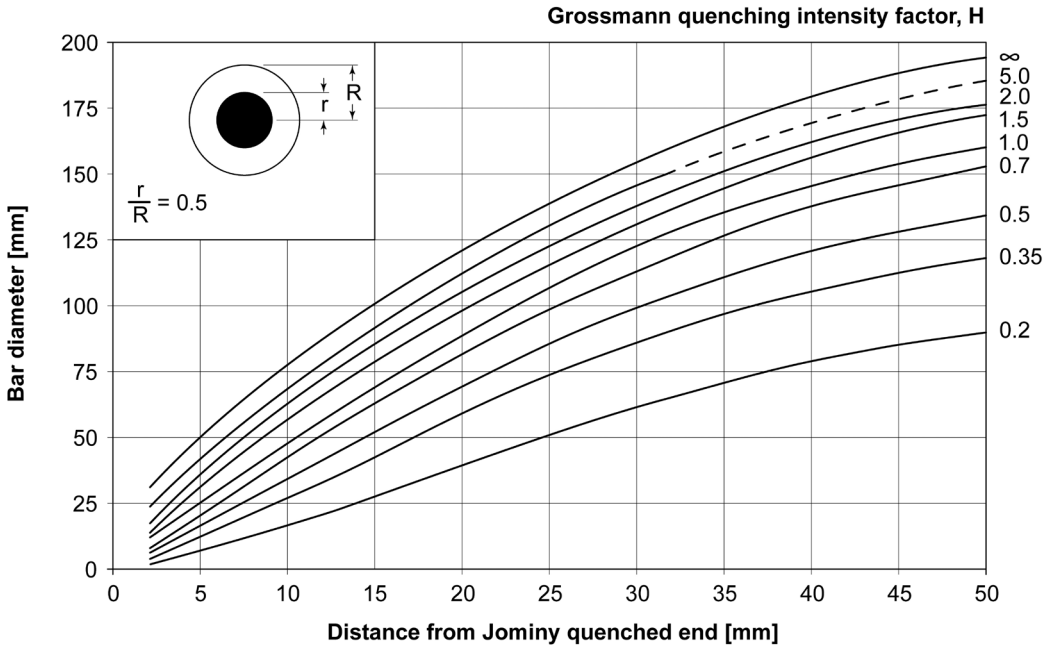

Figure 10.27 - Lamont diagram for points located at distance $r = 0.5 \cdot R$ from the center of the bar with radius R [from Lamont 1943].

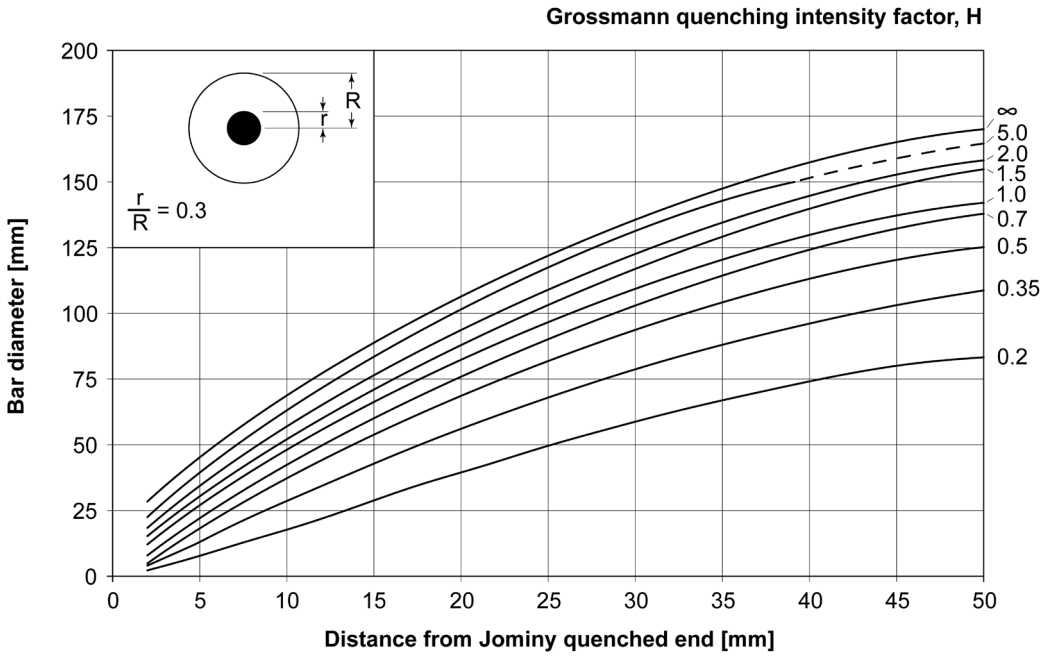

Figure 10.28 - Lamont diagram for points located at distance $r = 0.3 \cdot R$ from the center of the bar with radius R [from Lamont 1943].

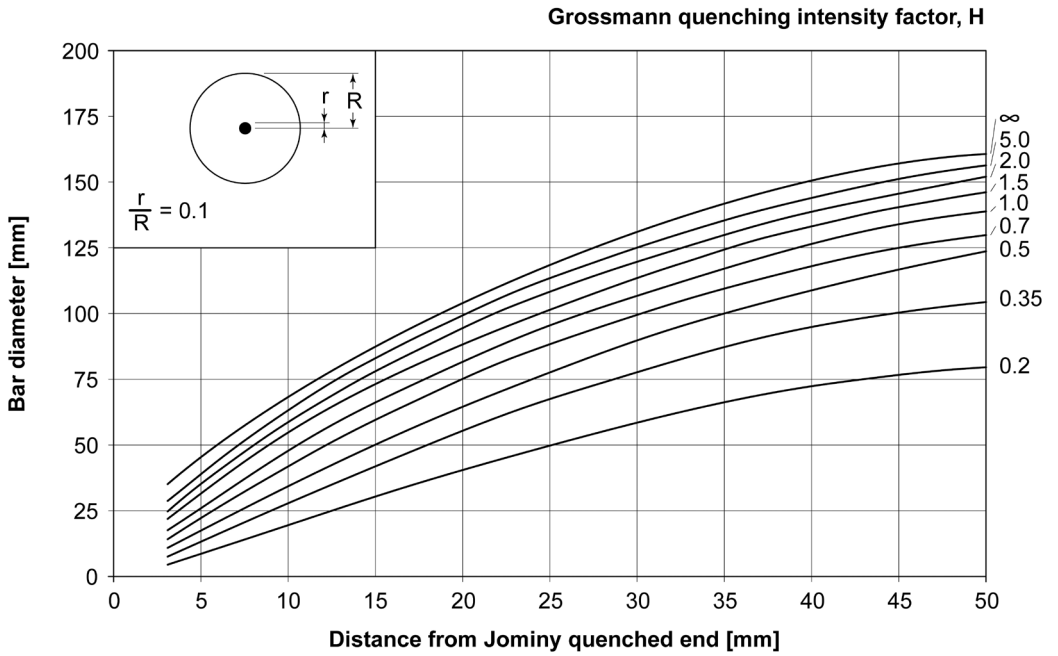

Figure 10.29 - Lamont diagram for points located at distance $r = 0.1 \cdot R$ from the center of the bar with radius R [from Lamont 1943].

The Lamont diagram are very useful because they correlate the hardness along the Jominy hardenability curve (in absicssa) with the hardness along the section of a cylindrical bar of radius R made with the same material of the Jominy sample (in ordinate), when the quenching intensity factor (H) of the quenching medium varies.

To understand the use of the Lamont diagrams let's take an example using Figure 10.25, that represents the generic radial position $\frac{r}{R} = 0.9$.

Let us suppose to quench a steel bar of 100mm in diameter in non-agitated oil ($H = 0.5$): the hardness at 45mm from the center of the bar (if $Ø = 100\text{mm} \rightarrow R = 50\text{mm}$ then $r = 0.9 \cdot R = 45\text{mm}$) is equal to the hardness that can be read on the Jominy hardeanbility curve at a distance of 17mm from the quenched end.

10.11 Practical applications of steel hardenability

Some practical application may be helpful in clarifying the use of the Just's formulas and the Lamont diagrams.

Case 1

The first problem is to estimate the Jominy hardenability curve of four hardened and tempered steel: EN C40, EN 25CrMo4, EN 36CrNiMo4, and EN 34CrNiMo6.

The nominal composition of the four types of steel is shown in Table 10.2. The Just formulas [equations 10.2, 10.3, and 10.5] can be used to estimate the Jominy hardenability curve starting from the nominal composition (Figure 10.30).

	C40	25CrMo4	36CrNiMo4	34CrNiMo6
C	0.40	0.25	0.36	0.34
Mn	0.75	0.75	0.70	0.70
Si	0.20	0.20	0.20	0.20
Cr	---	1.00	1.00	1.50
Ni	---	---	0.90	1.30
Mo	---	0.20	0.20	0.20

Table 10.2 - Nominal composition of four hardened and tempered steels EN C40, EN 25CrMo4, EN 36CrNiMo4, and EN 34CrNiMo6.

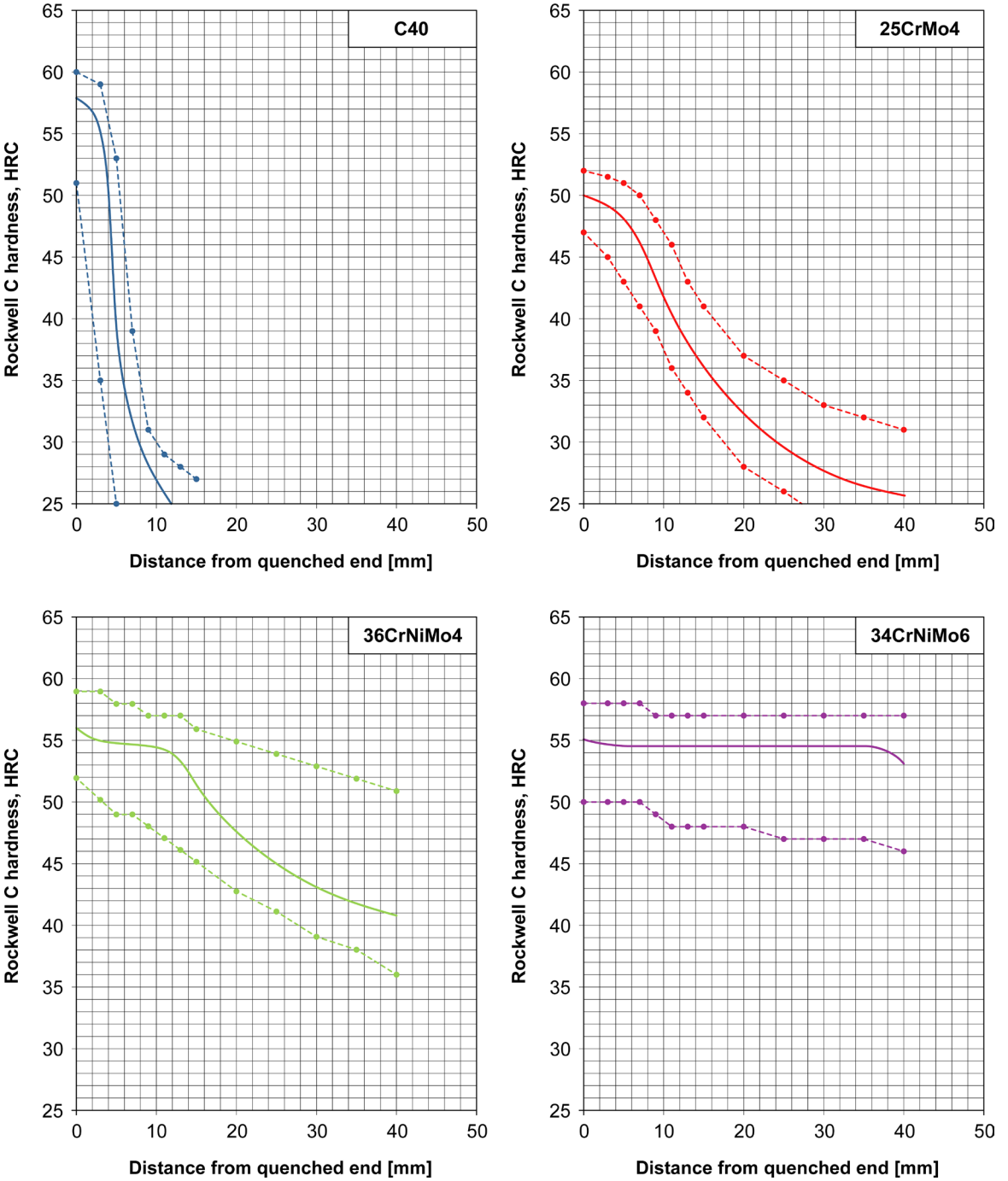

Figure 10.30 - Jominy hardenability curves for EN C40, EN 25CrMo4, EN 36CrNiMo4, and EN 34CrNiMo6 steels: estimate according to the Just's formulas (continuous lines), maximum and minimum hardenability limits (hardenability bands) according to EN ISO 683 standard, Parts 1 and 2 (dotted lines).

Case 2

Let us suppose to harden in non-agitated oil ($H = 0.5$, see Table 10.1) two cylindrical bars of 100mm in diameter, one made of EN 36CrNiMo4 steel and the other made of EN 34CrNiMo6 steel: what you want to know is the radial hardness profile at the end of the hardening.

The problem can be solved by using the Lamont diagrams (Figures 10.24 to 10.29) starting from the result of Case 1 (Figure 10.30[23]).

At first, we consider the EN 36CrNiMo4 steel and refer to the surface of the bar (Figure 10.24). If we use the curve defined by $H = 0.5$ and we enter the value of 100mm in ordinate, the value of 12mm is found in abscissa.This means that on the surface of the bar ($r = R$) the hardness is equal to that on the Jominy hardenability curve for EN 36CrNiMo4 steel at 12mm from the quenched end. In this case: 54HRC. Similarly, for the other radial positions:

- $r = 0.9 \cdot R$ ($r = 45$mm) → 17mm → 49.5HRC (Figure 10.25)
- $r = 0.7 \cdot R$ ($r = 35$mm) → 26mm → 44.5HRC (Figure 10.26)
- $r = 0.5 \cdot R$ ($r = 25$mm) → 30mm → 43HRC (Figure 10.27)
- $r = 0.3 \cdot R$ ($r = 15$mm) → 33mm → 42HRC (Figure 10.28)
- $r = 0.1 \cdot R$ ($r = 5$mm) → 35mm → 41.5HRC (Figure 10.29)

On the other hand, if EN 34CrNiMo6 steel is considered:

- $r = R$ ($r = 50$mm) → 12mm → 54.5HRC (Figure 10.24)
- $r = 0.9 \cdot R$ ($r = 45$mm) → 17mm → 54.5HRC (Figure 10.25)
- $r = 0.7 \cdot R$ ($r = 35$mm)→ 26mm → 54.5HRC (Figure 10.26)
- $r = 0.5 \cdot R$ ($r = 25$mm) → 30mm → 54.5HRC (Figure 10.27)
- $r = 0.3 \cdot R$ ($r = 15$mm) → 33mm → 54.5HRC (Figure 10.28)
- $r = 0.1 \cdot R$ ($r = 5$mm) → 35mm → 54.5HRC (Figure 10.29)

The radial hardness profiles of the EN 36CrNiMo4 and EN 34CrNiMo6 steel bars are shown in Figure 10.31. This example highlights that:

- the hardness of EN 39NiCrMo3 steel decreases rapidly just a few millimeters from the surface;
- the hardness of steel EN 34CrNiMo6 is substantially constant up to the center of the bar.

These two results are in perfect agreement with the Jominy hardenability curves of the two steel (Figures 10.30): the EN 36CrNiMo4 steel has a decreasing Jominy curve, while the Jominy curve of EN 34CrNiMo6 steel is almost flat, at least for the first 30mm from the quenched end. As already noted the radial hardness profile of a cylindrical steel bar is closely related to the Jominy hardenability curve of the same steel[24].

[23] If available, the actual Jominy hardenability curves of the steel should be used.

[24] The hardness profile (along the section of a component or along the Jominy sample) should not be confused with the absolute value of this mechanical property.

Figure 10.31 also shows a significant difference between the surface hardness values of the two cylindrical bars.
The surface hardness value of the cylindrical bar made of EN 36CrNiMo4 is much lower than that of the quenched end of the Jominy sample (54HRC has compared to 56HRC).
On the contrary the surface hardness value of the cylindrical bar made of EN 34NiCrMo6 is similar to that of the quenched end (54.5HRC as compared to 55HRC).

This difference depends on the different level of hardenability of the two steels.
The EN 34CrNiMo6 steel is more hardenable than the EN 36CrNiMo4 steel. Therefore, the higher hardenability allows to form martensite on the surface of the bar even if it is larger than the Jominy sample and the oil's quenching intensity factor is lower than that of water.
This result should not be surprising, the hardness values on the surface of a cylindrical bar is strongly influenced by the hardenability of the steel, as well as by the workpiece size and the quenching intensity factor of the quenched medium.

Figure 10.31 - Radial hardness profiles of two bars of 100mm in diameter made of EN 36CrNiMo4 steel and EN 34CrNiMo6 steel after quenching in non-agitated oil. The radial hardness profiles have been estimated with the Lamont diagrams.

10.12 Hardening and residual stresses

The austenite-martensite transformation occurs gradually along the section of the component: the transformation begins on the surface and ends in the core of the component.

A direct consequence is the creation of residual stresses at the end of the hardening since, martensite has a specific volume greater than austenite[25]. Residual stresses are formed when the core transformation occurs at a different time from that of the surface. Except for special cases, such as large-sized workpieces, the residual stresses are always of tension on the surface and compression in the core[26].

The phenomenon can be explained in a simplified way by observing Figure 10.32, that shows what occurs in a cylindrical bar during hardening; *S* and *C* represent the cooling curves of the surfaces and the core of the workpiece.

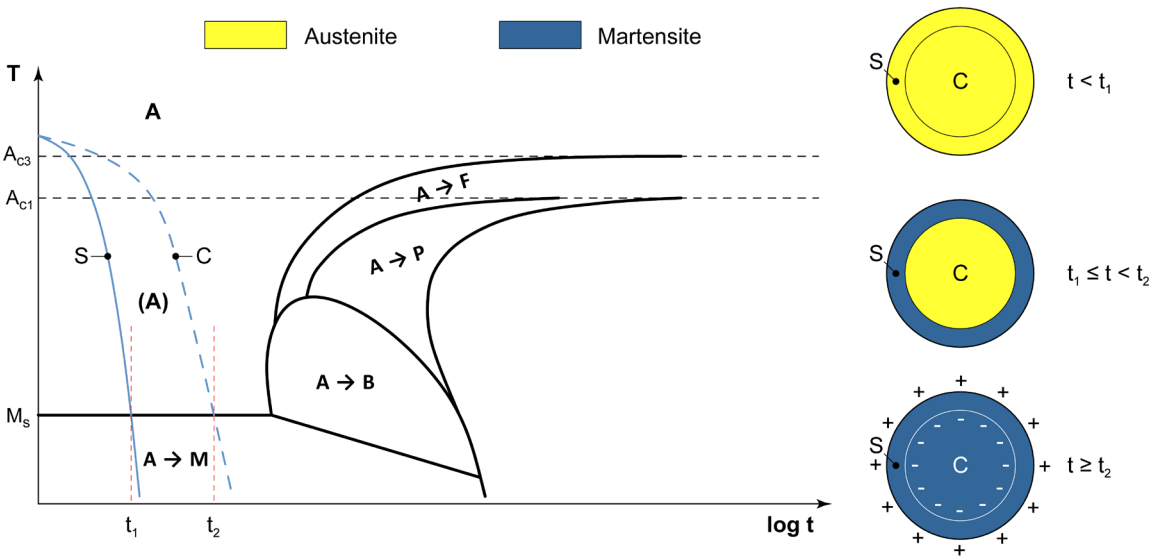

Figure 10.32 - Schematic representation of hardening for a medium/small-sized cylindrical bar made of a generic hypoeutectoid steel. The cooling curve of the surfaces *S* and the core *C* are superimposed on the C.C.T. diagram.

When time t is less than t_1, both the surface and the core are at high temperature and have an austenitic microstructure: internal stresses are practically nil. Beyond t_1 and up to t_2 only the surface forms martensite, while the core still has an austenitic microstructure.

[25] *The transformation of austenite into bainite, pearlite, ferrite, or cementite always produces an increase of the specific volume of the steel. However, the austenite-martensite transformation causes the greatest volumetric variations.*

[26] *See Note 4 of Chapter 4.*

At this stage any increase in volume are easily compensated by the austenite. Also in this second case, the residual stresses are practically nil.

Beyond t_2, the surface has a martensitic microstructure, while the core is still transforming. In this condition, the increase in volume of the core is prevented by martensite at the surface. The result is a thrust towards the surface, and the subsequent formation of tensile stresses that are compensated by the formation of compressive stresses in the core.

The level of residual stresses increases with the increase of the cooling rate, that depends on:

- the quenching procedures (the higher the quenching intesity factor of the quenching medium, the higher the residual stresses);
- the size and the shape of the semi-finished products (the larger the component and/or more complex the shape, the higher the residual stresses).

If the stress level is too high, permanent distortions and/or cracks may occur, which can make the workpieces useless (Figure 10.33). This is one of the reasons why you need to temper the as-quenched martensite, as described in Chapter 11.

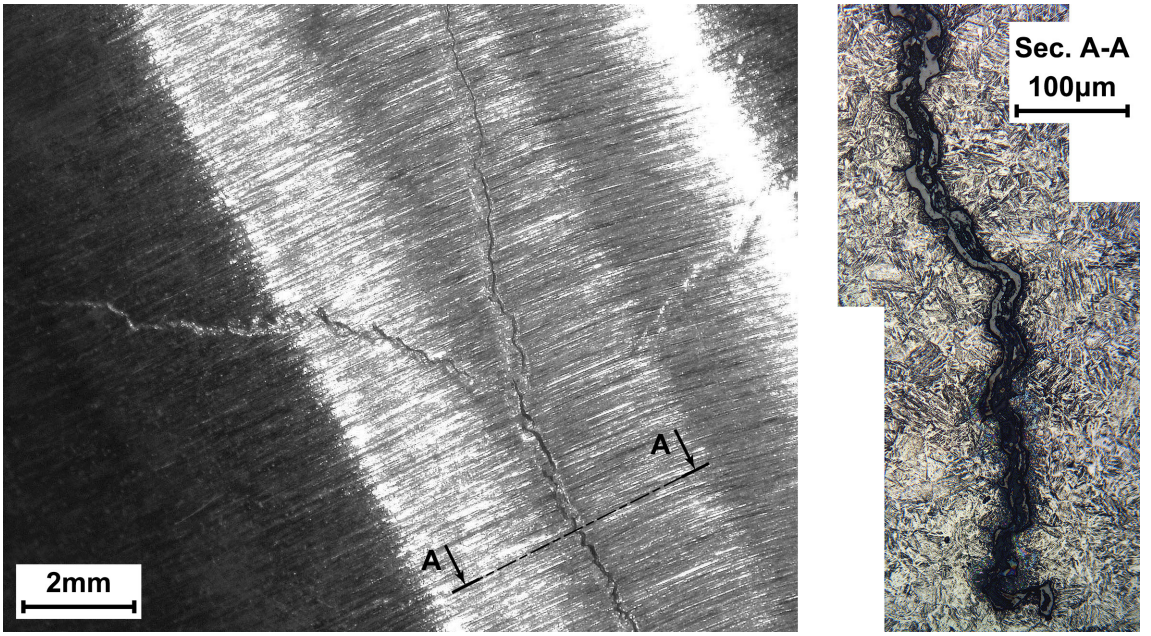

Figure 10.33 - Cracks in an EN 42CrMo4 steel bar after hardening: to the left, the outer surface, to the right, the microstructure along section A-A [Laboratories of the Department of Mechanical Engineering, Politecnico di Milano - Milano].

To limit residual stresses, steel should be chosen following the same rules used for hardenability. Large-sized components must be produced with very hardenable steel so that they can be cooled by using quenching media with a low quenching intensity factor; medium or small-sized components, on the other hand, can be produced with steel that is not very hardenable and cooled by using quenching media with a high quenching intensity factor.

10.13 Martempering and Austempering

The level of residual stresses produced by hardening can be drastically reduced by using two different heat treatments: martempering and austempering.

Martempering is similar to classic hardening, the main difference lies in the cooling phase, which is carried out using a thermal bath of molten salts at temperatures higher than M_s[27].

The holding time in the salt bath is long enough to equalize the temperature within the component, without intercept the bainitic transformation area on the T.T.T. diagrams.

Finally, when the temperature is uniform the component is cooled in oil or in air up to room temperature. The austenite-martensite transformation occurs only during the final part of the cooling phase. (Figure 10.34).

The purpose of martempering is to slow down the cooling before the austenite-martensite transformation takes place, in order to equalize the temperature within the workpiece. In this way the austenite-martensite transformation occurs almost simultaneously along the whole section of the component. Therefore martempering limits the residual stresses and the plastic deformations of the component, reducing the risk of cracks during the heat treatment.

After martempering, the microstructure is made of martensite, in the case of hypoeutectoid steels, or martensite plus carbides in the case of hypereutectoid steels. The microstructure has high toughness with low level of internal stresses and tempering can be carried out at low temperature (Chapter 11).

Martempering is a heat treatment that requires specific plants and, therefore, it has higher costs than traditional hardening and tempering. Martempering is carried out on semi-finished products of medium or large size or on components with very different sized sections. Martempering is also used for the heat treatment of tool steel, in order to prevent deformation or distortion.

[27] The temperature of M_s is between 200°-350°C depending on the type of steel, as calculated with the formulas proposed in Paragraph 7.5 of Chapter 7.

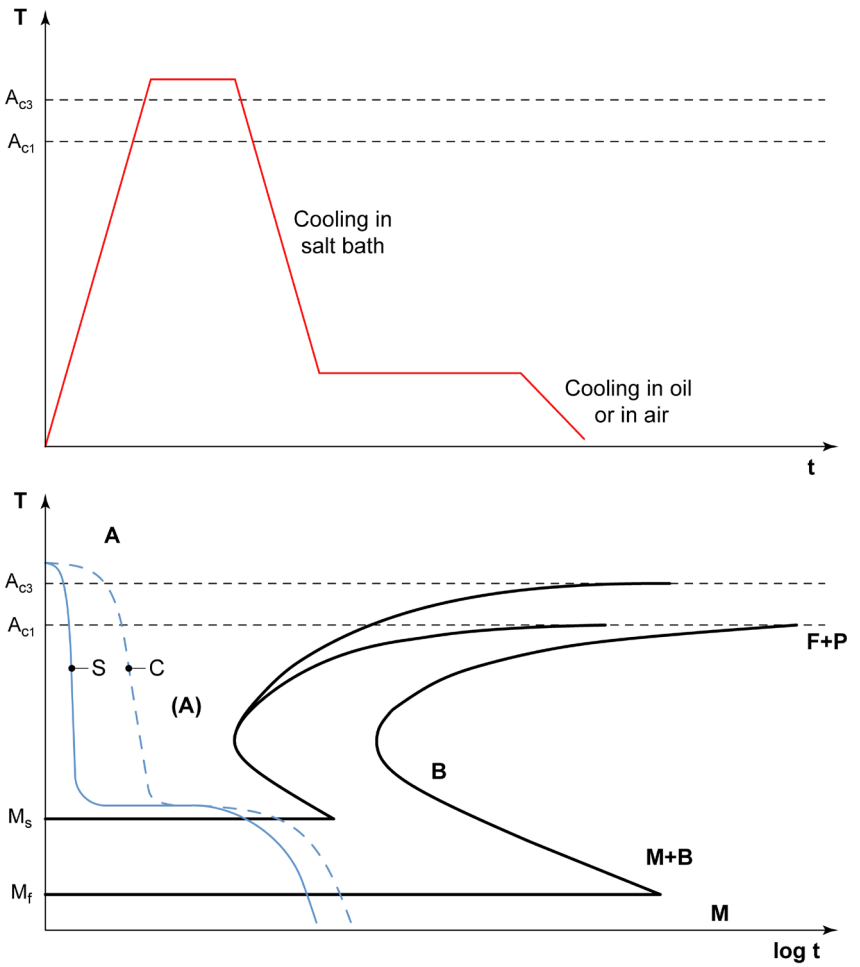

Figure 10.34 - Schematic representation of martempering for a generic hypoeutectoid steel (on the top). The cooling curve of surfaces *S* and core *C* are superimposed on the T.T.T. diagram (on the bottom).

Austempering is similar to martempering: steel is heated above the critical points and then cooled in a molten salt bath at a temperature slightly above M_s. In the case of austempering, however, the workpiece is holded in the salt bath until the isothermal transformation of the austenite into bainite is completed (Figure 10.35). Tempering is not required after austempering.

The purpose of austempering is to limit the risk of cracks or plastic deformations of the component, as well as to improve its mechanical properties. After the heat treatment the microstructure is made of very fine bainite characterized by higher mechanical properties, as compared to martensite after hardening and tempering.

Austempering is used for the same types of steel and components that are heat treated with martempering. The costs are also similar and higher than those of traditional hardening and tempering.

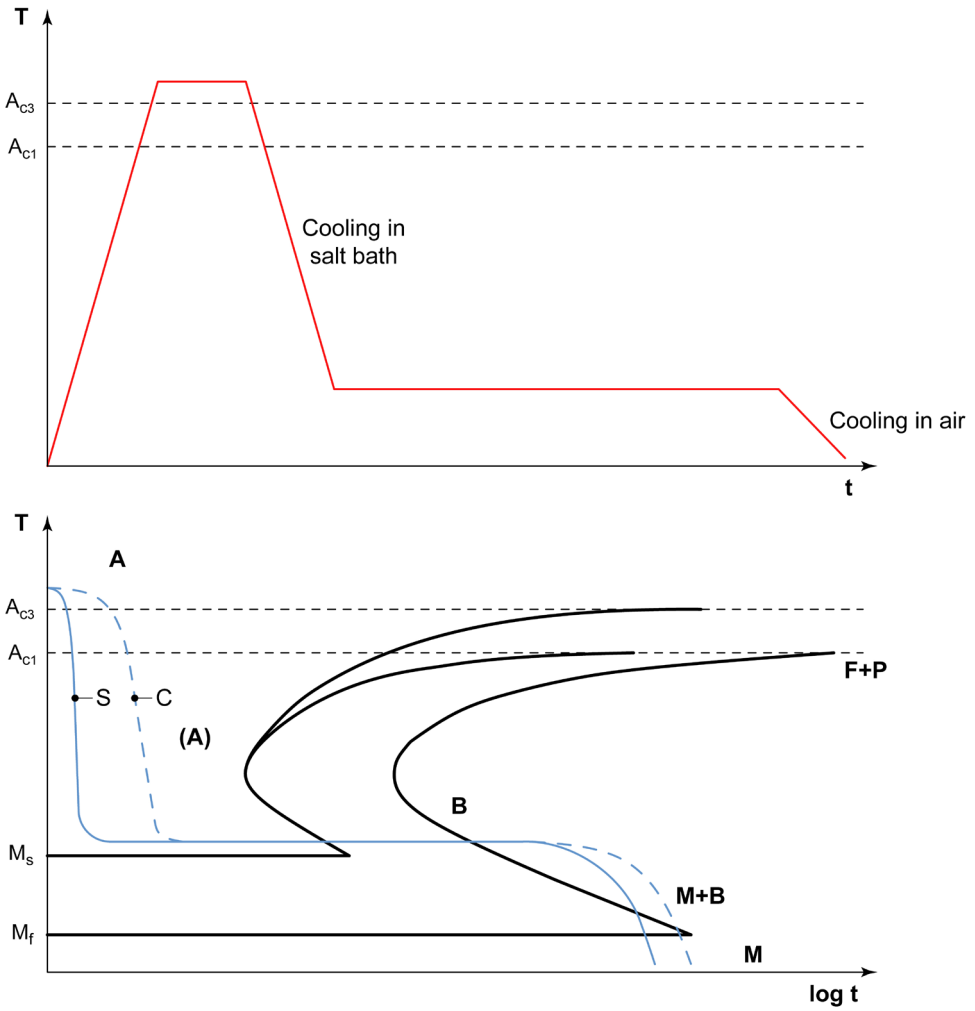

Figure 10.35 - Schematic representation of austempering for a generic hypoeutectoid steel (on the top). The cooling curve of surfaces *S* and core *C* are superimposed on the T.T.T. diagram (on the bottom).

11. HEAT TREATMENTS BELOW CRITICAL POINTS

11.1 Classification of subcritical treatments

Subcritical heat treatments have always the holding temperature below critical points and, therefore, they do not have the γ-phase $\rightarrow$ α-phase transformation. Consequently, at the end of the heat treatment the steel microstructure is almost unchanged. The subcritical heat treatments are divided into two categories:

- heat treatments that act on pearlitic-ferritic microstructure;
- heat treatments that act on martensitic microstructure.

At the first group was given the name of subcritical annealing, while at the second one was given the name of tempering. In both cases the soaking temperatures are similar, what makes the difference are the microstructural changes that occur during the heat treatment.

11.2 Subcritical annealing

The name subcritical annealing is used for various heat treatments. These heat treatments are quite similar (Figure 11.1) and their results depend mainly on the type of component to be treated and the microstructural changes that occur. The subcritical annealing are commonly divided into three categories:

- annealing for machinability: this heat treatment is performed to reduce the hardness in order to increase the machinability of the steel;
- stress-relief annealing: this heat treatment is performed to reduce residual stresses caused by previous manufacturing processes (i.e. welding, machining, etc.);
- recrystallisation annealing: this heat treatment is performed to reduce the level of cold work caused by previous manufacturing processes (i.e. drawing, cold rolling, etc.).

There are also heat treatments similar to subcritical annealing, but with a very specific purpose: a typical example is hydrogen annealing[1], which is performed to reduce the hydrogen content in casted or forged semi-finished products.

Annealing for machinability

The annealing for machinability has a holding temperature of 30°-50°C below critical point A_{c1}. The holding time depends on the microstructural changes that you want to create in the steel.

[1] *The hydrogen annealing has very long holding time (a several dozen hours) at temperatures between 600°C and 650°C, in order to diffuse hydrogen out from the semi-finished products (typically casted or forged workpieces).*

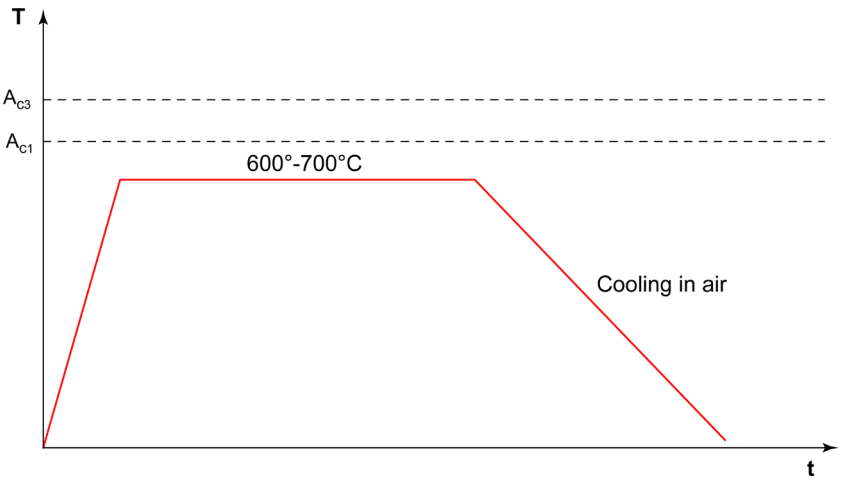

Figure 11.1 - Schematic representation of subcritical annealing.

Typically, the annealing for machinability has a holding temperature between 600°C and 700°C and a holding time of 2-4 hours. At the end of soaking, slow cooling is carried out in furnace or in air.
The main purpose of annealing for machinability is to modify the shape of the Fe_3C phase from lamellar to globular, in order to reduce the hardness and increase the machinability of the ferritic-pearlitic microstructure (Figure 11.2). However, if compared to spheroidizing annealing[2], the coalescence level of the Fe_3C phase is lower and is never complete.
Generally annealing for machinability is carried out after normalizing; often, however, this heat treatment is carried out on forged or laminated semi-finished products, immediately after hot working. In these cases, the non-homogeneities of the steel (segregation bands, chemical composition non-homogeneities, etc.) remain unaltered. Consequently, after annealing for machinability, the new microstructure is affected by original non-homogeneities.

Stress-relief annealing

Stress-relief annealing is similar to annealing for machinability. The main purpose of this heat treatment is to remove the residual stresses induced by previous manufacturing processes.

[2] *See paragraph 10.3 of Chapter 10.*

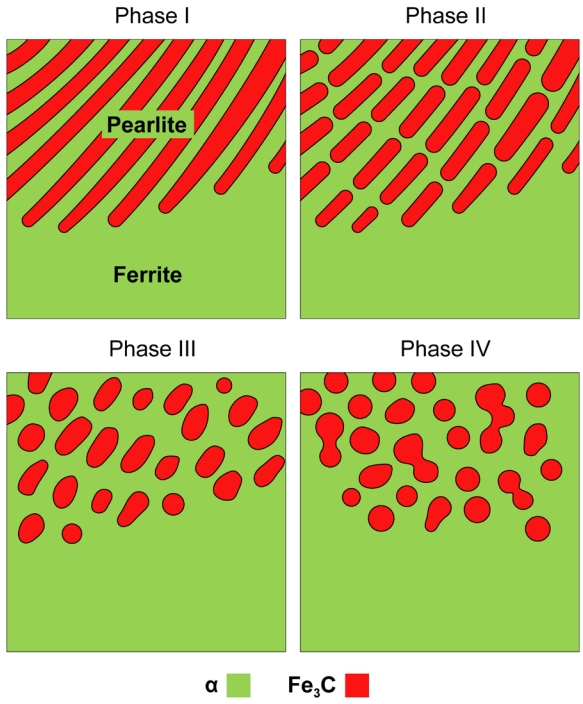

Figure 11.2 - Decomposition process of the Fe_3C phase from lamellar to globular. Phases II and III show the typical result of annealing for machinability, instead Phase IV shows the typical result of spheroidizing annealing [from Higgins 1993].

In the case of steel castings or after heavy mechanical machining, it is useful to carry out stress-relief annealing at temperatures between 600°C and 700°C for a few hours. Subsequently, the component is cooled in furnace up to 400°C and then in air. These subcritical treatments are performed to avoid brittle fracture or to limit the degradation phenomena caused by residual stresses[3].
Post weld heat treatments (P.W.H.T.) are also a type of subcritical annealing and are carried out to remove residual stresses and to improve the resistance to brittle fractures of welding structures (Figure 11.3).

[3] *Stress Corrosion Cracking is a degradation phenomenon that affect components with residual tensile stresses, made of a specific material and in contact with a specific aggressive environment. The elimination of one of these three factors makes the corrosive phenomenon impossible to happen (for more details, see Boniardi M., Casaroli A., Stainless Steels, ed.Lucefin, Esine, 2014).*

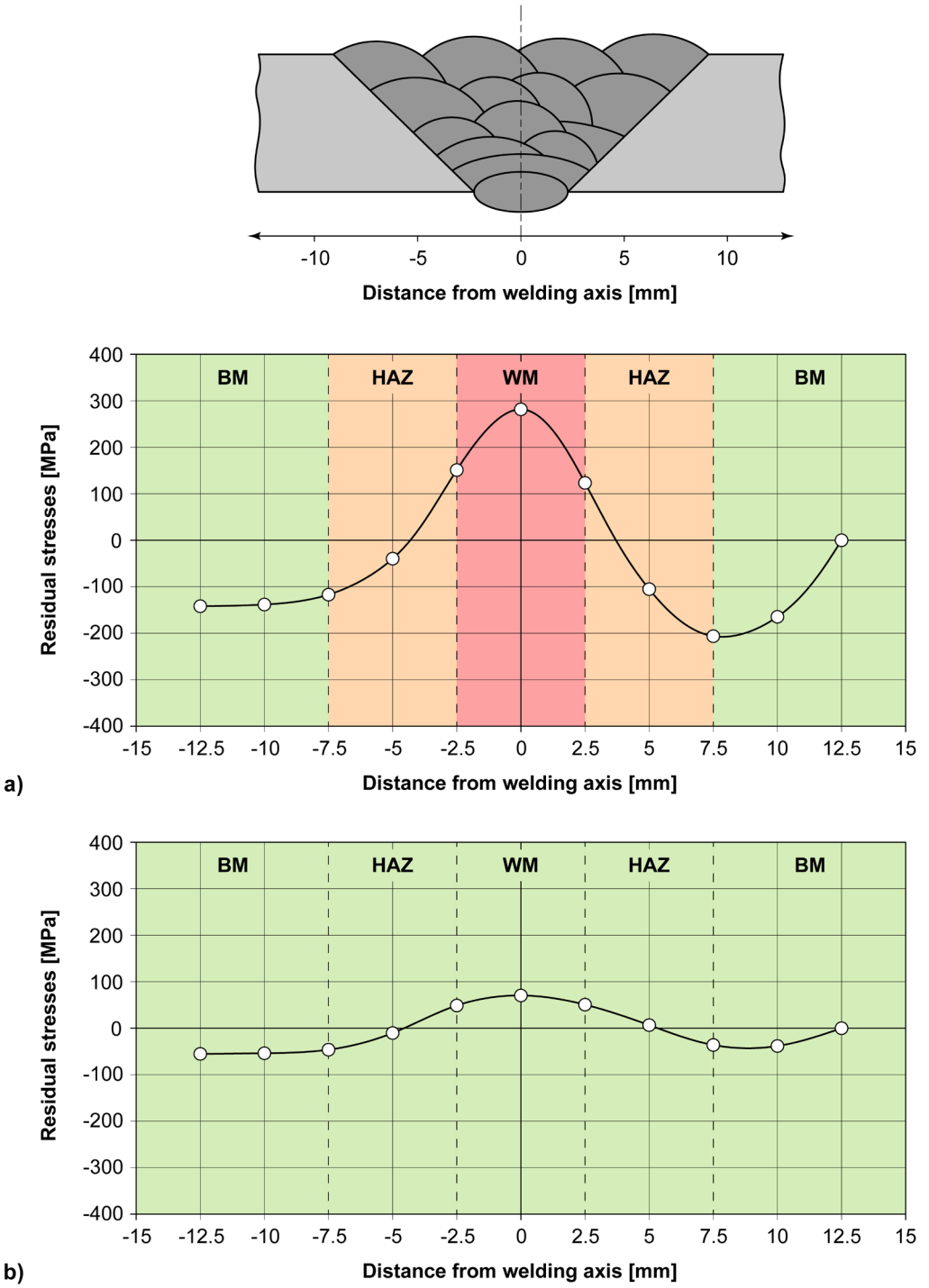

Figure 11.3 - Residual stresses field along the transverse direction of a welding joint made of low carbon steel: (a) before and (b) after stress-relief annealing at 650°C for 2 hours. The steel has been preheated at 250°-300°C and the welding has been made with automatic submerged arc welding.

Recrystallisation annealing

If the steel is cold worked, subcritical annealing always triggers recovery, recrystallisation, and grain growth phenomena described in Chapter 4. In these cases, the heat treatment is called recrystallisation annealing. Recrystallisation annealing can be carried out at different temperatures and holding times, depending on the desired level of recovery, recrystallisation, and grain growth. The initial level of strain hardening has a great influence on the final result (Figure 11.4). In general, the mean grain size increases (Figure 11.5):

- as the annealing temperature increases,
- as the holding time increases,
- as the strain hardening level of the steel decreases[4].

Recrystallisation annealing is very important in cold deformation processes because it restore the original deformability level of the steel. For example, during drawing or cold rolling, the strain hardening levels can exceed the maximum limit of the material, causing the component to break. In these cases, recrystallisation annealing is required to continue to reduce the section.

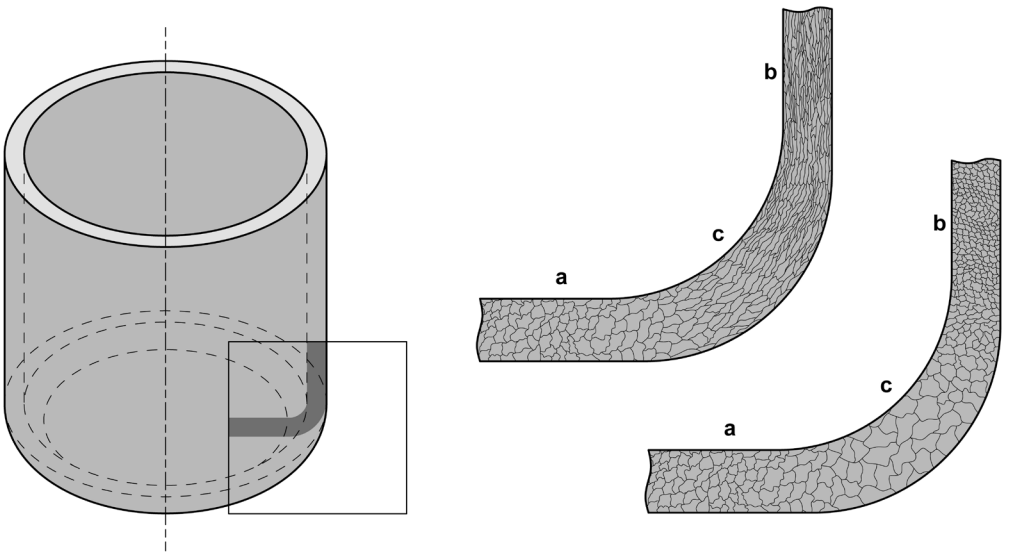

Figure 11.4 - Schematic representation of the mean grain size in a deep-drawn component before and after recrystallisation annealing: (a) in the bottom area the strain hardening is nil and therefore the recrystallisation is also nil; (b) in the side area the strain hardening is high and therefore the recrystallisation produces a very fine grain; (c) in the middle area the strain hardening level is lower than the side area but higher than the bottom one. In this area recrystallisation produces grains larger than the original ones [from Higgins 1993].

[4] Recrystallisation does not occur at any strain hardening level. In fact, recrystallisation starts only if a critical cold deformation threshold (called χ_{min} in Figure 11.5) is exceeded.

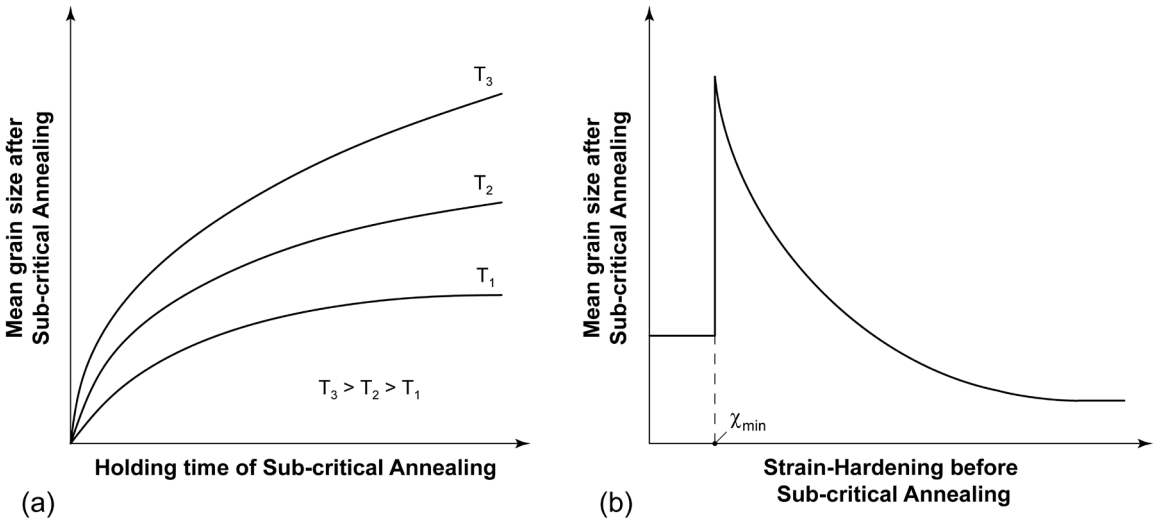

Figure 11.5 - The effect of holding temperature/time (a) and strain hardening level on mean grain size after recrystallisation (χ_{min} is the minimum level of strain hardening that activates recrystallisation).

11.3 Tempering

The as-quenched martensite[5] is very hard and, above all, very brittle and characterized by high level of residual stresses. Therefore, the workpieces cannot be immediately used after hardening, since they would risk sudden breakage. To overcome these problems, it is important to carry out another heat treatment after hardening, the so called "tempering".

Tempering should be started immediately after hardening, in order to limit the risk of cracks caused by residual stresses. Ideally, components should be tempered when they are not completely cool (50°-70°C). Tempering has a slow heating up to a temperature below the critical points. Generally a preheated furnace is used[6]. The heating time depends on the workpiece size and the type of the furnace.

[5] Generally, during hardening, austenite does not transform completely into martensite. The amount of martensite depends on the hardenability of the steel and the cooling rate of the workpiece. Therefore, the considerations in Paragraph 11.3 refers only to the portions of material where martensite is formed.

[6] If, for example, the heating temperature is equal to 600°C, it may be useful to preheat the furnace at temperatures of 250°C to 300°C. However, if the steel has high thermal conductivity (i.e. carbon steel) and the components have not complex shape, it is also possible to set the furnace at maximum temperature without preheating.

The typical soaking temperature is between 600°C and 650°C, even if soaking temperatures between 150°C and 200°C or 400°C and 460°C[7] are also used. In fact, the holding temperature and the holding time depend on the required mechanical strength at the end of the sub-critical annealing. Tempering ends with cooling in air, or sometimes in oil (Figure 11.6).

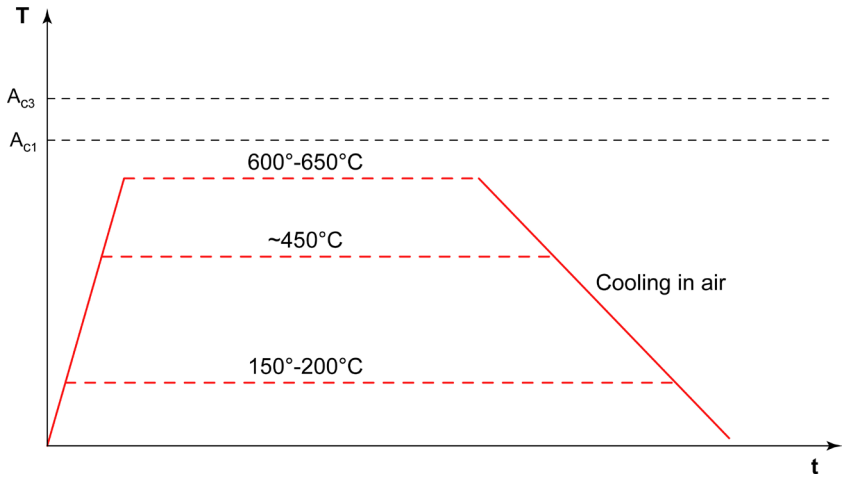

Figure 11.6 - Schematic representation of tempering.

Tempering has two important purposes:

- remove the typical brittleness of the as-quenched martensite;
- reduce the residual stresses caused by hardening.

These results are due to the microstructural changes that occur during tempering. Starting at 80°C, carbon diffuses out from the tetragonal lattice of the as-quenched martensite.

As a result, the as-quenched martensite transforms into "tempered martensite". This microstructure has a body-centered cubic lattice and is characterized by a toughness level higher than as quenched martensite; in fact, when the temperature increases, the lattice parameter c_α decreases until it becomes equal to the parameter a_α (Figures 8.20 and 8.22).

The diffusion of carbon out from the tetragonal lattice of the as-quenched martensite causes the formation of carbides. If temperature is between 100°C and 200°C carbides are made of $Fe_{2\text{-}3}C$ phase (ε carbides) while if temperature is between 200°C and 400°C carbides are made of Fe_3C phase and their shape is acicular.

[7] *Tempering between 250°C and 380°C or between 480°C and 570°C causes the embrittlement of the tempered martensite. In both cases, after tempering, steel is very brittle and shows low impact strength. Therefore, tempering should never be performed at these temperatures.*

At temperature between 450°C and 650°C carbides are still made of Fe_3C phase but their shape becomes globular. Finally, at temperature over 600°C carbides coalesce together, increasing in size. Tempering also causes the transformation of retained austenite, which turns to bainite for temperatures between 200°C and 400°C, or to martensite for temperature between 450°C and 650°C. The Figure 11.7 shows both a schematic representation of what previously described and the effect of tempering temperature on hardness of different iron-carbon alloys.

Alloying elements can influence the end result of tempering. Silicon and manganese counteracts the softening effect[8] since they delay the formation of carbides of Fe_3C phase. Chromium, molybdenum, vanadium, tungsten, and titanium form carbides harder than martensite, which preserve their hardness at high temperature and reduce the softening effect. Other chemical elements, such as nickel, have instead very limited effect on softening.

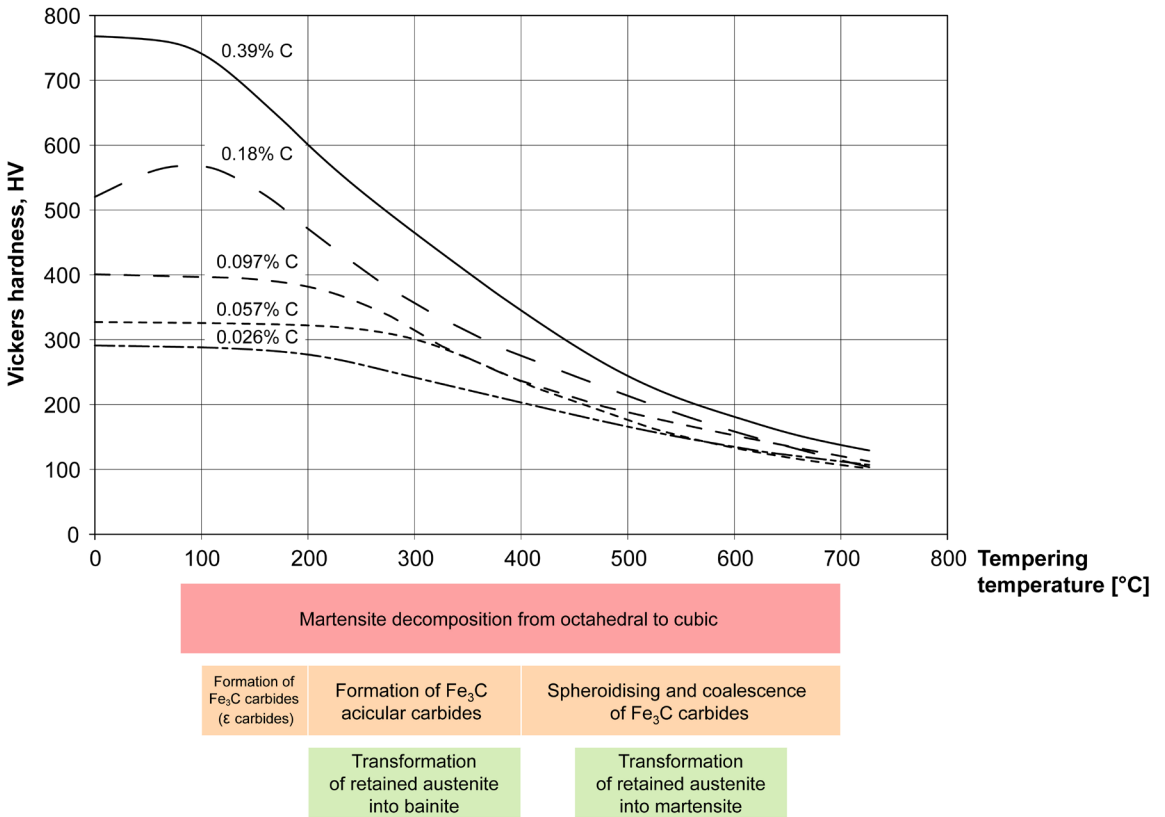

Figure 11.7 - The effect of tempering temperature (holding time:1 hour) on the hardness of different iron carbon alloys [from Speich 1969].

[8] *The term "softening" refers to the decay of hardness of steel components exposed to high temperature (up to ~500°C), such as tool steels.*

The tempering temperature has an important effect on all the engineering properties of steel. Figures 11.8 and 11.9 show the effect of tempering temperature on tensile strength, yield strength, elongation after fracture and impact strength of two commonly used hardened and tempered steels (EN C40 and EN 36CrNiMo4). As is typical of all hardened and tempered steels, when the tempering temperature increases, hardness and tensile strength decrease (UTS and YS) while elongation after fracture and impact strength increase.

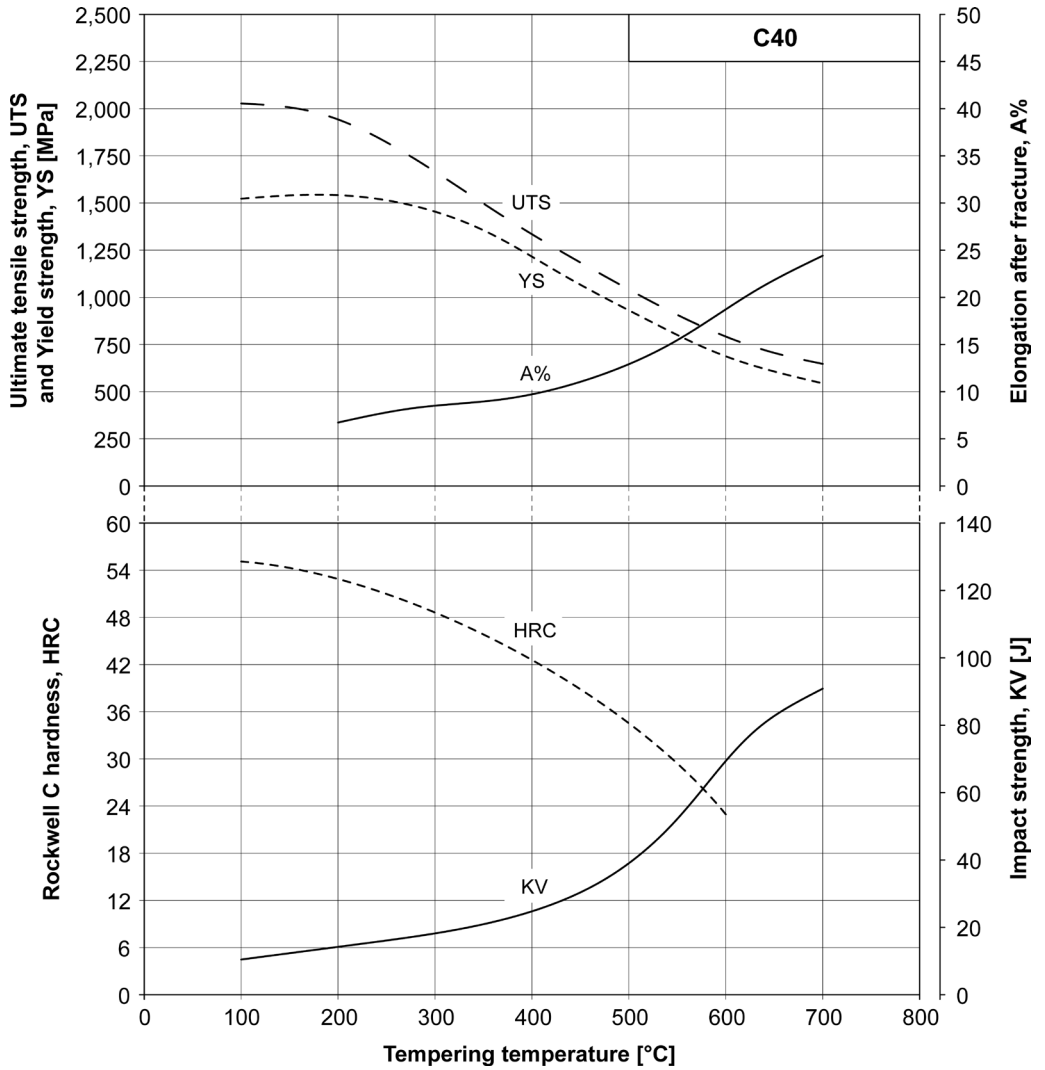

Figure 11.8 - The effect of tempering temperature on tensile strength (UTS and YS), elongation after fracture (A%), Rockwell C hardness (HRC), and impact strength (KV) of an EN C40 steel (cylindrical bars of 10mm in diameter austenitized at 840°C for 1 hour and hardened in water). [Laboratories of the Department of Mechanical Engineering, Politecnico di Milano - Milano].

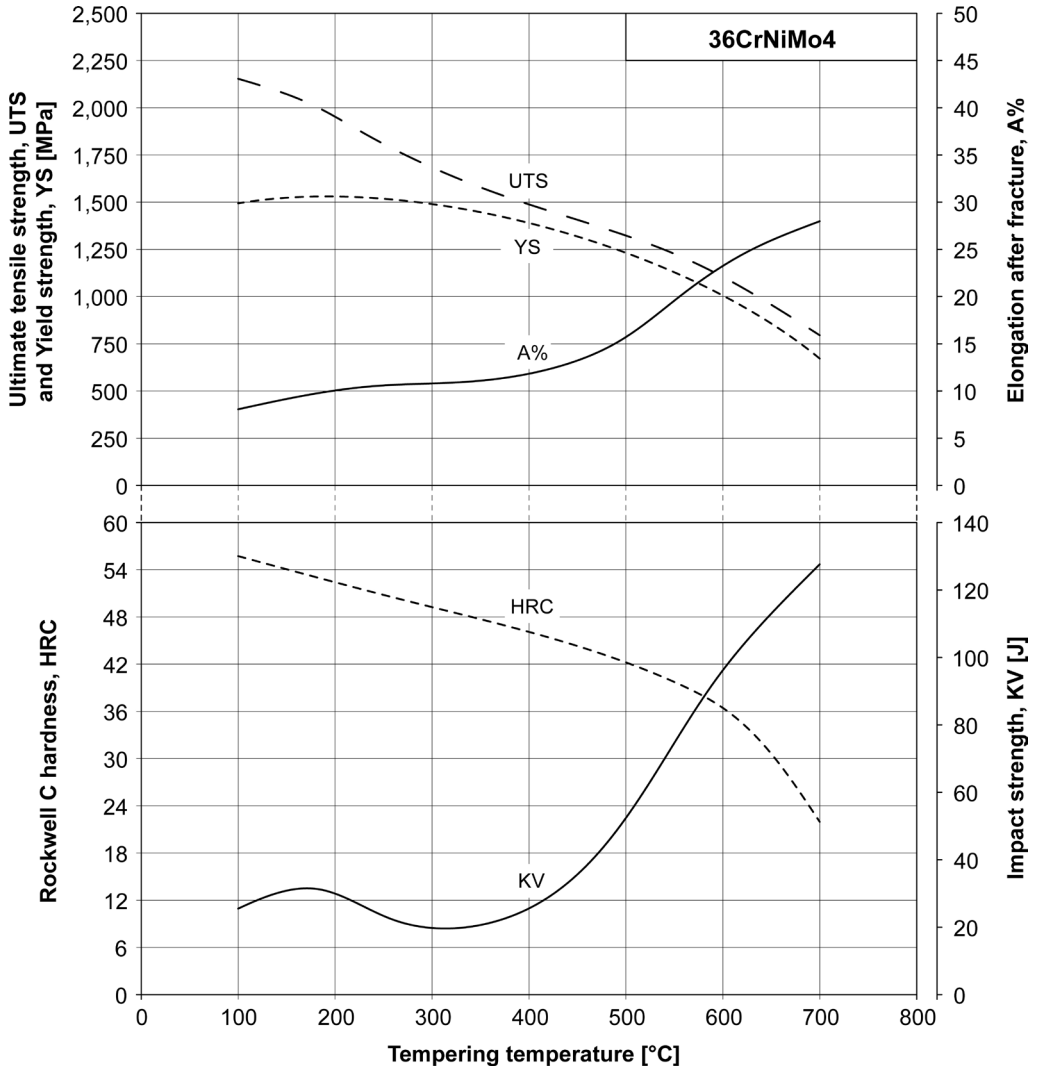

Figure 11.9 - The effect of tempering temperature on tensile strength (UTS and YS), elongation after fracture (A%), Rockwell C hardness (HRC), and impact strength (KV) of an EN 36CrNiMo4 steel (cylindrical bars of 10mm in diameter austenitized at 850°C for 1 hour and hardened in oil). [Laboratories of the Department of Mechanical Engineering, Politecnico di Milano - Milano].

Tempering has another important effect: the progressive decrease of residual stresses. Figures 11.10 and 11.11, show the effect of tempering temperature on the level of residual stresses, which is practically nil for tempering temperatures between 550°C and 600°C.

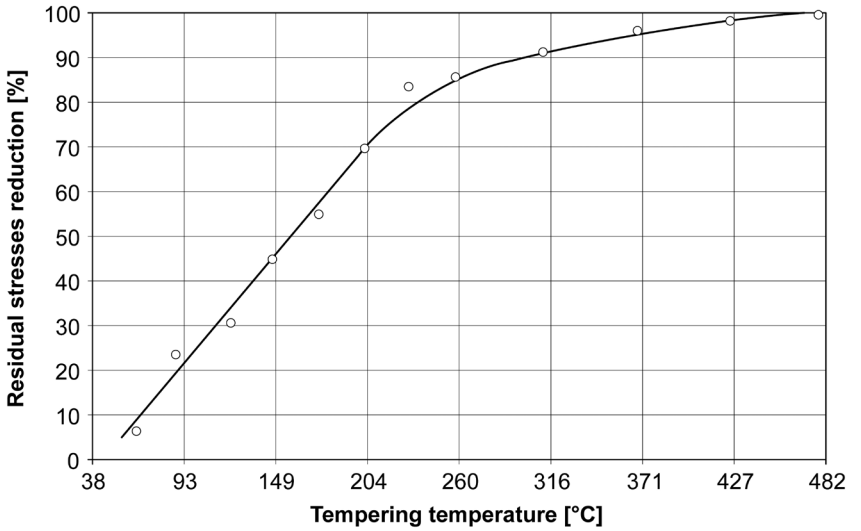

Figure 11.10 - The effect of tempering temperature on the level of residual stresses for a bearing steel (EN 100Cr6). The holding time is equal to 1 hour. [from Brown and Cohen 1962].

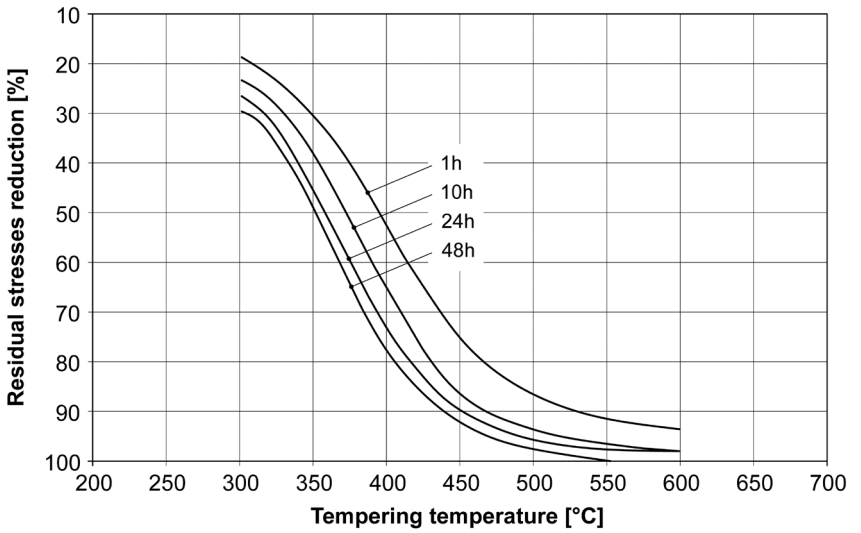

Figure 11.11 - The effect of tempering temperature and holding time on the level of residual stresses for an hardened and tempered steel [Spur and Stöferle 1980-1994].

11.4 Estimation of hardness after tempering

The hardness of tempered martensite can be estimated by various calculation methods. Here the formulas proposed by Hollomon and Jaffe[9] is presented. These formulas are valid for carbon steel but, thanks to the studies carried out by Grange and Baughman[10], their use has also been extended to low alloy steels. The calculation method proposed by Hollomon and Jaffe is based on the experimental evidence that the hardness of tempered martensite depends on a parameter called the Hollomon-Jaffe Parameter and indicated with the letter P. The parameter P in turn depends on temperature and holding time of tempering, according to the equation:

$$P = 1.8 \cdot T \cdot (C + log_{10}t) \cdot 10^{-3} \quad [11.1]$$

where T is the tempering temperature in Kelvin, t is the soaking time in hours, and C is a constant (for many steels $C = 18$). Figure 11.12 shows the effect of parameter P and carbon content on hardness of tempered martensite. If the steel has other alloying elements, besides carbon, the previously estimated hardness value must be increased by the ΔH quantity, which is defined by the equation 11.2:

$$\Delta H = f_{Mn} \cdot Mn + f_{Si} \cdot Si + f_{Ni} \cdot Ni + f_{Cr} \cdot Cr + f_{Mo} \cdot Mo + f_V \cdot V \quad [11.2]$$

The concentration of each alloying element must be multiplied by its f_{El} coefficients taken from Table 11.1. However, this calculation method does not apply to steel showing the secondary hardness phenomenon (Paragraph 11.5).

Case 1

We would like to know the hardness after hardening and tempering at 600°C for 2 hours on an EN C35 and EN 36CrNiMo4 steels; their nominal composition is shown in Table 11.2.
First of all, you have to evaluate the parameter P. From equation 11.1, we have:

$$P = 1.8 \cdot (600 + 273) \cdot (18 + log_{10}2) \cdot 10^{-3} \cong 28.76$$

The Figure 11.12 shows that, for $C = 0.36\%$ and $P = 28.76$, the Vickers Hardness of C35 steel after tempering is equal to[11]:

$$H_{C35} \cong 235\,HV$$

[9] *Hollomon J.H., Jaffe L.D., Time-temperature relations in hardened and tempered steel, Transactions of AIME, vol. 162, pp. 223- 249, 1945.*

[10] *Grange R.A., Baughman R.W., Hardness of tempered martensite in carbon and low alloy steels, ASM Transactions, vol. 48, pp.165- 197, 1956.*

[11] *The manganese and silicon contents are not to be considered because they are lower than those in Table 11.1. For these quantities the effect of the two alloying elements is already considered in the carbon effect shown in Figure 11.12.*

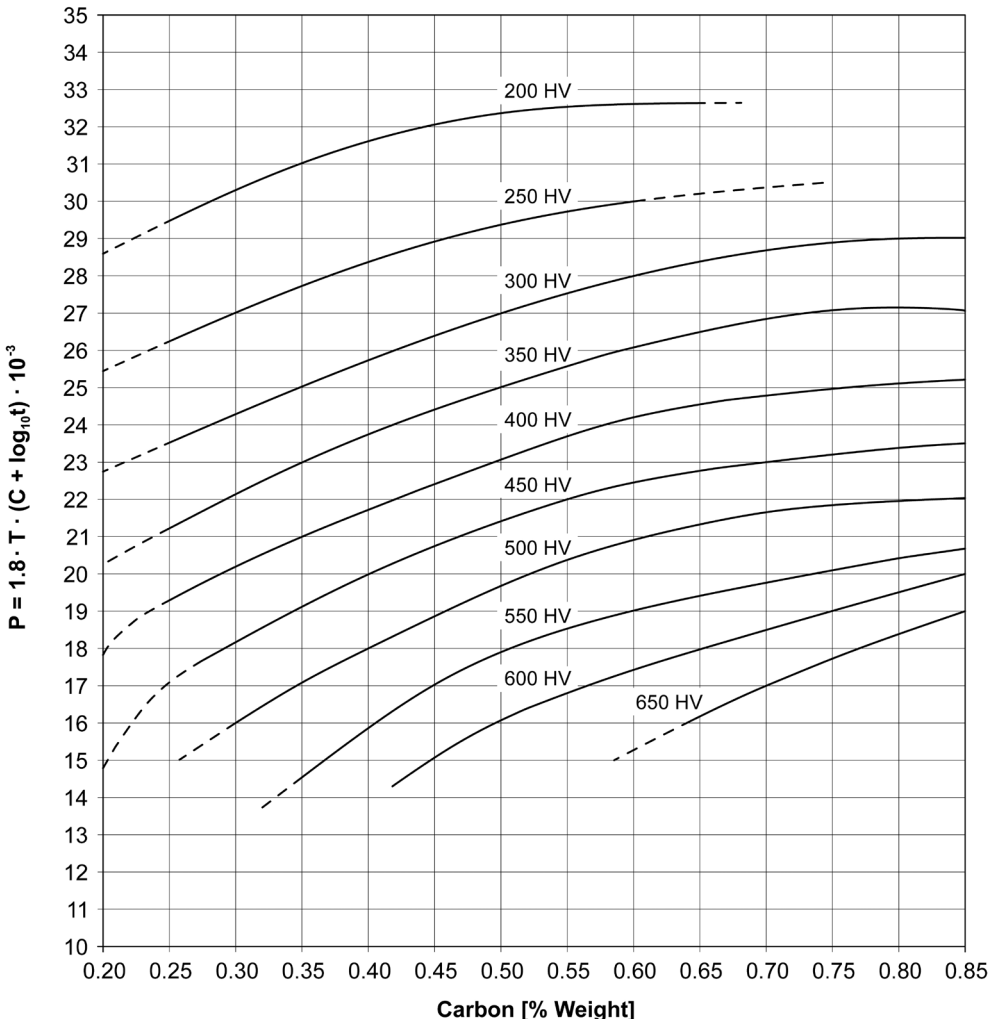

Figure 11.12 - The effect of parameter P and carbon content on hardness of tempered martensite [from Hollomon and Jaffe 1945].

In case of EN 36CrNiMo4 steel, the effect of alloying elements must be evaluated (the effect of carbon is the same because the content of carbon is the same for both types of steel).
The coefficients to be used in formula 11.2 are taken from table 11.1. Since $P = 28.76$ the effect of alloying element (ΔH) is between:

$$\text{for} \quad P = 28 \rightarrow \Delta H = 8 \cdot 0.90 + 55 \cdot 1.00 + 120 \cdot 0.20 = 86.20$$
$$\text{for} \quad P = 30 \rightarrow \Delta H = 6 \cdot 0.90 + 55 \cdot 1.00 + 105 \cdot 0.20 = 81.40$$

The linear interpolation between the two values is equal to:

$$\Delta H \cong 84$$

Therefore, the hardness after tempering of an EN 36CrNiMo4 steel is equal to:

$$H_{36CrNiMo4} = 235 + 84 \cong 320HV$$

		Value of parameter *P*					
Element	**level %**	**20**	**22**	**24**	**26**	**28**	**30**
Manganese (*Mn*)	0.85-2.1	35	25	30	30	30	25
Silicon (*Si*)	0.3-2.2	65	60	30	30	30	30
Nickel (*Ni*)	0-4	5	3	6	8	8	6
Chromium (*Cr*)	0-1.2	50	55	55	55	55	55
Molybdenum (*Mo*)	0-0.35	40 20 (*)	90 45 (*)	160 80 (*)	220 110 (*)	240 120 (*)	210 105 (*)
Vanadium (*V*) (**)	0-0.2	0	30	85	150	210	150

(*) Use these factors if the chromium content is between 0.5% and 1.2%.
(**) Use these factors for low alloy steels with chromium or chromium-vanadium; not valid for steels where vanadium is the only carbide forming element.

Table 11.1 - The $f_{E/}$ coefficients for various alloying elements in relation to parameter *P* [from Grange and Baughman 1956].

	C35	36CrNiMo4
C	0.36	0.36
Mn	0.75	0.70
Si	0.20	0.20
Cr	---	1.00
Ni	---	0.90
Mo	---	0.20

Table 11.2 - Nominal composition of EN C35 steel and EN 36CrNiMo4 steel.

Case 2

In this second example we would like to know the holding time t_x of a tempering carried out at 550°C on an EN 36CrNiMo4 steel, so that the hardness is the same as in the previous Case 1, i.e. $H_{36CrNiMo4} \cong$ 320HV (tempering at 600°C for two hours). Since we want the same hardness values, the parameter *P* must remain constant:

$$P_{550°C,\,t_x} = P_{600°C,\,2h} = 28.76$$

$$1.8 \cdot (550 + 273) \cdot (18 + log_{10} t_x) \cdot 10^{-3} = 28.76$$

Developing the calculations, the following occurs:

$$1{,}481.4 \cdot (18 + log_{10} t_x) = 28{,}760$$

$$log_{10} t_x \cong 1.41407$$

$$t_x \cong 25h \; and \; 56min$$

These result allow to estimate the effect of temperature and holding time on the effectiveness of tempering. In fact, case 2 shows an increase in soaking time of almost 13 times (from 2 hours to about 26 hours) if the temperature is reduced by 50°C (from 600°C to 550°C). Note that the hardness of tempered martensite is the same in both cases 1 and 2.

11.5 Tempering of high alloy steel and secondary hardness

Tempering produces always a progressive decrease in hardness of carbon or low alloy steel. However, if the steel has alloying elements such as chromium, molybdenum, tungsten, vanadium, and titanium, the metal mass forms very hard and very small carbides, during tempering. These carbides are uniformly dispersed in martensitic microstructure and act as obstacles to the dislocation motion, increasing the hardness of steel. This phenomenon is called secondary hardness to distinguish it from primary hardness of martensite.

This phenomenon is due to the higher affinity for carbon of the above mentioned alloying elements compared to iron. In fact, at high temperature the carbide forming elements promote the decomposition of Fe_3C carbides, forming at the same time stable carbides of MC type (i.e. VC, TiC and WC), M_2C type (i.e. Mo_2C and W_2C), M_6C type (i.e. Fe_3W_3C and Fe_3Mo_3C), and $M_{23}C_6$ type (i.e. $Cr_{23}C_6$), much harder than Fe_3C carbides (Figure 11.14).

The secondary hardness phenomenon generally occurs at temperatures between 400°C and 600°C, with a peak value of the hardness around 550°C. To this regard, Figure 11.15 shows the secondary hardness effect for several types of tool steels after hardening and three tempering[12].

The secondary hardness phenomenon is extremely important to reduce the softening effect that occurs in steels exposed to high temperature (up to ~500°C), such as tool steels. In fact, without the secondary hardness phenomenon, there would be a progressive decrease in hardness and a consequent loss of wear resistance.

[12] *Steel with significant quantities of alloying elements has a rather large amount of retained austenite, due to the downward shift of the horizontal line of martensite finish, M_f (see Paragraph 7.5 of Chapter 7). Therefore, you need to perform repeated tempering, in order to transform the retained austenite into martensite.*

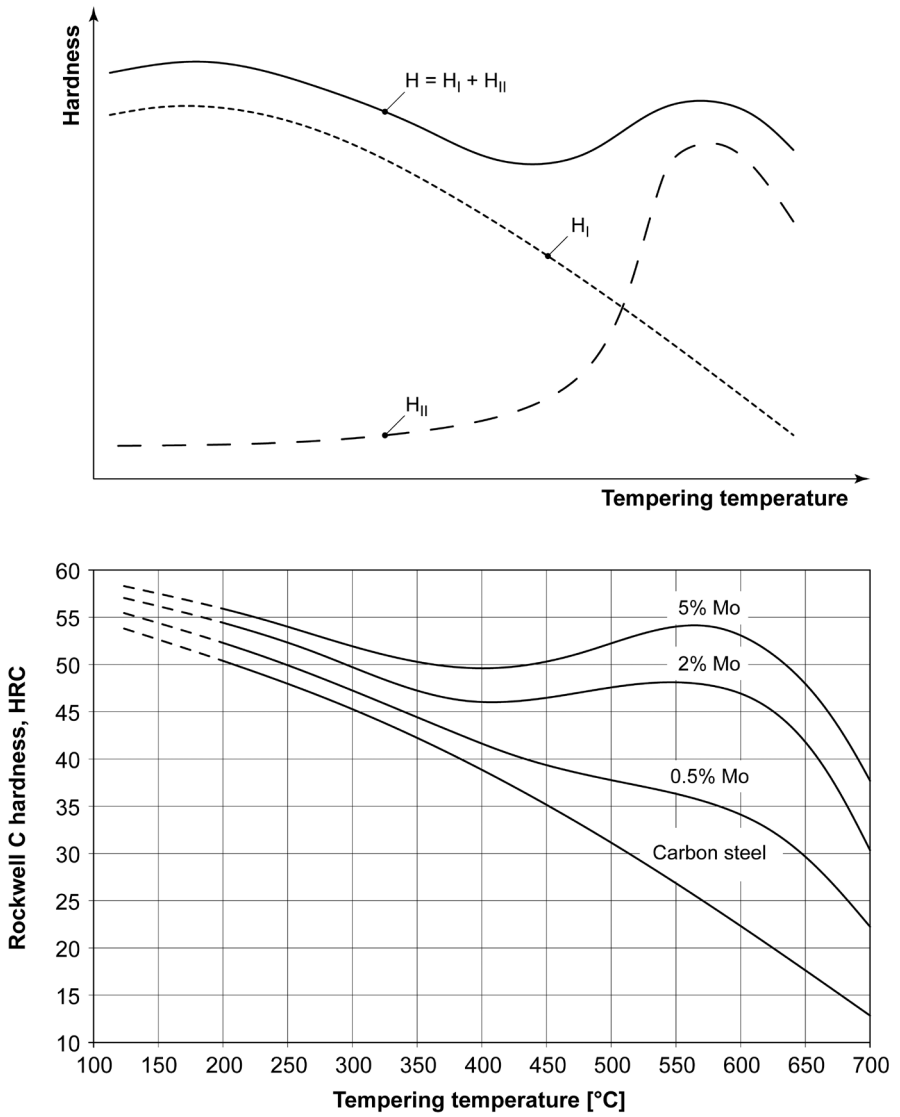

Figure 11.13 - (on the top) Schematic representation of the primary and secondary hardening effects (H_I: primary hardness due to solid solution of carbon in martensite; H_{II}: secondary hardness due to carbide precipitation; $H = H_I + H_{II}$: final steel hardness after tempering); (on the bottom) Example of the phenomenon for steels with increasing amount of molybdenum [from ASM-H4 1991].

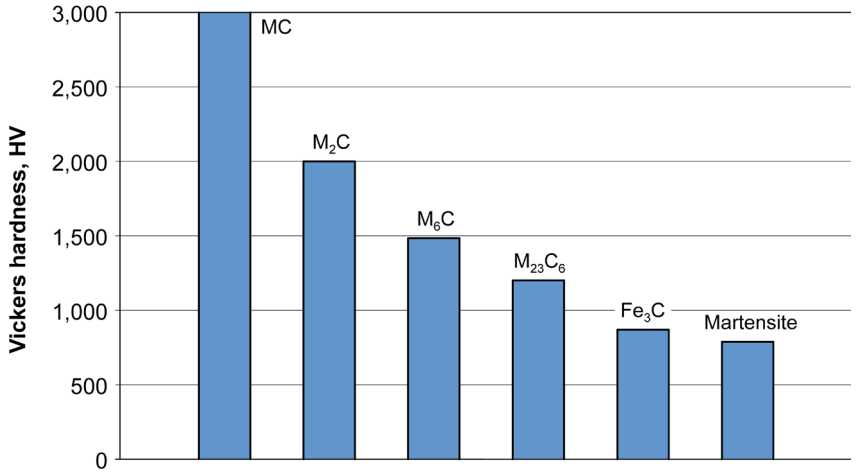

Figure 11.14 - Hardness of different types of carbides compared to martensite [from Wells and Lherbier 1980].

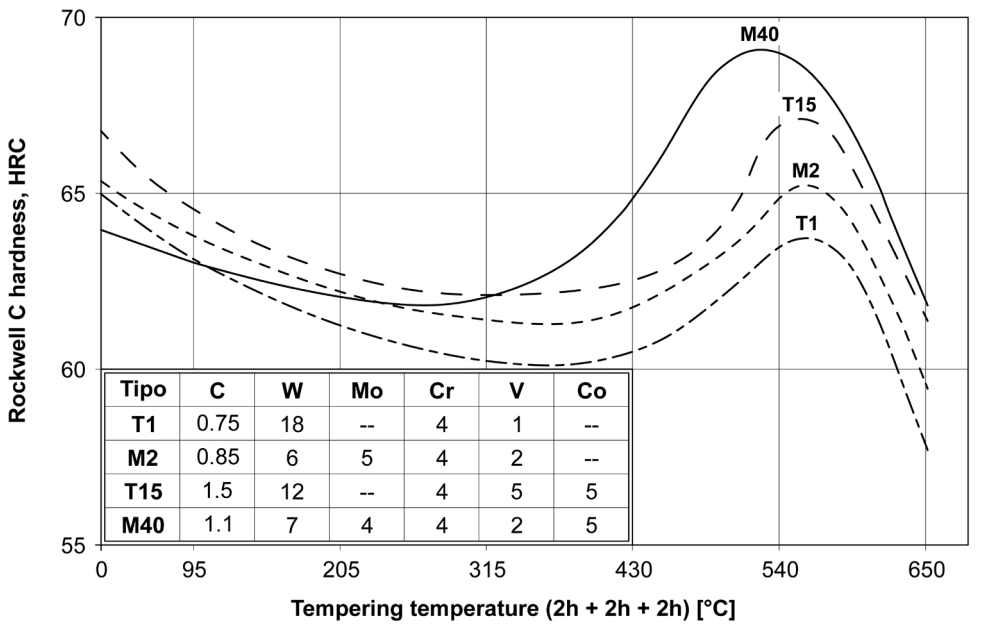

Tipo	C	W	Mo	Cr	V	Co
T1	0.75	18	--	4	1	--
M2	0.85	6	5	4	2	--
T15	1.5	12	--	4	5	5
M40	1.1	7	4	4	2	5

Figure 11.15 - Hardness for several types of tool steels after hardening and three tempering [from Hoyle 1988].

BIBLIOGRAPHIC RECOMMENDATIONS

It is not easy to give detailed advice regarding the topic of this book. In fact, a bibliography that deals with Steel Metallurgy is vast.

Two useful texts to begin with are those of Prof. Walter Nicodemi entitled: Metallurgia (volume 1) and Acciai e leghe non ferrose (volume 2) both published by Zanichelli in Bologna, in 2007 and 2008. These books not only concern steels (carbon, special, stainless, etc.), but also non-ferrous alloys (aluminum, copper, titanium, etc.).

The book by Prof. Aurelio Burdese, Metallurgia e tecnologia dei materiali metallici, UTET, Torino, Italia, 1992, and Claudio Cibaldi's volumes, I criteri di scelta e di trattamento degli acciai da costruzione e da utensili, 5 voll., AQM, Provaglio d'Iseo (BS), Italia, 2006-2010 are certainly useful for those who prefer to read in Italian. Numerous important bibliographic references exist in English.

Very interesting is the now unobtainable volume by Karl Erich Thelning, Steel and its Heat Treatment, Bofors Handbook, Butterworth, London, UK, 1975. Originally written in German and then translated into English, it contains all that can be useful with regard to steels and their heat treatment: not by chance this bibliographic reference is cited by all authors who, from that moment on, have been dealing with the metallurgy of steels.

The most recent American source is the collective volume edited by Flake C. Campbell, Elements of Metallurgy and Engineering Alloys, ASM International, Metals Park Ohio, USA, 2008. The author, a Boeing Engineer for 38 years, was awarded the Honorary Professorship of the University of Missouri (USA) in 2005.

Specifically on steels are also two books by George Krauss, Principles of Heat Treatment of Steels, ASM International, Metals Park, Ohio, USA, 1980 and Steels: Processing, Structure, and Performance, ASM International, Metals Park, Ohio, USA, 2005.

A great book, perhaps more for scientists than for technicians, is by the Persian author, Reza Abbaschian, Physical Metallurgy Principles, Cengage Learning, Stamford, USA, 2009, head of the Engineering Department of the University of California Riverside and emeritus professor of Mechanical Engineering.

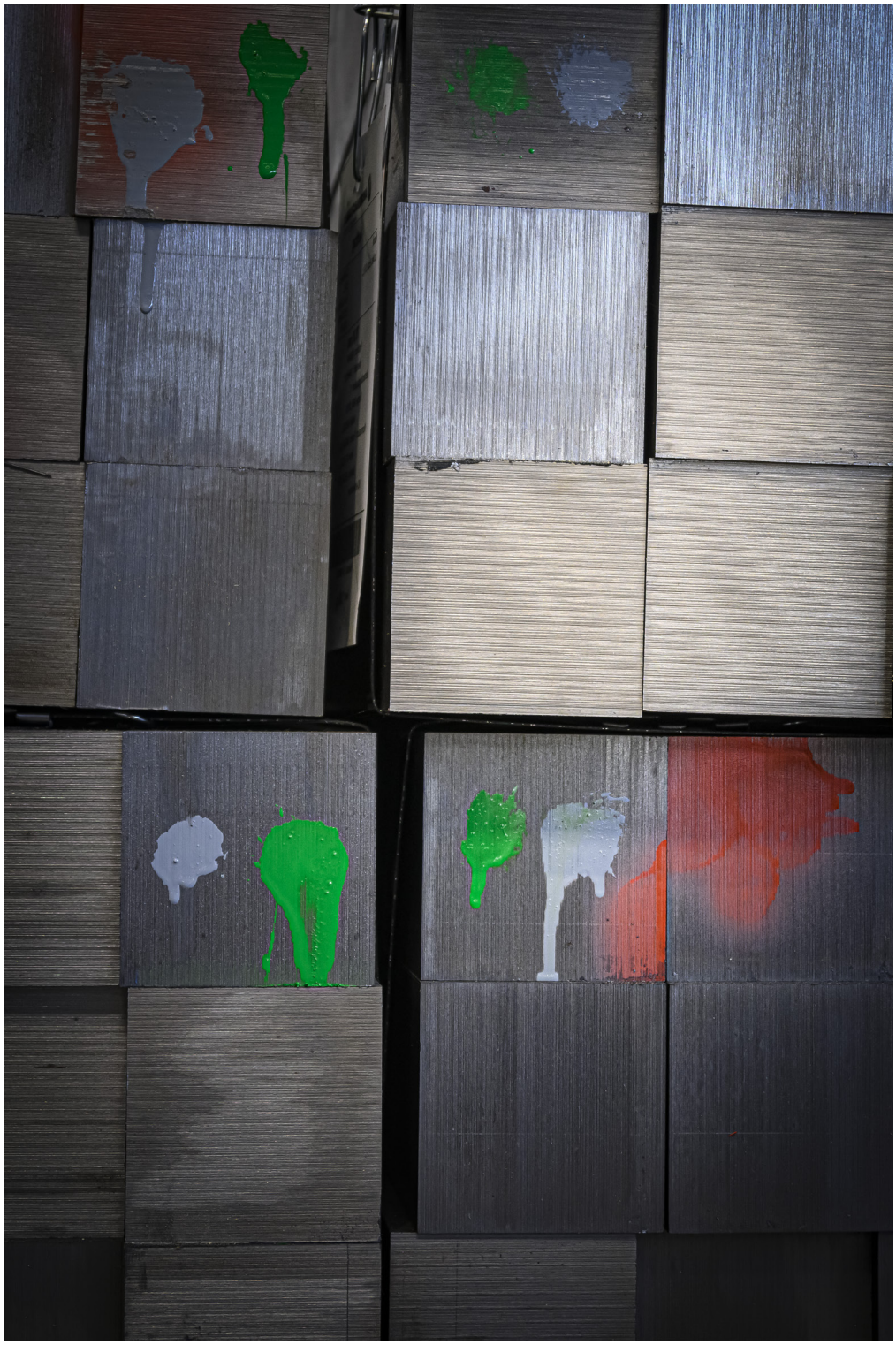

BIBLIOGRAPHY

[Abbaschian et al. 2009] Abbaschian R., Abbaschian L., Reed-Hill R. E., Physical Metallurgy Principles, 4th ed., Cengage Learning, Stamford, USA, 2009.

[Andrews 1965] Andrews K.W., Empirical formulae for the calculation of some transformation temperatures, Journal of the Iron and Steel Institute, n.7, pp.721-727, 1965.

[ASM-H.3 1992] ASM Handbook Committee, ASM Handbook, Vol. 3 - Alloy Phase Diagrams, 10th ed., ASM International, Metals Park, Ohio, USA, 1992.

[ASM-H.4 1991] ASM Handbook Committee, ASM Handbook, Vol. 4 - Heat Treating, 10th ed., ASM International, Metals Park, Ohio, USA, 1991.

[Bain e Paxton 1966] Bain E. C., Paxton H. P., Alloying Elements in Steel, 2nd ed., American Society for Metals, Metals Park, Ohio, USA, 1966.

[Briggs 1958] Briggs C. W., The Effect of Heat Treatment Variables on the Toughness of Cast Steel and Cast Armor, Steel Founders' Society of America, Cleveland, Ohio, USA, 1958.

[Brown e Cohen 1962] Brown R. L., Cohen M., Stress Relaxation of Hardened Steel, Metal Progress, n.2, pp. 66-71, 1962.

[Callister 2007] Callister W. D., Material Science and Engineering: An Introduction, 7th ed., John Wiley & Sons, New York, USA, 2007 (trad. it., Caneva C. (a cura di), Scienza e ingeneria dei materiali - un'introduzione, 2a ed., Edises, Roma, Italia, 2007).

[Campbell 2008] Campbell F. C. (ed.), Elements of Metallurgy and Engineering Alloys, ASM International, Metals Park Ohio, USA, 2008.

[Campbell 2003] Campbell J., Castings, 2nd ed., Butterworth-Heinemann, Oxford, UK, 2003.

[Cheng et al. 1991] Cheng L., Van der Pers N.M., Böttger A.,De Keuser Th.H., Mittemeijer E.J., Lattice Changes of Iron Carbon MartensiteAging at Room Temperature, Metallurgical Transaction A, Vol. 22, pp. 1957-1967, 1991.

[Chipman 1972] Chipman J., Thermodynamics and Phase Diagram of the Fe-C System, Metallurgical Transaction B, Vol. 3, pp. 55-64, 1972.

[Clayton e Danks 1990] Clayton P., Danks D., Effect of Interlamellar Spacing on the Wear Resistance of Eutectoid Steels under Rolling/Sliding Conditions, Wear, Vol. 135, p.369-387, 1990.

[Dieter 1988] Dieter G. E., Mechanical Metallurgy, McGraw Hill, London, UK, 1988.

[Gerold 1979] Gerold V., Precipitation Hardening; Dislocations in Solids, Vol. 4 - Dislocations in Metallurgy, North-Holland Publishing Company, Amsterdam, Holland, 1979.

[Ginzburg 2005] Ginzburg V.B., Metallurgical Design of Flat Rolled Steels, Marcel Dekker, New York, USA, 2005.

[Gladman 2004] Gladman T., Grain Size Control, Maney Pubblishing, London, UK, 2004.

[Grange e Baughman 1956] Grange R.A., Baughman R.W., Hardness of tempered martensite in carbon and low alloy steels, ASM Transactions, Vol. 48, pp.165-197, 1956.

[Higgins 1993] Higgins R.A., Engineering Metallurgy - Part I: Applied Physical Metallurgy, 6th ed., Arnold, London, UK, 1993.

[Hollomon e Jaffe 1945] Hollomon J.H., Jaffe L.D., Time-temperature relations in tempering steel, Transactions of AIME, Vol. 162, pp. 223-249 , 1945.

[Hosford 2005] Hosford W. F., Physical Metallurgy, Taylor & Francis Group, Boca Raton, Florida, USA, 2005.

[Hoyle 1988] Hoyle G., High Speed Steels, Butterworths, London, 1988.

[Krauss 1980] Krauss G., Principles of Heat Treatment of Steels, ASM International, Metals Park, Ohio, USA, 1980.

[Krauss 2005] Krauss G., Steels: Processing, Structure, and Performance, ASM International, Metals Park, Ohio, USA, 2005.

[Kurz e Fisher 1992] Kurz W., Fisher D.J., Fundamentals of Solidification, Trans Tech Publications, Switzerland, 1992.

[Jost et al. 1976] Jost S., Langer H., Pietsch D., Uligh P., Rechnerische Ermittlung der Erwärmdauer bei der Wärmebehandlung von Stahl, Fertigungstechnik und Betrieb, Vol. 26, pp.298-301, 1976.

[Lamont 1943] Lamont J.L., How to Estimate Hardening Depth in Bars, Iron Age, Vol. 152, pp. 64-70, 1943.

[Nicodemi 2007] Nicodemi W., Metallurgia, 2ª ed., Zanichelli, Bologna, Italia, 2007.

[Nicodemi 2008] Nicodemi W., Acciai e leghe non ferrose, 2ª ed., Zanichelli, Bologna, Italia, 2008.

[Ohmori e Honeycombe 1971] Ohmori, Y. and Honeycombe, R. W. K., Ohmori, Y. and Honeycombe, R. W. K. Proceedings ICSTIS, The Isothermal Transformation of Plain Carbon Austenite, Proceedings ICSTIS, Transactions of the Iron and Steel Institute of Japan, Vol. 11, pp. 1160-1164, 1971.

[Onink et al. 1993] Onink M., Brakman C. M., Tichelaar F. D., Mittemeijer E. J., van der Zwaag S., Root J. H., Konyer N. B., The Lattice Parameters of Austenite and Ferrite in Fe-C Alloys as functions of Carbon Concentration and Temperature, Scripta Metallurgica et Materialia, Vol. 29, pp. 1011-1016, 1993.

[Rocha et al. 2012] Rocha A.S., Nunes R.M., Hirsch T., Analysis by Design of Experiments of Distortion Potentials in Drawn and Induction Hardened Wire, Materials Research, Vol. 15(2), pp. 266-276, 2012.

[Singh 1999] Singh V., Physical Metallurgy, Standard Publishers Distributors, New Delhi, India, 1999.

[Smith e Hashemi 2006] Smith W.F., Hashemi J., Foundations of Materials Science and Engineering, 4th ed., McGraw-Hill, New York, 2006.

[Speich 1969] Speich G. R., Tempering of Low-Carbon Martensite, Transactions of TMS-AIME, Vol. 245, pp. 2552-2564, 1969.

[Spur e Stöferle 1980-1994] Spur G., Stöferle T. H. (ed.), Handbuch der Fertigungstechnik, 6 Vol., Carl Hanser Verlag, Munich, West Germany, 1980-1994.

[Steven e Haynes 1956] Steven W., Haynes A.G., The Temperature Formation of Martensite and Bainite in Low Alloy Steels, Journal of the Iron and Steel Institute, Vol. 183, pp. 349-359, 1956.

[Thelning 1975] Thelning K.E., Steel and its Heat Treatment, Bofors Handbook, Butterworth, London, UK, 1975.

[Thompson 1985] Thompson C.V., Secondary grain growth in thin films of semiconductors: Theoretical aspects, Journal of Applied Physics, Vol.58, pp.763-772, 1985.

[Totten 2006] Totten G. (ed.), Steel Heat Treatment: Metallurgy and Technologies, CRCnet base, Taylor & Francis Group, Boca Raton, Florida, USA, 2006.

[Wells e Lherbier 1980] Wells M.G.H. e Lherbier L.W., Processing and Properties of High Speed Tool Steels, TMS-AIME, New York, 1980.

[Wever et al. 1954/56/58] Wever F. et al., Atlas zur Warmebehandlung der Stahle, Verlag Stahleisen mbH, Dusseldorf, West Germany, 1954/56/58, Wever F., Rose A., Vol. 1; Rose A., Peter W., Strassburg W., Rademacher L., Vol. 2

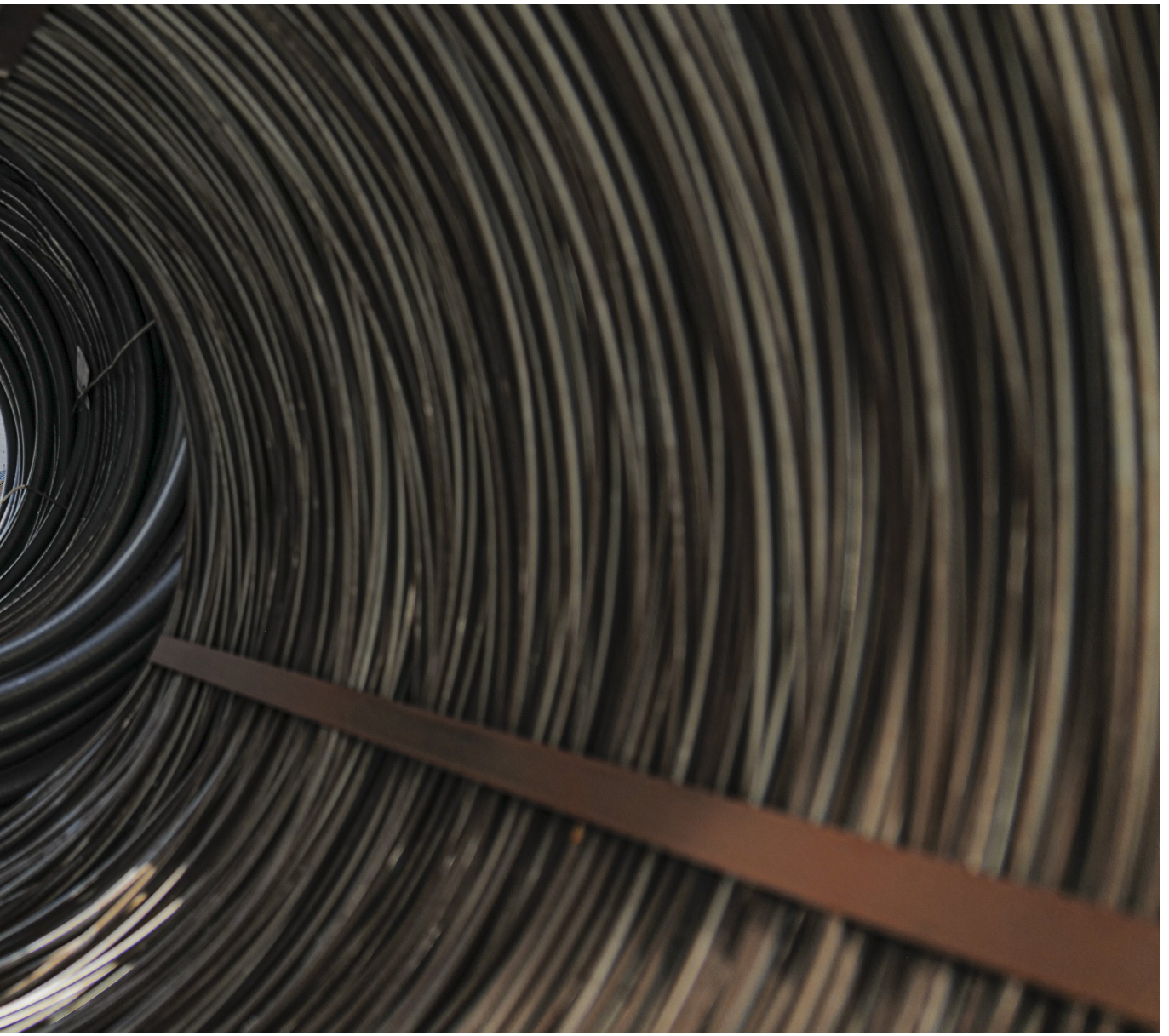

2nd edition, revised and corrected
Lucefin S.p.A.
I-25040 Esine - Brescia - Italy
www.lucefin.com

Graphics designed by: Lucefin
Photo by: Mino Martignano - Massimo Sperto
Printed by: Graphicscalve - Vilminore di Scalve - Bergamo - Italy

Photo by Fredi Marcarini

Marco V. Boniardi (Milano, 1964)

Full Professor of Metallurgy with the Department of Mechanical Engineering at Politecnico di Milano. For more than thirty years he has been involved in research and technological transfer activities in the sectors of Metallurgy and Materials Science. His main fields of interest are stainless steels, carbon and alloy steels, heat treatments and thermochemical treatments, fatigue, fracture mechanics, corrosion, steel production and transformation processes. In addition to standard issues in the sector of Metallurgy, his competence also includes fires, explosions and forensic ballistics. Author of more than 130 scientific publications, he cooperates with a number of Italian and international companies as regards forensic engineering, failure analysis and malfunctions during operation. He has also provided expert testimony in incidents widely covered by the media (such as the Viareggio train derailment and the Costa Concordia wreckage). He is the coordinator of the Failure Analysis & Forensic Engineering course that is held every two years.
Together with Andrea Casaroli he is the founder of the website **www.fa-fe.com**.

Andrea Casaroli (Piacenza, 1984)

Adjunct Professor of Metallurgy and Machine Design with the Department of Mechanical Engineering at Politecnico di Milano, and of Metallurgy at the University of Pavia. For more than ten years he has been involved in research activities in the metallurgical field as regards stainless steels, carbon and alloy steels, functional coatings and mechanical behaviour of materials. He also deals with failure analysis and industrial accidents and has acquired extensive expertise in fire investigations and fire resistance of materials. Author of more than 30 scientific publications, he cooperates with Italian and international companies in solving problems connected with mechanical failure, corrosion, fatigue and malfunctioning of industrial components and plants.
Together with Marco V. Boniardi he is the founder of the website **www.fa-fe.com**.

TRAFILIX
INDUSTRIES

Trafilix S.p.A.
I-25040 Esine - Brescia - Italia
www.trafilix.com

ISBN 978-88-909837-1-9